MECHANICAL CYCLIC STRAIN INDUCES CERAMIDE GENERATION IN ENDOTHELIAL CELLS

by

Oriana C. Hunter

Bachelor of Science, Massachusetts Institute of Technology, 1999

Submitted to the Graduate Faculty of

Swanson School of Engineering in partial fulfillment

of the requirements for the degree of

Doctor of Philosophy

University of Pittsburgh

2009

UNIVERSITY OF PITTSBURGH

SWANSON SCHOOL OF ENGINEERING

This dissertation was presented

by

Oriana C. Hunter

It was defended on

June 30th, 2009

and approved by

Michael T. Lotze, MD, Professor, Departments of Surgery and Bioengineering

Hannah Rabinowich, PhD, Professor, Departments of Pathology and Immunology

David A. Vorp, Professor, PhD, Departments of Surgery and Bioengineering

Dissertation Director: Andrew A. Amoscato, PhD,

Associate Professor, Departments of Pathology and Bioengineering

MECHANICAL CYCLIC STRAIN INDUCES CERAMIDE GENERATION IN ENDOTHELIAL CELLS

Oriana C. Hunter, PhD

University of Pittsburgh, 2009

The vascular endothelium is continuously subjected to a variety of mechanical and chemical stresses while it performs its duties in the maintenance of vascular permeability, tone, hemostasis, inflammation, and remodeling in health and disease. The mechanism by which endothelial cells respond to mechanical forces, or mechanotransduction, is not completely understood and is the subject of ongoing debate. Several theories involving proteins and reactive oxygen species have been proposed as components of the mechanotransduction process, however the role of the lipid microenvironment and lipid signaling remains largely unknown. We hypothesize that mechanical, uniaxial cyclic strain results in an increase in intracellular ceramide in vascular endothelial cells, which participates in signaling necessary to propagate mechanotransduction responses, potentially contributing to early events in the formation of atherosclerotic lesions.

To evaluate this hypothesis, we used electrospray mass spectrometry to study the lipid microenvironment, particularly with regards to ceramide signaling, in endothelial cells in response to cyclic strain within and beyond the physiological range, so as to gain a better understanding of the events that may ultimately contribute to endothelial dysfunction. The findings of these studies have elucidated the time scale of the ceramide response and the ceramide biosynthetic and metabolic pathways that occur during the early response to cyclic strain. Ceramide signaling results from distinct signaling events associated with nSMase,

aSMase, and *de novo* ceramide synthesis. The nSMase signaling event appears to be necessary for the later *de* novo event to occur. The endothelial response to cyclic strain is sensitive to strain magnitude, resulting in ceramide elevation at levels both above and below physiological strain magnitudes, suggestive of a wide variety of arterial pathological states.

These findings help to elucidate the early events in the mechanotransduction response to cyclic strain and represent a step towards bridging our understanding of the relationship between mechanotransduction and inflammation as it relates to endothelial cell activation and dysfunction and vascular disease. Establishment of the involvement of the ceramide biosynthetic pathway in endothelial cells and the vascular environment provides us with new biomarkers and therapeutic targets to potentially protect against vascular activation, dysfunction, and atherogenesis.

TABLE OF CONTENTS

LIST OF TABLES

LIST OF FIGURES

PREFACE

The first time I ever stepped foot in a real biological research lab was when I was a senior in high school. I do not recall what I had previously thought biomedical research actually involved, but at that moment, I knew that I liked it and that I was never going to be able to get away from it ever again. The path I have traveled since then has had many twists and turns and there have been many people who have guided my journey along the way. Certainly, I would not be the same person I am without them all.

Foremost, I want to thank Dr. Amoscato, who has been my "science dad" for the last ten years. When I was fresh out of college and an engineer besides, he took me into his lab, taught me to love lipids, trusted me to work independently from the first day, and has encouraged and supported me in all my scientific endeavors ever since. I cannot put into words my gratitude. May my work always reflect well on the solid foundation of scientific inquiry, integrity, and perseverance that he has instilled in me in his lab.

I want to thank Dr. Lotze, Dr. Rabinowich, and Dr. Vorp, not only for volunteering their time to serve on my committee and to guide me through their advice and discussion, but also for standing as role models. It was Dr. Lotze's lab into which I first stepped foot all those years ago as a high school student, and I don't know that I have ever really left it. Much of my desire to pursue science and the clinical life has been inspired by the example of his zeal for science,

dedication to students, and true generosity. If Dr. Amoscato is my "science dad," surely Dr. Lotze is my "science uncle." Although I have only known Dr. Rabinowich for a few years, I have known of her for far longer. Her name is one that I have known since I was a summer student throughout college and she has always been a role model to me as a woman in the sciences. Finally, and not least, I want to thank Dr. Vorp, without whom my thesis research really could not have happened. When I started this project, I knew that I wanted to study ceramide in vascular mechanotransduction, but I had no idea how to go about doing the mechano part of the transduction. He generously made his lab and his personnel available to me and has provided me with many opportunities to share my science with other bioengineers over the years.

I would also like to thank the entire Bioengineering department, and particularly Dr. Borovetz, for turning me from a mechanical engineer into a bioengineer. I have long suspected that Dr Borovetz always knew I would end up staying for a PhD, even if I thought I was just taking a few graduate classes for fun while applying to medical school. In the same breath, it is fitting to thank Lynette Spataro, for all the things she does to help graduate students get to do what we do. When we tell her that she is the best, we mean it.

Thank you as well to all the engineers, nurses, doctors, patients and families who have encouraged me in my education during my time at the Artificial Heart Program, and taught me as many lessons about life and human compassion as they have about heart failure.

On a more personal note, I want to thank my family and my friends. I especially want to thank Teresa, Jen, and Gloria. Thank you as well to the many friends I have had in the lab over the years. There are friends from the early days, like Anne, Sue, Masatoshi, and Kazuo. Then, there are also the new friends who have made the final years of my studies fun, like L.J. (my lab partner in all my best feats of nerdiness), Jessica, Tara, Nicole, Shelley, Adam, Antonio, and the

rest of the DAMP lab. In the Vorp lab, where I have occasionally spent more time than in my own lab, I want to thank Doug Chew and Tim Maul for helping me to even get through the front door of the building, let alone introducing me to the Flexcell.

I want to thank my loving family – mom, dad, Matt, and all the extended Hunter and DiNapoli families -- who have stood by me and cheered me on in all my endeavors. They have encouraged me to do what I love and have instilled in me the values of commitment, perseverance, and hard work. My parents and my brother, although not scientists, have patiently listened to me talk my way through scientific conundrums on more occasions than I can count and they have thoughtfully left me plates of leftovers in the refrigerator so that I would not go hungry after late nights in the lab. My family dogs have sat with me for countless hours while I studied and stayed up late writing papers. We have joked that Quincey is earning his own PhD, for all the journal articles and class notes that he ate as a puppy.

Although my entire extended family has encouraged me and cheered for me, I want to particularly acknowledge the encouragement of my Grandma DiNapoli who passed away this spring without getting to see me finish my PhD. My grandmother always valued the improvement of one's mind through learning and encouraged all her children and grandchildren to aspire to the higher education that she was not able to receive. She never missed an opportunity to tell others how proud she was of me.

The journey has been long and it has not always been easy, but it is not an experience I would trade for anything in the world. Thank you again, to everyone who has helped me to get here. I could not have done it without you.

Finally, I would like to acknowledge the funding sources for this work, including NIH grants 1 R01 092389, 5 P30 CA47904-17, 1 U19 AI068021-01, and 1 P01 CA101944-04.

1.0 INTRODUCTION

1.1 VASCULAR ENDOTHELIAL FUNCTION AND CARDIOVASCULAR DISEASE

The vascular endothelium forms the lining of blood vessels and the heart, separating blood from the intimal and medial layers of arteries and veins, and very importantly, regulates vessel permeability to leukocytes and inflammatory mediators [1]. Furthermore, the vascular endothelium is responsible for maintaining vascular tone and for regulating platelet aggregation, thrombogenesis, and proliferation and remodeling of blood vessels, in response to biochemical and mechanical signaling [2]. Dysfunction or loss of integrity of the vascular endothelium, consequently, may compromise vasoregulation, increase blood coagulation, and promote leukocyte and inflammatory cytokine infiltration into the intima and increase smooth muscle cell (SMC) migration and proliferation, potentially contributing to the formation of atherosclerotic lesions [1, 3-5].

Atherosclerosis is a progressive disease characterized by the formation of lesions within the arterial wall characterized by inflammation, lipid accumulation, cell death, and fibrosis. Progressing lesions develop into mature plaques, which can cause vessel occlusion or can rupture, leading to acute thrombotic occlusion of the vessel. Depending on the arteries affected by atherosclerosis, the clinical outcome may manifest as an acute myocardial infarction, heart failure, ischemic stroke, hypertension, or organ or limb ischemia and functional impairment [6-

8]. Endothelial dysfunction, a precursor to the onset of atherosclerosis, has been implicated in the clinical manifestation and disease pathogenesis of most cardiovascular diseases [9-11].

1.1.1 Cardiovascular disease and atherosclerosis: incidence and impact on health care

Cardiovascular disease is the primary cause of 35.3% of deaths each year in the United States and contributes to as many as 56% of all deaths. Furthermore, as many as 80 million American adults have at least one form of cardiovascular disease manifesting as hypertension, coronary heart disease such as myocardial infarction or angina pectoris, heart failure, or stroke. Taken together, these patients accounted for more than 7 million hospital discharges in 2006 and the total cost of care for cardiovascular disease in 2009 is projected to be $475.3 billion. Atherosclerosis, whether of the coronary or peripheral arteries, is responsible for nearly three fourths of all deaths from cardiovascular disease in this country, including deaths from stroke and myocardial infarction [8]. Atherosclerotic vascular disease remains a major cause of death worldwide in both developed and developing countries [4, 7, 8]. Thus, atherosclerotic vascular disease represents a serious clinical problem worldwide.

Owing to the profound impact of atherosclerosis as a global health crisis, substantial efforts have been made to educate the public about risk factors for cardiovascular disease [8] and to improve diagnostic methods to monitor endothelial dysfunction and to detect subclinical vascular disease before patients become outwardly symptomatic of cardiovascular disease [5, 10, 12]. Although traditional methods of determining vascular dysfunction have focused on measures of vasomotion of arteries, whether by the administration of an endothelium-dependent vasodilator such as acetylcholine or brief occlusion of a peripheral artery to study the vessel's response to the resulting flow-mediated vasodilation, efforts are now being made to identify

surrogate biochemical markers of vascular health in an effort to provide a more specific analysis of the underlying mechanisms of a patient's vascular dysfunction, response to therapy, and prognosis [4, 12].

1.1.2 Vascular anatomy

The vascular wall, whether that of an artery or a vein, contains three distinct layers: the intima, the media, and the adventitia. The intima, or tunica intima, consists of the endothelial lining, which directly interacts with the blood, supported by a basement membrane and thin extracellular matrix overlying the internal elastic lamina. The structure of the internal elastic lamina is an open meshwork that allows movement of cells between the intima and media as well as exchange of soluble factors between the endothelium and cells of the media. This aspect is of particular note in the development of atherosclerotic lesions [13-15].

The media, or tunica media, is comprised of smooth muscle cells and collagen, bounded by an external elastic lamina on the opposite side. The smooth muscle cells provide the tonus that allows arteries to dampen pulsatile blood flow from the heart, and together with the elasticity of the various elastic laminae contributes to a relatively smooth flow of blood through the arterial system. Owing to this property, the media in arteries is generally thicker than in veins, and varies in thickness corresponding to the pressure head in the artery [13, 14]. The internal and external elastic laminae are also absent in the typical vein [14, 16]. In elastic arteries such as the aorta, which sees increased pressures and pulsatility across the cardiac cycle, the media is comprised of several layers of lamellae, which are layers of smooth muscle cells bounded on each side by a thin elastic lamina and the number of lamellae increases along the artery in the cephalad direction [13].

The outermost layer on the abluminal surface of the artery is the adventitia, or the tunica externa. The tunica externa consists primarily of collagen, some elastin, some smooth muscle cells, fibroblasts, macrophages, lymphocytes, a system of nerves, and the arterioles, capillaries, and venules of the vasa vasorum, which nourishes cells across the outer thickness of arteries. In thicker arteries such as the aorta, the vasa vasorum also extends into the media of the vessel [13, 14, 16, 17]. The adventitial vasa vasorum has also been implicated as the source of intraplaque vasculature in advanced atherosclerotic lesions, correlating with increased inflammation and propensity for intraplaque rupture [17, 18].

The largest arteries, such as the aorta, pulmonary trunk, and their major branch arteries including the pulmonary, common carotid, subclavian, and common iliac arteries, are classified as elastic or conducting arteries and can have a diameter up to approximately 2.5cm [14]. These arteries have a highly organized medial structure that reduces oscillation and dampens pulsatility as blood flow progresses towards the arterioles. This alleviates pulsatile stresses on the perfused organs [13, 14, 19]. Medium diameter arteries, known as muscular or distribution arteries, typically have a luminal diameter of 0.5mm to 0.4cm and are characterized by a thick, highly cellular media. Examples of muscular arteries include the external carotid, brachial, mesenteric, and femoral arteries. Arterioles tend to have a luminal diameter of less than 30 μm, have a relatively thin media, and have a poorly defined adventitia [14]. Atherosclerotic lesions occur primarily in large elastic arteries and medium muscular arteries [13].

1.1.3 Function of the healthy endothelium

The vascular endothelium consists of a single, continuous monolayer of endothelial cells lining the blood vessels and the heart, thus separating the blood from underlying layers of the vessel intima and media of arteries and veins [1, 20, 21]. Under conditions of laminar flow, endothelial cells elongate and align in the direction of flow/ shear stress, but retain a polygonal cobble-stone-like morphology in regions of disturbed flow where flow may be sluggish or characterized by eddying [13, 22]. There is evidence that the endothelium of arteries and veins are distinct entities with inherently different responses to stimuli, reflective of environmental inputs and differential gene expression [16, 22, 23]. In its unique location, the endothelium has been described as a biophysical sensor, capable of releasing numerous autocrine, endocrine, and paracrine factors in response to changes in the physical, metabolic, and inflammatory environment to maintain vascular homeostasis [4, 5, 9, 10]. In addition to responding to changes in blood flow and blood composition, the endothelium is capable of reacting to signaling from the other cells of the vessel wall and extracellular matrix components [22-24].

One of the most notable functions of the endothelium is the regulation of vascular tone in response to changes in hemodynamic forces and blood-borne chemical signals through the release of vasoactive substances, including vasodilators like nitric oxide, prostacyclin, endothelium-derived hyperpolarizing factor, bradykinin, adrenomedullin, and C-natriuretic peptide; and vasoconstrictors like endothelin-1, angiotensin-II, thromboxane A_2, prostaglandins, hydrogen peroxide and free radicals [9, 21, 25]. The balance of these factors is crucial to vascular homeostasis and impacts the systemic blood circulation [4, 9, 16]. Nitric oxide in particular is crucial in the maintenance of vascular tone and vascular reactivity and as such, is the subject of extensive study [4, 9].

The function of the endothelium goes beyond regulation of vascular tone. Under normal physiological conditions, endothelial cells regulate the bi directional transport of gases and macromolecules from the blood by way of receptor-mediated and receptor-independent transcytosis and endocytosis [4, 20] and biosynthesis of numerous factors that influence hemostasis and angiogenesis [13, 16, 20, 21, 25]. The endothelium also plays a critical role in trafficking of leukocytes, modification of lipoproteins from the plasma, and vessel permeability [13, 16, 23, 25].

The endothelium is highly dynamic and heterogeneous, allowing for local adaptations necessary to maintain the health and function both of the vasculature and the tissues and organs it services. In the disease state, its ability to optimally adapt to changes in environmental stimuli is compromised. Not surprisingly, endothelial function is associated not only with traditional vascular disease like atherosclerosis, but with most diseases, ranging from cancer to renal failure to sepsis to chronic inflammatory disease, and may play a role in disease causality or may exist in a state of dysfunction secondary to the initial disease pathology [23].

1.1.4 Endothelial cell activation

Under normal conditions, the quiescent endothelial cells express a phenotype that is anticoagulant, anti-inflammatory, antiadhesive, and vasodilatory. When exposed to certain environmental factors indicative of damage or danger, such as TNF-α, IL-1, or endotoxin, endothelial cells change their phenotype to one that is more procoagulant, proadhesive, and vasoconstrictive with increased antigen-presenting capacity. This broad set of changes occurs as a normal part of both physiological and pathophysiological conditions [23, 24].

One of the earliest events of endothelial cell activation, occurring within minutes of activation, is the exocytosis of Weibel-Palade bodies (WPBs) into both the apical and basolateral spaces. WPBs release numerous proteins responsible for regulating hemostasis, vascular tone, inflammation, and angiogenesis [22, 25-27]. The major component of WPBs is von Willebrand factor (vWF), which is involved in platelet adhesion to the activated endothelial cell [22, 26, 27]. P-selectin, a receptor that mediates adhesion of platelets and leukocytes to the endothelium is present in the membranes of WPBs and fuses with the plasma membrane of the endothelial cell upon exocytosis. WPBs have also been reported to contain endothelin (vasoconstrictor), tissue plasminogen activator (thrombolytic), osteoprotegerin (bone remodeling), angiopoietin-2 (vascular remodeling, inflammation), and even coagulation factor VIII [22, 28]. WPBs of the microvasculature and those produced during active inflammation contain the proinflammatory chemokine IL-8, which is involved in chemotaxis of target leukocytes. IL-8 is retained in WPBs even after reversal of endothelial activation, arguing that this property helps the pre-activated endothelium mount a more robust inflammatory response upon reactivation [29, 30].

While WPB exocytosis represents a rapid and general response to inflammation during activation, there are also a number of signaling events and changes in gene expression occurring over the period of the first few hours that refine the immune response. Numerous adhesion molecules, including VCAM-1 and E-selectin are upregulated, which, combined with cytokines like IL-6 and chemokines like IL-8, promote leukocyte adhesion prior to trafficking across the endothelium. The combination of cytokines, chemokines, and adhesion molecules necessary for leukocyte adhesion, rolling, activation, and transendothelial migration varies depending on the type of target leukocyte (i.e. T lymphocyte, neutrophil, or monocyte) [22, 25, 27]. TNF-α activation of endothelial cells has also been shown to decrease endothelial nitric oxide synthase

(eNOS), thereby promoting a vasoconstrictive state [31]. Activation of endothelial cells by pro-inflammatory cytokines has also been shown to upregulate production of Tissue Factor, a major initiator of the extrinsic coagulation cascade, thus promoting a pro-coagulant state [25].

Signaling through NF-κB, which has been studied best in response to the inflammatory cytokines TNF-α and IL-1, but is also known to be triggered by Toll-like receptors on the endothelial cell surface, leads to expression of an assortment of genes for pro-inflammatory adhesion molecules including E-selectin, ICAM-1, and VCAM-1; cytokines such as IL-6; chemokines such as IL-8; cyclooxygenase-2; and inducible nitric oxide synthase (iNOS) as well as a number of other protective genes, which protect against apoptosis and exert anti-inflammatory effects, providing some degree of protection to the endothelium against damage during activation [25, 32]. The high degree of regulatory feedback mechanisms assure that NF-κB transcriptional products are only transiently activated during activation, although there is evidence that enhanced NF-κB signaling occurs during aging and in some inflammatory diseases like rheumatoid arthritis and Crohn's disease [25, 33]. Additionally, the MAPK signaling pathways – including ERK, JNK, and p38 MAPK pathways – are also activated during endothelial cell activation, which have been implicated in a variety of cellular outcomes from proliferation, and differentiation to apoptosis, stress responses, and inflammation [25].

Another interesting, but less understood facet of endothelial activation is the generation of microparticles, which are submicron vesicles shed from the plasma membrane in response to cellular activation, injury, or apoptosis [20, 34, 35]. Microparticles of platelet, leukocyte, and endothelial cell origin have been identified under both healthy and pathological conditions and their composition with regards to surface markers and lipid content depends on the cell type of origin and disease state. Endothelial microparticles, which are particularly rich in Tissue Factor

at their plasma membrane, have been shown to decrease nitric oxide-dependent vasodilation and to promote arterial stiffness, inflammation, and thrombogenesis [34].

Thus, the broad variety of signaling, cellular recruitment, and transcriptional changes present during activation demonstrates not only the complex and multifaceted functionality of the endothelial cell, but also suggests the many potential ways in which an imbalance of this well-orchestrated self-regulation can lead to or exacerbate disease (Figure 1.1).

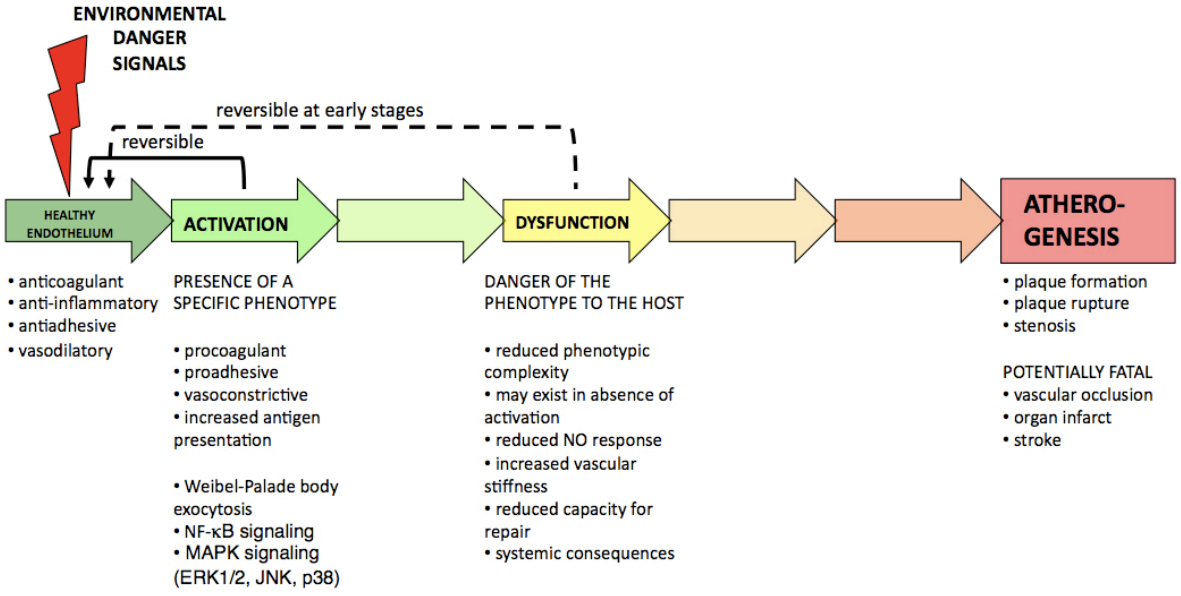

Figure 1.1. The vascular endothelium undergoes many changes contributing to the onset of vascular disease.

1.1.5 Endothelial cell dysfunction

Endothelial dysfunction is believed to be one of the earliest events contributing to the onset of atherosclerotic cardiovascular disease (Figure 1.1), and has been described in patients with risk factors for vascular disease such as diabetes, hyperlipidemia, hypertension, and smoking, as well as in patients without traditional risk factors [4, 5, 10, 24]. Endothelial dysfunction has also been associated with mechanical removal of or trauma to the endothelium or when the endothelial continuity is compromised [24, 35]. Whereas endothelial activation describes the presence of a specific endothelial phenotype, endothelial dysfunction describes the danger of the endothelial phenotype to the host and may exist even in the absence of endothelial activation. Unlike the healthy endothelium, which is highly heterogeneous in its phenotype and functionality, the dysfunctional phenotype loses complexity and becomes more uniform in its response to stimulation as endothelial cells approach quiescence [23]. Cellular senescence, whether associated with age or with disease states, particularly under conditions that require a high degree of cell turnover, has also been implicated in the progression of endothelial dysfunction as part of many vascular pathologies [36].

While endothelial dysfunction is believed to be reversible prior to the development of advanced, lesional, structural changes to the vascular wall, methods to screen for its presence have not been widely utilized at the clinical level. Likewise, guidelines for the identification of appropriate screening populations in otherwise clinically asymptomatic patients without traditional risk factors remain vague, since most patients do not present until they have clinically significant endpoint events, such as myocardial ischemia [4, 24]. The ability to effectively detect early endothelial dysfunction and to monitor subclinical vascular disease has the potential to

improve our understanding of conventional risk factors and to expand the efficacy and use of preventative pharmacological and medical therapies [10, 37].

The traditional definition of endothelial dysfunction is a reduction in the bioavailability of vasodilators, and more specifically nitric oxide (NO), relative to the increase in endothelium-derived vasoconstrictors and reactive oxygen species, leading to an impaired endothelium-dependent vasodilatory response [9, 10]. As such, conventional methods to assess endothelial dysfunction rely on detection of a paradoxical failure of vasodilation or even vasoconstriction in response to administration of an endothelium-dependent vasodilator like acetylcholine followed by a brief period of mechanical vascular occlusion [12]. Other methods like pulse wave velocity assess the overall stiffness of an artery and may represent a cause or an effect of vascular disease depending on the underlying etiology without assessing the actual health of the endothelium [19].

As our understanding of the complexity of normal endothelial function and vascular disease progression improves, it becomes clear that this limited definition of endothelial cell dysfunction does not properly take into account the numerous contributions of the endothelium to the vascular milieu, nor does it take into account the potential detriment of their loss or the systemic nature of endothelial dysfunction as a syndrome. As such, some scholars have suggested an expanded view of endothelial dysfunction to also include assessment of the antithrombotic, metabolic, platelet and leukocyte adhesion, and anti-inflammatory properties of the endothelial cells as well as the ability to regulate the movement of fluid volume and electrolytes in the intra- and extravascular spaces to provide a more finely tuned evaluation of the extent of endothelial dysfunction and capacity to predict the potential course of disease progression [12, 19, 23, 24]. Others note that endothelial dysfunction is characterized not only

by the loss of functionality of the endothelial cells present, but also by a reduced ability of the endothelium to repair desquamation whether through proliferation or recruitment of circulating endothelial progenitor cells (EPCs) [24]. The relatively young field of biomarkers of endothelial dysfunction stands to provide the greatest benefit to this broader view of endothelial dysfunction.

1.1.6 Atherosclerosis

The formation of the atherosclerotic lesion is complex and multistep. Due to exposure to oxidized lipoproteins or oxidized LDL resulting from diet or inflammation, activated endothelial cells (ECs) upregulate surface markers responsible for recruitment and intravisation of circulating monocytes into the subendothelial space where they differentiate into macrophages and take up oxidized LDL and other lipids, leading to the formation of foam cells which comprise the early lesion, known as the "fatty streak." The developing atherosclerotic lesion consists of foam cells of macrophage and smooth muscle cell origin, extracellular pools of lipids, apoptotic cells, and other immune cells such as T cells and mast cells, and is accompanied by SMC migration and proliferation. In the late stages of plaque development, the lesion also contains foam cells of endothelial cell origin. As the lesion progresses, it becomes increasingly fibrotic and calcified, making it more susceptible to plaque rupture, leading to thrombosis, which can cause vessel occlusion or embolization or can contribute to further growth of the lesion and increased vessel stenosis, all with the potentially catastrophic outcome of stroke, myocardial or other organ infarction, or peripheral vascular occlusion [3, 6, 20].

Similarly, loss of integrity of the endothelium due to endothelial apoptosis, as may also occur in the process of vascular graft occlusion, is also believed to cause increased vascular

permeability, SMC proliferation, and blood coaguability, potentially contributing to lipid, monocyte, and SMC deposition in the intimal space leading to plaque development [1, 38].

1.1.7 Transplant vasculopathy

Transplant vasculopathy remains one of the most significant limitations in solid organ allograft transplantation. Approximately 50% of transplant patients exhibit significant allograft vasculopathy within five years and 90% exhibit significant disease within ten years. During transplant vasculopathy, the vasculature of the allograft organ develops severe, diffuse intimal hyperplasia, leading to stenosis and eventual graft ischemia [15].

Within the first year, a phenomenon of vessel shrinkage in transplanted organs has been observed and is believed to be due to a transient adventitial hyperplasia characterized by increased adventitial scarring and contraction due to initial perivascular inflammation. Later, vascular stenosis in transplanted organs tends to be characterized by intimal hyperplasia, which involves the recruitment and proliferation of smooth muscle cells into the intima. Regardless of whether intimal, medial, or adventitial hyperplasia is initiated, the net effect on the vessel without compensatory remodeling, is often increased vascular stiffness [15].

Unlike conventional atherosclerotic lesions, areas of transplant vasculopathy tend to be concentric around the graft rather than focal. Although the composition of the media across these lesions is somewhat different from a traditional atherosclerotic plaque, the initiating events of lesion formation are still believed to be loss, impaired remodeling, and dysfunction of the endothelium. Also, as with conventional atherosclerosis, inflammation and its impact on the endothelium are also believed to be a very important factor in the early stages of lesional development [1, 15].

1.1.8 Vascular graft occlusion

Annually, more than 350,000 patients in the United States and more than 800,000 patients worldwide undergo coronary artery bypass grafting for revascularization therapy due to coronary artery disease. Graft occlusion following gradual graft stenosis remains a daunting challenge to bypass grafting and grafts of venous origin (i.e. saphenous vein) have a substantially higher rate of occlusion by ten years post-operative than do arterial grafts (i.e. internal mammary artery). Studies also show that even when the graft remains patent, vascular disease of the graft is often present [39, 40].

Vein graft occlusion has been extensively documented to be the result of excessive intimal hyperplasia or atherosclerosis, often occurring at the artery-vein anastomotic site [41]. Experimental vein grafts may see as much as 140 times the circumferential strain encountered compared to that encountered at the harvest site. Additionally, the anastomotic site, due to ballooning of the graft because of compliance mismatch, is frequently exposed to eddying shear flow conditions [42]. Histological evaluation of the vein grafts near the anastomotic site has shown that they experience intimal hyperplasia as well as loss of the endothelial layer across this region [41]. This phenomenon has also been observed along the entire length of the graft in experimental vein graft models, with and without reduction in eddying shear flow [38, 42]. There is also evidence that in arterial and vein grafts in which the bypassed coronary artery is "too patent," that increased stenosis, due to reduced arterial flow in the graft, may occur [40].

1.2 VASCULAR ENDOTHELIAL BIOMECHANICS AND MECHANOBIOLOGY

Blood vessels experience a variety of mechanical forces due to blood flow, mainly hydrostatic pressure, acting radially; cyclic strain, acting circumferentially; and fluid shear stress, acting longitudinally in the direction of blood flow [43], as shown in Figure 1.2. Together, these forces influence the endothelium and its role in maintaining proper blood flow, vascular tone, remodeling, inflammation, and thrombosis. During mechanical injury and disease, blood vessels may encounter abnormal levels of these forces, which have been shown to affect the function of ECs and SMCs, potentially contributing to atherogenesis [44, 45].

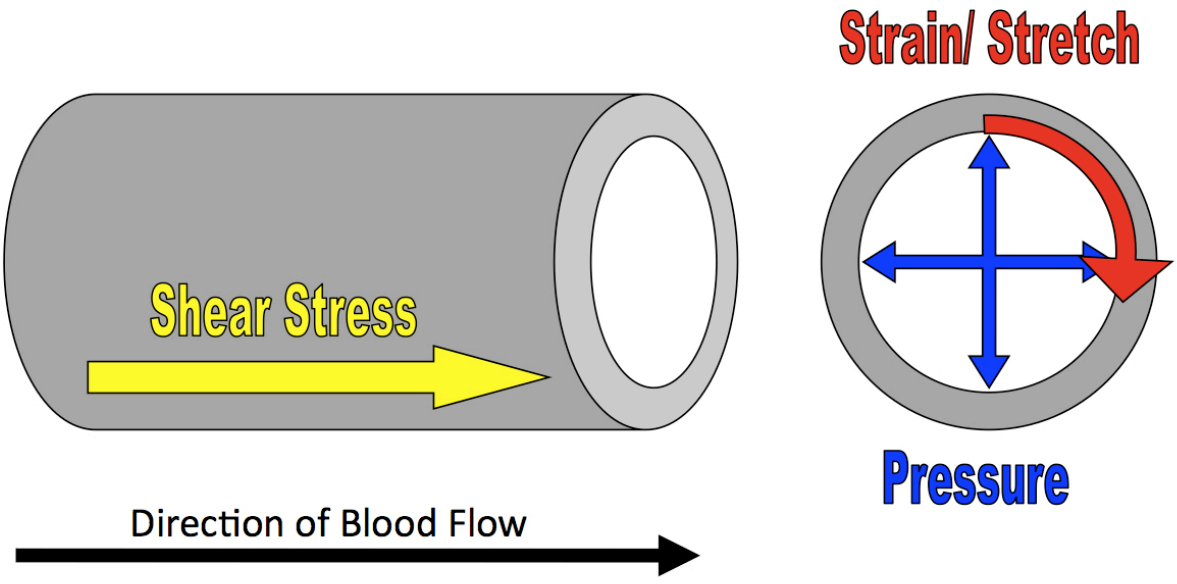

Figure 1.2. Mechanical forces act upon a blood vessel during pulsatile blood flow.

1.2.1 Mechanotransduction

The process by which applied mechanical forces are transformed into cellular biomolecular responses, is known as mechanotransduction [46]. Several possible mechanisms have been proposed for mechanotransduction including ion channels, G-proteins, mitogen-activated protein kinases (MAPKs), integrins and focal adhesions, the cytoskeleton, and reactive oxygen species (ROS) [44, 45, 47], as shown in Figure 1.3.

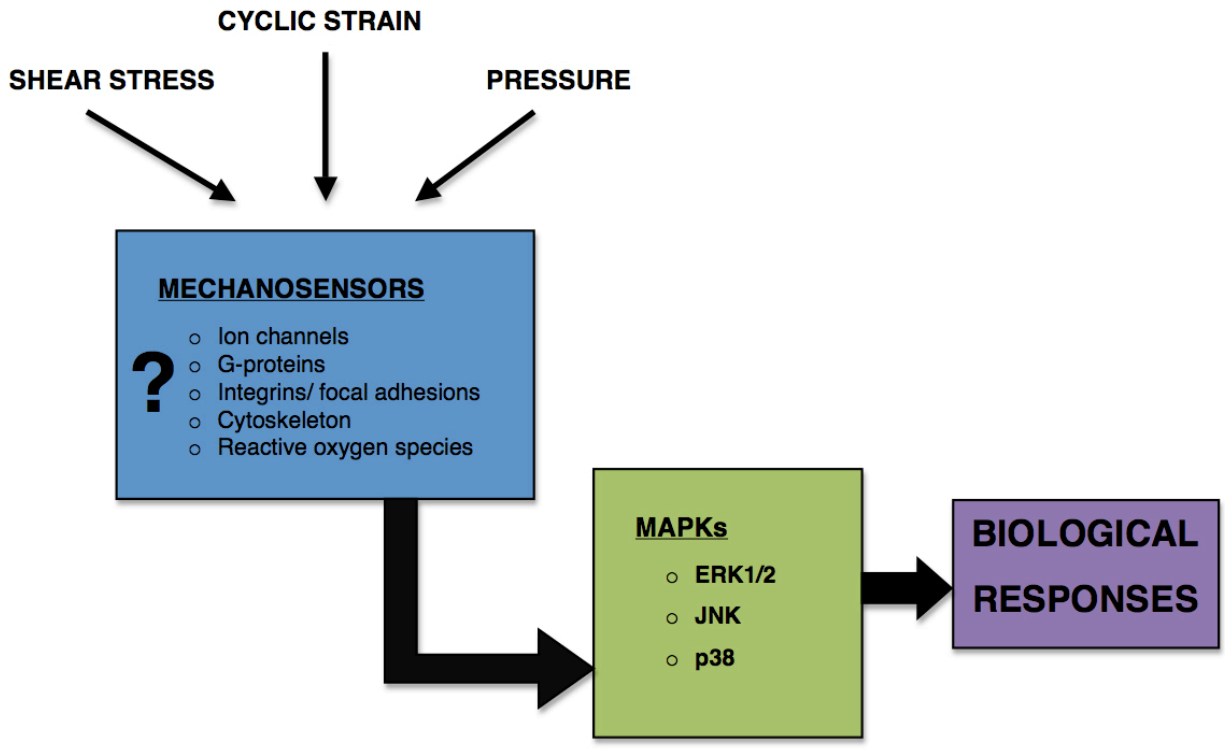

Figure 1.3. Several possible mechanisms for mechanotransduction have been proposed.

Upon activation, stretch-activated (SA) cation channels allow a non-selective influx of K^+, Na^+, and Ca^{2+} ions into the cell followed by membrane depolarization. This response is blocked by the removal of extracellular Ca^{2+} or addition of the stretch-activated channel inhibitor gadolinium, but not by the addition of Ca^{2+} channel blockers. SA cation channels have been identified in ECs and SMCs of various species and vascular origins and are involved in cell differentiation, proliferation, morphological changes, and superoxide production in response to cyclic strain. SA cation channels have also been known to signal through a number of second messenger pathways, including ERK1/2. Specific mechanosensitive K+ ion channels have also been reported in ECs and SMCs [44, 48].

Heterotrimeric G-proteins on the apical surface of endothelial cells have been proposed as mechanosensors of stretch and shear stress, in isolated membranes and whole cell models, suggesting an initiating role for changes in membrane fluidity in response to mechanical perturbation. Cyclic strain-induced p38 phosphorylation can be blocked by addition of G protein agonists and the level of activation has been show to be sensitive to both the magnitude and rate of strain [44, 48].

Mitogen-activated protein kinases (MAPKs), including ERK1/2, JNK, and p38, have been implicated in the process of mechanotransduction, but it is unclear whether they function in direct mechanosensing, second messenger signaling, or both. Although the intermediate steps are not well understood, mechanotransduction due to SA cation channels, and actin filaments have been shown to activate ERK1/2. Cyclic strain induces JNK activation in an integrin-independent manner, but it is unclear whether reactive oxygen species may be the cause of JNK activation. Activation of p38 by cyclic stretch, which is time- and stretch-dependent, appears to

occur as a second messenger pathway mediated by reactive oxygen species or other signaling pathways like PKC-ras/rac1 [44].

Mechanical stretch is known to reinforce integrin adhesions and produce integrin-dependent signaling, observed in both ECs and SMCs [48]. In most cases, the cytoplasmic domain of integrins is functionally linked to cytoskeletal proteins and kinases like focal adhesion kinase, placing them in an optimum location for initiation of mechanotransduction [45, 47]. It is speculated that the α subunit acts as the mechanosensor and that subsequent signal transduction occurs through the cytoplasmic domain of the β_1 integrin. Additionally, $\beta 1$ integrin protein expression and activity are observed in rat aortic SMCs in response to mechanical stress, further supporting this argument [44]. The specific signaling response appears to vary between species and vascular beds, reflecting a specificity for extracellular matrix composition and integrin combination [44, 45, 48].

Owing to the complex and interconnected structural elements of the cell cytoskeleton, it has been proposed that the stresses applied locally are distributed globally through movement of the cytoskeletal structure throughout the cell. Thus, through the cytoskeletal structure of microfilaments, intermediate filaments, internal microtubule struts, and extracellular matrix adhesions, surface forces could be transmitted along the cytoskeleton deep into the cell, potentially causing spatial associations of otherwise separated enzymes and substrates to promote signaling events. This process is generally known as the tensegrity concept [44, 47].

Another possible route for sensing of mechanical forces, particularly shear stress, is the glycocalyx. The glycocalyx covers the luminal surface of the blood vessel and provides a barrier to shear stress such that the shear stress acting on the actual apical plasma membrane of the endothelial cells is essentially zero. In theory, mechanical forces would be transmitted along the

glycosaminoglycan chains of the glycocalyx to transmembrane anchors, and enzymatic digestion of the glycocalyx has been shown to negate certain shear-induced outcomes like NO production, but the specificity of such models is unclear [46, 48, 49].

Reactive oxygen species (ROS), which are capable of signaling through a variety of signaling pathways in the endothelium have also been proposed as an initial signaling event for mechanotransduction, most notably because ROS can activate FAK, which has been implicated in mechanotransduction due to its location at focal contacts and ability to signal through a number of downstream signaling pathways. ROS appear to be involved in endothelial cell expression of MCP-1 on endothelial cells exposed to mechanical strain, but the source of ROS and whether it is the initial signal remains unclear [47].

The true mechanism of mechanosensing is hotly debated, but it seems likely that endothelial cells employ a variety of such mechanisms with potential for overlap of second messenger signaling pathways.

1.2.2 Cyclic strain and the vasculature

In particular, cyclic strain is of interest to this study because of its clinical relevance to hypertension, vein grafting, balloon angioplasty over-stretch injury and possibly intra-aortic balloon pumping, tissue engineering, and atherosclerotic lesions. Cyclic strain influences a variety of vascular cell functions including proliferation, migration, apoptosis, morphology, and production and secretion of a variety of soluble molecules inherent to EC function [44]. Cyclic strain appears to affect EC proliferation biphasically, with lower levels of strain causing reduced proliferation and higher levels of strain causing enhanced proliferation. EC migration, on the

other hand, appears to vary directly with cyclic strain magnitude, such that increased strain causes an increase in the rate of migration [44]. One of the hallmarks of cyclic uniaxial strain in vascular cells is the phenomenon of cellular alignment perpendicular the direction of strain [44, 50]. This perpendicular alignment is believed to cause a reduction of net intracellular stress during long-term exposure to cyclic uniaxial strain and is absent in response to cyclic biaxial stress [50]. With increasing magnitude of uniaxial stretch, actin stress fibers align more closely perpendicular to strain, with significant alignment at and above ~5% strain [44, 50]. Microfilament rearrangement is almost complete by 15 minutes after the onset of strain and cellular alignment is complete within 12 to 48 hours [44].

Spontaneous atherosclerotic lesions tend to develop in regions of elevated cyclic strain, including sites of vein to artery grafting [42, 51]. Not surprisingly, vein grafts used in coronary artery bypass grafting are more prone to atherosclerosis than arterial grafts in the same application [40]. Interestingly, in both ECs and SMCs, physiological levels of cyclic strain (~6-10%) do not increase apoptosis, whereas in both cell types, superphysiological levels (15-20%) promote apoptosis [44, 52, 53]. Moreover, physiological cyclic strain in ECs inhibits TNF-α and serum starvation induced apoptosis in both human and bovine aortic ECs [52]. Furthermore, cyclic strain has been shown to increase ROS production in aortic and venous ECs and in SMCs [51, 54, 55]. It is theorized that high biomechanical stress results in elevated oxidative damage and cell death, contributing to inflammation and SMC hyperplasia ultimately resulting in atherogenesis [38, 42, 44, 51, 55].

1.2.3 Shear stress and the vasculature

Although not the focus of this study, it is worth noting that of the forces acting on blood vessels, shear stress has been studied the most in the context of vascular endothelial cells, as this is the only cell type of the vascular wall exposed to shear stress associated with blood flow [56-59]. Very notably, laminar shear stress is associated with a protective induction of eNOS expression and NO release, whereas in areas of disturbed shear such as at bifurcations, low eNOS expression occurs in a manner that makes the vessel more prone to atherosclerosis [56, 60].

1.3 CERAMIDE AND SPHINGOLIPIDS

1.3.1 Ceramide

Ceramide is a sphingolipid with diverse activity relevant to atherosclerosis and vascular biology. As such, ceramide is produced in response to a multitude of cellular stressors including cytokines (TNF-α, IL-1β, etc.), hypoxia/reperfusion, lipopolysaccharide, and oxidized LDL, growth factors, and other stimuli present in the vascular environment [2, 61]. Depending upon the site and source of synthesis, ceramide can participate directly in signaling or can assist in signaling through its involvement in lipid rafting [2, 62]. Lipid rafts are regions of the plasma membrane that are enriched in sphingomyelin and cholesterol. Upon hydrolysis of sphingomyelin to ceramide, these lipid rafts self-associate to form larger ceramide-enriched membrane domains, thereby assisting in the aggregation and clustering of receptor molecules and contributing to the reorganization of intracellular signaling molecules to allow signal propagation within the cell

[62]. Depending on the source and type of ceramide involved, ceramide signaling may lead to cell proliferation, differentiation, growth, or apoptosis [61].

This diversity of outcomes is evident within the vascular setting. In bovine aortic ECs, TNF-α, UV, heat shock, H_2O_2, and γ-irradiation all signal through ceramide, resulting in apoptosis. Conversely, in vascular SMCs, oxidized LDL signals through ceramide to cause SMC proliferation, LDL aggregation, and foam cell formation. IL-1, on the other hand, promotes differentiation of human dendritic cells and E-selectin upregulation in human umbilical vein ECs (HUVECs) by way of ceramide signaling [63].

1.3.2 Ceramide biosynthesis and signaling

Ceramide is central to sphingolipid biosynthesis and may be generated *de novo*, or may be produced during the hydrolysis of sphingomyelin and other complex sphingolipids [63, 64], as shown in Figure 1.4. Ceramide can act directly, or can be further metabolized into sphingomyelin (SM), ceramide-1-phosphate, glucosylceramide and higher gangliosides or glyclolipids, or to sphingosine, which can be further processed into sphingosine-1-phosphate (S-1-P) [63-66]. Stressors such as γ-irradiation or TNF-α stimulate several of these pathways simultaneously [63, 65]. Thus, it is believed that the fate of a cell is determined by the net effect of the activity of all of these pathways in response to stresses [65]. Known targets of ceramide include ceramide-activated protein kinase (CAPK), protein kinase Cζ (PKCζ), and ceramide-activated protein phosphatase (CAPP) [63, 65, 67]. Additionally, ceramide interacts with MAPK, JNK, caspase, and mitochondrial signaling pathways [63, 67]. The numerous downstream targets of ceramide have been reviewed excellently by others [68, 69].

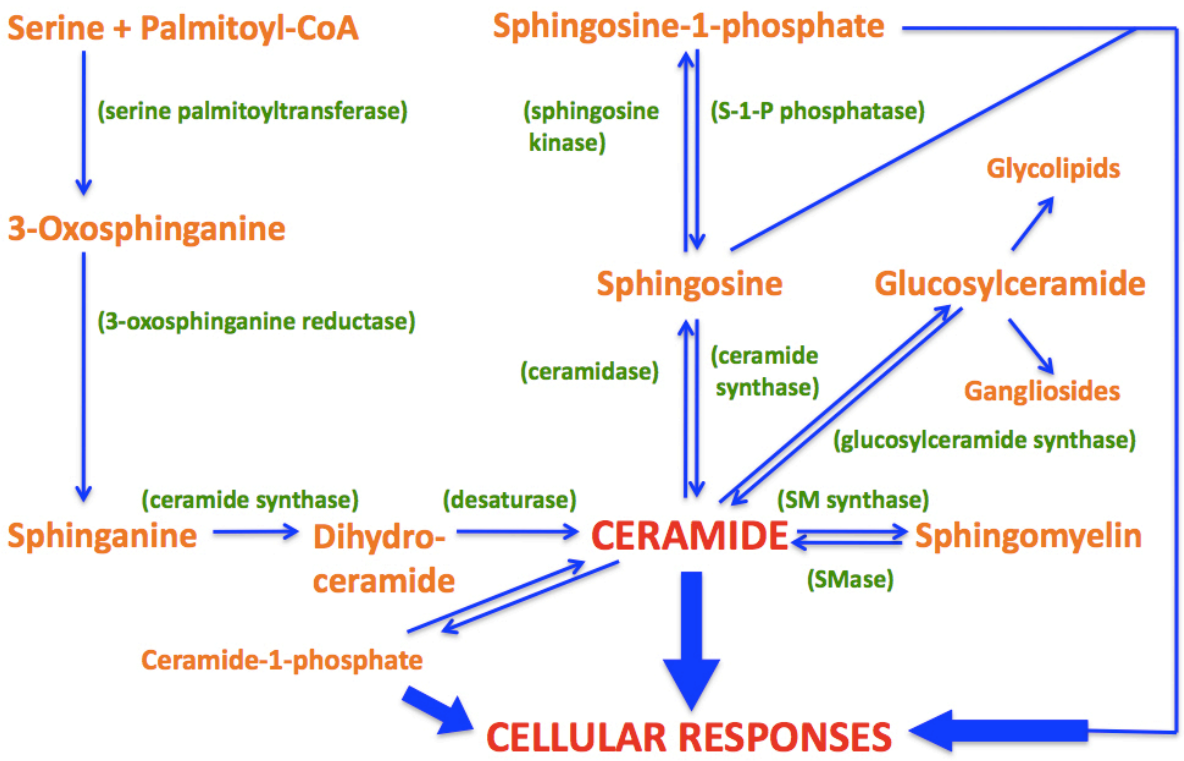

Figure 1.4. Ceramide is central to sphingolipid biosynthesis.

As a sphingolipid, ceramide is structurally characterized by a sphingosine base with a fatty acid attached to the carbon-2 position by an amide bond [64] (Figure 1.5). The predominant physiological forms of ceramide contain fatty acids of C_{16} to C_{26} chain length [62, 70]. C_{16} and C_{24} ceramides specifically have been implicated in apoptosis [70]. A hydrophilic head group can be attached to the OH-group in the carbon-1 position to yield more complex sphingolipids. For example, addition of a sugar yields glycosphingolipids, including glucosylceramide or lactosylceramide, or addition of phosphorylcholine yields sphingomyelin (SM) [64].

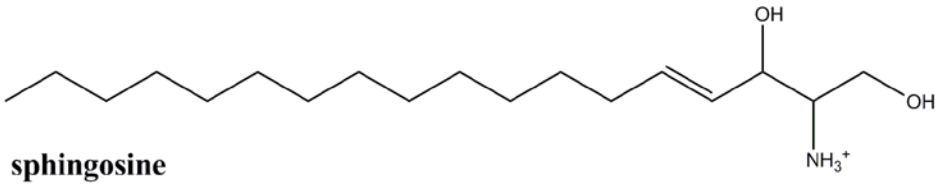

sphingosine

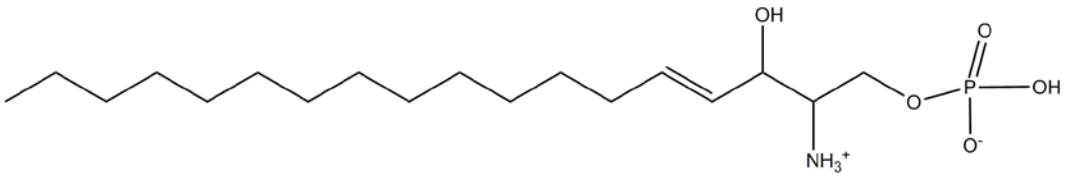

sphingosine-1-phosphate (S-1-P)

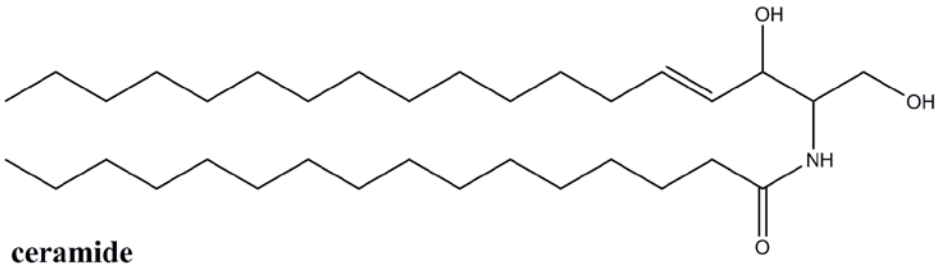

ceramide

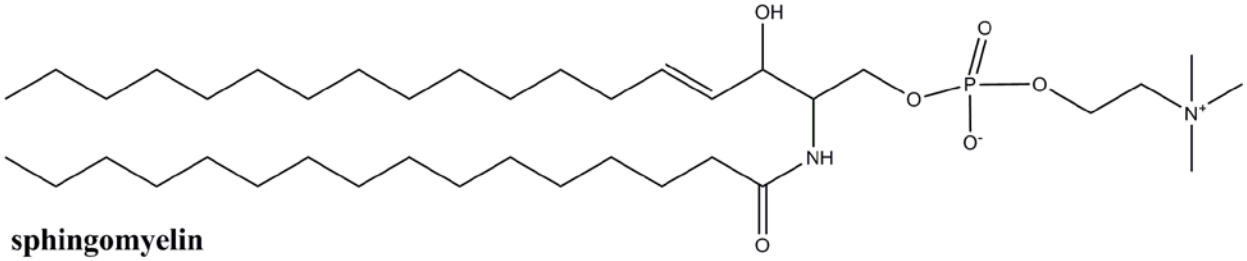

sphingomyelin

Figure 1.5. Sphingolipids l ike c eramide, s phingosine-1-phosphate, an d s phingomyelin ar e ch aracterized by a sphingosine base.

SM is the predominant sphingolipid in biological membranes and is hydrolyzed into ceramide by sphingomyelinase (SMase). Several forms of secreted or membrane-bound SMases have been identified and they are characterized by their pH optima – acidic (aSMase), neutral (nSMase), or basic [62, 65]. nSMase is found primarily in the plasma membrane whereas aSMase is located in the lysosomes and endosomes, where it is hypothesized that it may be rapidly mobilized to the extracellular membrane upon stimulation [65, 66, 71]. Basic SMase has been identified in the intestinal mucosa and bile, where it may be involved in digestion [63].

Stress stimuli may trigger ceramide accumulation from either *de novo* synthesis, SM hydrolysis, or both, and both pathways have been implicated in the same cellular outcomes. SM hydrolysis into ceramide has been observed in response to numerous stimuli including TNF-α, Fas ligand, vitamin D_3, IFN-γ, various chemotherapeutic agents, ionizing irradiation, heat stress, ischemia/reperfusion, nitric oxide, and IL-1 [63, 65, 72]. Potentially interesting in the vascular setting is the observation that ceramide signaling due to aSMase-mediated hydrolysis of SM is necessary for eNOS activation by some cytokines and growth factors in various cell types and a coregulatory role for ceramide and NO has been suggested [73, 74]. *De novo* synthesis of ceramide has been observed in response to TNF-α, ionizing irradiation, and chemotherapeutic agents [63, 65, 70, 75]. Sphingomyelin hydrolysis occurs rapidly and transiently within minutes as an early ceramide response, although prolonged SMase activity has been observed, whereas *de novo* synthesis usually occurs over a period of several hours as a late response [63, 65, 70].

1.3.3 Ceramide metabolites

Both ceramide and its many metabolites are biologically active [2, 61, 64]. Of particular note in the vascular setting is the metabolite sphingosine-1-phosphate (S-1-P) (Figure 1.5). Ceramide may be degraded to sphingosine by ceramidase and sphingosine can then be converted to S-1-P by sphingosine kinase (Figure 1.4). S-1-P can either be converted back to sphingosine or can be further degraded by S-1-P lyase to ethanolamine phosphate and hexadecanal for removal from the sphingolipid biosynthetic pathway [64, 76]. Platelets store and release S-1-P upon activation [76, 77]. Normal plasma and serum contain S-1-P at concentrations of 200-500nM [77]. S-1-P acts as an autocrine activator of platelets and helps to synergistically amplify aggregation induced by weak platelet agonists [76]. As such, S-1-P may play a strong role in accelerating hemostasis and thrombosis [76, 77]. In HUVECs, S-1-P binds to certain endothelial differentiation gene (EDG) receptors to enhance morphogenic differentiation, formation of adherens junctions and cortical actin, and chemotactic migration in angiogenic models [78]. In human aortic SMCs, S-1-P inhibits actin filament assembly and formation of focal adhesions, thus inhibiting SMC spreading and migration. [79].

Since S-1-P tends to enhance growth, whereas ceramide tends to promote cell death and cell cycle arrest, it has been hypothesized that the relative amounts of ceramide and S-1-P in a cell balance each other and serve as a sphingolipid rheostat [80]. Addition of S-1-P is capable of preventing exogenous ceramide-induced apoptosis in HUVECs [78]. This further underscores the importance of understanding the balance of ceramide and its metabolites within the cellular setting.

1.3.4 Ceramide and its metabolite in atherosclerosis

Ceramide has been directly implicated in atherosclerotic lesions. Sections of atherosclerotic aorta contain substantially higher levels of ceramide by wet tissue weight than similar segments of healthy tissue [2]. Lactosylceramide is prevalent in atherosclerotic lesions at all stages of formation [81] and macrophages present in atherosclerotic lesions have been found to produce a soluble sphingomyelinase capable of degrading sphingomyelin associated with oxidized LDL into ceramide [2, 81]. Endothelial cells at the site of lesions have also been found to secrete a soluble form of acidic sphingomyelinase [71]. Furthermore, *in vitro*, exogenous ceramide and exogenous neutral sphingomyelinase have been shown to cause Weibel-Palade body exocytosis from human aortic ECs, which may trigger inflammation and thrombosis [26]. Thus, ceramide may play a significant role in the propagation of cellular and molecular events critical to the formation of atherosclerotic lesions.

1.4 SUMMARY AND LIMITATIONS OF PREVIOUS RESEARCH

The vascular endothelium is continuously subjected to a variety of mechanical forces including cyclic strain, shear stress, and pressure from pulsatile blood flow, as well as chemical stresses. Together, these factors influence the endothelium's ability to maintain appropriate vascular permeability, vascular tone, and hemostasis, and to regulate inflammation and remodeling in health and disease. During mechanical injury or disease, blood vessels may encounter abnormal levels of mechanical forces, which can affect the function of endothelial cells and may contribute to formation of atherosclerotic lesions [43-45].

The mechanism by which endothelial cells respond to mechanical forces, or mechanotransduction, is not completely understood and is the subject of ongoing debate. Several possible mechanisms including G-protein-linked receptors, mitogen-activated protein kinases (MAPKs), integrins and focal adhesions, the cytoskeleton, ion channels, and reactive oxygen species (ROS) have been proposed as components of the mechanosensing process and likely, several of these processes are activated concurrently [44, 45, 47]. However, the role of the lipid microenvironment and lipid signaling, and more particularly ceramide signaling, in mechanotransduction, remains largely unknown.

While, ceramide has been studied in response to numerous molecular stressors [2, 61], almost no work has been done to explore the role that ceramide might play during mechanotransduction in response to mechanical stresses on cells, in particular in the vascular endothelium. Exogenous ceramide generation has been shown to cause increased cell proliferation as well as apoptosis in the walls of an experimental *in vivo* vein graft model [38]. In an elevated pressure/flow model in isolated rat lung, transient activation of neutral SMase in the cell membrane has also been observed to generate ceramide, suggesting that it is a possible step in mechanosensing [82, 83]. Another study has shown that exogenously added ceramide or hydrolysis of SM to ceramide by exogenously added SMases is capable of causing vasorelaxation in SMCs of phenylephrine-contracted rat aortic rings *in vitro* [84]. However, the role of ceramide and its metabolites remains unexplored in the model of cyclic strain.

In our studies, we examined the virtually unexplored and critical role of the lipid microenvironment, particularly with regards to ceramide signaling, in endothelial cells in response to cyclic strain within and beyond the physiological range, so as to gain a better understanding of the events which may ultimately contribute to endothelial dysfunction and

eventual atherosclerosis. This research specifically focused on the ceramide biosynthetic pathway because we hypothesize that these lipid pathways play a critical role in endothelial cell mechanotransduction at several levels, as shown in Figure 1.6:

1. Ceramide plays a critical role in plasma membrane dynamics. The involvement of G-proteins, MAPKs, and other plasma membrane proteins in mechanotransduction pathways within endothelial cells has been demonstrated. However, the influence and function of the ceramide and sphingolipid component of the plasma membrane must be considered because these lipids serve as membrane anchors for many of these proteins and function in the formation of lipid rafts to aid in the coalescence of membrane proteins and receptors into caveolae, which is necessary for efficient signaling [62].

2. Ceramide is required for activation of some protein kinases. While various protein kinases appear to be associated with the mechanotransduction response, it should be noted that some kinases require ceramide for activation, directly or indirectly [63, 65, 67], suggesting a further potential role of ceramide and sphingolipids.

3. Ceramide can form channels in membranes. Protein-based ion channels have been proposed as endothelial cell mechanosensors. Again, ceramide and the sphingolipid component must be considered because of its necessity in proper ion channel formation, as well as for ceramide's ability to self-form channels in lipid membranes without protein involvement [62, 85].

4. Ceramide can generate ROS and ROS can generate ceramide. Ceramide has been shown to promote ROS generation and the correlation between ROS formation and ceramide signaling has been observed in numerous models [62, 67, 86]. Furthermore, ROS

production promotes ceramide generation. Together, this perpetuating relationship would provide an efficient mechanism of signal amplification in ECs during mechanotransduction.

5. The ceramide-sphingomyelinase pathway has been suggested as a mechanosensor. Rapid generation of ceramide due to neutral SMase activity in caveolae in a pressure/flow model has been observed, suggesting its potential role in mechanosensing [82, 83]. The ceramide-sphingomyelinase pathway has also been implicated in vasodilation, strengthening its potential role in mechanosensing [84].

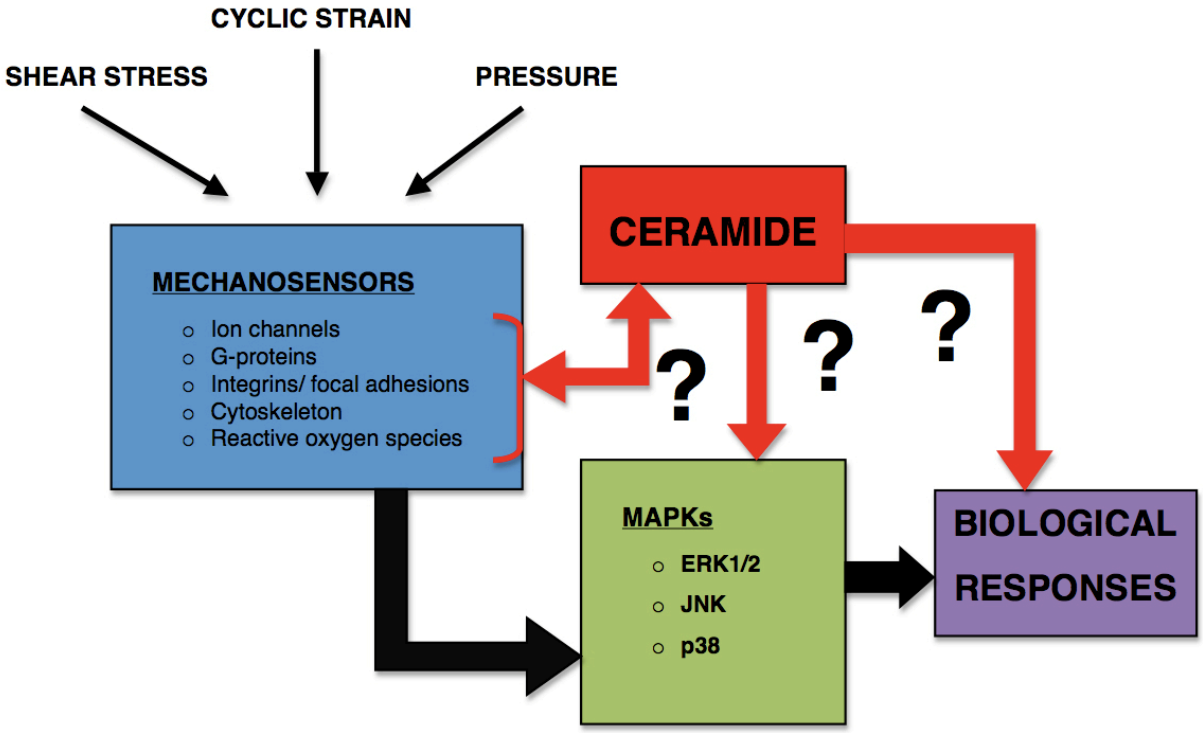

Figure 1.6. Ceramide signaling may play a critical role in endothelial cell mechanotransduction at several levels.

Thus, a detailed study of the role of the lipid microenvironment, and more particularly the role of ceramide and its metabolites, during cyclic strain will provide new opportunities for manipulation and monitoring of endothelial health and function. Such manipulation strategies could have direct translational applications in protective therapies for compromised or pathophysiological states such as atherosclerosis, hypertension, following vein grafting, or to enhance vascular tissue engineering efforts.

1.5 HYPOTHESIS AND SPECIFIC AIMS

The presented experiments were designed to test the following hypothesis:

Mechanical, uniaxial cyclic strain results in an increase in intracellular ceramide in vascular endothelial cells, which participates in signaling necessary to propagate mechanotransduction responses to cyclic strain, potentially contributing to early events in the development of endothelial dysfunction and the formation of atherosclerotic lesions.

The specific aims that we established to test this hypothesis are as follows:

Specific Aim 1: **Determine the profile of phospholipids and sphingolipids present in aortic endothelial cells.**

a. Identify the major species of phosphatidyl choline (PC), phosphatidyl ethanolamine (PE), phosphatidyl inositol (PI), phosphatidyl serine (PS), and phosphatidyl glycerol (PG) present in human and bovine aortic endothelial cells.
b. Identify the major species of ceramide and sphingomyelin (SM) present in human and bovine aortic endothelial cells.

c. Determine whether aortic endothelial cells in static culture respond similarly to exogenous C_8 and C_{16} ceramides, representing species of nonphysiological and physiological fatty acid chain lengths respectively.

Specific Aim 2: **Determine whether aortic endothelial cell ceramide levels are altered in response to uniaxial, cyclic mechanical strain.**

a. Identify the molecular forms of ceramide generated in response to cyclic strain.
b. Determine whether ceramide signaling in response to cyclic strain involves an early response within minutes, suggesting membrane sphingomyelin as the source of ceramide generation; a late response after several hours, suggesting *de novo* ceramide generation; or both.
c. Determine if the duration, frequency, and intensity of cyclic strain affects the magnitude and molecular forms of ceramide generated.

Specific Aim 3: **Determine which ceramide biosynthetic pathways are activated upon exposure of aortic endothelial cells to cyclic, uniaxial strain and determine the abundance of ceramide metabolites.**

a. Determine if levels of sphingomyelin, sphingosine, and sphingosine-1-phosphate are altered in response to cyclic strain.
b. Determine the effects of inhibitors of *de novo* ceramide synthesis and hydrolysis of sphingomyelin to ceramide, on cyclic strain-induced ceramide levels.

To summarize the experimental design, we began by defining the lipid environment of aortic endothelial cells to establish the foundation for a more in-depth study of ceramide signaling. We then set out to thoroughly evaluate how ceramide and its metabolites change in response to a

panel of physiological and pathological strain conditions with regards to magnitude and frequency over time. Then, to further define the place of ceramide signaling within the mechanotransduction response to cyclic strain, we evaluated which biosynthetic pathways appeared to be activated in response to strain and the accumulation of select matabolites with known biological activity in the vascular microenvironment. The findings of these studies will help to elucidate the early events in the mechanotransduction response to cyclic strain and to bridge our understanding between the relationship between mechanotransduction and inflammation as it relates to endothelial cell activation and dysfunction and vascular disease.

2.0 DETERMINATION OF THE LIPID PANEL FOR AORTIC ENDOTHELIAL CELLS

2.1 INTRODUCTION

Before examining the modulation of a single lipid species – ceramide -- and its metabolites, it is helpful to first define the entire panel of phospholipids and sphingolipids present in aortic endothelial cells and to identify variations between the lipid profiles of bovine aortic endothelial cells (bAECs) and human aortic endothelial cells (hAECs). Many biologically active lipid species such as sphingosine-1-phosphate, diacylglycerols, platelet-activating factor, lysophosphatidic acid, and eicosanoids can be derived from the degradation or modification of other phospholipids and sphingolipids [87, 88]. Loss of appropriate lipid biosynthesis has extensive implications in disease [87]. Thus, one must look at the entire lipid panel of the cell to properly understand the signaling potential of the cell.

Lipids play important roles not only in the structures and metabolic functions of cells and organelles, but also in signal transduction directly, as second messengers, or indirectly through lipid rafting [87, 89, 90]. In addition to the functional specificity of the polar head-group of a lipid, the fatty acid side-chain composition, chain-length, and bond characteristics can affect membrane fluidity and rigidity – characteristics necessary for maintaining proper membrane structure/function and signaling [91, 92]. Sphingolipids, as a part of lipid rafts, are critical for

facilitating and amplifying receptor signaling within cells [62]. To date, there have been no thorough evaluations of the specific lipid composition of aortic endothelial cells, particularly by mass spectrometry.

Electrospray ionization tandem mass spectrometry (ESI-MS/MS) has been used by a number of groups including our own to identify the specific composition of lipids from whole-cell lipid extractions, alone or following HPLC or thin-layer chromatography purification [89, 93-96].

This chapter will specifically address the first specific aim:

Determine the profile of phospholipids and sphingolipids present in aortic endothelial cells.

1. Identify the major species of phosphatidyl choline (PC), phosphatidyl ethanolamine (PE), phosphatidyl inositol (PI), phosphatidyl serine (PS), and phosphatidyl glycerol (PG) present in human and bovine aortic endothelial cells.
2. Identify the major species of ceramide and sphingomyelin (SM) present in human and bovine aortic endothelial cells.
3. Determine whether aortic endothelial cells in static culture respond similarly to exogenous C_8 and C_{16} ceramides, representing species of nonphysiological and physiological fatty acid chain lengths respectively.

2.2 METHODS

2.2.1 Cell culture

Cryopreserved stocks of primary culture hAECs and bAECs were obtained from Lonza Walkersville (Walkersville, MD). Purchased hAECs were obtained from single donors and frozen in the third passage following isolation. Purchased bAECs were obtained pooled from three to five donors and frozen in the first passage following isolation. Pooled bovine endothelial cells were chosen to reduce donor variation in endothelial cell phenotype. Cells were expanded in endothelial cell growth medium (EGM, Lonza Walkersville), obtained as a BulletKit containing proprietarily protected concentrations of bovine brain extract with heparin, hydrocortisone, GA-100, human endothelial growth factor (hEGF), and a final concentration of 2% serum. Upon reconstitution, hAECs and bAECs were expanded and frozen as stocks, as described below, so that a fresh vial of cells could be used for each experiment and each experiment within a set of experiments would be done using cells in the same passage from the same cell lot. By doing so, all experiments could be done at the same passage following isolation, within the number of guaranteed passages for endothelial cell phenotype and variation from donor to donor could be eliminated within the same set of experiments.

2.2.1.1 Thawing of frozen aortic endothelial cells

Prior to thawing frozen AECs, 5mL complete EGM was added to each of four T-25 vented polystyrene tissue culture flasks (BD Biosciences, San Jose, CA) and warmed for 30 minutes in a tissue culture incubator at 37^{o}C, 5% humidity to condition the flasks. Immediately upon removal from liquid nitrogen storage, the cryopreserved AECs (Lonza Walkersville) were

thawed quickly in a 37°C water bath before sterile transfer to the pooled, warmed medium from the preconditioned flasks. The diluted cells were gently aspirated for mixing and then equally distributed across the T-25 flasks at a distribution of approximately 4000 cells/cm^2). The flasks were quickly returned to the 37°C incubator where they were allowed to adhere overnight. On the following day, the initial thawing medium was removed by aspiration and replaced with fresh EGM medium warmed to 37°C. Media was replaced every two days thereafter until passage. All cell culture manipulations were performed using aseptic technique.

2.2.1.2 Aortic endothelial cell passage and stocking

When cells reached approximately 80% confluence, they were passed into new flasks at a distribution of 5000 cells/cm^2 to prevent growth inhibition due to cell-cell contact. As described previously (Section 2.2.1.1), 1 mL/5 cm^2 EGM was added to the new flasks and conditioned at 37°C prior to use in passage.

For passage, media was gently aspirated. 5 mL phosphate buffered saline (PBS, Invitrogen, Carlsbad, CA) was then added per 25 cm^2 of culture area, rocked gently, and removed by aspiration to remove residual serum from the cell monolayer surface. 1 mL of 0.25% trypsin-EDTA (Invitrogen) per 25 cm^2 of culture area was immediately added to the flasks and cell detachment was monitored closely using an inverted light microscope (Olympus, Center Valley, PA). When cells were 80% rounded, the flasks were gently tapped to dislodge the cells. The trypsin was immediately diluted with room temperature EGM at a ratio of at least 1:4. Cells were counted on a hemacytometer (Fisher Scientific) and viability was determined by trypan blue exclusion (Sigma, St. Louis, MO). Cells were then centrifuged in a benchtop centrifuge at 1500 rpm for 5 minutes at 4 °C to pellet the cells. Cells were immediately resuspended in freezing medium consisting of 10% FBS (Invitrogen), 80% EGM, and 10%

DMSO (Fisher Scientific, Pittsburgh, PA) at a density of $1x10^6$ live cells/mL. Cells were quickly aliquotted into 2 mL round-bottom cryopreservation vials (Fisher Scientific), distributing $1x10^6$ cells per vial. Vials were insulated in a styrofoam rack and frozen immediately in a -80°C freezer. The next morning, cells were transferred to a liquid nitrogen freezer for long-term storage.

Approximately 50-70 vials of frozen AECs were obtained from each initial cryovial. Upon stocking of a new lot of AECs, the lipid profile of the new cells at 80% confluence in static culture was determined by electrospray mass spectrometry (ESI-MS) as described below (section 2.2.2 through 2.2.4) and compared to that of previous lots to ensure similarity of the baseline lipid profile across donors. For all experiments, cells were used in the first passage after thawing (fourth passage following receipt of initial primary culture and within seven passages following isolation).

2.2.2 Preparation of AECs for ESI-MS Lipid Profile Determination

Two vials ($2x10^6$ total live cells) were thawed (Section 2.2.1.1) and transferred into three T-75 vented polystyrene tissue culture flasks (BD Biosciences), each preconditioned with EGM at 37°C. Cells were cultured before passage (Section 2.2.1.2) into 6-well polystyrene tissue culture plates (BD Biosciences) at a density of approximately 5-8000 cells/cm^2 in 2 mL EGM per well. The medium was replaced with 2 mL EGM on the first day following passage and every two days thereafter.

When cells reached 80% confluence, they were non-sterilely harvested, combining two wells per sample. The media from both wells was transferred to a 15 mL conical centrifuge tube (BD Biosciences). Both wells were washed with 2 mL PBS and the wash was added to the conical

tube. To induce cell detachment, 600 µL 0.25% trypsin-EDTA was added to each well. The cells were dislodged by aspiration with the pooled media/wash and returned to the conical tube. The wells were then washed to remove any remaining cells with 2 mL PBS per well, adding the wash to the same tube. The harvested cells were centrifuged for five minutes at 1500 rpm, 4°C to pellet the cells. The supernatant was then decanted and the cells were resuspended by aspiration in 10 mL PBS. The cells were centrifuged again for 5 minutes at 1500 rpm, 4°C to pellet the cells and the supernatant was discarded. The cells were then resuspended in 1 mL of PBS, they were counted on a hemacytometer, and the viability was determined by trypan blue exclusion.

2.2.3 Lipid extraction

Two wells of a 6-well plate grown to 80% confluence generally yielded 5-10x10^5 cells, corresponding to an appropriate total lipid content for analysis by our ESI-MS techniques.

Lipid extractions were performed in 13x100 mm borosilicate glass tubes (VWR, West Chester, PA) that had been prepared by washing them first with HPLC grade methanol (Spectrum, Gardena, CA) followed by chloroform (EMD, Gibbstown, NJ). The tubes were allowed to air dry in a ventilated chemical fume hood.

After cell counts and viability were determined, the endothelial cells were transferred to a prepared glass tube, which was then placed inside a new 15 cc polypropylene conical and capped. The cells were then centrifuged for 5 minutes at 1500 rpm, 4°C to pellet the cells. The supernatant was decanted in a single pour to avoid dislodging the pelleted cells. Immediately, 500 µL of methanol containing butylated hydroxytoluene (BHT, Sigma) was added to the glass tube using a polypropylene pipette tip and the tube was briefly centrifuged. 1 mL of chloroform

was then added using a glass serological pipet prewashed with chloroform to reduce contamination of the extraction and the tube was again briefly vortexed. The final extraction concentration of methanol:chloroform was 1:2. The glass extraction tube was then replaced in the polypropylene tube, the tube was flushed with a stream of nitrogen gas, and the tube was capped and sealed with Parafilm. Extraction was allowed to occur in the dark, overnight, at 4°C.

To separate the aqueous and organic phases, 300 µL of 0.15 M NaCl (Sigma) was added to the glass extraction tube. The tube was vortexed for 5 seconds followed by centrifugation for 5 minutes at 1500rpm, 4°C. The organic layer, containing the lipids from the cell sample partitions at the bottom of the tube below the NaCl. The bottom 90% of the organic layer was carefully removed using a glass Pasteur pipette and transferred to a fresh glass extraction tube prepared as described earlier in this section and untouched without clean latex gloves to reduce contamination from oils on the fingers. The organic layer was then evaporated under a steady stream of nitrogen gas over a warm water bath, leaving the isolated lipids as a dry film on the bottom of the tube. The glass tube containing the dried lipid extract was then replaced in the 15 mL polypropylene conical, the conical was flushed with nitrogen gas, capped, and sealed with Parafilm. The lipid extracts were then stored in the dark at -20°C until ESI-MS analysis.

2.2.4 ESI-MS analysis of lipids

2.2.4.1 Principles of electrospray mass spectrometry

Electrospray mass spectrometry (ESI-MS) works by solubalizing the sample molecules in a compatible running solution which is passed through a high voltage capillary tube into a strong electrostatic field (positive or negative) at atmospheric pressure, resulting in a fine aerosol of highly charged droplets containing the sample. The running solvent evaporates leaving a stream

of sample ions that are then passed through a focusing lens and on into the first set of quadrupole analyzers under vacuum followed by the first detector (Figure 2.1).

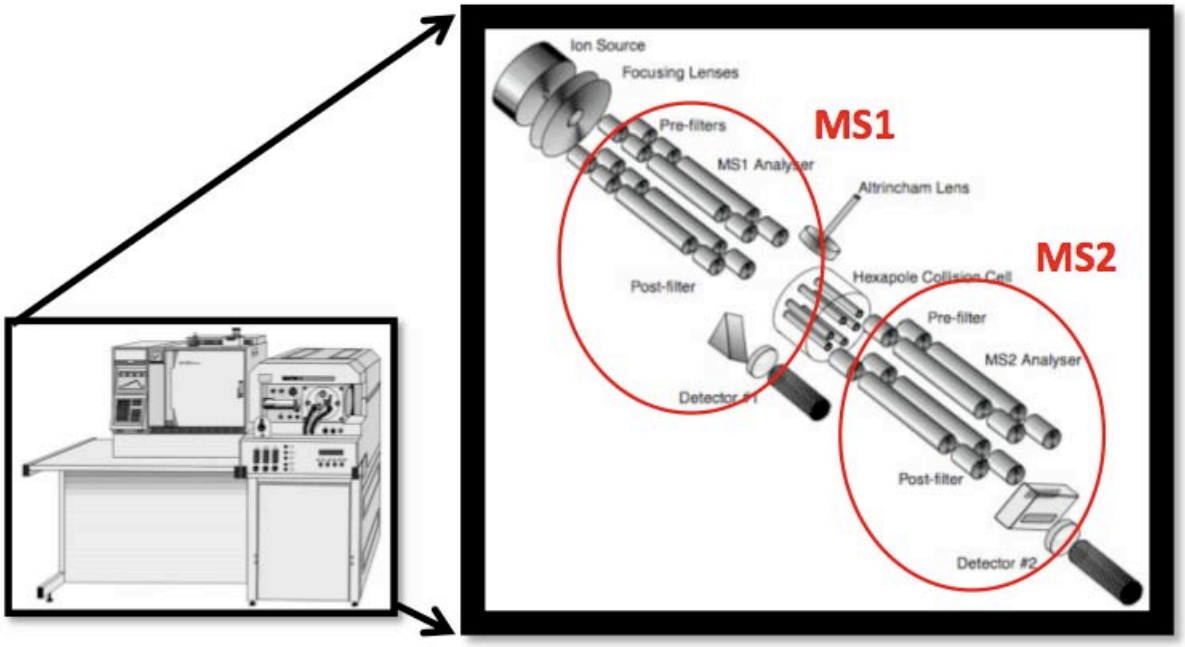

Figure 2.1. Electrospray mass spectrometry (ESI-MS) works by creating a stream of sample ions that are passed through a focusing lens (upper left of expanded view) and through a first set of quadrupole analyzers (MS1), yielding a spectrum of the relative intensity of each of the detected ions. For further structural characterization of the sample, the sample ions can then be passed through a hexapole collision cell (center of expanded view) where they are bombarded with argon gas to induce fragmentation. The fragmented ions are then passed through a second set of quadrupole analyzers (MS2). The resulting spectrum reveals the mass/charge of any resulting charged fragments. Comparison of the resulting fragments yields information that can be used to identify the structural composition of the parent ion. See the text for a detailed description of ESI-MS and ESI-MS/MS analysis. Figure adapted from [97].

This first detector produces the MS1 analysis, providing a spectrum of relative intensity of signal at each mass/charge (m/z) in total ion counts. A single ion may hold several charges. The m/z reflects the ratio of the ion's molecular mass to the number of its charges using the

formula (m+n)/n where m is the molecular mass and n is the number of charges on the molecule. As such, the total population of a molecule of 900 Da that can hold up to three charges may be distributed across the spectrum with peaks at 901 for the m+1 ion, 451 for the m+2 ion, and 301 for the m+3 ion.

For structural determination (MS/MS), the sample ions can then be passed through the hexapole collision cell where they are bombarded with argon gas to induce molecular fragmentation. The fragments are then passed through the second set of quadrupoles and the second analyzer where the MS2 analysis occurs. The resulting spectrum reveals peaks corresponding to the m/z of any charged fragments. Fragment masses of known structural components and mass differences corresponding to the masses of known structural components (i.e. amino acids for protein determination) can be used to identify the structural composition of the parent ion.

2.2.4.2 MS/MS analysis of lipids

Determination of lipid structure relies upon the abilities of phospholipids to hold a negative charge on the phosphate group, allowing for their detection in the negative ion mode by ESI-MS. Occasionally, a lipid does not hold its own negative charge, as is the case with sphingolipids like ceramide, but will form a negatively charged adduct by associating with free Cl^- ions (a chloride adduct) which can also be detected in the negative mode or Na^+ ions (a sodium adduct) which can be detected in the positive mode. The abundance of such adducts is strongly affected by the abundance of Cl^- or Na^+ ions in the sample preparation and the variable sensitivity of the instrument under different operating conditions.

Typically, a lipid molecule may fragment within the head group, between the head group and the phosphate group, between the phosphate group and the glycerol backbone, or between the glycerol backbone and the side-chains. Individual fragments may form adducts with Cl^- or Na^+, or may gain or lose a water molecule and the resulting fragmentation spectrum reflects a mixture of those fragments that hold a charge in the chosen ion mode. Not all fragments are detectable. Typically, in the negative ion mode, certain lipid head groups, the phosphate group with or without the glycerol backbone, and the fatty acid side chains will carry a charge.

There are a variety of MS/MS operating scans. The three types of MS-MS scans that were utilized in this study are the daughter ion scan, a parent ion scan, or a constant neutral loss scan (Figure 2.2). In a daughter ion scan, MS1 is used to scan for a single parent mass and only ions of that m/z are allowed to pass into the second quadrupole, MS2, which scans for the daughter ions that result after suffering fragmentation in the collision cell. In a parent ion scan, the MS2 scans for a single daughter ion while the first quadrupole is used to scan for all parent ions that will fragment to the product selected as the daughter ion. Only those parent ions producing the specified daughter ion are reported in the spectrum. In a neutral loss scan, both quadrupoles are scanning in synchrony, such that the any parent ion that loses a specified mass between the first quadrupole and the second quadrupole will be detected at the final detector and reported in the spectrum.

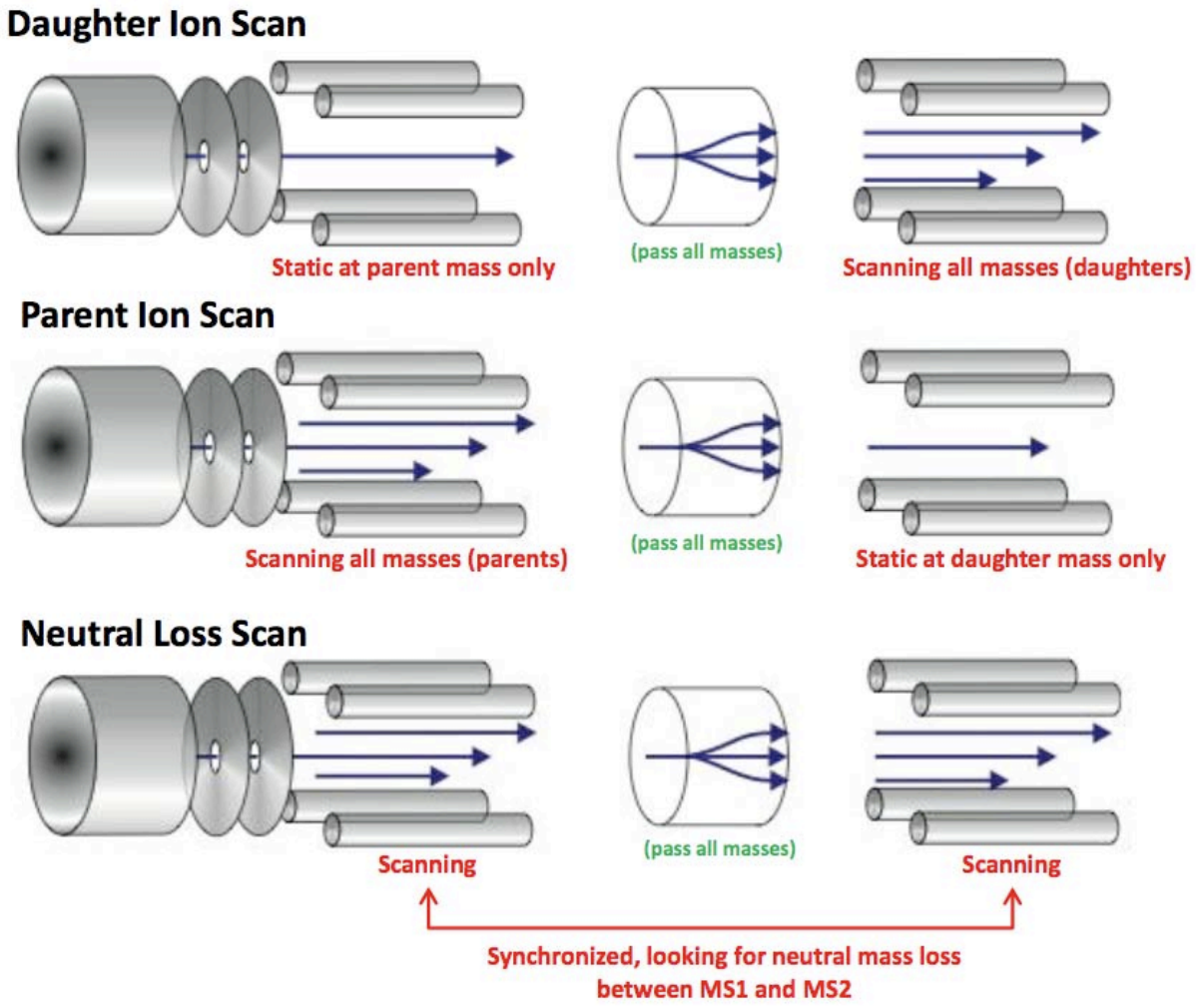

Figure 2.2. Three types of ESI-MS/MS operating scans were utilized in this study. In a daughter ion scan, MS1 is used to scan for a single parent mass and only ions of that m/z are allowed to pass into the second quadrupole, MS2, which scans for the daughter ions that result after suffering fragmentation in the collision cell. In a parent ion scan, the MS2 scans for a single daughter ion while the first quadrupole is used to scan for all parent ions that will fragment to the product selected as the daughter ion. Only those parent ions producing the specified daughter ion are reported in the spectrum. In a neutral loss scan, both quadrupoles are scanning in synchrony, such that the any parent ion that loses a specified mass between the first quadrupole and the second quadrupole will be detected at the final detector and reported in the spectrum. Figure adapted from [97].

2.2.4.3 MS/MS determination of bAEC and hAEC lipid profiles

All ESI-MS analysis was performed on a Fisons VG Quattro II triple quadrupole mass spectrometer (formerly Fisons Instruments/Micromass, Inc.; currently Waters Corp., Milford,

MA) with an electrospray source, using the MassLynx software system (Fisons). All lipid analysis was performed using a chloroform:methanol solvent system at a ratio of 1:2. Fragmentation was inducted by argon gas. In all discussion of lipid species, to denote the fatty acid composition, the notation of $C_{n:m}$ is used whereby "n" represents the carbon chain length of the fatty acid and "m" represents the number of double bonds in the fatty acid.

Techniques for identifying lipid species for a cell population using ESI MS/MS have been establish previously by our group and others [89, 93-96].

To establish the appropriate target species of ceramide and sphingomyelin, it was necessary to first determine the major species present. bAECs were used for these experiments because they are the cell type used for the majority of cyclic strain experiments in this study. Ceramide does not fragment into a definitive fragmentation pattern in our system, despite the ease and reliability of detection of chloride adducts of ceramide by our technique. Our group has previously verified the fragmentation of ceramide species using alternate mass spectrometry techniques [96].

Likewise, sphingomyelin, due to its structural properties, poses similar challenges for fragmentation. Sphingomyelin is detectable alone and as a sodium adduct in the positive mode, and to a much lesser extent as a chloride adduct in the negative mode, making standard fragmentation in the negative mode less practical. Sphingomyelin and PC have the same choline head group, which, due to the positive charge held by the nitrogen, means that both lipids are easily detectable in the positive mode and are the overwhelming majority of lipids detectable in the positive mode. Attempts to identify species of sphingomyelin by a neutral loss scan based on the properties of the choline head group would also reveal species of PC. Because of the sphingosine side chain, sphingomyelin typically runs at an odd m/z value while PC typically runs

as an even m/z value. Unfortunately, the fatty acid side chains do not charge in the positive mode and true verification of composition would need to be performed in the negative mode by doing a daughter ion scan of the corresponding chloride adduct. However, this could be complicated by the wide acquisition window necessary for fragmentation in that some species of sphingomyelin and PC differ by only a single Da, meaning that it is likely that both would fragment together, complicating the identification process. Our group has previously verified the structure of several sphingomyelin species that had previously been isolated by TLC separation to eliminate PC [95].

Because our group has verified the structures of physiological ceramide and sphingomyelin species previously, that work was not repeated. To examine the relative abundance of ceramide species in bAECs, a standard negative ion scan over the range of 400-950 m/z was performed for six separate lipid extractions from statically cultured control bAECs extracted at approximately 80% confluence as described in Sections 2.2.2 and 2.2.3. Natural species of ceramide contain a $C_{18:1}$ sphingosine base (Figure 2.3). Because this group is not variable, ceramide species will hereafter be described only by their fatty acid side-chain. For simplicity, when the number of double bonds is not specified, all bonding combinations analyzed for that species are being described (i.e. C_{16} refers to both the $C_{16:0}$ and $C_{16:1}$ forms). The total ion counts (TIC) of peaks corresponding to the m/z appropriate for chloride adducts of ceramides with unsaturated or singly saturated fatty acid chain lengths from C_2 through C_{28} were recorded and normalized in relationship to the (TIC) of a chloride adduct of PC at a m/z of 794 for each sample. This particular species of PC has $C_{16:0}$ and $C_{18:1}$ fatty acid side chains and is a structural lipid found in consistent prevalence in cells.

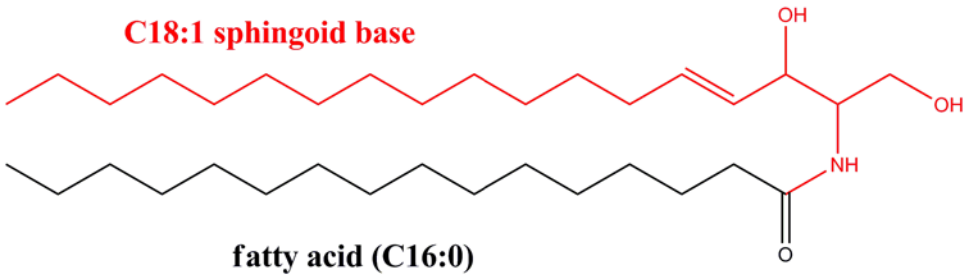

Figure 2.3. $C_{16:0}$ ceramide denotes a naturally occurring ceramide containing a $C_{18:1}$ sphingosine base and a $C_{16:0}$ fatty acid side-chain.

To examine the relative abundance of sphingomyelin species in bAECs, a standard positive scan of 400-950 m/z was performed for lipid extractions from the same six control bAEC lipid extractions. The positive scan for each sample was performed immediately following the negative ion scan and all pairs of scans were timed identically to assure consistent MS analysis. Natural species of sphingomyelin contain a $C_{18:1}$ sphingosine base (Figure 2.4). Because this group is not variable, sphingomyelin species will hereafter be described only by their fatty acid side-chain. The total ion counts (TIC) of peaks corresponding to the m/z appropriate for sodium adducts of sphingomyelins with unsaturated or singly saturated fatty acid chain lengths from C_2 through C_{28} were recorded and normalized in relationship to the (TIC) of a sodium adduct of PC at a m/z of 782 for each sample. PC at a m/z of 782 in the positive mode is the sodium adduct corresponding to the chloride adduct of PC at a m/z of 794 in the negative mode.

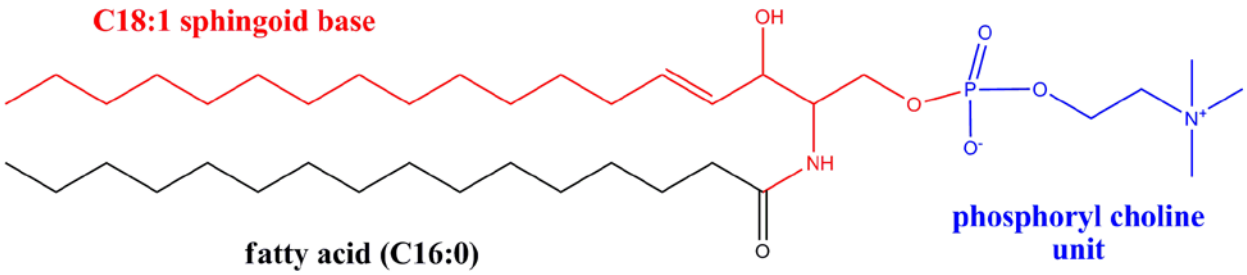

Figure 2.4. $C_{16:0}$ sphingomyelin denotes a naturally occurring sphingomyelin containing a $C_{18:1}$ sphingosine base and a $C_{16:0}$ fatty acid side-chain.

By normalizing TIC of the lipid species of interest against that of a single naturally occurring lipid of relatively constant abundance instead of to cell count, there is better control against variations in cell handling and isolation techniques prior to extraction as well as control against some amount of geometric morphological variation in cells with treatment or growth. Use of the same species of PC for normalization in both the positive and negative mode assures that variation of levels in ceramide and sphingomyelin are compared against the same standard. This normalization strategy is employed in all MS analysis discussed in this study.

The baseline of reliable detection for our MS analysis system is approximately 1×10^5 TIC, hereafter called the threshold. Below this threshold, it is difficult to distinguish between signal noise and detection and the signal is not strong enough to allow for fragmentation to determine structure. Statistical significance of the relative abundance of ceramide and sphingomyelin species was determined by performing a paired t-test using Prism Version 4 (GraphPad Software, San Diego, CA) relative to the threshold normalized against the corresponding PC $C_{16:0}$, $C_{18:1}$ Cl^- TIC for each sample.

Determination of PC, PE, PI, PS, and PG profiles was performed using lipid extractions of statically cultured control hAECs extracted at 80% confluence, prepared as described in

Section 2.2.2 and 2.2.3. Figure 2.5 shows the structural properties of the typical phospholipids we profiled in this study. hAECs were chosen for this set of experiments due to anticipated interest in such profiles for human cells by a larger audience.

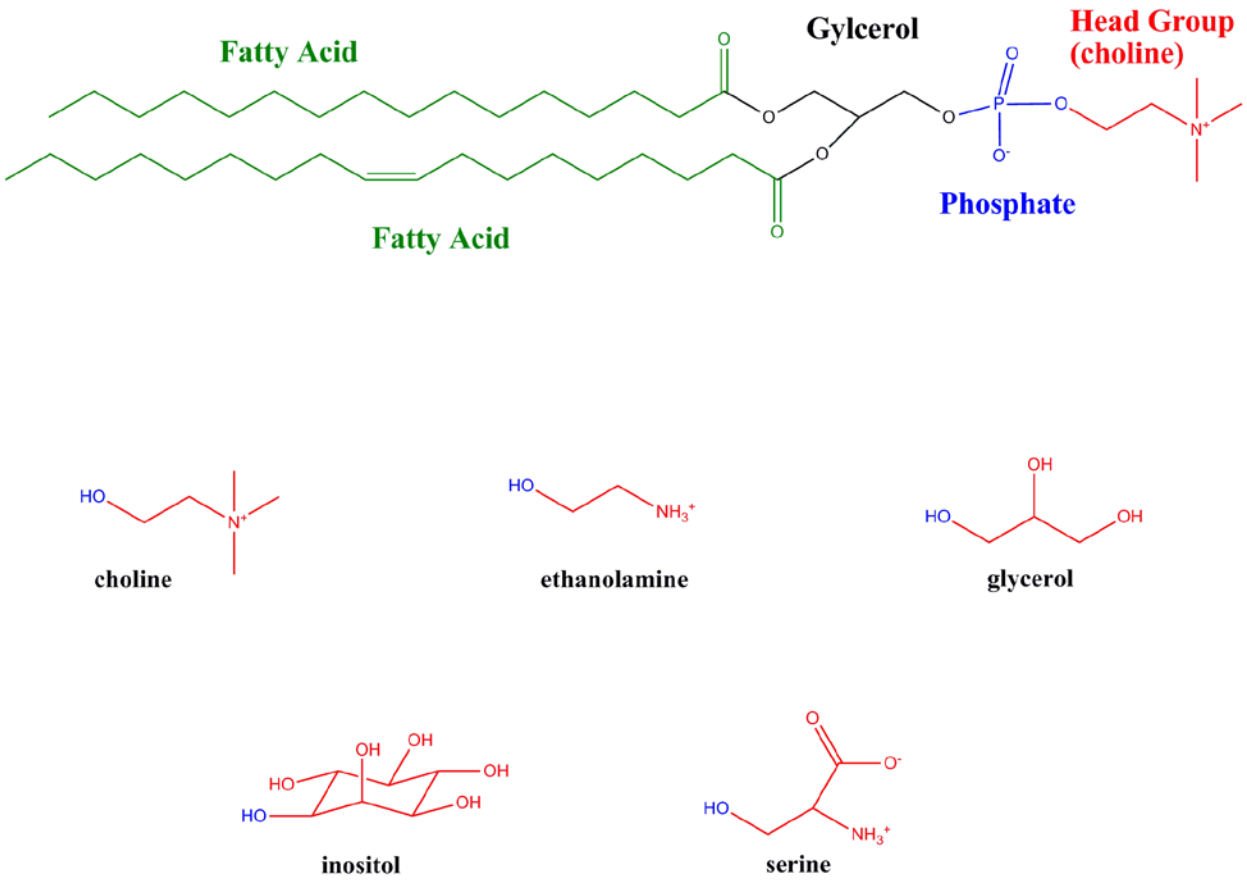

Figure 2.5. A typical phospholipid -- in this example $C_{16:0}/C_{18:1}$ phosphatidyl choline (PC) -- is characterized by a glycerol back-bone with two fatty acid side-chains at the C_1 and C_2 positions and a phosphate linked to the head group at the C_3 position. In all discussion of phospholipid species, to denote the fatty acid composition, the notation of $C_{n:m}$ is used whereby "n" represents the carbon chain length of the fatty acid and "m" represents the number of double bonds in the fatty acid.

The profile of major species of PE was determined by performing a negative mode parent ion scan of all ions producing a fragment with a m/z of 196, corresponding to a loss of the

glycerol-ethanolamine head group with the loss of one water and carrying a negative charge on the oxygen. The profile of major species of PI was determined by performing a negative mode parent ion scan of all ions producing a fragment with a m/z of 241, corresponding to the phosphoinositol head group with the loss of a single water molecule. The profile of major species of PS was determined by performing a neutral loss ion scan of all ions producing a fragment at a m/z of 87 less than the parent ion. This shift corresponds to the loss of the phosphoserine head group, minus one molecule of H_3PO_4. Daughter ion scans were then performed on the prominent parent ions detected in the parent ion scans and neutral loss scan to verify that these species do indeed correspond to PE, PI, and PS respectively and to determine the corresponding lengths of the fatty acid side chains.

Finally, to compare the occurrence of the same lipid species in both hAECs and bAECs, spectra from standard lipid extractions of both cell types (Section 2.2.3) were compared across the m/z range of 250-950 in the negative ion mode and 400-950 in the positive ion mode.

2.2.4.4 Specificity of the AEC response to exogenously added physiological C_{16} ceramide and nonphysioloigcal C_8 ceramide

Because of the ease of solubility with decreasing fatty acid chain length, short-chain ceramides (C_2-C_8) are frequently used in exogenous ceramide studies, despite being nonphysiological. To assess the validity of this model and to further explore the distinction between physiological and non-physiological species of ceramide and the EC response, we subjected bAECs to increasing concentrations of exogenous C_8 and deuterated C_{16} ceramide (C_{16}-D_{31} ceramide) and compared cell viability and the ceramide profile. The synthetic C_{16}-D_{31} ceramide has a mass 31 Da higher than C_{16} ceramide, allowing for distinction by ESI-MS between exogenously added and endogenous C_{16} ceramide in these cells.

Stocks of C_8 and deuterated C_{16} ceramide (D_{31}-C_{16} ceramide) were prepared in pure ethanol at a concentration of 5 mg/mL and stored at -20°C. Prior to use, D_{31}-C_{16} ceramide stock was solublized by sonication in a water bath for 30 minutes. Stock concentrations of ceramide were added to EGM medium pre-warmed to 37 °C and were examined for precipitation. Treatment media was used immediately.

bAECs were cultured in 6-well plates (BD Biosciences) using EGM as described previously (Section 2.2.2). When cells had reached approximately 70-80% confluence, the media was replaced with 2mL of control or treatment media. Two wells for each treatment at each time point were treated with either control EGM; EGM supplemented with C_8 ceramide at a concentration of 10 μM, 25 μM, or 50 μM; or EGM supplemented with D_{31}-C_{16} ceramide at a concentration of 10μM, 25μM, or 50μM. At each timepoint – 1, 3, 6, 12, 24, 48, and 72 hours -- two wells were harvested and extracted for each treatment as described previously (Section 2.2.3) and analysis was performed by ESI-MS. For each sample, sequential negative and positive ion mode scans were performed across the m/z range of 250-950. Levels of $C_{16:0}$, $C_{24:0}$, and $C_{24:1}$ species of ceramide and $C_{16:0}$ sphingomyelin were compared and cell viability was assessed by trypan blue exclusion. The experiment was performed four times.

2.3 RESULTS

2.3.1 Common phospholipid panel

ESI-MS/MS revealed a broad distribution of species of PC, PE, PG, PI, and PS in hAECs. The MS-MS spectra are shown in Appendix A and the findings are summarized in Tables 2.1, 2.2,

2.3, 2.4, 2.5, and 2.6 below. Fatty acid chain-length composition is expressed with regards to both the diacyl species and the individual species. The fatty acid containing the vinyl ether is notated by an adjacent "p" in the description of the individual group description. Interestingly, a number of species of plasmalogens – plasmenyl PE – were also identified. The presence of the same parent ions in bAECs is confirmed by side-by-side comparison between MS spectra of bAECs and hAECs (Appendix B).

Table 2.1. Predominant species of phosphatidyl choline (PC) in hAECs by ESI-MS/MS

Phosphatidyl choline (PC)			
Diacyl species		m/z (M-H)-	acyl/acyl
32:1	Cl^- salt	766	14:0/18:1 and 16:0/16:1
34:2	Cl^- salt	792	16:1/18:1
34:1	Cl^- salt	794	16:0/18:1
36:4		781	16:0/20:4 and 14:1/22:3
36:2	Cl^- salt	820	18:1/18:1
36:1	Cl^- salt	822	18:0/18:1

Table 2.2. Predominant species of phosphatidyl ethanolamine (PE) in hAECs by ESI-MS/MS

Phosphatidyl ethanolamine (PE)		
Diacyl species	m/z (M-H)-	acyl/acyl
34:1	716	16:0/18:1 and 16:1/18:0
36:1	744	16:1/20:0, 16:0/20:1, and 18:0/18:1
38:4	766	16:0/22:4 and 18:0/20:4
40:6	791	18:1/22:5

Table 2.3. Predominant species of plasmenyl PE in hAECs by ESI-MS/MS. The fatty acid containing the vinyl ether is notated by an adjacent "p" in the description of the individual group description.

Plasmenyl species of PE		
Diacyl species	m/z (M-H)-	acyl/acyl
36:4	721	16:0p/20:4
28:2	754	16:0/22:2 and 18:1/20:1
38:5	747	16:0p/22:5 and 18:1p/20:4
40:6	773	18:1p/22:5
40:5	775	16:0p/24:5 and 18:0p/22:5

Table 2.4. Predominant species of phosphatidyl glycerol (PG) in hAECs by ESI-MS/MS.

Phosphatidyl glycerol (PG)		
Diacyl species	m/z (M-H)-	acyl/acyl
32:1	719	14:0/18:1 and 16:0/16:1
32:0	721	14:0/18:0 and 16:0/16:0
34:1	747	16:0/18:1
36:2	773	18:1/18:1
36:1	775	16:0/20:1 and 18:0/18:1

Table 2.5. Predominant species of phosphatidyl inositol (PI) in hAECs by ESI-MS/MS.

Phosphatidyl inositol (PI)		
Diacyl species	m/z (M-H)-	acyl/acyl
28:0	754	14:0/14:0
30:1	779	14:1/16:0
36:1	863	18:0/18:1
38:4	885	18:0/20:4
40:5	911	18:1/22:4
40:4	913	18:0/22:4

Table 2.6. Predominant species of phosphatidyl serine (PS) in hAECs by ESI-MS/MS.

Phosphatidyl serine (PS)		
Diacyl species	m/z (M-H)-	acyl/acyl
34:1	760	16:0/18:1 and 16:1/18:0
36:1	788	18:0/18:1
38:3	812	18:0/20:3
40:5	836	18:0/22:5
42:1	871	18:0/24:1 and 18:1/24:0

2.3.2 Ceramide distribution

MS analysis has allowed us to determine the major species of ceramide present in bAECs grown in static (unstrained) culture. Figure 2.6 shows that $C_{16:0}$, $C_{24:0}$, and $C_{24:1}$ ceramides are the major species of ceramides present in these cells. Results are expressed as mean ± SEM. Although C_2 ceramides can be found in nature, C_4 thorough C_{12} ceramides are non-physiological and as such,

are observed in trace levels at or below the noise level. Low, but significant levels of $C_{14:0}$, $C_{16:1}$, C_{18}, C_{20}, C_{22}, C_{26}, and C_{28} were also detected.

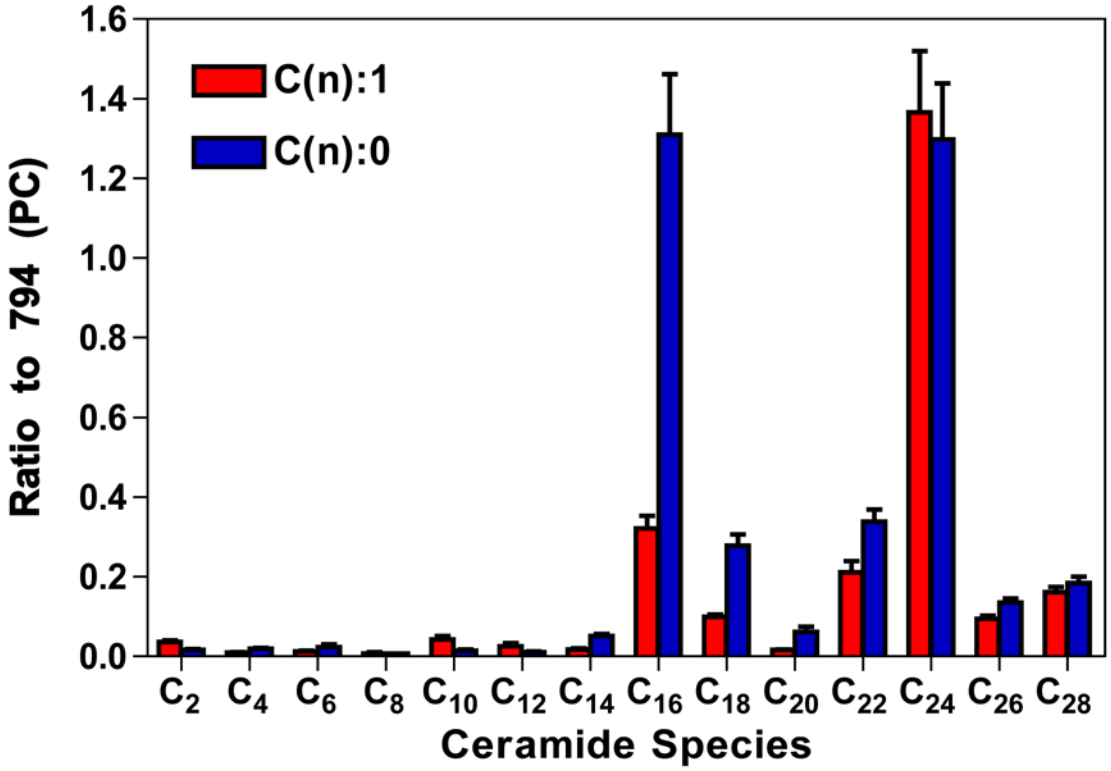

Figure 2.6. $C_{16:0}$, $C_{24:1}$, and $C_{24:0}$ are the major species of ceramide in bAECs. Results are expressed as a ratio of total ion count of ceramide to that of a physiological structural phospholipid (phosphatidyl choline). $P<0.0001$ for C_{16}, C_{18}, C_{22}, C_{24}, C_{26}, and C_{28} ceramide. $P<0.001$ for $C_{20:1}$. $P<0.01$ for $C_{14:0}$. $P<0.05$ for $C_{20:0}$. (n=6)

2.3.3 Sphingomyelin distribution

MS analysis has allowed us to determine the major species of sphingomyelin (SM) present in bAECs grown in static culture. SM is detectable in the positive mode as a sodium adduct and in its native form at different levels and precisions (Figure 2.7). Results are expressed as mean ± SEM. The ratio of TIC to 782 PC ($C_{16:0}/C_{18:1}$) for the unsodiated form of $C_{16:0}$ SM has a mean of 0.113 ± 0.033, whereas the mean is 0.311 ± 0.015 for the sodiated form ($p<0.005$, n=6). For this reason, evaluation of the distribution of SM species was performed for the sodium adduct forms. Since sphingomyelin is synthesized from ceramide, it is not surprising that the predominant species of SM (Figure 2.8) reflect the predominant species of ceramide in these cells (Figure 2.6). The predominant species of SM are the $C_{16:1}$, $C_{16:0}$, $C_{20:0}$, $C_{22:1}$, $C_{22:0}$, $C_{24:1}$, and $C_{24:0}$ forms of SM. In interpreting the relative abundance of the longer chain SMs, however, it is important to recall that these species fall within the same m/z range as many other phospholipids. For example, sodiated $C_{22:0}$ SM falls at m/z of 781, which is only one Da less than sodiated $C_{16:0}/C_{18:1}$ PC, the abundant structural phospholipid against which the SM TIC is normalized. As such, the TIC at m/z 781 represents a mixture of sodiated $C_{22:0}$ SM as well as sodiated $C_{16:0}/C_{18:1}$ PC with naturally occurring isotope variation in carbon atoms. Normally, the contribution of the isotopic form of a lipid species to the TIC detected at a given m/z value is relatively insignificant, but in this instance, the normal species of sodiated $C_{16:0}/C_{18:1}$ PC at m/z 782 is so abundant that the contribution of the isotopic form occurring at m/z 781 is not negligible.

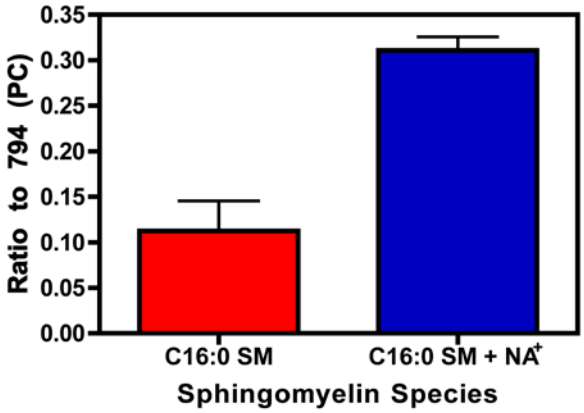

Figure 2.7. The sodium adduct of $C_{16:0}$ sphingomyelin is present in greater abundance than the unsodiated form in bAECs in static culture. Results are expressed as a ratio of total ion count of ceramide to that of a physiological structural phospholipid (phosphatidyl choline). $P<0.005$. (n=6)

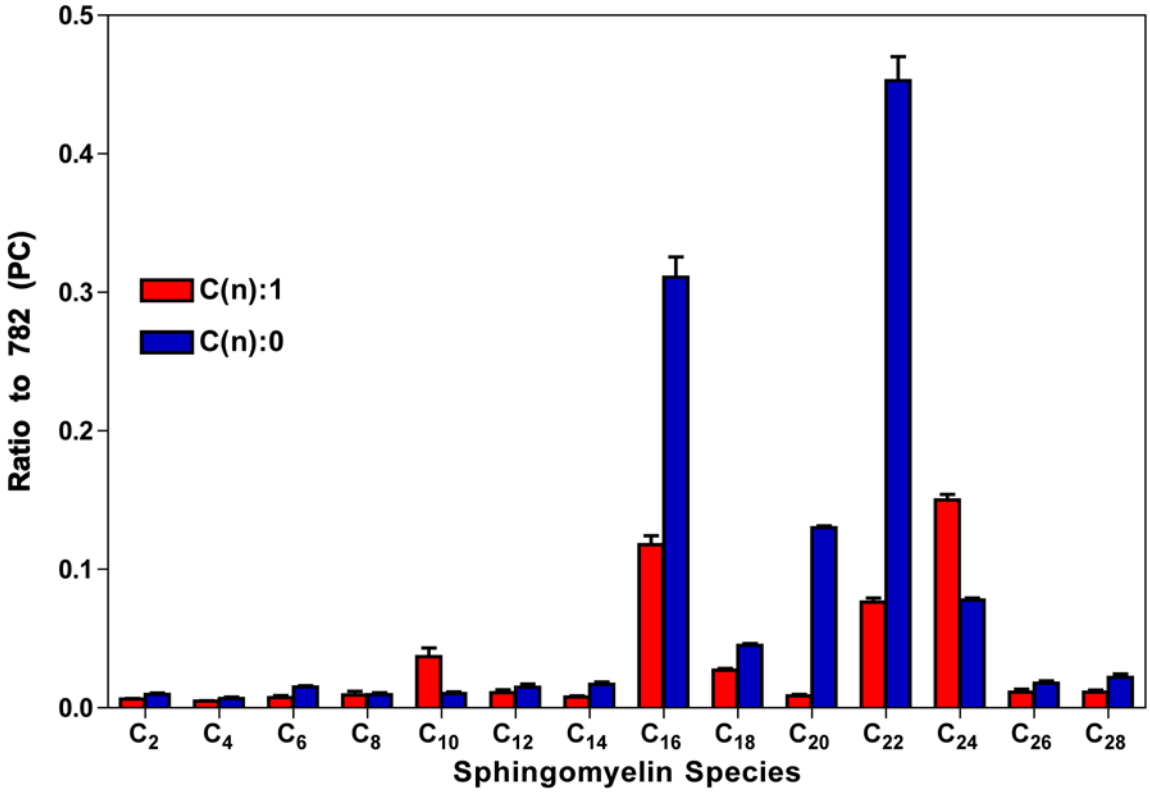

Figure 2.8. $C_{16\text{-}24}$ through C_{24} are the major species of sphingomyelin in bAECs. Results are expressed as a ratio of total ion count of sphingomyelin to that of a physiological structural phospholipid (phosphatidyl choline). $P<0.0001$ for all species except $C_{4:0}$, $C_{6:1}$, $C_{10:0}$, C_{12}, C_{24}, and $C_{26:1}$ SM, which had $P<0.0005$ and $C_{8:1}$ SM, which had $P=0.0056$. (n=6)

2.3.4 Specificity of response to exogenously added physiological C_{16} ceramide and nonphysiological C_8 ceramide

Exogenous C_8 and D_{31}-C_{16} ceramides were both rapidly taken up by bAECs in static culture (Figures 2.9.A and 2.10.A). In these figures, levels of the exogenously added ceramides are expressed as the TIC of ceramide normalized to the TIC of 794 PC. For all other figures, the normalized ceramide content of treated cells is expressed as a ratio to the corresponding

normalized ceramide content of control cells, allowing better correlation of data sets. The data shown is the average of two experimental repeats.

The endogenous ceramide response to exogenous ceramide is very different between C_8 and D_{31}-C_{16} ceramides. Treatment with exogenous C_8 ceramide causes an expected increase in bAEC C_{16} and C_{24} ceramides (Figures 2.9.B and 2.9.C) with a corresponding concentration-dependent decrease in viability (Figure. 2.9.D). Interestingly, treatment with exogenous C_{16}-D_{31} ceramide causes a sustained decrease in bAEC levels of endogenous C_{16} and C_{24} ceramides (Figures 2.10.B and 2.10.C) and does not compromise cell viability (Figure 2.10.D). These findings were confirmed in cells treated with exogenous synthetic C_{16} ceramide (not deuterated) with regards to C_{24} ceramide levels and viability (data not shown).

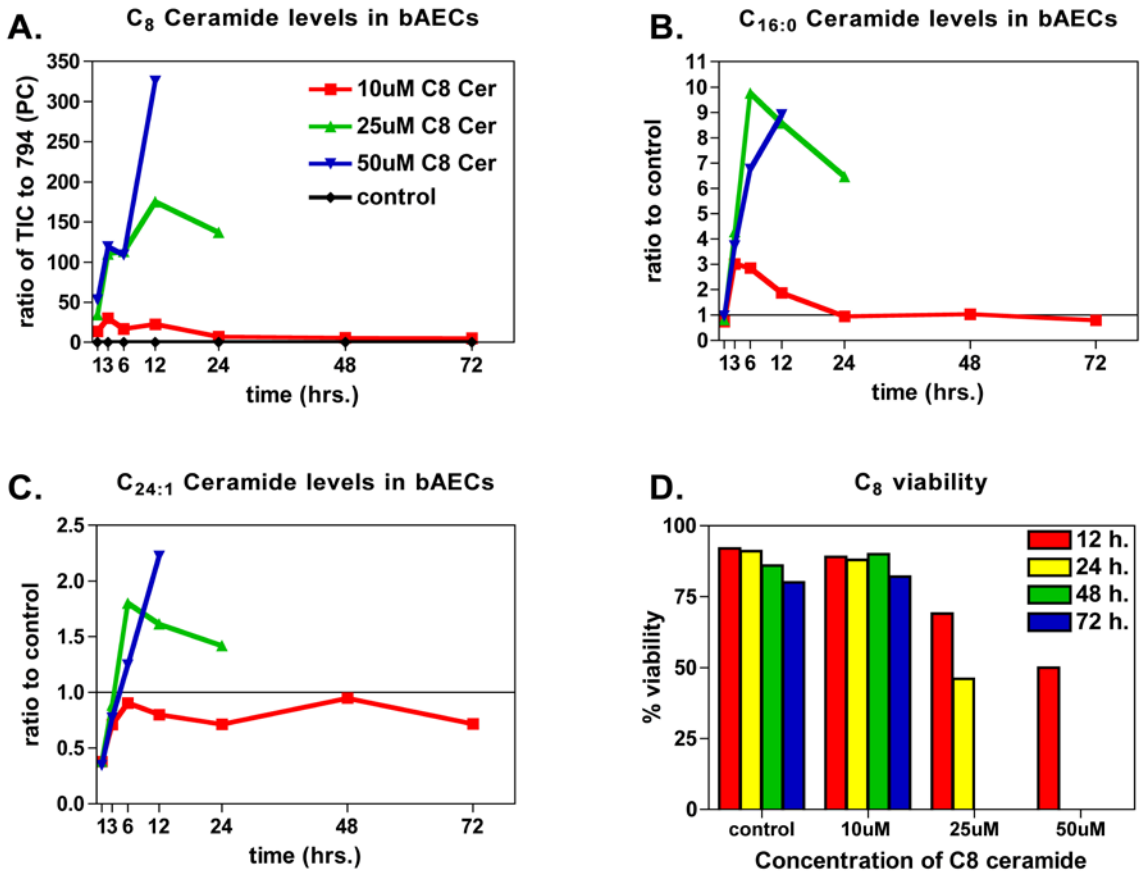

Figure 2.9. Exogenous C_8 ceramide is taken up by bAECs, resulting in increased intracellular C_{16} and C_{24} ceramides and concentration dependent decrease in viability. (A) shows changes in intracellular levels of C_8 ceramide following treatment and (B) shows changes in intracellular $C_{16:0}$ ceramide following treatment. (C) shows changes in intracellular $C_{24:1}$ following treatment and (D) shows changes in cell viability by trypan blue exclusion with increasing concentration of C_8 ceramide treatment. Data shown is representative of two experiments.

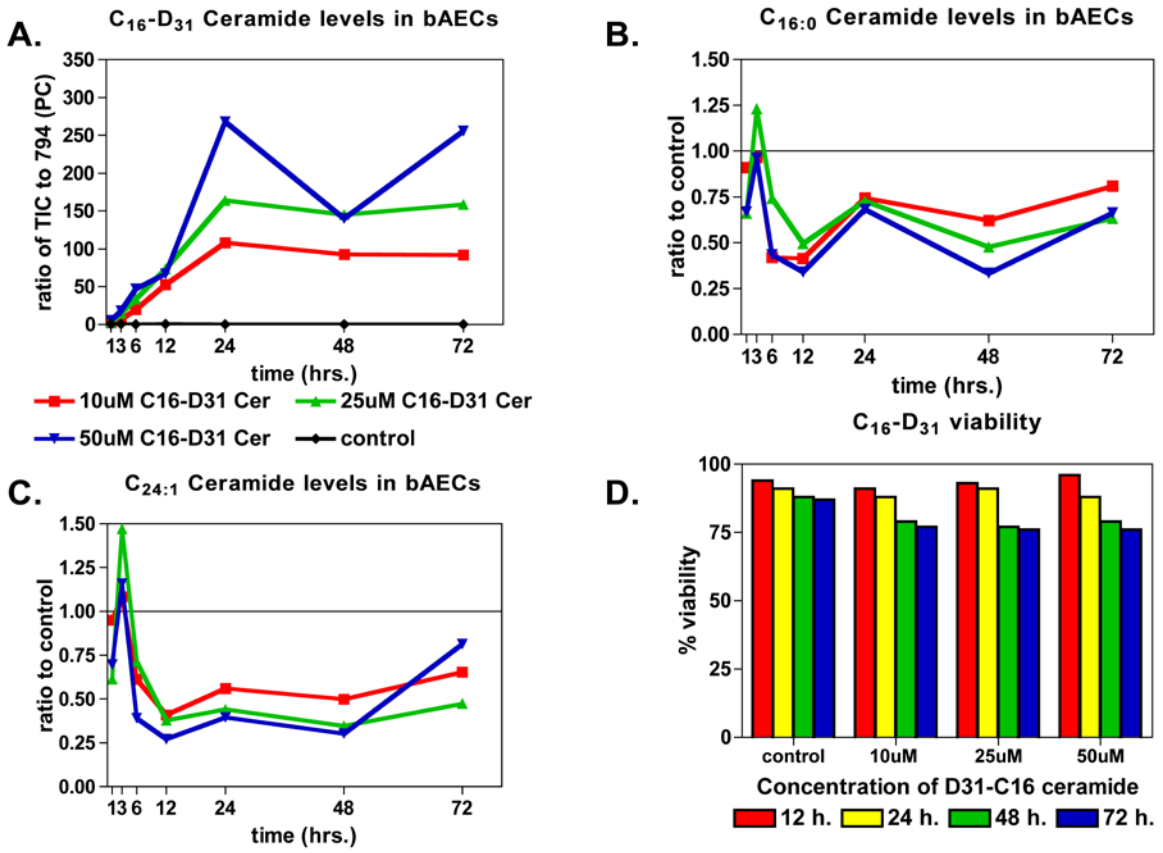

Figure 2.10. Exogenous C_{16}-D_{31} ceramide is taken up by bAECs, resulting in decreased intracellular C_{16} and C_{24} ceramides, and preserved cellular viability. (A) shows changes in intracellular levels of C_{16}-D_{31} ceramide following treatment, (B) shows changes in intracellular endogenous $C_{16:0}$ ceramide following treatment, (C) shows changes in intracellular $C_{24:1}$ ceramide following treatment, and (D) shows changes in cell viability by trypan blue exclusion with increasing concentration of C_{16}-D_{31} ceramide treatment. Data shown is representative of two experiments.

2.4 DISCUSSION

2.4.1 Phospholipid profile

The major species of phospholipids present in hAECs, as listed in Tables 2.1, 2.2, 2.3, 2.4, 2.5, and 2.6, show a broad distribution of fatty acid chain lengths within the physiological range (C_{14}-C_{24}). It is also interesting to note the abundance of cholesterol, at a m/z of 421 in the negative mode or 409 in the positive mode, representing the chloride and sodium adducts respectively (Appendix B). Many of these species have been identified by others as predominant species in circulating human blood cells [93].

This list is extensive, but not exhaustive. As alluded to previously, there are limitations to ESI-MS/MS analysis of total lipid pools from cellular extracts. Parent ion scans based upon phospholipid head-group characteristics may reveal multiple lipid species, as is the case with plasmenyl PE (plasmalogen of PE) and PE, or PC and SM, which share the same choline head-group but differ in side chain composition. Furthermore, identification of the fatty acid side-chains requires MS/MS analysis in the negative ion mode, which does not always favor species of phospholipids or sphingolipids that are detected more abundantly in the positive ion mode, like PC or SM.

Not all lipid species fragment in such a way that a definitive fragmentation pattern can be determined, as is the case for PC in the negative ion mode and PG. Potential species of a phospholipid may be identified by a parent ion scan, as was the case of our evaluation of PE and PI, but verification and determination of side chain composition depends on performing a daughter ion scan on each potential target, as was performed in this study. As is clear in the numerous spectra exhibited in Appendix A, it is not uncommon when scanning, to find that a

single mass ion peak is a mixture of not only multiple fatty acid chain lengths of the same phospholipid, but may also be a mixture of multiple phospholipids.

Assessment of the fatty acid pairings relies upon mathematical calculation based on the fragmentation pattern. Occasionally, peaks corresponding to low abundance of longer fatty acid chains are present, but a probable phospholipid structure cannot be assigned to them. Additionally, depending on the bonding pattern and carbon chain length, not all fatty acid fragments are easily detectable at an abundance corresponding to their paired shorter fatty acid side-chain. Thus, fragmentation efficiencies do exist and vary with chain length. Sometimes, these discrepancies in the fatty acid fragmentation pattern can be accounted for because of low levels of suggestive fragmentation patterns for a different phospholipid. For example, when performing a daughter ion scan for a species of PE, there may be detection of a m/z loss of 50 suggesting the presence of PC due to loss of a CH_3Cl during fragmentation in the negative ion mode, revealing the presence of a mixture of phospholipids (PE and PC) corresponding to that mass ion, and allowing for assignment of low abundance fatty acids.

Another potential difficulty in assessing the distribution of fatty acid chain compositions is that the window of detection through the MS1 detector must be broad enough to allow for adequate signal intensity following fragmentation. Between this variability and normal isotopic variation in molecules, it is not uncommon to have fragmentation of lipids corresponding to adjacent mass ion peaks (i.e. 779 PC with 780 PI) or even possibly to detect fragmentation from diacyl combination differing by one double bond, corresponding to a mass shift of two Da. If the target parent is in between the m:n and m:n+1 total diacyl compositions, fragmentation may reveal an overlapping pattern of all constituent acyl/acyl combinations, making exact characterization more difficult.

When scanning for higher mass ions, above m/z 700, there is also the potential for detection of doubly charged species of cardiolipin. Cardiolipin is formed by two PG molecules sharing the same head-group, allowing for the molecule to contain four fatty acid side-chains and up to two negative charges. The doubly charged form of cardiolipin, not surprisingly, falls in a similar m/z range as native PG and may overlap with other phospholipid species.

Ultimately, the list of phospholipid species generated is indicative of major species of phospholipids, but there are likely many species that are absent due to some of the detection difficulties discussed above. To form a more complete list, it would be helpful to purify the phospholipids first by TLC (thin layer chromatography) to separate lipids by their chemical properties, and then to perform ESI-MS/MS on the purified lipid pools.

Although not directly related to the present study of ceramide metabolism, the ability to detect and measure species of plasmalogens by ESI-MS is also an interesting finding. Several species of plasmenyl PE were found during the evaluation of AEC lipids (Table 2.3). Plasmalogens are a type of lipid characterized by a vinyl ether at the C_1 position on the glycerol backbone where the sn-1 moiety is usually a $C_{16:0}$, $C_{18:1}$, or $C_{18:0}$ fatty acid (Figure 2.11). The sn-2 moiety is usually a polyunsaturated fatty acid and the head-group is typically choline or ethanolamine and the abundance of these forms varies in different tissues [98]. Plasmenyl PE is abundant in brain myelin and platelets [93, 98-100], while plasmenyl PC is abundant in cardiac muscle and platelets [98]. Cleavage of arachidonic acid ($C_{20:4}$ fatty acid) from plasmenyl PE in platelets stimulated by thrombin [100] and from plasmenyl PC in coronary artery endothelial cells stimulated by thrombin and hypoxia [101] via phospholipase A_2 (PLA_2) has been reported. Plasmalogens, and particularly plasmenyl PE, have been shown to protect platelet phospholipids from oxidative degradation [99].

Thus, the ability to monitor selective changes in both total plasmalogen content as well as specific species of plasmalogens, for example those containing arachidonic acid, by mass spectrometry during suspected mechanisms of endothelial activation, may provide further insight into the extent of damage to the lipid functionality of the endothelium. Given the potential role of reactive oxygen species in mechanotransduction, the plasmalogen profile may be affected in such a system and may be involved in the contribution of mechanical insults to the endothelium during initiation and progression of vascular disease.

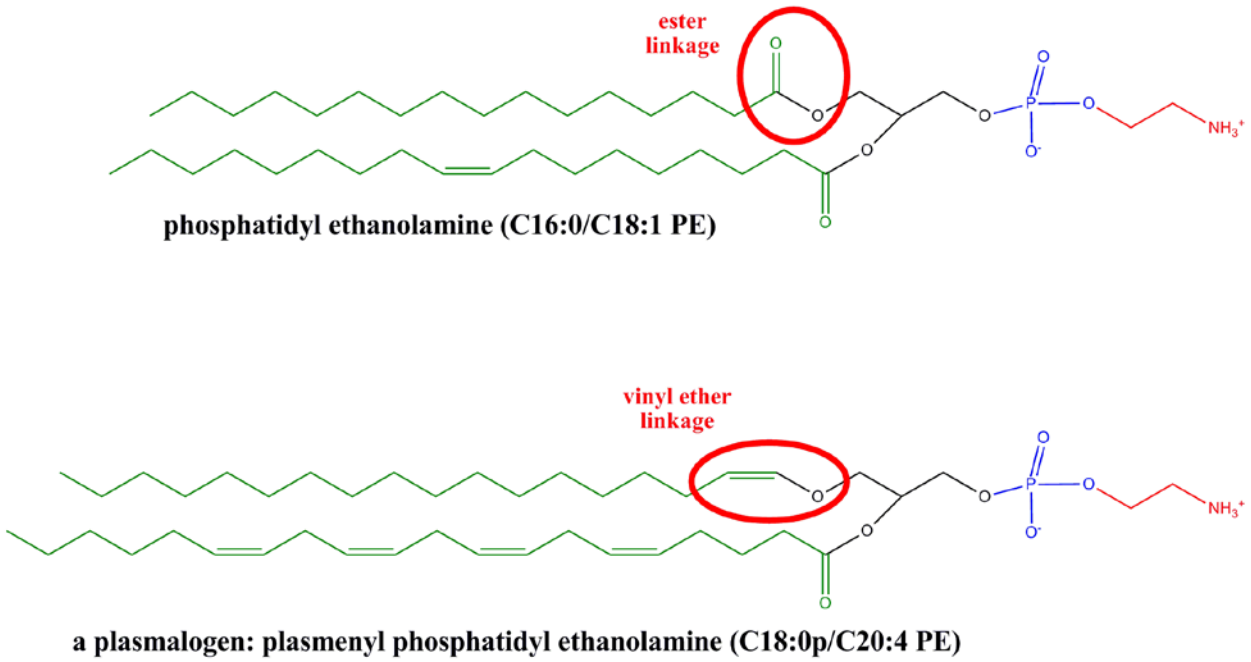

Figure 2.11. Plasmalogens are a type of lipid characterized by a vinyl ether at the C_1 position on the glycerol backbone where the sn-1 moiety is usually a $C_{16:0}$, $C_{18:1}$, or $C_{18:0}$ fatty acid. The sn-2 moiety is usually a polyunsaturated fatty acid and the head-group is typically choline or ethanolamine.

2.4.2 Ceramide and sphingomyelin profile

The predominant physiological forms of ceramide contain fatty acids of C_{16} to C_{26} chain length [62, 70]. C_{16} and C_{24} ceramides specifically have been implicated in apoptosis [70, 102]. Not surprisingly, the major forms of ceramide detected in AECs by ESI-MS are $C_{16:0}$, $C_{24:1}$, and $C_{24:0}$ ceramides (Figure 2.6). The overall proportions of physiological species of ceramides in our analysis are comparable to those observed by others in human umbilical vein endothelial cells (HUVECs) as detected by HPLC/MS [94]. Because of their known biological specificity and abundance in both bovine and human AECs, ceramide evaluation for further studies is limited to the $C_{16:0}$, $C_{24:1}$, and $C_{24:0}$ species of ceramide.

One of the potential drawbacks of our technique of detecting ceramides by MS is that the chloride adduct is measured. The ability to form adducts and to detect them by ESI-MS is sensitive to extraction technique and solvent conditions. To a lesser extent, this is also a problem with sphingomyelin detection, although the unsodiated form can be detected with less reliability (Figure 2.7). As such, variation in aqueous buffer use and cell preparation techniques has been limited to reduce that source of variation in this study and ESI-MS analysis is always performed with fresh solvent.

Since ceramide is a building block for sphingomyelin, it is not surprising to see that there is a similar prevalence of the same fatty acid chain lengths in ceramide in Figure 2.6 as there is in sphingomyelin in Figure 2.8. Specifically, $C_{16:0}$ is one of the most abundant forms of both ceramide and sphingomyelin detected. The proportional abundance of SM in AECs is similar to that observed by others using ESI-MS/MS of human circulating blood cells [93] and has been identified by our group as a major species of SM in other cell types [95]. As is discussed in

Section 2.3.3, in the positive ion mode, many of the larger forms of SM fall at adjacent m/z to those of abundant species of PC, making it difficult to distinguish the relative contribution of naturally occurring sphingomyelin and isotope species of PC. Although there would likely be differences in the fatty acid composition of the PC species and the SM species, fragmented fatty acids are not detectable in the positive mode, in which SM and PC run at greatest abundance. Furthermore, performing MS/MS analysis on every lipid sample generated is tedious and would increase the amount of sample needed. To reduce the contribution of overlap of SM with other lipid species, and to maintain consistency of detection across sample preparations, only the sodium adduct of $C_{16:0}$ SM, corresponding to m/z of 725, is evaluated in further studies.

2.4.3 Response to exogenous physiological C_{16} ceramide and nonphysiological C_8 ceramide

Because of the ease of solubility with decreasing fatty acid chain length, short-chain ceramides (C_2-C_8) are frequently used in exogenous ceramide studies, despite being nonphysiological. Our evaluation of the specificity of the aortic endothelial cell response to both physiological C_{16} and non-physiological C_8 species of ceramide reveals that short-chain ceramide is not a direct functional substitute for physiological long-chain ceramide, with regards to change in viability and intracellular physiological ceramide content (Figures 2.9 and 2.10).

Treatment with exogenous C_8 ceramide causes an expected increase in bAEC C_{16} and C_{24} ceramides (Figures 2.9.B and 2.9.C) with a corresponding concentration-dependent decrease in viability (Figure 2.9.D). Interestingly, treatment with exogenous C_{16}-D_{31} ceramide causes a decrease in bAEC levels of endogenous C_{16} and C_{24} ceramides (Figure 2.10.B and 2.10.C) and does not compromise cell viability (Figure 2.10.D).

Both C_8 and C_{16}-D_{31} ceramides are taken up rapidly by bAECs in static culture (Figures 2.9.A and 2.10.A), following thorough washing of the cells prior to extraction, suggesting that the difference in outcome is not due to difference in uptake kinetics associated with the fatty acid chain length or precipitation of the C_{16} ceramide out of solution prior to treatment.

Although the data is not shown, these same findings were observed in bAECs treated with synthetic, non-deuterated C_{16} ceramide species. In those initial studies, only the change in C_{24} ceramide species was visible as well as the preservation of cell viability, since exogenous and endogenous forms of C_{16} ceramide could not be distinguished. The use of D_{31}-C_{16} ceramide has shown that all the major species of ceramide are downregulated following the addition of the exogenous physiological source of ceramide, unlike the concentration-dependant increase in endogenous ceramide and decrease in viability preset in bAECs following addition of nonphysiological C_8 ceramide.

Thus, exogenous sources of C_{16} ceramide are well tolerated by bAECs and the data suggests that bAECs may be capable of converting the exogenous physiological ceramide into a more palatable metabolite like SM, S-1-P, or a higher glycolipid, whereas the nonphysiological ceramide may not be able to be processed. This seems especially possible given the reduction in endogenous ceramide species relative to untreated control cells (Figures 2.10.B and 2.10.C). C_{16} ceramide may also be capable of autoregulating ceramide synthesis in bAECs such that in response to increases in C_{16} ceramide -- a species with known biological activity -- endogenous synthesis of ceramides may be downregulated in the absence of other stress events to prevent inappropriate signaling.

Furthermore, this data may further support the concept that specificity of fatty acid chain length plays a role in specific activity of different ceramide species. Different species of

ceramide have specific ceramide synthases, each of which is encoded on a different gene. For example, in humans, each of the six longenvity assurance genes, *LASS1-6*, encodes for ceramide synthases that selectively utilize specific fatty acid chain lengths between C_{16} and C_{24} and different genes may be activated under different circumstances [102]. This evidence further supports the notion that different chain lengths of ceramide may play different roles and that measurement of a single species of ceramide may not be a surrogate for all species of ceramide with regards to biological activity.

The outcome of ceramide signaling is also associated with the site and source of ceramide generation within the cell. Exogenous C_{16} ceramide may not partition into the appropriate intracellular pools to evince a change in viability, whereas C_8 ceramide causes rapid generation of ceramide, potentially through removal of the C_8 chain and reacylation with $C_{16:0}$ (palmitic acid), similar to *de novo* synthesis [88].

If this is indeed the case, it may partially explain the apparent pro-survival outcome for exogenous C_{16} ceramide treatment. Ceramide has also been implicated in autophagy in HUVECs following binding to glycated collagen substrates [94] and in response to a number of chemotherapeutic agents in cancer cells [103, 104]. Autophagy in response to C_2 ceramide occurs rapidly over a few hours [103, 104], consistent with the timeframe of ceramide accumulation and cell death experienced by bAECs in response to C_8 ceramide. In HT-29 colon cancer cells, C_2 ceramide has been shown to promote autophagy by the accumulation of intracellular physiological ceramides, and that autophagy is reduced in the presence of myriocin, an inhibitor of *de novo* ceramide synthesis [103]. Thus, if bAECs downregulate *de novo* ceramide synthesis in response to exogenous C_{16} ceramide synthesis whereas addition of exogenous C_8 ceramide promotes it, one might expect cells treated with C_{16} ceramide to be

spared from autophagic death. Interestingly, the ceramide generation associated with induction of autophagy in HUVECs appears to result from aSMase activity, not *de novo* synthesis [94]. Autophagy may be modulated by ceramide and its metabolites, including S-1-P, through different pathways, suggesting, as often occurs with ceramide, that the final fate of the cell is determined not by a single pathway, but by the sum of concurrent stress signaling processes [104].

Of course, our initial studies do not explore whether cell death occurs by apoptosis, autophagy, or necrosis, and further evaluation of apoptotic and autophagic markers would be necessary, but the similarity of outcomes in response to short- and long-chain ceramides to autophagy data is intriguing. Furthermore, when evaluating ceramide data in endothelial cells, it is appealing to believe that autophagy, and not just apoptosis, may contribute to impaired endothelial cell function.

2.5 CONCLUSIONS

Evaluation of the phospholipid and sphingolipid profiles of bAECs and hAECs confirms that both cell types possess a similar lipid profile. Examination of the sphingolipid profile confirms that $C_{16:0}$, $C_{24:2}$, and $C_{24:0}$ ceramides are the predominant species in AECs and identifies sodiated $C_{16:0}$ SM as an appropriate measure of SM by ESI-MS, establishing them as suitable endpoint measures for future experiments. Furthermore, evaluation of the bAEC response to exogenous C_8 and C_{16} ceramides reveals that bAECs have a specific regulatory response to physiological but not non-physiological ceramides.

3.0 THE CERAMIDE RESPONSE TO MECHANICAL CYCLIC STRAIN

3.1 INTRODUCTION

The effect of cyclic strain on the endothelium is of particular relevance in the clinical setting because of its involvement in hypertension, vein grafting, balloon angioplasty over-stretch injury and possibly intra-aortic balloon pumping, tissue engineering, and atherosclerotic lesions. As discussed in Section 1.2.2, cyclic strain has been shown to influence a variety of vascular cell functions including proliferation, migration, apoptosis, morphology, and production and secretion of a variety of soluble molecules inherent to EC function. Changes in biological endpoints may vary biphasicly or linearly in response to strain magnitude [44]. Signaling events may occur transiently or may be sustained, depending on the strain conditions [50]. Furthermore, the endothelium in disease may be affected not only by unusually high strain, as one would expect to result in injury, but may also experience unusually low strains. This would occur as part of stress-shielding of the endothelium in the case of arterial stiffening which can occur in any region of the arterial bed, including the aorta. Arterial stiffness, even in the absence of hypertension, leads to increased left ventricular afterload and decreased coronary artery perfusion, suggesting that vascular stiffness can also contribute to cardiovascular disease progression [105, 106].

Thus, in evaluating the contribution of the mechanotransduction response to cyclic strain, it is important to look at not only whether a change occurs in a biological endpoint in response to strain compared to static culture, but to evaluate the dose response over time and over a variety of strain conditions. J.D. Humphrey further elaborates on the importance of such data by suggesting that mechanical dose response curves may be as important to understanding vascular health as pharmacological dose response curves, and points to the limited availability of such data in the field [105].

Changes in endogenous ceramide levels in endothelial cells remains unexplored. As such, a full assessment of how the dominant forms of ceramide change in response to duration, magnitude, and frequency of cyclic strain regimen is important to establish appropriate conditions for assessment of the role of ceramide in the mechanotransduction response.

This chapter will specifically address the second specific aim:

Determine whether aortic endothelial cell ceramide levels are altered in response to uniaxial, cyclic mechanical strain.

1. Identify the molecular forms of ceramide generated in response to cyclic strain.
2. Determine whether ceramide signaling in response to cyclic strain involves an early response within minutes, suggesting membrane sphingomyelin as the source of ceramide generation; a late response after several hours, suggesting *de novo* ceramide generation; or both.
3. Determine if the duration, frequency, and intensity of cyclic strain affects the magnitude and molecular forms of ceramide generated.

3.2 METHODS

3.2.1 Cyclic strain apparatus

Cyclic uniaxial stretch was applied to bAECs using a Flexcell FX4000T cyclic tension system (Figure 3.1, Flexcell International, Hillsborough, NC). The use of the FX4000T to apply cyclic strain to vascular endothelial cell monolayers has been well documented [107-109]. Briefly, the FX4000T is a computer-regulated bioreactor that can apply cyclic or static tensile strains to *in vitro* cell cultures grown on a deformable silicone substrate. Computer-regulated valves allow for the application and release of vacuum pressure to the underside of the deformable culture substrate, stretching the substrate over a rigid loading post such that a reproducible, predetermined tensile strain is applied to the cells. Frequency and magnitude of the cyclic strain is set by the user. A baseplate holds up to four specialty 6-well plates containing the deformable substrate as the bottom of each well and applies the same strain regimen to all plates.

For these experiments, rectangle loading posts were used to apply uniaxial strain to BioFlex 6-well culture plates (Flexcell International) factory-coated with ProNectin, a synthetic polypeptide containing multiple repeats of the RGD binding sequence of fibronectin. Fibronectin was chosen because it is commonly found as a component of the extracellular matrix supporting vascular endothelial cells [110]. Furthermore, fibronectin is recruited from the plasma during tissue injury [110], making it an appropriate substrate for a model of biological stress in the endothelium.

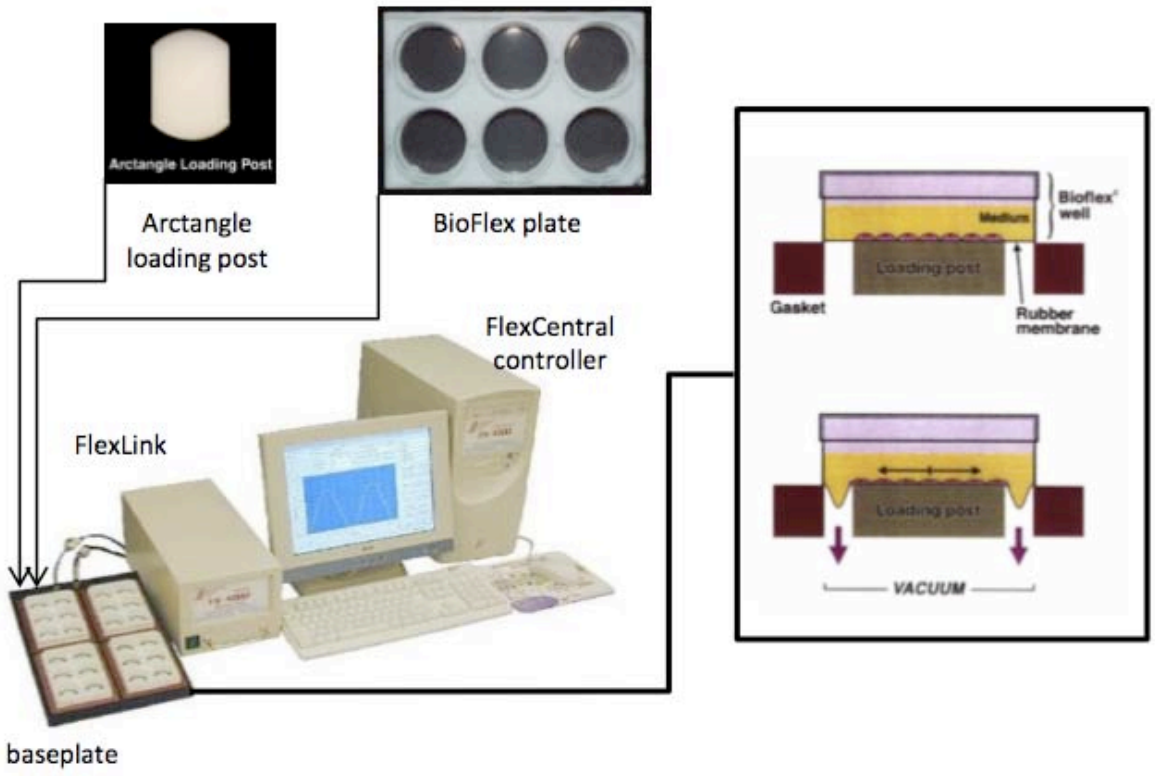

Figure 3.1. The FX4000T system (lower left) applies cyclic strain/stretch to *in vitro* cell cultures grown on a deformable silicone substrate. The computer (the FlexCentral controller) controls valves in the FlexLink module, applies and releases vacuum pressure to the underside of the culture plates fitted with a deformable culture substrate that are positioned on the baseplate. Stretching the substrate over a rigid loading post applies a reproducible, predetermined tensile strain that is applied to the cells (far right). Frequency and magnitude of the cyclic strain is set by the user. The baseplate holds up to four specialty 6-well plates (top center) containing the deformable substrate as the bottom of each well and applies the same strain regimen to all plates. An arctangle loading post (upper left) is used in each well to apply uniaxial strain to the cells. Figure adapted from www.flexcelliint.com.

3.2.2 Panel of cyclic strain conditions

To fully explore how bAEC ceramide levels change in response to the addition of cyclic uniaxial strain, a variety of strain regimens were employed. The panel of conditions is detailed in Table 3.1 and tests how ceramide changes in response to isolated variation of duration, magnitude, and

frequency of cyclic strain. Each pairing of strain frequency and magnitude represents a different experiment. Three independent repeats were generated for each experiment and each experiment was performed twice such that n=6 for each time-point.

Table 3.1. Panel of strain regimens to test isolated changes in duration, magnitude, and frequency of cyclic strain.

Strain Regimen Variable	Cyclic Strain Magnitude	Cyclic Strain Frequency	Time-points (hrs)
Duration	10%	1 Hz	0.5, 1, 3, 6, 12, 24, 48, 72
Cessation	10%	1 Hz	Strain applied for 24 hrs, then evaluation at 1.5, 3, 6, and 12 hrs post-strain
Magnitude	3%, 6%, 10%, 12%	1 Hz	0.5, 1, 3, 6, 12, 24, 48, 72
Frequency	6%	0.5 Hz, 1 Hz, 1.5 Hz, 2 Hz	0.5, 1, 3, 6, 12, 24, 48, 72

For initial studies of changes in ceramide in response to strain, bAECs were exposed to 10% cyclic uniaxial strain at a frequency of 1 Hz. These conditions are widely used in the literature [44, 50, 52, 54]. Time-points of 0.5, 1, 3, 6, 12, 24, 48, and 72 hrs were chosen so that both early and late changes in ceramide, suggestive of sphingomyelin hydrolysis or *de novo* synthesis respectively, could be explored. To determine whether changes in ceramide levels require constant application of cyclic strain, cyclic uniaxial strain was applied to bAECs for 24 hours (10%, 1 Hz) and changes in ceramide over time following cessation of strain were studied.

The cyclic strain regimens were chosen to reflect a broad range of physiological and pathophysiological conditions. We examined the ceramide response of bAECs to subphysiological (3%), normal physiological (6%), and high physiological strain intensities (10% and 12%) [44, 50, 52], all at 1Hz frequency. To explore the ceramide response to varied

frequency, bAECs were subjected to cyclic strain at 6% intensity, which is a normal physiologic value [44, 52], but with varied frequency ranging from 0.5Hz (below physiological, representing a heart rate of 30 bpm), 1Hz (normal physiological, representing a heart rate of 60 bpm), 1.5Hz (high physiological, representing a heart rate of 90 bpm), and 2 Hz (abnormally high physiological, representing a heart rate of 120 bpm).

The FX4000T system is capable of testing up to four plates at a time at a single strain frequency and magnitude. Thus, to test four different strain frequencies, four separate experiments had to be performed. For each time-point, three isolated repeats were generated and each experiment was performed twice such that n=6.

To evaluate more than four time-points per experiment, a system of cycling 6-well plates through the baseplate was adopted. Prior evaluation of changes in the total lipid profile of bAECs in static culture revealed that there were negligible changes in C_{16} and C_{24} species of ceramide over time (data not shown). To rotate the plates through the baseplate, as the plates being harvested for time-points between 0.5 and 6 hrs were removed from the baseplate, new plates were installed on the baseplate to be harvested for the later time-points. The contribution of the minimal change in ceramide levels prior to the onset of strain in the plates that are added to the baseplate later is minimized by using these plates for the latest time points at which there are substantially larger time increments between time-points (12-24 hr intervals between the later time-points compared to 0.5-3 hr intervals between the earlier time-points). This process is outlined in Table 3.2.

Table 3.2. Explanation of plate rotation system.

Time (hr:min)	Process
00:00	Plates 1-4 loaded on baseplate, plates 5-8 in incubator
00:30	Plate 1 removed from baseplate for 0.5 hr time-point, plate 5 loaded on baseplate
01:00	Plate 2 removed from baseplate for 1 hr time-point, plate 6 loaded on baseplate
03:00	Plate 3 removed from baseplate for 3 hr time-point, plate 7 loaded on baseplate
06:00	Plate 4 removed from baseplate for 6 hr time-point, plate 8 loaded on baseplate
12:30	Plate 5 removed from baseplate for 12 hr time-point (12 hrs total strain time)
25:00	Plate 6 removed from baseplate for 24 hr time-point (24 hrs total strain time)
51:00	Plate 7 removed from baseplate for 48 hr time-point (48 hrs total strain time)
78:00	Plate 8 removed from baseplate for 72 hr time-point (72 hrs total strain time)

3.2.3 Cell culture for cyclic strain time-course experiments

For each cyclic strain experiment, two vials of bAECs ($2x10^6$ total live cells) were thawed and passed into three T-75 flasks containing EGM (Section 2.2.2). When cells achieved 80% confluence, they were passed into seventeen BioFlex ProNectin-coated 6-well plates using the same technique as described in Section 2.2.2. For strain cessation experiments, only eight BioFlex ProNectin plates were seeded with cells. For the initial benchmark assessment of ceramide response to cyclic strain, only two BioFlex ProNectin plates were seeded with cells. The media was replaced with 2 mL EGM on the first day after plating and every two days thereafter. When the cells achieved 80% confluence, after approximately four to five days, the

media was replaced with 2 mL fresh EGM, warmed to 37°C. The plates were then returned to the humidified incubator @ 37°C, 5% CO_2 for 2 hours to allow the cells to adjust to the media exchange prior to loading the plates on the baseplate of the FX4000T strain apparatus.

3.2.4 Sample collection and preparation of lipid extractions

3.2.4.1 Benchmark assessment of ceramide response to cyclic strain

To determine whether cyclic strain affects whole-cell levels of $C_{16:0}$, $C_{24:1}$, and $C_{24:0}$ ceramides, one plate of bAECs, prepared as described in Section 3.2.3, was loaded onto the FX4000T baseplate and exposed to 10% strain at 1 Hz for 24 hrs. An identical plate of unstrained bAECs incubated in the same humidified incubator as the one containing the FX4000T (37°C, 5% CO_2) served as the paired control. At the end of the strain period, cells were immediately harvested and the lipids were extracted as described in Sections 2.2.2 and 2.2.3. Cell count and viability by trypan blue exclusion were also assessed as described in Section 2.2.2 to assure cell survival.

For each extraction, two wells were pooled during harvest, allowing for the preparation of three separate repeats of each time-point per plate. Each pair of wells (one sample) was harvested and processed using separate pipets, conicals, and cell count/viability assessments to ensure that they were truly independent samples. This technique was employed in all strain experiments.

An ESI-MS scan across the m/z range of 250-950 in the negative mode was performed and $C_{16:0}$, $C_{24:1}$, and $C_{24:0}$ ceramide levels were measured and normalized to $C_{16:0}$:$C_{18:1}$ PC (m/z of 794) as described in Section 2.2.4.3. Statistical significance of the change in ceramide species

was determined by a paired t-test comparing the strained cells to the unstrained controls using Prism Version 4.

3.2.4.2 Cessation of strain

To determine whether changes in ceramide required continuous application of cyclic strain, four plates of bAECs, prepared as described in Section 3.2.3, were loaded onto the FX4000T baseplate and exposed to 10% strain at 1 Hz for 24 hrs. Four identical plates of unstrained bAECs incubated in the same humidified incubator as the one containing the FX4000T (37^{o}C, 5% CO_2) served as the paired controls. At the end of the strain period, all plates were removed from the baseplate and returned to the incubator in static culture. Cells were harvested and the lipids were extracted as described in Section 2.2.2 and 2.2.3 at 1.5, 3, 6, and 12 hrs post-strain. For each plate, three independent repeats were generated and the experiment was performed twice.

The extractions were timed so that the chloroform:methanol was added to the cells at the indicated time-points. This ensured that the lipid extraction reflected the lipid levels at that period of time following the cessation of strain. Because the total lipid extraction process takes approximately one hour, it was not possible to generate a true 0 hr time-point for comparison; the 1.5 hr time-point is equivalent to the extraction process utilized in all other experiments in this study.

Consecutive ESI-MS scans across the m/z range of 250-950 in the negative and positive ion modes were performed. $C_{16:0}$, $C_{24:1}$, and $C_{24:0}$ ceramide, sphingosine (m/z of 299), and S-1-P (m/z of 379) levels were measured in the negative ion mode scan and $C_{16:0}$ sphingomyelin levels were measured in the positive ion mode scan. The TICs of these sphingolipid species were

normalized to $C_{16:0}$:$C_{18:1}$ PC (m/z of 794 in the negative mode and 782 in the positive ion mode) as described in Section 2.2.4.3. Statistical significance of the change in sphingolipid species was determined by a paired t-test comparing the strained cells to the unstrained controls using Prism Version 4.

3.2.4.3 Variation of duration of strain

To determine how whole-cell levels of $C_{16:0}$, $C_{24:1}$, and $C_{24:0}$ ceramides vary over time in response to cyclic strain, eight plates of bAECs, prepared as described in Section 3.2.3, were loaded onto the FX4000T baseplate and exposed to 10% strain at 1 Hz, using the plate rotation scheme outlined in Table 3.2. Nine identical plates of unstrained bAECs incubated in the same humidified incubator that contains the FX4000T (37^{o}C, 5% CO_2) served as the paired controls. One control plate was harvested immediately after the initial loading of the strain apparatus as a 0 hr control time-point. At 0.5, 1, 3, 6, 12, 24, 48, and 72 hrs, a strained and a control plate were each harvested and the lipids were extracted as described in Sections 2.2.2 and 2.2.3. Cell count and viability by trypan blue exclusion were also assessed as described in Section 2.2.2 to assess cell survival.

For each extraction, two wells were pooled during harvest, allowing for the preparation of three separate repeats of each time-point per plate. Each pair of wells (one sample) was harvested and processed using separate pipets, conicals, and cell count/viability assessments to ensure that they were truly independent samples.

Consecutive ESI-MS scans across the m/z range of 250-950 in the negative and positive ion modes were performed. $C_{16:0}$, $C_{24:1}$, and $C_{24:0}$ ceramide, sphingosine (m/z of 299), and S-1-P (m/z of 379) levels were measured in the negative ion mode scan and $C_{16:0}$ sphingomyelin levels

were measured in the positive ion mode scan. The TICs of these sphingolipid species were normalized to $C_{16:0}$:$C_{18:1}$ PC (m/z of 794 in the negative mode and 782 in the positive ion mode) as described in Section 2.2.4.3. Statistical significance of the change in sphingolipid species was determined by a paired t-test comparing the strained cells to the unstrained controls using Prism Version 4.

Data regarding changes in sphingomyelin, sphingosine, and S-1-P are presented in Chapter 4.

3.2.4.4 Variation of magnitude of strain

To determine how whole-cell levels of $C_{16:0}$, $C_{24:1}$, and $C_{24:0}$ ceramides vary over time in response to different magnitudes of cyclic strain, a set of four separate experiments was performed. Each experiment was performed using the same frequency (1 Hz), but different strain magnitudes – 3%, 6%, 10%, or 12%. Each experiment was performed twice and yielded three isolated repeats per experiment.

All experiments used the same method as that described in Section 3.2.4.3. For each experiment, one control plate was harvested immediately after the initial loading of the strain apparatus as a 0 hr control time-point. At 0.5, 1, 3, 6, 12, 24, 48, and 72 hrs, a strained and a control plate were each harvested and the lipids were extracted as described in Sections 2.2.2 and 2.2.3. Cell count and viability by trypan blue exclusion were also assessed as described in Section 2.2.2 to assess cell survival.

Consecutive ESI-MS scans across the m/z range of 250-950 in the negative and positive ion modes were performed. $C_{16:0}$, $C_{24:1}$, and $C_{24:0}$ ceramide, sphingosine (m/z of 299), and S-1-P (m/z of 379) levels were measured in the negative ion mode scan and $C_{16:0}$ sphingomyelin levels

were measured in the positive ion mode scan. The TICs of these sphingolipid species were normalized to $C_{16:0}$:$C_{18:1}$ PC (m/z of 794 in the negative mode and 782 in the positive ion mode) as described in Section 2.2.4.3. Statistical significance of the change in sphingolipid species was evaluated by one-way ANOVA with a Bonferroni posttest using Prism Version 4.

Data regarding changes in sphingomyelin, sphingosine, and S-1-P are presented in Chapter 4.

3.2.4.5 Variation of frequency of strain

To determine how whole-cell levels of $C_{16:0}$, $C_{24:1}$, and $C_{24:0}$ ceramides vary over time in response to different frequencies of cyclic strain, a set of four separate experiments was performed. Each experiment was performed using the same strain magnitude (10%), but different strain frequencies – 0.5 Hz, 1 Hz, 1.5 Hz, and 2 Hz. Each experiment was performed twice and yielded three isolated repeats per experiment.

All experiments used the same method as that described in Section 3.2.4.3. For each experiment, one control plate was harvested immediately after the initial loading of the strain apparatus as a 0 hr control time-point. At 0.5, 1, 3, 6, 12, 24, 48, and 72 hrs, a strained and a control plate were each harvested and the lipids were extracted as described in Sections 2.2.2 and 2.2.3. Cell count and viability by trypan blue exclusion were also assessed as described in Section 2.2.2 to assure cell survival.

Consecutive ESI-MS scans across the m/z range of 250-950 in the negative and positive ion modes were performed. $C_{16:0}$, $C_{24:1}$, and $C_{24:0}$ ceramide, sphingosine (m/z of 299), and S-1-P (m/z of 379) levels were measured in the negative ion mode scan and $C_{16:0}$ sphingomyelin levels were measured in the positive ion mode scan. The TICs of these sphingolipid species were

normalized to $C_{16:0}$:$C_{18:1}$ PC (m/z of 794 in the negative mode and 782 in the positive ion mode) as described in Section 2.2.4.3. Statistical significance of the change in sphingolipid species was evaluated by one-way ANOVA with a Bonferroni posttest using Prism Version 4.

Data regarding changes in sphingomyelin, sphingosine, and S-1-P are presented in Chapter 4.

3.3 RESULTS

3.3.1 Benchmark assessment of ceramide response to cyclic strain

With the addition of 10% cyclic strain at 1 Hz for 24 hours, bAECs undergo a marked increase in intracellular accumulation of $C_{16:0}$, $C_{24:1}$, and $C_{24:0}$ ceramides (Figure 3.2). All data are presented as mean ± SEM, with n=5. In the strained cells, normalized levels of $C_{16:0}$ ceramide were 2.34 ± 0.14 compared to 1.14 ± 0.20 in control cells; normalized levels of $C_{24:1}$ ceramide were 3.15 ± 0.25 compared to 1.36 ± 0.29 in control cells; and normalized levels of $C_{24:0}$ ceramide were 2.51 ± 0.25 compared to 1.14 ± 0.21 in control cells. Statistical significance was achieved in each comparison ($p<0.005$). Thus, in response to 24 hours of 10% cyclic uniaxial strain at 1 Hz frequency, all three of the major species of ceramide experience at least a two-fold increase compared to controls.

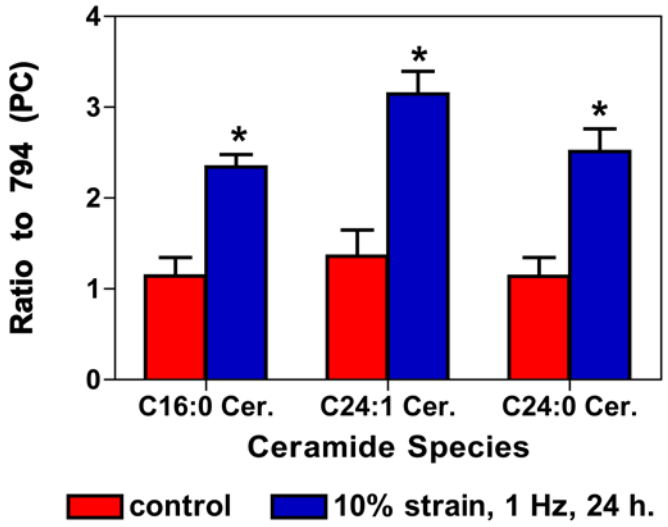

Figure 3.2. Cyclic strain causes increases in C_{16}, $C_{24:1}$, and $C_{24:0}$ ceramides. bAECs were subjected to 10% uniaxial, cyclic strain, 1 Hz for 24h. Results are expressed as mean ± SEM of the ratios of total ion counts for specific ceramide species to that of phosphatidyl choline (PC). * = $p<0.005$ (n=5)

3.3.2 Cessation of strain

Following cessation of strain, the ceramide changes initially seen are rapidly lost, suggesting that strain-induced ceramide changes only occur while the cell is actively being strained (Figure 3.3). The same is true for changes in the metabolite sphingomyelin (SM). Changes in sphingosine and S-1-P were not significant. By 12 hours, a small, but significant increase in ceramide species relative to control is again observed. The normalized ceramide or metabolite content of strained cells is expressed as a ratio to the corresponding normalized ceramide or metabolite content of the matched unstrained control. The data shown are the average of three experimental repeats.

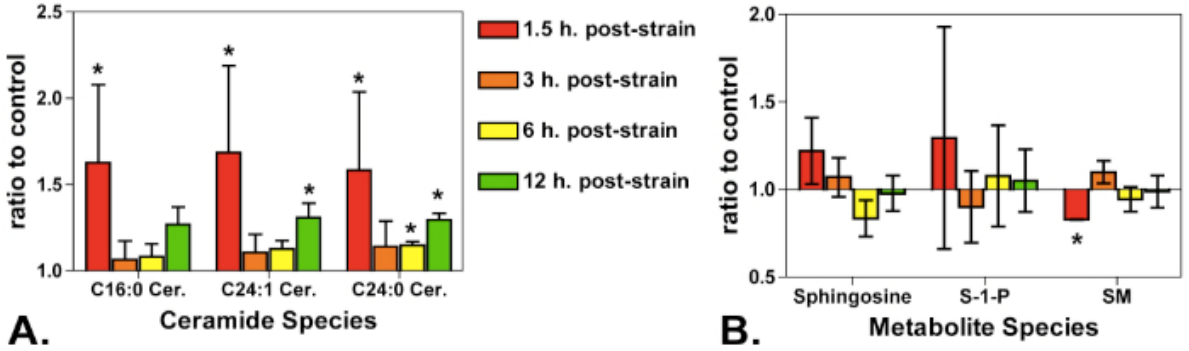

Figure 3.3. Ceramide and sphingomyelin changes are lost upon cessation of strain. bAECs were subjected to 10% uniaxial strain, 1Hz for 24 hrs. Cells were harvested and processed such that the time of lipid extraction occurred at 1.5, 3, 6, or 12 hrs following cessation of strain. The total ion count of the species of interest was normalized to PC and the data shown expresses the ratio of the strained group to matched controls (mean ± SEM). (A) shows how ceramide increases are lost following strain cessation and (B) shows how ceramide metabolite changes vary following strain cessation (only sphingomyelin demonstrated a statistically significant initial change compared to control). * = $p<0.05$ (n=3)

3.3.3 Variation of duration of strain

When cells are exposed to 10% cyclic strain at 1 Hz, the time response reveals that whole-cell ceramide levels are not constant over time (Figure 3.4). Although the lack of cellular synchrony between experiments complicates the statistical evaluation of the early time points, the results still suggest the presence of an early rise in ceramide within the first few hours as well as a prolonged rise in ceramide levels over the first few days. This observation is in agreement with the time scale of ceramide generation in response to other cellular stresses. These observations in the cyclic strain model will be confirmed later with studies using pharmacological inhibitors against *de novo* synthesis and SM hydrolysis to elucidate the specific contribution of these

pathways to total ceramide accumulation. Results for $C_{24:1}$ and $C_{24:0}$ ceramide are comparable to those of C_{16} ceramide. The normalized ceramide content of strained cells is expressed as a ratio to the corresponding normalized ceramide content of the matched unstrained control. None of the data were statistically significant ($p \leq 0.05$), although most data points were trending towards significance ($p \leq 0.15$). The data shown are the average of five experimental repeats.

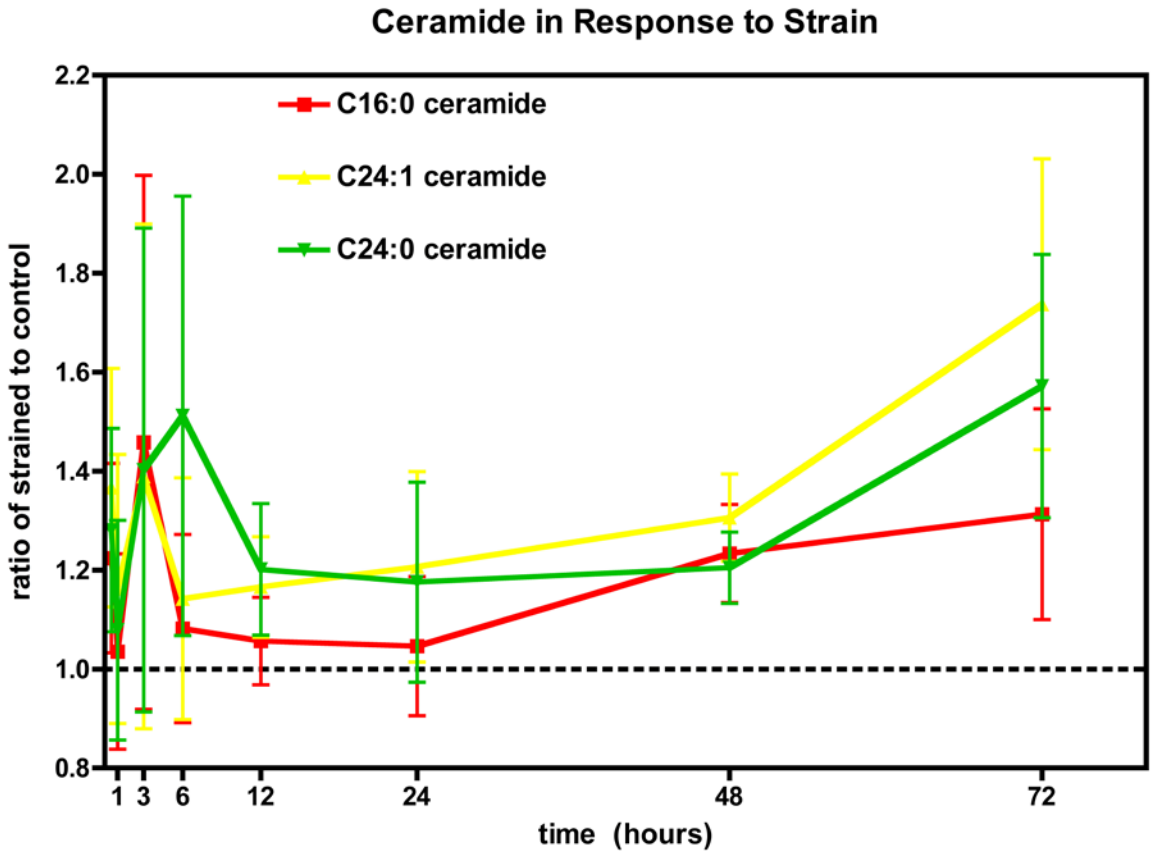

Figure 3.4. Time scale of ceramide accumulations suggests the contribution of both early membrane-associated ceramide production and late *de novo* ceramide synthesis. bAECs were subjected to 10% uniaxial strain, 1Hz for 0-72h. and harvested at time points shown for lipid extraction and ceramide analysis. As previously, total ion count of ceramide is normalized to that of PC and the data shown is expressed as a ration of the strained group to the control. (n=5)

3.3.4 Variation of magnitude of strain

When bAECs were exposed to different strain magnitudes from 3%-12%, all at a frequency of 1 Hz, it should be noted that the previously described early and late ceramide responses can still be observed in all but the 3% strain intensity (subphysiological) (Figure 3.5). The data also suggests that above or below a normal physiological level of 6% strain, that bAECs exhibit elevated levels of $C_{16:0}$ and $C_{24:1}$ ceramides, particularly within the first 24 hours.

The normalized ceramide content of strained cells is expressed as a ratio to the corresponding normalized ceramide content of the matched unstrained control. None of the data were statistically significant ($p \leq 0.05$), although many data points were trending towards significance ($p \leq 0.15$). The data shown are the average of five experimental repeats.

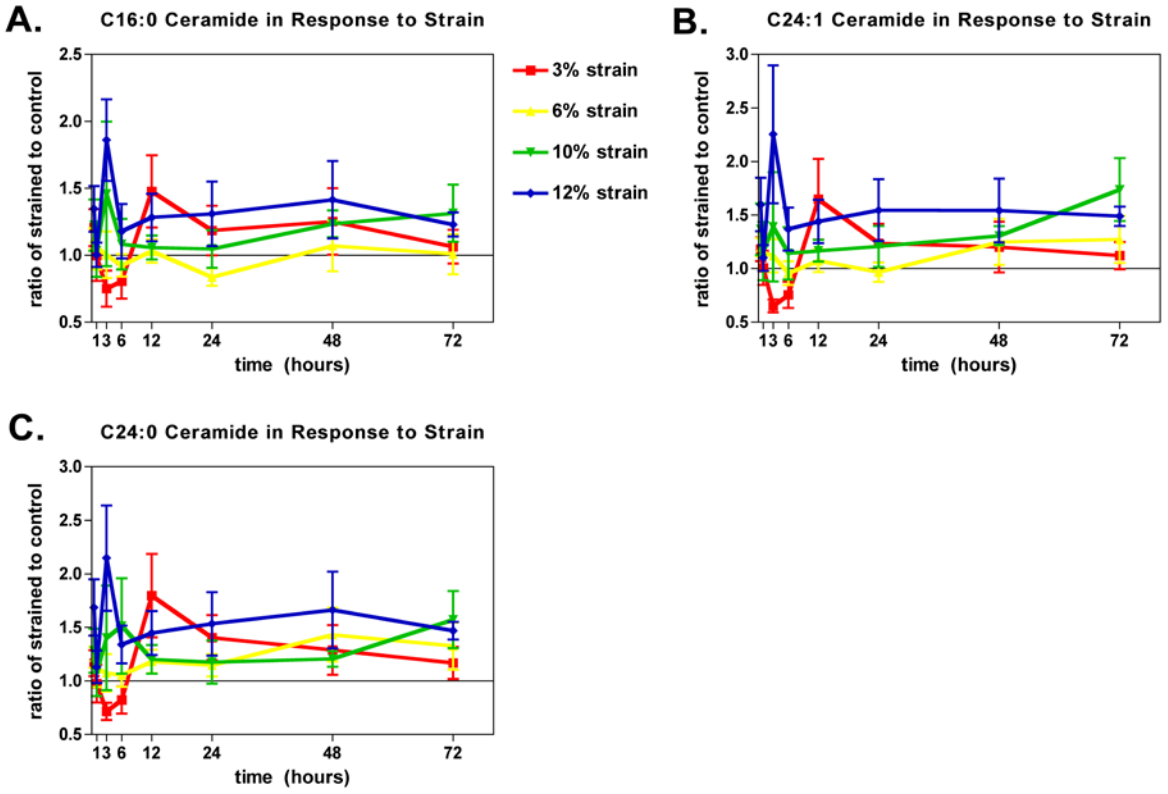

Figure 3.5. Ceramide regulation is tuned to strain intensity. Above or below normal physiological strain intensity (6%), bAECs exhibit elevated C_{16} (A) and C_{24} ceramide levels (B and C). Also observe that at all but the subphysiological strain intensity (3%), the previously described early and late ceramide responses appear to be involved. bAECs were exposed to 3, 6, 10, or 12% strain at 1Hz for up to 72hrs with harvest and lipid extraction for ceramide analysis performed at time points shown between 30 min and 72 hrs. The total ion count of ceramide is normalized to that of PC and the data shown is expressed as a ratio of the strained group to the control. (n=5)

3.3.5 Variation of frequency of strain

At 6% cyclic strain, variation of strain frequency between 0.5 Hz and 2 Hz did not appear to affect long-term ceramide accumulation compared to a frequency of 1 Hz (Figure 3.6).

The normalized ceramide content of strained cells is expressed as a ratio to the corresponding normalized ceramide content of the matched unstrained control. None of the data were statistically significant ($p \leq 0.05$). The data shown are the average of four experimental repeats for 0.5 Hz and 1 Hz data and three experimental repeats for 1.5 Hz and 2 Hz data.

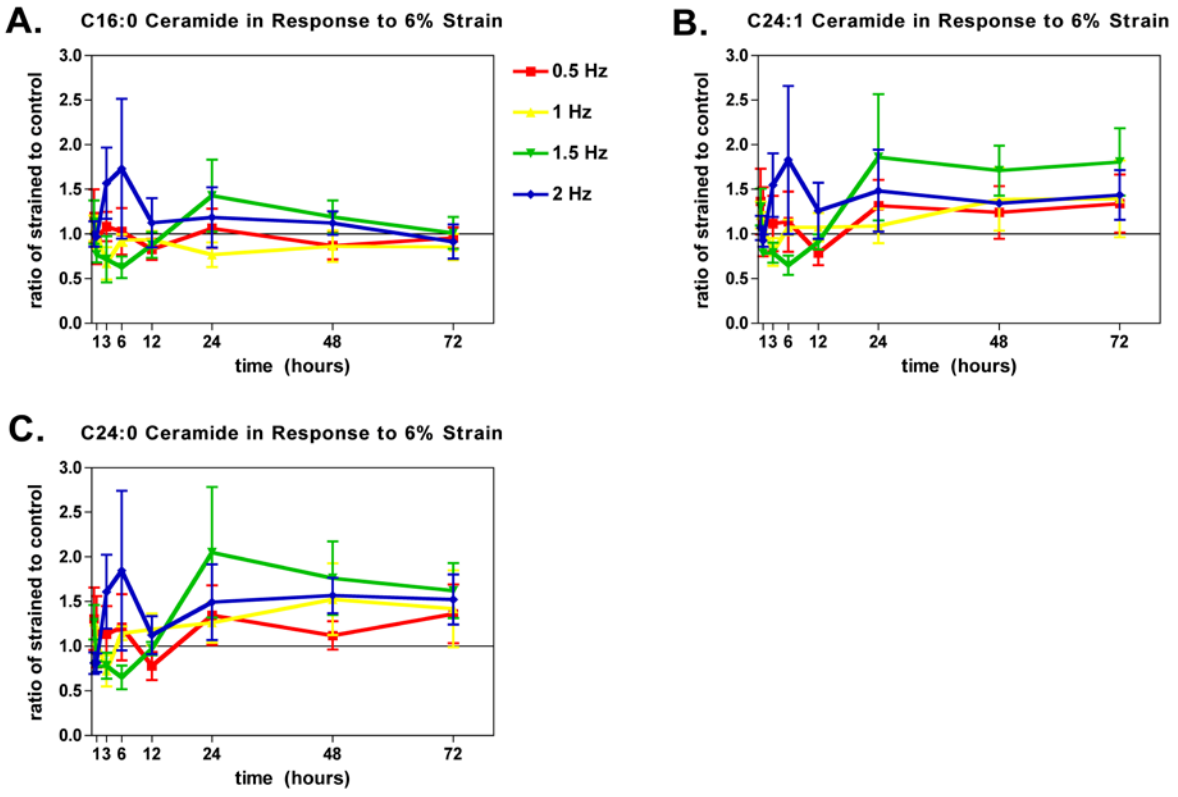

Figure 3.6. Ceramide levels do not vary with frequency at 6% cyclic strain. bAECs were exposed to 6% strain at 0.5, 1, 1.5, or 2 Hz for up to 72 hrs with harvest and lipid extraction for ceramide analysis performed at time points shown between 30 min and 72 hrs. (A) shows changes in $C_{16:0}$ ceramide levels, (B) shows changes in $C_{24:1}$ ceramide, and (C) shows changes in $C_{24:0}$ ceramide. As previously, total ion count of ceramide is normalized to that of PC and the data shown is expressed as a ratio of the strained group to the control. (n=3-4)

3.4 DISCUSSION

3.4.1 Application and cessation of cyclic strain

Evaluation of a single time-point and strain regimen on bAECs – 10% strain at 1 Hz for 24 hrs – reveals that all the major species of ceramide do change in response to uniaxial cyclic strain (Figure 3.2). When discussing a change in a signaling molecule like ceramide, the next natural question is to ask whether the observed increases in ceramide require the continuous application of strain to maintain the change, or whether an initial period of application sets the cells down a committed path of signaling events, such that removal of the strain stimulus would not change the resulting outcome.

To test this, we exposed bAECs again to the same regimen of cyclic strain for 24 hours and, at the end of this period, removed the plates from the strain apparatus and returned them to static culture. Interestingly, the initial elevations in ceramide were quickly lost upon removal of the strain stimulus (Figure 3.3), as were any changes in sphingomyelin. This suggests that the observed ceramide signaling requires active straining of the cells and that removal of the strain stimulus returns the cells to the unstrained state.

Considered in the context of mechanotransduction, this finding makes sense. If a cell encounters an increase in the local forces being applied to it (i.e. acute hypertension or vein-to-artery grafting), it needs to trigger appropriate signaling pathways in response. Once the strain stimulus is removed (i.e. return to normotension or remodeling of the vessel to compensate for increased strain), prolonged signaling, particularly ceramide signaling, could be detrimental to the cell survival.

This data also stresses the importance of consistent experimental technique and potential introduction of experimental error in this type of experiment. The first time-point chosen for the strain cessation experiments is 1.5 hrs, which is slightly longer than the amount of time necessary to disassemble the strain apparatus, harvest the cells, and extract the lipids, and as such, closely represents the technical conditions of a standard lipid extraction as used in this body of work. By three hours, the detectable change in ceramide is lost, which means that it is absolutely critical to employ consistent technique with regards to the timing of the extraction and potentially even the person performing the extraction.

It should be noted that there is a small but significant increase in ceramide relative to control by 12 hrs post-strain, although this difference is considerably less than that observed at 1.5 hrs post-strain. Between 6 and 12 hours following cessation of strain, the typical cellular alignment observed in response to strain is lost, as observed by light microscopy, indicating that the cells are changing their orientation and potentially their integrin profile as well. This process may require an increase in ceramide to participate in lipid rafting to facilitate integrin and focal adhesion rearrangement. Further studies of lipid raft content and focal adhesions following cessation of strain would be necessary to confirm this possibility as it cannot be proved by changes in the whole-cell lipid profile.

It is worth noting that one of the potential difficulties expected with the use of the Flexcell FX4000T is the fact that strain is not uniformly applied across the entire culture substrate of the BioFlex plate, only across the region over the loading post. Thus, we may encounter some degree of variability of ceramide detected based upon the distribution and homogeneity of cells across the strained surface compared to regions on the periphery. During culture, bAECs and hAECs tend to grow most heavily in the centers of the wells in the region

that is positioned over the loading post, which somewhat minimizes the contribution of these nonhomogeneous strain regions around the periphery of the well. The BioFlex plate, which has the culture adhesion surface across the entire well, was chosen for these experiments rather than the similar UniFlex plate, which has the culture adhesion surface only in a defined rectangular region over the arctangle loading post, because it was felt that the contribution of adhesion matrix composition affecting any cells that persist in growing on the uncoated regions of the UniFlex plate (i.e. cellular stress associated with culture on the untreated silicone membrane) was potentially greater and less controlled from experiment to experiment than the contribution of uneven strain distribution towards the periphery of the BioFlex plate.

Another potential problem with the FX4000T system is that a small amount of media evaporation is to be expected in the strained cultures compared to the static controls. ECs are sensitive to preconditioning of their microenvironment and prefer to be grown at a specific ratio of cell density to media volume. This makes it difficult to offset evaporation with a larger culture volume or exchanging the media of the system, which as introduced cellular stresses, can be expected to affect ceramide expression. It should be noted, however, that any contribution to cellular stress from evaporation in the strain apparatus or uneven strain distribution across the membrane are encountered in all strain experiments and will thus be routine across treatment conditions in comparisons of strain parameters by lipid profile.

3.4.2 Variation of time, magnitude, and frequency of cyclic strain over time

To examine whether ceramide generation due to cyclic strain is indicative of an early response, suggesting membrane-associated ceramide formation from sphingomyelin; a later response, suggesting *de novo* synthesis; or both types of responses, bAECs were subjected to 10% uniaxial

cyclic strain, 1Hz with lipid extractions for ceramide analysis performed after 0.5, 1, 3, 6, 12, 24, 48, and 72 hrs of strain (Figure 3.4). Although the lack of cellular synchrony between experiments complicates the statistical evaluation of the early time points, the results still suggest the presence of an early rise in ceramide within the first few hours as well as a prolonged rise in ceramide levels over the first few days. This observation is in agreement with the time scale of ceramide generation in response to other cellular stresses. Very interestingly, the data within the first 6 hours suggests that there may be two rises in ceramide at 0.5 and 3 hours, suggesting that there may even be two signaling events occurring within this period. The presence of two ceramide increases within that time frame suggests the possible involvement of two different sphingomyelinases.

These observations in the cyclic strain model will be confirmed in Chapter 4 with studies using pharmacological inhibitors against *de novo* synthesis and SM hydrolysis to elucidate the specific contribution of these pathways to total ceramide accumulation.

When the same time-course was repeated but strain magnitude was varied to reflect subphysiological (3%), normal physiological (6%), and high physiological strain intensities (10% and 12%), all at 1Hz frequency, similar time-dependant increases in ceramide were observable for all regimens except the 3% strain intensity (Figure 3.5). If the time response is indeed reflective of the presence of an early ceramide increase due to membrane-associated sphingomyelin hydrolysis whereas the later, prolonged increase in ceramide may be due to *de novo* synthesis, this finding suggests that a threshold level of strain may be necessary to elicit sphingomyelin hydrolysis. Being that ECs do not align perpendicular to strain below 5% strain magnitude, it may be possible that either this early ceramide increase is caused by or is necessary for cell alignment. Of course, further experiments using inhibitors to ceramide synthetic

pathways at physiological strain levels as well as experiments examining whether increasing endogenous ceramide, potentially through bacterial S Mase, at subphysiological strain levels would be necessary to determine whether the lack of the early ceramide response at 3% strain is associated with the failure of cells to align.

When viewing the change in ceramide levels in response to change in strain magnitude (Figure 3.5), it is also interesting to consider that the data suggests that subphysiological (3%) and high physiological (10% and 12%) magnitudes of strain show a greater increase in ceramide relative to that occurring in response to normal physiological strain (6%). This would suggest that endothelial cells require a certain amount of strain to achieve optimum growth conditions, but that elevation beyond that point can be harmful to the cell. One would expect levels of ceramide generated to have something of a linear response to increasing strain such that cells exposed to 3% strain would have lower ceramide levels than cells exposed to 6% strain. However, if one considers that ECs align to reduce net intracellular stress, one might expect to see an increase in a cellular stress signaling molecule like ceramide in a cell that was unable to accomplish this goal without alignment, hence the relative increase in ceramide in cells exposed to 3% strain compared to 6% strain.

These findings regarding 3% strain are particularly interesting in the context of arterial stiffness associated with calcified atherosclerotic plaques and progressive vascular disease. If one defines endothelial cell health in terms of the activity of cellular stress signaling pathways, reduction in cellular strain in the wrong population of ECs (aortic ECs), may be as detrimental as an elevation in strain. This observation should also be considered in the context of tissue engineered vascular conduits in which maintenance of an intact and normally functioning endothelium is necessary for conduit success [42].

Of course, when considering strain magnitude, which is also reflective of pulse pressure, it is important to consider that these findings utilize aortic ECs, and that different results might be observed in ECs of microvascular or venous origin reflective of phenotypic differences.

Variation of cyclic strain frequency across a range to include 0.5 Hz (below physiological, representing a heart rate of 30 bpm), 1 Hz (normal physiological, representing a heart rate of 60 bpm), 1.5 Hz (high physiological, representing a heart rate of 90 bpm), and 2 Hz (abnormally high physiological, representing a heart rate of 120 bpm), all maintaining a normal physiological strain magnitude of 6% does not appear to affect long-term ceramide accumulation (Fig. 3.6). In the context of normal arterial conditions, this suggests that a change in heart rate at a normal blood pressure is less detrimental than an increase in blood pressure at a normal heart rate.

Another clinical situation that could be modeled using the existing FX4000T system would be to evaluate 3% strain at 2 Hz. This regimen would model the vasculature during cardiogenic shock in which a patient encounters hypotension and tachycardia. It would be interesting to see whether such conditions resulted in a further change in ceramide compared to 3% strain at 1 Hz, particularly if changes in ceramide signaling in the arterial circulation result in endothelial activation and production of soluble factors that could affect the microvasculature, all potentially contributing to the end stage organ and vascular dysfunction encountered by these patients.

Of course, there are several experimental limitations to consider when evaluating these frequency findings. The ability to generate experimental strain magnitude and frequency in the FX4000T strain apparatus is limited by the ability to generate an appropriate vacuum and to shuttle air through the system as vacuum is applied and released at the underside of the

deformable culture substrate membrane. Thus, in order to generate higher magnitudes of strain, one is limited to a lower range of frequencies. Similarly, when generating higher frequencies of strain, one is limited to lower strain magnitudes. Initial assessment revealed that 6% strain could be achieved at 2 Hz, but that 10% strain could not. It is very possible that at high physiological strains such as 10 or 12%, that elevated strain frequency may produce a change in ceramide levels within the cell. This would correspond to the clinical occurrence of a patient with hypertension and high heart rate.

At high frequencies and high magnitudes, the deformable culture substrate on the BioFlex plates may also experience some amount of creep over time, which would have resulted in a reduction in the strain magnitude encountered by the cell. Creep describes the tendency of a material to permanently deform over time in response to a stress, and in this case would suggest a ballooning of the deformable membrane over time causing the application of the same force over a greater surface area to result in lower strain magnitudes. While endothelial cells strained at or above 6% did retain their alignment, suggesting that a magnitude of at least 5% was maintained under these conditions, it is possible, particularly at the later time points of 48 and 72 hrs, that the true strain encountered by the cells was less than the intended strain, which may in part account for the closeness of many of the variables at the 72 hr time-points in Figures 3.5 and 3.6. Evaluation of the deformation properties of the substrate membrane alone over time at the various strain regimens employed would be necessary to confirm or deny the possible influence of creep at the later experimental time-points.

3.4.3 Statistical considerations

The time-course data presented in this chapter frequently show strong evidence towards conclusions, but fail to achieve statistical significance of $p \leq 0.05$. Often, this is reflective of the low numbers of experimental repeats presented, as may be the case with the strain frequency data for which results express only three or four data repeats. The number of times an experiment was performed is described in the methods, whereas the results describe the number of times an experiment was analyzed by mass spectrometry.

At the earliest time-points occurring within six hours, lack of synchrony of cells across experiments and even between two wells on the same plate may contribute to subtle differences in ceramide detected. Ceramide levels detected in whole cell extracts represent a snapshot of the sum of the contributions of all ceramide biosynthetic and metabolic pathways. If a transient spike in signaling occurs fifteen minutes sooner or later in one sample than in other samples, it will potentially increase the sample variation at two time-points. Thus, in describing the early ceramide signaling increases that appear to occur at 30 minutes and 3 hours, caution has been used. Especially at the 30-minute time-point, the amount of ceramide detected is likely the trailing shoulder of a ceramide spike that has occurred prior to 30 minutes, which is consistent with the timeframe of membrane-associated sphingomyelin hydrolysis, particularly by nSMase.

Some researchers choose to compensate for lack of cellular synchrony by serum starving the cells prior to introducing the cellular stress, but since serum starvation is a cellular stress in itself and can affect ceramide levels, this method was not employed in these studies so that the results we present describe only the effects of cyclic strain on ceramide generation and not that

associated with serum withdrawal. To partially reduce the contribution of culture variation from well to well within the same plate, two wells were always combined for each lipid extraction.

Additionally, to normalize the data presented to account for signal variation between mass spectrometry runs and to adjust for cell count and volume across samples, ratios were frequently employed, and at times, ratios of ratios. Ratios are inherently asymmetrical, making a t-test, for example, somewhat ambiguous.

Finally, when discussing whole-cell levels of a molecule active in signaling, it is important to consider that *functionally significant* and *statistically significant* are not synonymous. Advocates of the dose-response approach to analyzing mechanotransduction signaling support a focus on functional significance beyond just statistical significance [105]. Since the impact of ceramide on cell fate is dependent on the site and source of ceramide generation, it is important to recognize that functionally relevant differences may be reflected by a statistically small increase. Prior studies have shown that atherosclerotic tissue has approximately 1.5-fold increase in ceramide compared to normal arterial tissue by wet weight [2]. This is consistent with the fold increase in ceramide observed at later time-points illustrated in Figures 3.2 and 3.4. Thus, true validation of the ceramide data presented rests in linking ceramide changes to biological outcomes in cyclically strained ECs.

3.5 CONCLUSIONS

Cyclic, uniaxial strain applied at a variety of magnitudes (3% - 12%) and frequencies (0.5 Hz - 2 Hz) representing variation from subphysiological to elevated, pathophysiological states of

arterial strain conditions, demonstrates that $C_{16:0}$, $C_{24:1}$, and $C_{24:0}$ ceramides are elevated in bAECs in response to cyclic strain. Furthermore, application of cyclic strain is necessary to sustain elevated ceramide levels; removal of the strain stimulus results in a rapid return to ceramide levels comparable to those seen in unstrained control cells. Evaluation of the time response suggests that bAECs exhibit an early and a late ceramide signaling event, suggestive of the involvement of both hydrolysis of membrane-associated sphingomyelin as well as *de novo* synthesis in ceramide generation.

4.0 CERAMIDE BIOSYNTHESIS AND METABOLISM DURING CYCLIC STRAIN

4.1 INTRODUCTION

The data presented in Chapter 3 indicate that ceramide is generated in response to cyclic, uniaxial strain. Ceramide represents a central molecule in sphingolipid signaling and biology, and can be generated through *de novo* synthesis or through hydrolysis of sphingomyelin or other complex sphingolipids [63, 64]. Ceramide as well as its metabolites, like S-1-P, are biologically active and the ultimate fate of a cell is believed to be determined by the net effect of the activity of all these pathways in response to a stress [65]. In particular, the concept of the balance of ceramide and S-1-P activity acting as a rheostat to push a cell towards death or survival has been proposed [80]. Both ceramide and S-1-P have been shown to cause autophagy. Ceramide generated by SM hydrolysis induces an autophagic death while S-1-P was associated with a pro-survival type of autophagy [104].

The time-course response of ceramide in bAECs in response to cyclic strain described in Section 3.3.3 and supported in Section 3.3.4 suggests that ceramide generation has an early and a late response, suggesting that both SM hydrolysis and *de novo* synthesis are at work. There is evidence that both neutral SMase, active in the plasma membrane, and acidic SMase, predominant in lysosomes but capable of translocating to the plasma membrane, may be active in ECs in response to stressors [62, 82, 83]. The appearance of a spike in ceramide levels at 30

minutes and again at 3 hours suggests that both aSMase and nSMase may be responsible for early ceramide signaling.

The finding that continuous application of cyclic strain is necessary to maintain elevated ceramide levels (Section 3.3.2), suggests that regulation of ceramide synthesis is linked to mechanosensing. Thus, SM hydrolysis and *de novo* synthesis may work together to regulate and maintain the ceramide signaling response to cyclic strain.

To test this hypothesis, more extensive evaluation of changes in major ceramide metabolites like sphingosine and S-1-P as well as hydrolysable sphingolipids like SM will be necessary. To specifically assess the roles of SM hydrolysis and *de novo* synthesis of ceramide in the EC response to strain, inhibition of the appropriate enzyme pathways will be necessary.

This chapter will specifically address the third specific aim:

Determine which ceramide biosynthetic pathways are activated upon exposure of aortic endothelial cells to cyclic, uniaxial strain and determine the abundance of ceramide metabolites.

1. Determine if levels of sphingomyelin, sphingosine, and sphingosine-1-phosphate are altered in response to cyclic strain.
2. Determine the effects of inhibitors of *de novo* ceramide synthesis and hydrolysis of sphingomyelin to ceramide, on cyclic strain-induced ceramide levels.

4.2 METHODS

4.2.1 Response of sphingosine, S-1-P, and sphingomyelin to cyclic strain

Studies of changes in whole-cell levels of sphingosine, S-1-P, and sphingomyelin in bAECs were performed concurrently with evaluation of ceramide level changes in response to the varied time, magnitude, and frequency regimens described in Table 3.1. Thus, the experimental methods are outlined in Section 3.2.

During ESI-MS analysis, consecutive scans across the m/z range of 250-950 in the negative and positive ion modes were performed. In addition to $C_{16:0}$, $C_{24:1}$, and $C_{24:0}$ ceramides, sphingosine (m/z of 299), and S-1-P (m/z of 379) levels were measured in the negative ion mode scan and $C_{16:0}$ sphingomyelin levels were measured in the positive ion mode scan. The TICs of these sphingolipid species were normalized to $C_{16:0}$:$C_{18:1}$ PC (m/z of 794 in the negative mode and 782 in the positive ion mode) as described in Section 2.2.4.3. Statistical significance of the change in sphingolipid species was determined by paired t-test comparing the strained cells to the unstrained controls for the benchmark assessment at 24 hrs, following 10% strain at 1 Hz and by one-way ANOVA with a Bonferroni posttest for magnitude and frequency data using Prism Version 4.

4.2.2 Selective inhibition of aSMase, nSMase and *de novo* ceramide synthesis

Three pharmacological inhibitors were employed to selectively inhibit hydrolysis of acid or neutral sphingomyelinase or *de novo* ceramide synthesis. The inhibitors and the concentrations used are described in Table 4.1. Manumycin A prepared from *Streptomyces parvulus*,

desipramine, and L-cycloserine were purchased from Sigma. Manumycin A (hereafter called manumycin) is maintained as a stock 5 mg/mL solution in pure ethanol. Desipramine and L-cycloserine are both stored as powders and were prepared as 1 mM stocks in EGM medium and were sterile filtered through a syringe filter (Fisher Scientific). All media containing inhibitors were prepared fresh immediately prior to use. The concentrations used were chosen because they were previously demonstrated in pilot studies to be the highest concentration capable of eliciting inhibitory function in hAECs during 10% cyclic strain at 1 Hz without compromising cell viability by trypan blue exclusion.

Table 4.1. Inhibitors of ceramide synthesis

Inhibitor	Ceramide synthetic pathway blocked by inhibitor	Specific target of inhibitor	Concentration used
Manumycin A	SM hydrolysis	nSMase	2 μM
Desipramine	SM hydrolysis	aSMase	50 μM
L-cycloserine	*de novo* synthesis	ketosphinganine synthatase	1 mM

hAECs were chosen for the inhibitor experiments because future experiments assessing direct EC functionality in response to perturbation of ceramide signaling will be performed in hAECs due to the expanded clinical relevance of the human cell source as well as the increased availability of commercial immunoassays for human cell systems. While some of these assays could be done in bovine cells, relying upon species cross-reactivity, it was more logical to switch to human cells for the inhibitor studies.

For each inhibitor experiment, two vials of hAECs ($2x10^6$ total live cells) were thawed and passed into three T-75 flasks containing EGM (Section 2.2.2). When cells achieved 80% confluence, they were passed into sixteen BioFlex ProNectin-coated 6-well plates using the same technique as described in Section 2.2.2. For strain cessation experiments, only eight BioFlex

ProNectin plates were seeded with cells. The media was replaced with 2 mL EGM on the first day after plating and every two days thereafter.

When the cells achieved 80% confluence, after approximately four to five days, the media in fifteen of the plates was replaced with 2 mL/well fresh untreated EGM or EGM containing 2 μM manumycin, 50 μM desipramine, or 1 mM L-cycloserine, pre-warmed to 37°C. Two wells received untreated EGM and two wells received EGM containing the inhibitor of interest. The media in the sixteenth plate was replaced with 2 mL/well untreated EGM, the cells were immediately harvested, and the lipids were extracted, pooling two wells per sample as a pre-treatment control as described in Sections 2.2.2 and 2.2.3. Cell count and viability by trypan blue exclusion were also assessed as described in Section 2.2.2 to assure cell survival.

The fifteen treated plates were then returned to the humidified incubator @ 37°C, 5% CO_2 for 2 hours for manumycin studies and for 3 hours for desipramine and L-cycloserine studies to allow for full enzyme inhibition prior to loading the plates on the baseplate of the FX4000T strain apparatus.

To determine how whole-cell levels of $C_{16:0}$, $C_{24:1}$, and $C_{24:0}$ ceramides vary over time in response to cyclic strain in the presence of inhibitors to aSMase, nSMase, and *de novo* synthesis, seven plates of the inhibitor pre-treated hAECs were loaded onto the FX4000T baseplate and exposed to 10% strain at 1 Hz, using the plate rotation scheme outlined in Table 3.2. Seven identical plates of unstrained inhibitor pre-treated hAECs incubated in the same humidified incubator containing the FX4000T (37°C, 5% CO_2) served as the paired controls. One inhibitor pre-treated control plate was harvested immediately after the initial loading of the strain apparatus as a 0 hr control time-point. At 0.5, 1, 3, 6, 12, 24, and 48 hrs, a strained and a control plate were each harvested and the lipids were extracted as described in Sections 2.2.2 and 2.2.3.

Cell count and viability by trypan blue exclusion were also assessed as described in Section 2.2.2 to assure cell survival.

For each extraction, both wells containing either the control media or the inhibitor-treated media were pooled during harvest. As a result, each experiment yielded only one experimental repeat with a matched control. Each inhibitor experiment was performed three separate times.

Consecutive ESI-MS scans across the m/z range of 250-950 in the negative and positive ion modes were performed. $C_{16:0}$, $C_{24:1}$, and $C_{24:0}$ ceramide levels were measured in the negative ion mode scan and $C_{16:0}$ sphingomyelin levels were measured in the positive ion mode scan. The TICs of these sphingolipid species were normalized to $C_{16:0}$:$C_{18:1}$ PC (m/z of 794 in the negative mode and 782 in the positive ion mode) as described in Section 2.2.4.3.

4.3 RESULTS

4.3.1 Response of sphingosine, S-1-P, and sphingomyelin to cyclic strain

4.3.1.1 Benchmark assessment of sphingosine, S-1-P, and sphingomyelin to cyclic strain

After 24 hrs of 10% cyclic strain at 1 Hz, only sphingosine and sphingomyelin showed significant changes in bAECs, both resulting in decreases (Figure 4.1). Results are expressed as the ratio of TIC to PC. All data are presented as mean ± SEM, with n=5. After 24 hours of 10% cyclic strain at 1 Hz, sphingosine levels dropped from 0.120 ± 0.015 to 0.0783 ± 0.0090 ($p=0.046$) and sphingomyelin levels dropped from 0.326 ± 0.008 to 0.282 ± 0.010 ($p=0.013$). As shown in Figure 3.3, changes in sphingomyelin levels following cessation of strain rapidly return to baseline, comparable to the findings shown for ceramide changes. This suggests that

sphingomyelin/ceramide metabolism is intimately linked to mechanical strain. In Figure 3.3, it should be noted that the sphingosine levels at 1.5 hrs following cessation of strain, also strained for 24 hrs at 10% strain at 1 Hz, show an initial increase in sphingosine levels relative to control, whereas the benchmark data taken immediately following cessation of strain shows a decrease (Figure 4.1).

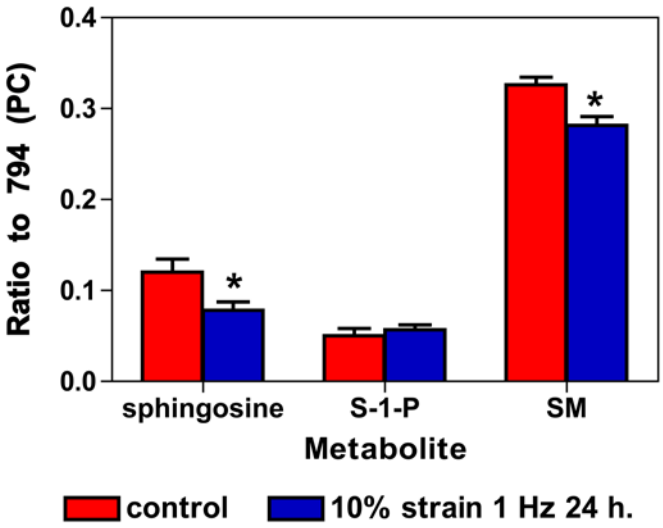

Figure 4.1. Cyclic strain causes decreases in sphingosine and sphingomyelin, but not S-1-P. bAECs were subjected to 10% uniaxial, cyclic strain, 1Hz for 24h. Results are expressed as mean ± SEM of the ratios of total ion counts for specific sphingolipids to that of phosphatidyl choline (PC). * = $p<0.005$ (n=5)

4.3.1.2 Response of sphingosine, S-1-P, and sphingomyelin to variation in magnitude and frequency of strain

Because the responses of sphingomyelin, S-1-P, and sphingomyelin to cyclic strain over time do not follow a standard response pattern, as ceramide species do, the time response of these sphingolipids will not be expressed separately, but will instead be discussed in the context of strain magnitude and frequency.

4.3.1.2.1 Metabolite response to variation of strain magnitude

When bAECs were exposed to different strain magnitudes from 3% -12%, all at a frequency of 1 Hz, it should be noted that each sphingolipid metabolite varies distinctively and not all follow a standard dose or time response to strain intensity. At all magnitudes except 10%, bAECs appear to experience a reduction in sphingosine, as seen in figure 4.2.A. This reduction is particularly evident at later timepoints in the 12-72 hr range. S-1-P levels do not appear to experience a consistent change over time (Figure 4.2. B), but the presence of clear response curves at all strain magnitudes suggest a transient early (<3 hrs) and intermediate (12-24 hrs) elevation in S-1-P levels. Only SM (Figure 4.2.C) appears to demonstrate a consistent reduction in response to strain at all but the subphysiological strain intensity (3%); this phenomenon is particularly pronounced at the high physiological strain intensity of 12%.

The normalized sphingolipid content of strained cells is expressed as a ratio to the corresponding normalized sphingolipid content of the matched unstrained control. None of the data were statistically significant ($p \leq 0.05$). The data shown are the average of five experimental repeats.

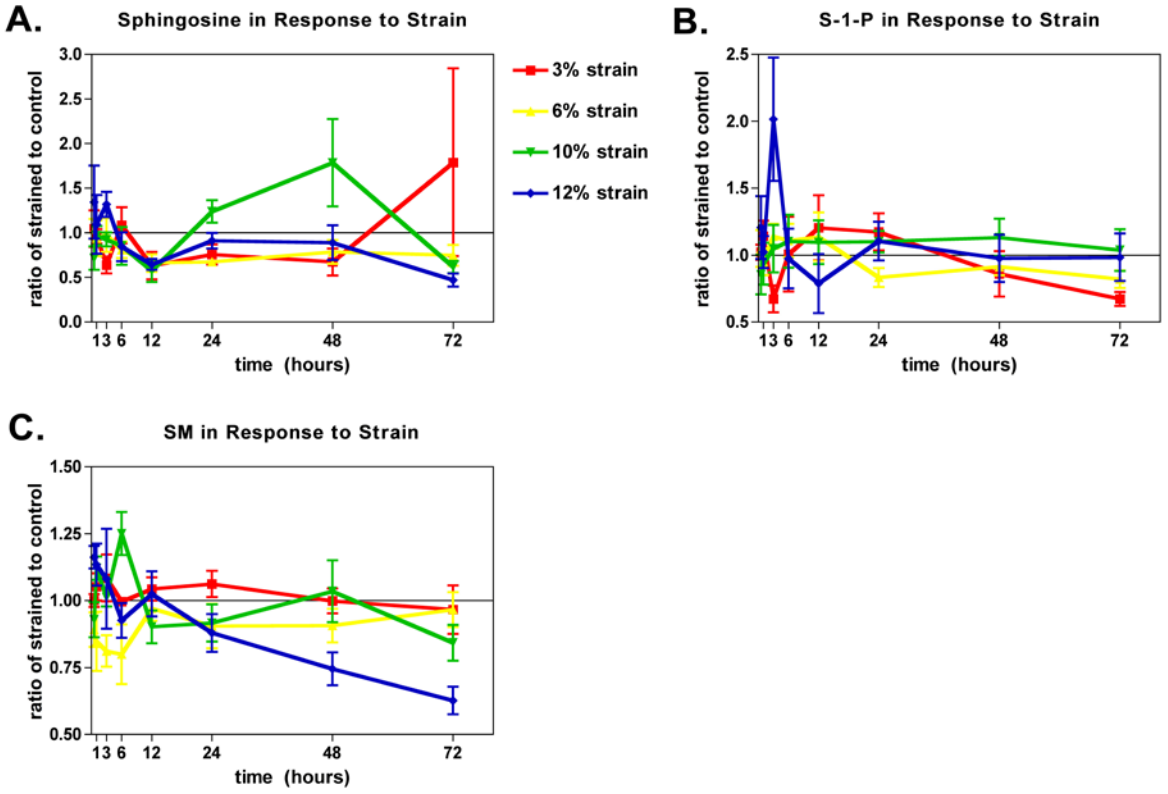

Figure 4.2. Sphingolipid metabolites of ceramide show some variation in response to cyclic strain magnitude. At all magnitudes except 10%, bAECs appear to experience a reduction in sphingosine (A). S-1-P levels do not appear to experience a consistent change over time, but the response curves at all strain magnitudes suggest a transient early (<3 hrs) and intermediate (12-24 hrs) elevation in S-1-P levels (B). Only SM (C) appears to demonstrate a consistent reduction in response to strain at all but the subphysiological strain intensity (3%); this phenomenon is particularly pronounced at the high physiological strain intensity of 12%. bAECs were exposed to 3, 6, 10, or 12% strain at 1Hz for up to 72 hrs with harvest and lipid extraction for sphingolipid analysis performed at time points shown between 30 minutes and 72 hours. The total ion count of each sphingolipid metabolite is normalized to that of PC and the data shown is expressed as a ratio of the strained group to the control. (n=5)

4.3.1.2.2 Metabolite response to variation of strain frequency

At 6% cyclic strain, variation of strain frequency between 0.5 Hz and 2 Hz did not appear to affect long-term changes in sphingosine, S-1-P, or sphingomyelin compared to a frequency of 1 Hz (Figure 4.3).

The normalized ceramide content of strained cells is expressed as a ratio to the corresponding normalized ceramide content of the matched unstrained control. None of the data were statistically significant ($p \leq 0.05$). The data shown are the average of four experimental repeats for 0.5 Hz and 1 Hz data and three experimental repeats for 1.5 Hz and 2 Hz data.

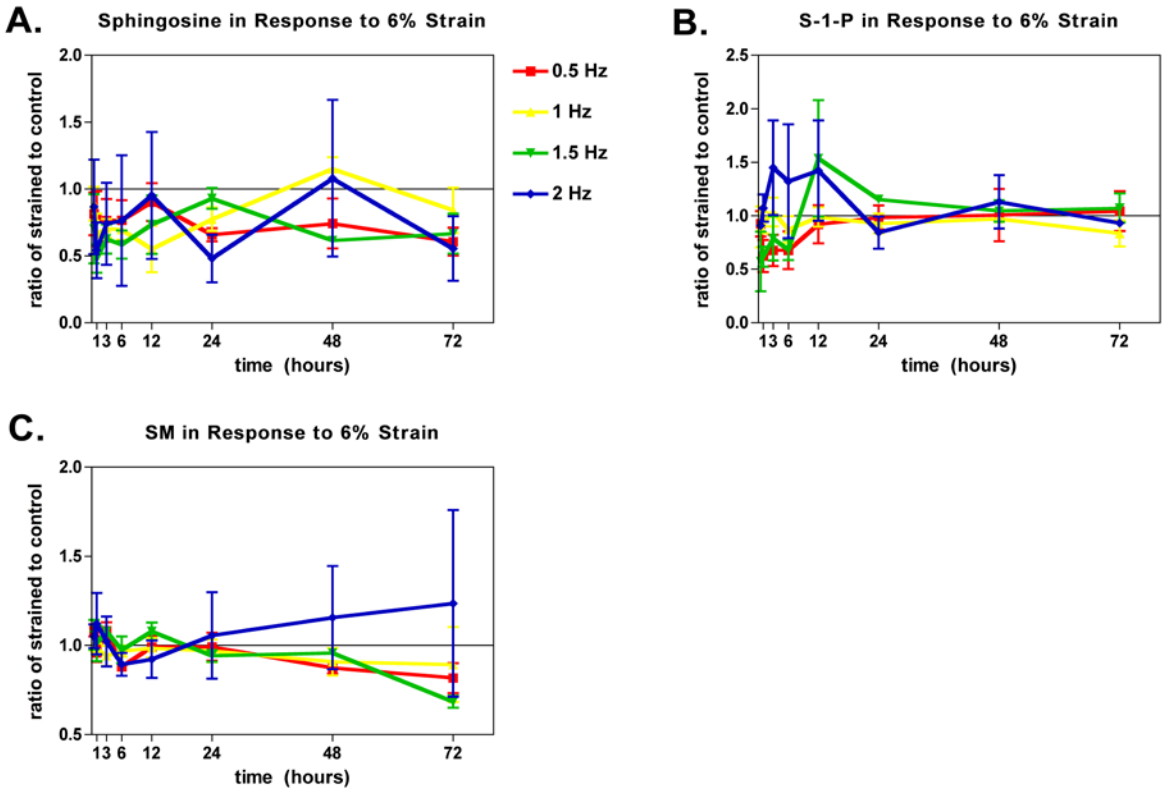

Figure 4.3. Sphingolipid metabolites do not vary with frequency at 6% cyclic strain. bAECs were exposed to 6% strain at 0.5, 1, 1.5, or 2 Hz for up to 72 hrs with harvest and lipid extraction for sphingosine, S-1-P, and SM analysis performed at time points shown between 30 minutes and 72 hours. (A) shows changes in sphingosine levels, (B) shows changes in S-1-P, and (C) shows changes in sphingomyelin levels. As previously, total ion count of sphingolipid metabolite is normalized to that of PC and the data shown is expressed as a ratio of the strained group to the control. (n=3-4)

4.3.2 Selective inhibition of aSMase, nSMase and *de novo* ceramide synthesis

4.3.2.1 Inhibition of aSMase

Pretreatment of hAECs with desipramine, an inhibitor of aSMase, prior to and concurrently with exposure to 10% cyclic strain at 1 Hz, blocks the early, but not the late increase in ceramide associated with 10% cyclic strain at 1 Hz (Figure 4.4). The $C_{16:0}$, $C_{24:1}$, and $C_{24:0}$ ceramide increase typically encountered at 3 hrs is abrogated in response to desipramine treatment, however the prolonged ceramide increase normally encountered at later timepoints is still present and even seems to be elevated for all major ceramide species. Sphingomyelin levels are not substantially decreased following desipramine treatment. Data shown represent a single experiment.

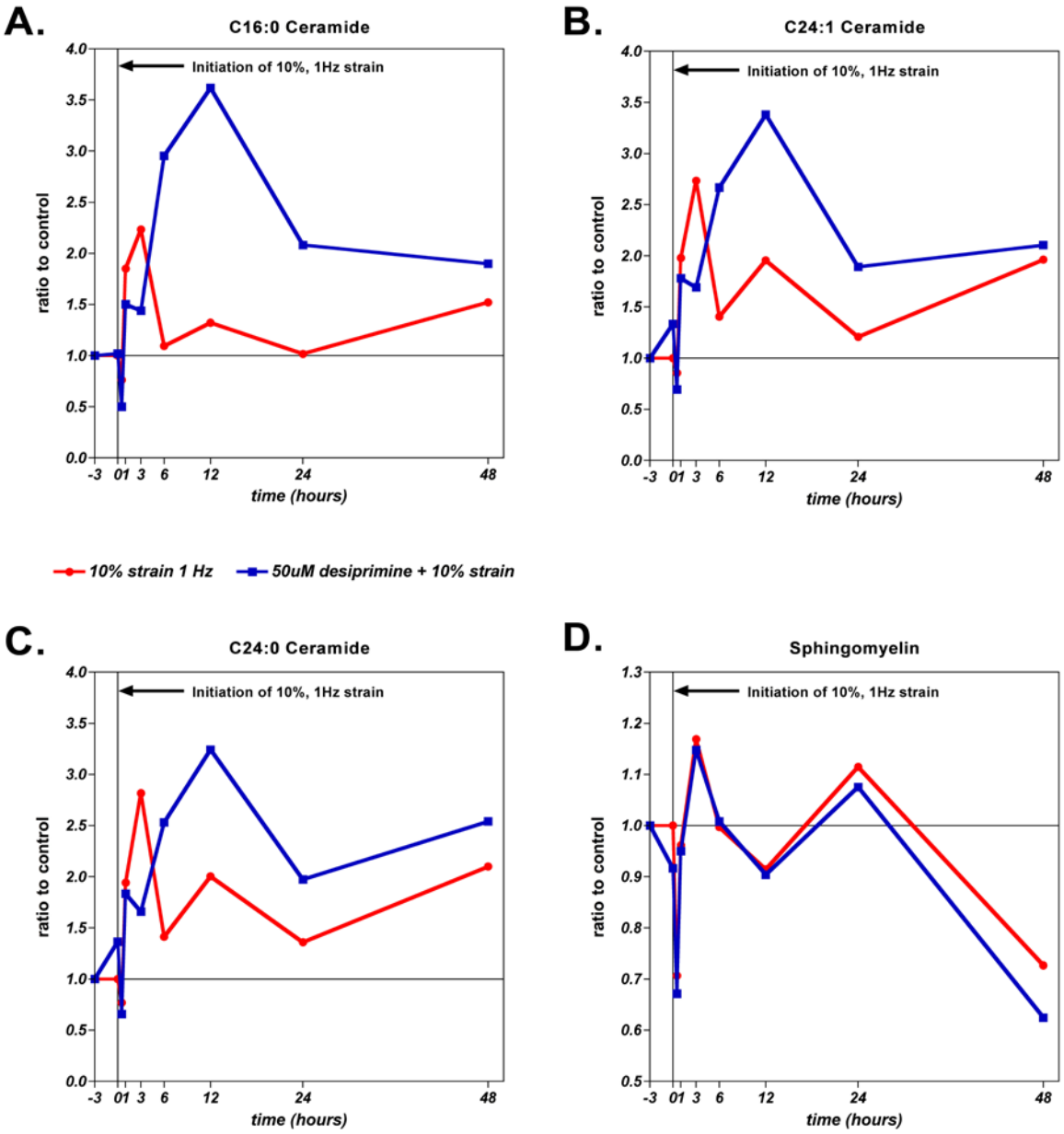

Figure 4.4. Desipramine inhibition of aSMase blocks only the early ceramide increase. (A) shows changes in $C_{16:0}$ ceramide, (B) shows changes in $C_{24:1}$ ceramide, (C) shows changes in $C_{24:0}$ ceramide, and (D) shows changes in sphingomyelin. hAECs were pretreated with 50 μM desipramine for 3 hrs prior to exposure to 10% cyclic strain at 1Hz for up to 48 hrs, maintaining desipramine in the culture medium. Cells were harvested for lipid extraction for ceramide analysis at time points shown between 30 minutes and 48 hours. As previously, total ion count of ceramide or sphingomyelin is normalized to that of PC and the data shown is expressed as a ratio of the strained group to the control. (n=1)

4.3.2.2 Inhibition of nSMase

Pretreatment of hAECs with manumycin A, an inhibitor of nSMase, prior to and concurrently with exposure to 10% cyclic strain at 1 Hz, blocks the very early and the late increase in ceramide associated with 10% cyclic strain at 1 Hz (Figure 4.5). The $C_{16:0}$, $C_{24:1}$, and $C_{24:0}$ ceramide increase typically encountered at about 30 minutes to 1 hr is abrogated, as well as the prolonged ceramide increase typically encountered at later time-points. Interestingly, it appears that a small increase in ceramide at 3 hrs is still present for all species of ceramide, even during manumycin treatment. Sphingomyelin levels are substantially decreased following manumycin treatment. Data shown represent a single experiment.

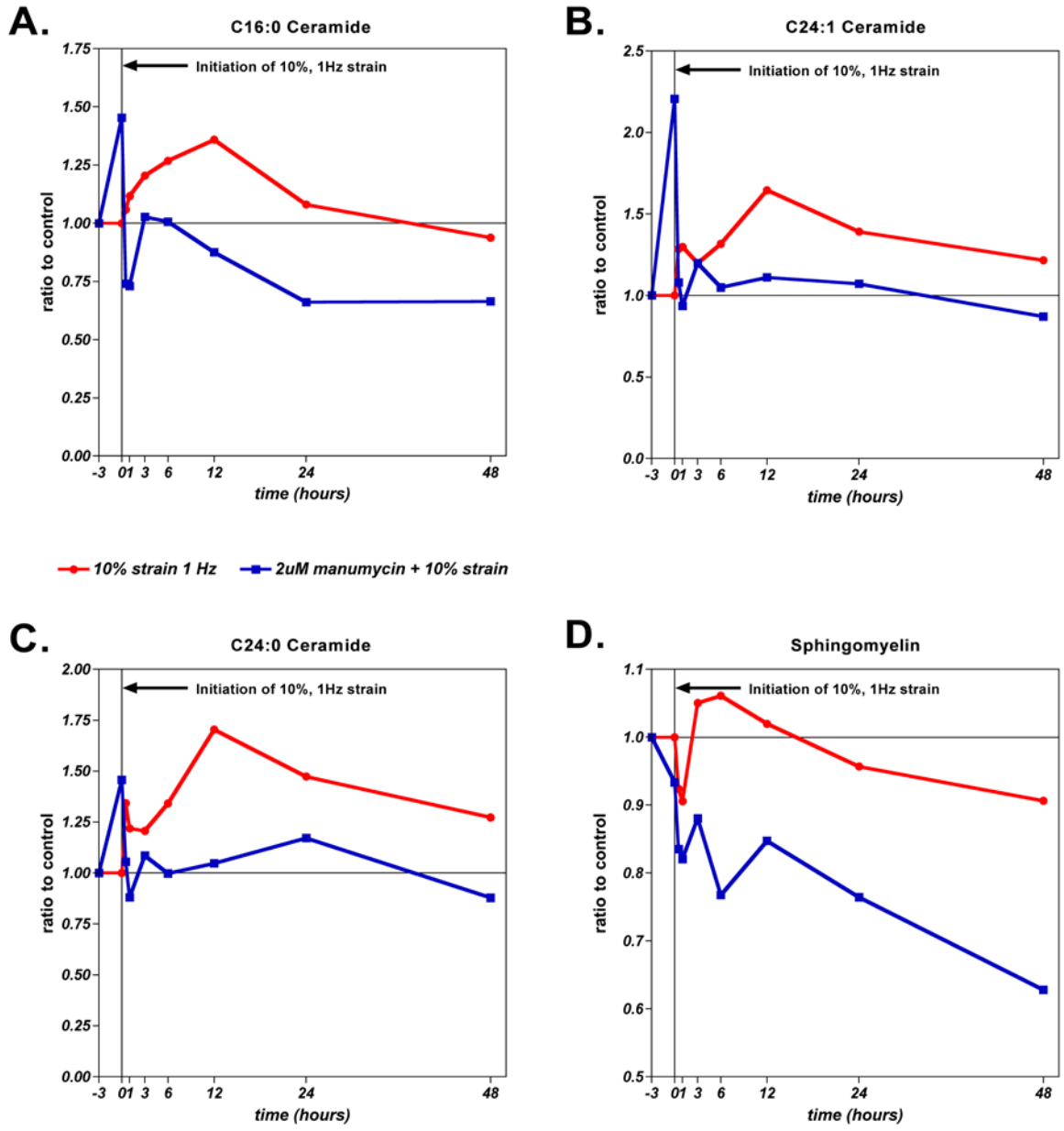

Figure 4.5. Manumycin A inhibition of nSMase blocks both early and late ceramide increases. (A) shows changes in $C_{16:0}$ ceramide, (B) shows changes in $C_{24:1}$ ceramide, (C) shows changes in $C_{24:0}$ ceramide, and (D) shows changes in sphingomyelin. hAECs were pretreated with 2 μM manumycin A for 2 hrs prior to exposure to 10% cyclic strain at 1Hz for up to 48 hrs, maintaining manumycin A in the culture medium. Cells were harvested for lipid extraction for ceramide analysis at time points shown between 30 minutes and 48 hours. As previously, total ion count of ceramide or sphingomyelin is normalized to that of PC and the data shown is expressed as a ratio of the strained group to the control. (n=1)

4.3.2.3 Inhibition of *de novo* ceramide synthesis

Pretreatment of hAECs with L-cycloserine, an inhibitor of *de novo* ceramide synthesis, prior to and concurrently with exposure to 10% cyclic strain at 1 Hz, blocks only the late increase in ceramide associated with 10% cyclic strain at 1 Hz (Figure 4.6). The $C_{16:0}$, $C_{24:1}$, and $C_{24:0}$ ceramide increase typically encountered between 30 minutes and 3 hrs is still present, but the prolonged ceramide increase is markedly reduced below even unstrained control levels. Sphingomyelin levels are substantially decreased following L-cycloserine treatment as well. Data shown represent a single experiment.

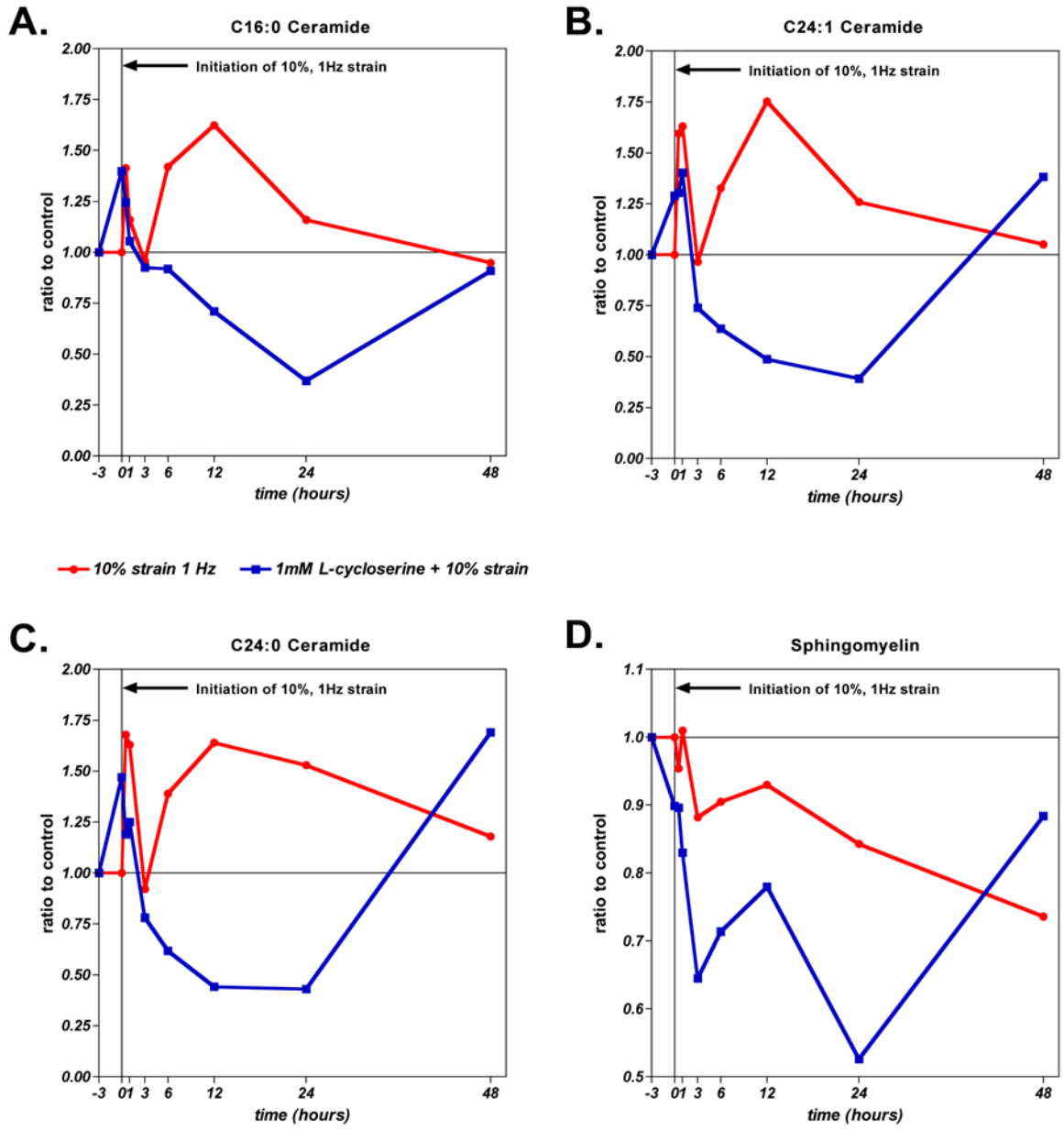

Figure 4.6. L-cycloserine inhibition of *de novo* ceramide synthesis inhibits late, but not early ceramide accumulation. (A) shows changes in $C_{16:0}$ ceramide while (B) shows comparable changes in $C_{24:1}$ ceramide and (C) shows comparable changes in $C_{24:0}$ ceramide. (D) shows changes in sphingomyelin. hAECs were pretreated with 1mM L-cycloserine for 3 hrs prior to exposure to 10% cyclic strain at 1 Hz for up to 48 hrs, maintaining L-cycloserine in the culture medium. Cells were harvested for lipid extraction for ceramide analysis at time points shown between 30 minutes and 48 hours. As previously, total ion count of ceramide or sphingomyelin is normalized to that of PC and the data shown is expressed as a ratio of the strained group to the control. (n=1)

4.4 DISCUSSION

4.4.1 Sphingosine and cyclic strain

Evaluation of a single time-point and strain regimen on bAECs – 10% strain at 1 Hz for 24 hrs – reveals that only sphingomyelin and sphingosine show a change relative to unstrained control cells, both exhibiting decreases (Figure 4.1). In Figure 3.3, it should be noted that the sphingosine levels at 1.5 hrs following cessation of strain, also for 24 hrs at 10% strain at 1 Hz, shows an initial increase in sphingosine levels relative to control, whereas the benchmark data taken immediately following cessation of strain shows a decrease (Figure 4.1). The question is then how these conflicting data should be viewed. As discussed in Section 3.4.1, the 1.5 hr post-strain timepoint lipid extraction (addition of chloroform and methanol) is performed at approximately the same time following removal from the strain apparatus as the standard lipid extractions described in the rest of this study, so one would expect agreement of the data. These are separate experiments performed on separate occasions and the variability may reflect Type I error indicating that the change in sphingosine at this timepoint may not actually exist.

Alternatively, the reduction in sphingosine with strain relative to control, as seen in the benchmark assessment, may be lost very quickly following cessation of strain, more quickly than even the changes in ceramide or sphingomyelin. The total time to extraction of a standard lipid extraction as performed in the benchmark experiment is approximately 1 hour, whereas the total time between cessation of strain and actual extraction for the first strain cessation time-point is 1.5 hours. Being that sphingosine is an intermediate between ceramide and protective S-1-P, it is possible that during strain, sphingosine is utilized readily to generate S-1-P to shift the cell towards a more protective phenotype, but that upon removal of the strain stimulus, S-1-P

generation slows and sphingosine levels back up, resulting in the increase relative to control seen at 1.5 hrs in the strain cessation experiment. This explanation is supported by the observations that sphingosine shows a reduction across most time-points at all strain magnitudes (Figure 4.2) and frequencies (Figure 4.3) tested.

4.4.2 S-1-P and cyclic strain

When considering sphingosine changes, changes in S-1-P must be compared as well, since sphingosine is an intermediate in the metabolism of ceramide to S-1-P. If one tries to look at net change in S-1-P across strain regimen magnitudes, there does not appear to be a statistical significance (Figure 4.2.A). However, looking at the time-response of each frequency together, it is clear that at all strain magnitudes tested, bAECs experience an early spike in S-1-P, followed by a reduction, followed by a second, more sustained rise. These patterns generally follow the pattern of ceramide increase over time in response to strain and may represent conversion of increased ceramide to S-1-P, potentially as a protective mechanism. Variation of frequency at 6% strain does not appear to affect S-1-P levels (Figure 4.3.A).

Taken together with the sphingosine data, it appears that during active strain, sphingosine is readily utilized and does not remain as an intermediate. Whether it is being utilized in the conversion of S-1-P to ceramide or in the conversion of ceramide to S-1-P cannot be determined from these studies, but it is probable that both pathways occur within ECs during strain, potentially as part of the theorized sphingolipid rheostat [80].

4.4.3 *de novo* synthesis of ceramide

Synthesis of ceramide by the *de novo* pathway, which usually occurs over a period of several hours as a late response to cellular stress, has been shown in response to a number of cellular stresses including TNF-α, ionizing radiation, and chemotherapeutic agents and has been implicated in apoptosis [63, 65, 70, 75].

When L-cycloserine is introduced into culture concurrent with 10% cyclic strain at 1 Hz, hAECs exhibit the characteristic early increase in ceramide through 3 hrs, but after 6 hrs, the ceramide response is considerably depressed compared to strain alone and even compared to unstrained control cells (Figure 4.6). This suggests that the late ceramide response, as expected, is associated with *de novo* synthesis. Furthermore, sphingomyelin levels in hAECs are substantially reduced with addition of L-cycloserine during strain relative to strain alone, suggesting that SMase activity is still functional and that inhibition of *de novo* synthesis of ceramide reduces the level of available sphingomyelin (Figure 4.6.D).

4.4.4 Sphingomyelin and cyclic strain

The sphingomyelin response to cyclic strain is arguably the most straight-forward of the metabolite responses tested. The standard ceramide response to time, as shown in Figure 3.4, appears to have two early spikes in ceramide generation prior to 1 hr and again at approximately 3 hrs, followed by a sustained increase in ceramide after 12-24 hrs. Based on these findings, we hypothesized that sphingomyelin hydrolysis was responsible for the early ceramide increase while *de novo* ceramide synthesis was responsible for the late ceramide increase.

Addition of manumycin A, an inhibitor of neutral SMase, during 10% strain at 1 Hz causes an early and immediate decrease in all of the major species of ceramide as well as an absence of the late ceramide response (Figure 4.5). Interestingly, there is still a spike in all ceramide species measured occurring at 3 hrs. This suggests that the initial ceramide spike occurring prior to 1 hour is due to hydrolysis of SM by nSMase in the plasma membrane, consistent with the notion of initiation of mechanotransduction signaling at the membrane. This is also consistent with the finding the nSMase activity is observed in response to elevated pressure/flow in an isolated lung graft model [82, 83]. The presence of the 3 hr spike in ceramide even with the addition the nSMase inhibitor, as well as the continued reduction in sphingomyelin compared to strain alone, suggests that there is a second early ceramide response, probably due to another form of SMase and that nSMase activity accounts for a relatively small amount of SM hydrolysis (Figure 4.5). However, the absence of the late ceramide response following manumycin A treatment suggests that ceramide signaling resulting from nSMase hydrolysis is necessary for the later *de novo* synthesis of ceramide. If *de novo* synthesis is indeed blocked by the inhibition of nSMase-associated hydrolysis of sphingomyelin to ceramide, the pronounced reduction in sphingomyelin seen in Figure 4.5. D may be due to a reduction in the available sphingomyelin caused by a reduction in available ceramide without *de novo* synthesis. Further studies assessing the functional activity of enzymes active in the *de novo* biosynthetic pathways would be necessary to confirm this observation. However, it is important to recognize that manumycin A is also a known inhibitor of the Ras pathway by way of inhibiting Ras farnesyl transferase. It has been proposed that some of the Ras inhibitory activities of manumycin A may be attributable to nSMase inhibition [111]. To confirm that nSMase is

responsible for observed apparent changes in *de novo* synthesis, it would be helpful to repeat these experiments using other known inhibitors of nSMase like scyphostatin.

The data from experiments using desipramine, an inhibitor of aSMase, clarify these findings. When desipramine is added to hAEC culture during 10% strain at 1 Hz, the ceramide spike at 3 hrs is abrogated for all major species of ceramide, but the late response is still present and is actually more pronounced than in hAECs exposed to 10% strain alone (Figure 4.4). This suggests that the 3 hr spike in ceramide is attributable to aSMase hydrolysis of sphingomyelin, potentially after lysosomal translocation to the membrane, but that ceramide signaling from aSMase does not affect *de novo* ceramide synthesis. When one looks at the very meager sphingomyelin changes in response to aSMase inhibition (Figure 4.4.D) relative to the pronounced changes in sphingomyelin in response to manumycin (Figure 4.3.D), it appears that the majority of SM hydrolysis observed in response to cyclic strain is attributable to aSMase. The relevance of this finding in the setting of the endothelial response to mechanical stresses is supported by studies that have shown that ceramide signaling by aSMase-mediated hydrolysis of sphingomyelin are necessary for eNOS activity [73, 74]. Although the relationship between eNOS activity and ceramide during cyclic strain is not tested in this body of work, it is an intriguing target for future experiments.

In the bAECs exposed to 6%, 10%, and 12% strain, sphingomyelin shows a prolonged reduction relative to unstrained controls, suggesting that sphingomyelin hydrolysis occurs at physiological and high physiological levels of strain, whereas at 3% strain (subphysiological), there is actually an elevation in sphingomyelin relative to unstrained controls. At 3% strain, the major species of ceramide did not exhibit the characteristic early increase in ceramide at approximately 3 hrs that was observed in response to 6%, 10%, and 12% strain. Taken together

with the inhibitor studies, this information is very interesting. Recalling that the ceramide spike at 3 hrs appears to be a result of aSMase hydrolysis of SM, it is possible that aSMase activity requires a strain threshold to occur. It is intriguing, since the apparent lack of aSMase activity at 3 hrs occurs in cells exposed to 3% strain, which do not align perpendicular to strain, to think that aSMase activity is either required for alignment, or that alignment is required for aSMase activity. Certainly, in the context of integrin rearrangement and formation of focal adhesions in conjunction with cellular alignment, it seems likely that one would expect an increase in ceramide enriched membrane domains to facilitate reorganization and clustering of receptors or adhesion molecules, potentially through aSMase. aSMase translocation to the membrane accompanying the formation of ceramide-enriched membrane domains in response to CD95 ligand stimulation has been shown in bAECs [62].

As with ceramide, sphingosine, and S-1-P, sphingomyelin does not appear to vary with changes in strain frequency at 6% strain (Figure 4.3.D). As discussed previously (Section 3.4.2), due to limitations of the Flexcell FX4000T system, it is not possible to impose a strain regimen at 2 Hz using a strain magnitude higher than 6%. At higher strain magnitudes, higher frequencies might affect ceramide generation and consequently sphingomyelin hydrolysis, in a more profound manner, but these studies do not suggest that strain frequency affects ceramide synthesis.

4.5 CONCLUSIONS

Cyclic, uniaxial strain applied at a variety of magnitudes (3%-12%) and frequencies (0.5 Hz – 2 Hz) representing variation from subphysiological to elevated, pathophysiological states of

arterial strain conditions, demonstrates that whole-cell levels in sphingosine and sphingomyelin are reduced in bAECs in response to cyclic strain. As with ceramide, continuous application of cyclic uniaxial strain is necessary to maintain these changes and removal of the strain stimulus causes sphingosine and sphingomyelin levels to return to baseline. Based on similarly shaped curves for the S-1-P response to strain over time compared to ceramide, it appears the sphingosine, as an intermediate, is being utilized in conversion of ceramide to S-1-P and vice versa during strain. Sustained reduction in sphingomyelin levels suggests that sphingomyelin is being hydrolyzed to form ceramide during strain. Similar to ceramide findings, variation of strain frequency at a strain magnitude of 6% does not appear to alter levels of sphingosine, S-1-P, or sphingomyelin.

Studies of selective inhibition of aSMase, nSMase, and *de novo* synthesis of ceramide reveal that all three enzymes are involved in the ceramide response to cyclic strain, as shown in Figure 4.7. Neutral SMase hydrolysis of sphingomyelin occurs within the first hour of strain application and appears to be necessary for triggering the sustained *de novo* synthesis of ceramide following strain. Acid SMase hydrolysis of sphingomyelin occurs at approximately 3 hours after the onset of strain and may represent the majority of SM hydrolysis that occurs in response to strain. Finally, *de novo* synthesis of ceramide seems to begin after 6 hrs of strain and appears to be predominantly responsible for the prolonged ceramide response observed after 12-24 hours of cyclic strain.

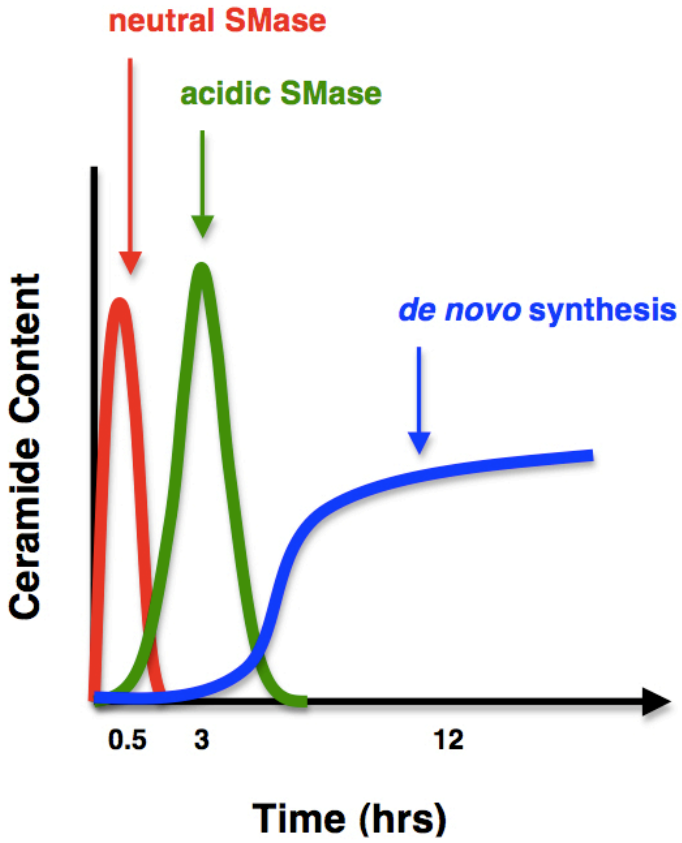

Figure 4.7. The ceramide response to cyclic strain involves the generation of ceramide from both the *de novo* synthetic pathway and from hydrolysis of sphingomyelin to ceramide by nSMase and aSMase.

5.0 CLOSING DISCUSSION

5.1 RESTATEMENT OF THE BIOLOGICAL PROBLEM

The purpose of this body of research was to examine the virtually unexplored and critical role of the lipid microenvironment, particularly with regards to ceramide signaling, in aortic endothelial cells in response to cyclic strain within and beyond the physiological range, so as to gain a better understanding of the events which may ultimately contribute to endothelial activation and dysfunction and to eventual atherosclerosis.

Cyclic strain, acting circumferentially through the wall of the blood vessel, in addition to hydrostatic pressure acting radially, and fluid shear stress, acting longitudinally in the direction of blood flow are the major mechanical forces encountered by blood vessels in response to pulsatile blood flow [43]. Together, these forces influence the endothelium and its ability to maintain appropriate vascular permeability, tone, and hemostasis, and to regulate inflammation and remodeling in health and disease. During mechanical injury or disease states, blood vessels may encounter abnormal levels of mechanical forces, which can alter endothelial and smooth muscle cell function, which in turn may contribute to the formation of atherosclerotic lesions [43-45].

Clinically, cyclic strain is associated with hypertension, vein grafting, balloon angioplasty over-stretch injury and possibly intra-aortic balloon pumping, tissue engineering, and

formation of atherosclerotic lesions. Atherosclerotic lesions tend to develop in regions of elevated strain, including sites of vein to artery grafting [42, 51]. Thus, an improved understanding of how aberrant mechanical forces trigger dysfunction and inflammation in the vasculature has the potential to greatly improve our understanding of vascular disease pathology and etiology.

The means by which cells convert mechanical forces into biomolecular responses is known as mechanotransduction [46]. Numerous possible mechanisms for mechanotransduction have been proposed, including ion channels, G-proteins, MAPKs, integrins and focal adhesions, the cytoskeleton, and reactive oxygen species [44, 45, 47]. While it is debated which of these mechanisms in the true mechanosensor in the vascular setting, it is very likely that several of these processes are activated concurrently.

Ceramide, the central molecule in sphingolipid biosynthesis, is widely known to participate in stress signaling in response to a multitude of cellular stress stimuli pertinent to the vascular setting, including cytokines (TNF-α, IFN-γ, IL-1β, etc.), lipopolysaccharide, oxidized LDL, various chemotherapeutic agents, ionizing irradiation, heat stress, ischemia/reperfusion, and nitric oxide [2, 61, 63, 65, 72] and has been implicated in signaling through many versatile targets including MAPKs, JNK, and caspases, amongst others [63, 67]. Depending on the site and source of synthesis, ceramide can participate directly in signaling or can assist in signaling through its involvement in lipid rafting [2, 62], leading to cell proliferation, differentiation, growth, or arrest [61].

Furthermore, ceramide and its metabolites have been found in elevated levels in atherosclerotic lesions [2, 81], and areas of lesion development have exogenous and endogenous sources of sphingomyelinases and sphingomyelin, capable of contributing to ceramide

generation through sphingomyelin hydrolysis [2, 71, 81]. Within the context of vascular inflammation and activation, ceramide introduced from exogenous sources as well as endogenously through the hydrolysis of sphingomyelin has been shown to trigger Weibel-Palade body exocytosis in endothelial cells [26].

Despite the breadth of its signaling potential and influences on cell fate, the role of ceramide signaling remains largely unexplored in the context of mechanotransduction. Ceramide has the potential to be involved in all aspects of mechanotransduction, whether through involvement in plasma membrane dynamics and lipid rafting to facilitate coalescence of membrane proteins and receptors, particularly in the caveolae, for signaling and signal amplification [62]; through direct or indirect activation of protein kinases [63, 65, 67]; through its ability to self-associate into lipid channels and to aid in the proper formation of ion channels [62, 85]; and through the ability of ceramide to generate reactive oxygen species and vice versa, suggesting its potential role in signaling amplification [62, 67, 86]. Furthermore its historical implication in the development of inflammation, cellular stress, and endothelial cell activation make it a very likely link between mechanical trauma and eventual development of vascular disease.

5.2 RESTATEMENT OF THE HYPOTHESIS AND REVIEW OF EXPERIMENTAL DESIGN

Our central hypothesis is that mechanical, uniaxial cyclic strain results in an increase in intracellular ceramide in vascular endothelial cells, which participates in signaling necessary to propagate mechanotransduction responses to cyclic strain, potentially contributing to early

events in the development of endothelial dysfunction and the formation of atherosclerotic lesions.

To test this hypothesis we began by defining the phospholipid and sphingolipid environment of aortic endothelial cells by a detailed mass spectrometric analysis to establish the foundation for a more in-depth study of ceramide signaling. We then explored the response of aortic endothelial cells to exogenous sources of C_8 and C_{16} ceramides, representing species of nonphysiological and physiological fatty acid chain lengths respectively, to test the specificity of the endothelial cell response to different species of ceramides.

We then set out to thoroughly evaluate how ceramide and its metabolites -- namely sphingosine, S-1-P, and sphingomyelin -- change in response to a panel of physiological and pathological strain conditions with regards to magnitude and frequency over time. Sphingosine and S-1-P were chosen because the intracellular balance between ceramide and S-1-P activity has been suggested as a determining factor -- a sphingolipid rheostat -- for whether a cell's fate favors survival (S-1-P) or death (ceramide) [80]. Sphingomyelin was chosen because its hydrolysis is a ready source of ceramide and it is a prominent sphingolipid involved in lipid rafting and cell signaling [65, 66, 71].

Then, to further define the place of ceramide signaling within the mechanotransduction response to cyclic strain, through the use of pharmacological inhibitors to acid sphingomyelinase, neutral sphingomyelinase, and *de novo* ceramide synthesis, we evaluated which biosynthetic pathways appeared to be activated in response to strain and we examined the accumulation of select metabolites with known biological activity in the vascular microenvironment.

5.3 SUMMARY OF RESULTS AND DISCUSSION

In Chapter 2, we established the sphingolipid and phospholipid microenvironment through an extensive mass spectrometric analysis. The list of phospholipids in Tables 2.1, 2.2, 2.3, 2.4, 2.5, and 2.6 reveal that the major species of phospholipids present in AECs show a broad distribution of fatty acid chain lengths within the physiological range (C_{14}-C_{24}). By nature of limitations inherent in ESI-MS/MS analysis of whole-cell lipid extractions, this list is not absolute and is only indicative of major species present, as discussed in Section 2.4.1.

In addition to expected phospholipids like PC, PE, PG, PI, and PS, we also found abundant cholesterol and a number of species of PE plasmalogens, which possess a vinyl ether at the C_1 position on the glycerol backbone instead of the typical ether linkage connecting the fatty acid. As such, plasmalogens are particularly susceptible to attack by reactive oxygen species at the vinyl ether linkage (Figure 2.11), thereby conferring anti-oxidant function by causing them to be especially effective in protecting other membrane phospholipids and components from oxidative damage in platelets [99]. Plasmenyl PE and plasmenyl PC are also cleaved by PLA_2 to release arachidonic acid in coronary artery ECs stimulated by thrombin and hypoxia [101]. The ability to detect and monitor changes in specific plasmalogen species by ESI-MS may prove to be an insightful tool in future studies assessing the extent of damage to lipid functionality in the endothelium, particularly with regards to the potential role of reactive oxygen species in mechanotransduction, as well as in evaluating the initiation and progression of vascular disease.

In assessing the sphingolipid profile of AECs, we established that $C_{16:0}$, $C_{24:1}$, and $C_{24:0}$ species of ceramide are abundant and easily detectable by ESI-MS in both bovine and human AECs. Evaluation of the profile of sphingomyelin species present revealed species with a broad distribution of length of the non-sphingoid fatty acid side-chain. $C_{16:0}$ sphingomyelin was found

to be abundant and easily detectable. By nature of its lower mass than the abundant species of PC detected in the positive ion mode, it is relatively isolated on the MS spectrum. These properties established $C_{16:0}$ sphingomyelin as a suitable measure of sphingomyelin activity in ECs. These studies also established $C_{16:0}$, $C_{24:1}$, and $C_{24:0}$ ceramide; $C_{16:0}$ sphingomyelin; and sphingosine and S-1-P as the panel of sphingolipids to be measured in all further endothelial cell experiments in this study.

Because of the ease of solubility with decreasing fatty acid chain length, short-chain ceramides (C_2-C_8) are frequently used in exogenous ceramide studies, despite being nonphysiological. Our evaluation of the specificity of the aortic endothelial cell response to both physiological C_{16} and non-physiological C_8 species of ceramide reveals that short chain ceramide is not a direct functional substitute for the other, both with regards to change in viability and intracellular physiological ceramide content (Figures 2.9 and 2.10).

Treatment with exogenous C_8 ceramide causes an expected increase in bAEC C_{16} and C_{24} ceramides with a corresponding concentration-dependent decrease in viability (Figure 2.9), while treatment with exogenous C_{16}-D_{31} ceramide causes a decrease in bAEC levels of endogenous C_{16} and C_{24} ceramides and does not compromise cell viability (Figure 2.10). Thus, exogenous sources of C_{16} ceramide are well tolerated by bAECs and the data suggests that bAECs may be capable of converting the exogenous physiological ceramide into a more palatable metabolite like SM, S-1-P, or a higher glycolipid, whereas the nonphysiological ceramide may not be able to be processed and is instead deacylated and reacylated to form longer-chain ceramides. This seems especially possible given the reduction in endogenous ceramide species relative to untreated control cells following treatment with exogenous C_{16}-D_{31} ceramide (Figure 2.10). C_{16} ceramide may also exhibit feedback inhibition of ceramide synthesis in bAECs such that in

response to increases in C_{16} ceramide, a species with known biological activity, endogenous synthesis of ceramides may be downregulated in the absence of other stress events to prevent inappropriate signaling.

This data may further support the concept that specificity of fatty acid chain length plays a role in specific activity of different ceramide species. Different species of ceramide are associated with distinct ceramide synthases, each of which is encoded on a different gene. For example, in humans, each of the six longevity assurance genes, *LASS1-6*, encode for ceramide synthases that selectively utilizes specific fatty acid chain lengths between C_{16} and C_{24} and different genes may be activated under different circumstances [102]. This evidence further supports the notion that different chain lengths of ceramide may play different roles and that measurement of a single species of ceramide may not be a surrogate for all species of ceramide with regards to biological activity.

The outcome of ceramide signaling is also associated with the site and source of ceramide generation within the cell. Exogenous C_{16} ceramide may not partition into the appropriate intracellular pools to evince a change in viability, whereas C_8 ceramide causes rapid generation of long-chain ceramide, potentially through removal of the C_8 chain and reacylation with $C_{16:0}$ (palmitic acid), similar to *de novo* synthesis.

The ability of endothelial cells to respond to extracellular sources of sphingolipids is highly applicable in the vascular setting where endothelial cells are exposed to sphingolipids circulating in serum or associated with extracellular lipid-protein complexes, and pools of sphingolipids within atherosclerotic lesions.

To fully explore how endothelial cells respond to cyclic strain, a series of experiments was performed to test how ceramide levels vary in bAECs in response to a variety of strain

regimens encompassing subphysiological through physiological strain conditions encountered within the arterial vasculature, each assessing the time response that accompanies selective variation of the magnitude and frequency of strain. Further experiments in hAECs, using selective inhibitors against *de novo* ceramide synthesis or hydrolysis of sphingomyelin to ceramide by acidic or neutral sphingomyelinases, clarified many of these findings.

A feature of the ceramide response to cyclic strain by bAECs over the first 72 hrs, which was conserved across normal physiological and pathophysiological strain magnitudes at all strain frequencies tested, was the presence of a two-part early rise in ceramide within the first few hours as well as a prolonged rise in ceramide levels over the first few days (Figures 3.4, 3.5, and 3.6). The inhibitor studies performed in hAECs revealed that the very early rise in ceramide at 30 minutes corresponds to nSMase hydrolysis of SM to ceramide, while the second early rise in ceramide at 3 hrs corresponds to aSMase hydrolysis of SM to ceramide. The late, prolonged response occurring after 12 hrs and lasting for the remainder of the 72 hr experiment was found to be due to *de novo* ceramide synthesis (Figure 4.7). Very interestingly, when nSMase was inhibited, the cells experienced neither the initial spike in ceramide generation, nor the later prolonged response, suggesting that nSMase-associated ceramide signaling may be necessary to initiate *de novo* synthesis. Thus, we propose that ceramide signaling due to nSMase and aSMase hydrolysis of sphingomyelin to ceramide and *de novo* ceramide synthesis plays a role in the mechanotransduction to cyclic strain, although further studies are needed to determine how ceramide signaling is specifically linked to known mechanisms of mechanotransduction (Figure 5.1).

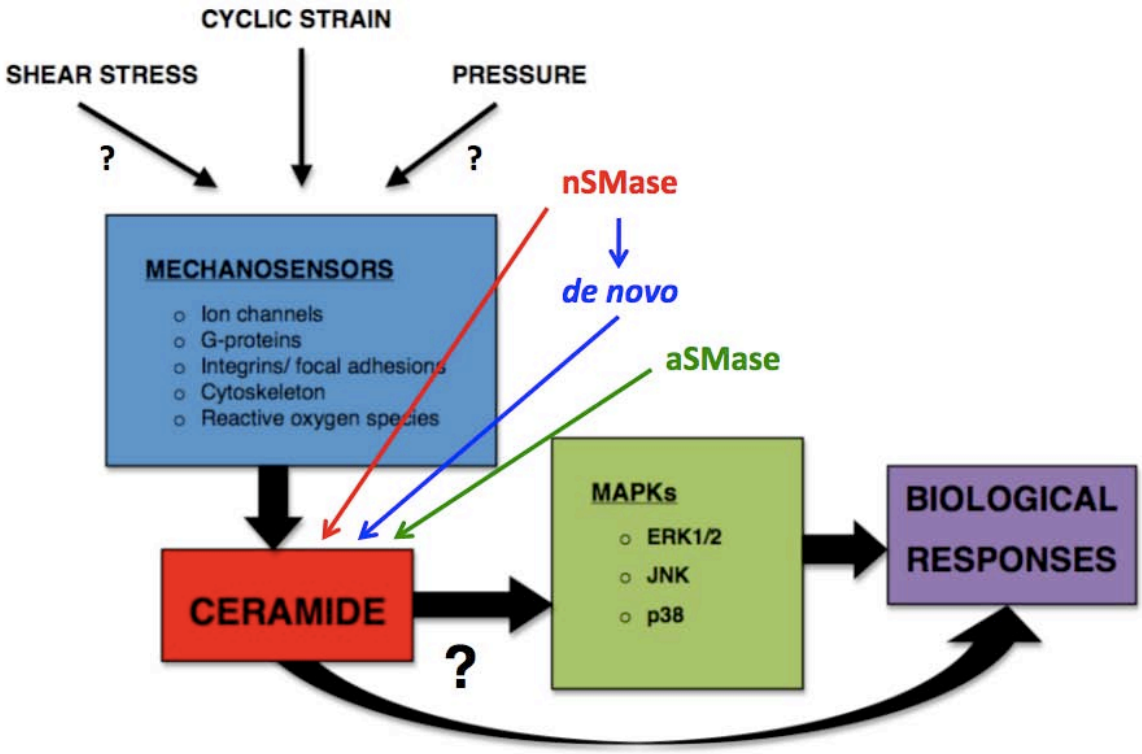

Figure 5.1. Ceramide is involved in the mechanotransduction response to cyclic strain and is generated from hydrolysis of sphingomyelin to ceramide by both nSMase and aSMase, as well as by the *de novo* synthetic pathway. The specifc relationship of ceramide signaling to proposed mechanisms of mechanotransduction must still be determined.

More plainly, this data suggests that the initial ceramide signaling event due to nSMase activity occurring at the onset of strain, and localized to the plasma membrane appears to be necessary to stimulate *de novo* synthesis that may be necessary for the cell to mount a sustained mechanotransduction response to cyclic strain. Thus, nSMase activity at the plasma membrane, where sphingomyelin is abundant in caveolae and in lipid rafts necessary for receptor and surface molecule arrangement, may be critical to the initial steps of mechanotransduction, either through the direct action of ceramide signaling, or through the role of ceramide in lipid rafts to enhance

receptor coalescence. This phenomenon has also been proposed in studies of elevated pressure/flow in isolated lung grafts [82, 83].

The finding that nSMase is activated in response to cyclic strain further supports the hypothesis that ceramide signaling in ECs in response to cyclic strain contributes to early events leading to EC dysfunction. Ceramide generated by nSMase activation in hAECs has been shown by others to cause exocytosis of Weibel-Palade bodies [26], a hallmark of endothelial activation, which may over time contribute to endothelial dysfunction [23].

Interestingly, the early ceramide response, particularly that occurring at 3 hrs, appears to be absent in the response to 3% strain (subphysiological), while being present at all higher strain magnitudes tests (6-12%). If the time response is indeed reflective of the presence of an early ceramide increase due to membrane-associated sphingomyelin hydrolysis, this finding suggests that a threshold level of strain may be necessary to elicit sphingomyelin hydrolysis. Being that ECs do not align perpendicular to strain below 5% strain magnitude, it may be possible that this early ceramide increase is either caused by or is necessary for cell alignment within this time period. The 3 hr peak in ceramide, which we have shown is associated with aSMase activity, may reflect either translocation of lysosomal aSMase to the cell membrane to participate in membrane receptor coalescence [62] necessary for signaling or to facilitate integrin rearrangement during alignment. Alternatively, it may represent the involvement of the sphingolipid salvage pathway, which recycles sphingolipids like sphingomyelin or glucosylceramide to sphingosine which may then be converted to S-1-P or to ceramide [88]. The transience of this peak in the higher strain magnitude suggests that aSMase is being employed to assist in a specific transient membrane event, rather than a basal metabolic function of the cell,

further strengthening the notion that a SMase-mediated ceramide generation is specifically associated with strain alignment.

The AEC response to subphysiological strain is still clinically relevant, since vascular disease is also characterized by regions of arterial stiffness occurring in any region of the arterial bed including the aorta and across calcified atherosclerotic lesions. If one defines endothelial cell health in terms of the activity of cellular stress signaling pathways, reduction in cellular strain in the wrong population of ECs (aortic ECs), may be as detrimental as an elevation in strain. Thus, the absence of a SMase-associated ceramide signaling in ECs experiencing a reduction in strain magnitude in the aorta or across atherosclerotic lesions, may result in endothelial dysfunction which could affect vascular cells both locally and in the distal circulation, potentially contributing to the gross pathological manifestations of cardiovascular disease.

Variation of strain frequency (0.5 Hz – 2 Hz) at a normal physiological strain magnitude (6%) yielded less variation in ceramide and ceramide metabolite regulation than did variation of strain magnitude (3%-12% at a physiological frequency (1 Hz). In the context of normal arterial conditions, this suggests that a change in heart rate at a normal blood pressure is less detrimental than an increase in blood pressure at a normal heart rate.

One of the other very interesting findings of the cyclic strain studies is the notion that continuous application of cyclic strain is required to maintain changes in ceramide, sphingomyelin, and sphingosine and that removal of the strain stimulus causes the cell to rapidly return to sphingolipid levels commensurate with unstrained control cells (Figure 3.3). This further strengthens the link between ceramide signaling and the act of mechanosensing.

Considered in the context of mechanotransduction, this finding makes sense. If a cell encounters an increase in the local forces being applied to it (i.e. acute hypertension or vein-to-artery grafting), it needs to trigger appropriate signaling pathways in response. Once the strain stimulus is removed (i.e. return to normotension or remodeling of the vessel to compensate for increased strain), prolonged signaling, particularly ceramide signaling, could be detrimental to the cell survival. This further strengthens the observations from the exogenous ceramide and inhibitor studies that ECs appear to tightly regulate ceramide synthesis and that ceramide signaling employs some measure of autoregulation.

Cyclic strain, at all magnitudes (Figure 4.2) and frequencies (Figure 4.3) tested encountered an S-1-P response curve similar in shape to that observed for ceramide, showing a brief early spike in S-1-P and a second later rise, suggesting that S-1-P is being modulated concurrently with ceramide, potentially as a protective mechanism as part of the theorized sphingolipid rheostat [80]. Ceramide generation has been associated with both apoptosis [61] and autophagy [94, 103, 104], while S-1-P has been associated with cell survival [80] and protective autophagy [104].

The concept of autophagy in the setting of cyclic strain is interesting. For our studies, we monitored cell viability throughout all experiments and found that viability was preserved in response to all strain regimens employed, consistent with studies by others leading some to speculate that cyclic strain confers a protective effect to ECs and SMCs [44, 52, 53]. Autophagy in HUVECs following binding of glycated collagen substrates is dependent on aSMase [94]. The presence of the aSMase-associated peak in ceramide signaling in bAECs and hAECs in response to cyclic strain at physiological levels begs the question of whether autophagy may occur in these cells as part of the response to cyclic strain. Of course, a cell need not be dead in

order to have aberrant cell function and autophagy, which is potentially linked to ceramide signaling, may provide some insight into mechanical induction of endothelial activation and dysfunction.

5.4 STUDY LIMITATION AND FUTURE DIRECTIONS

The data presented reveal great insight into how ceramide varies in AECs during the time response to mechanical cyclic strain and makes large steps towards defining the ceramide dose response to strain in AECs. Furthermore, the evaluation of changes in levels of ceramide metabolites, like sphingosine and S-1-P, and higher sphingolipids like sphingomyelin taken together with inhibitor studies exploring SM hydrolysis and *de novo* ceramide synthesis, begin to shed light on the mechanism of ceramide generation in response to strain and into how it is utilized. Comparison of these findings with known ceramide activity in other cell systems and disease models suggests that ceramide generation may contribute to pro-inflammatory and dysfunctional cell phenotypes associated with cellular stress, not to be confused with mechanical stress in this definition.

What is clearly missing from these studies is a direct relationship of ceramide to a cellular stress phenotype in response to cyclic strain, particularly through repetition of inhibitor studies in strain models, looking at biological endpoint assessments. To prove that ceramide signaling in ECs during strain definitively contributes to an activated phenotype, it would be helpful and necessary to repeat these experiments looking for markers of EC activation, like vWF and IL-8 release associated with Weibel-Palade body exocytosis, which has been shown to be triggered by both exogenous ceramide as well as endogenous ceramide from nS Mase

activation [26]. Likewise, an assessment of how ceramide regulation affects the standard model of endothelial cell function – NO production – would be essential. To explore whether ceramide contributes to a pro-inflammatory state in this system with an eye towards the eventual onset of atherosclerotic lesion formation, one should study inflammatory molecules like TNF-α or HMGB1 and adhesion molecules traditionally associated with monocyte recruitment, like MCP-1. Correlations of ceramide signaling and SMase activation in ECs in response to strain compared to other disease models makes a strong argument for further study of whether cyclic strain induces autophagy in endothelial cells. As such, it would be helpful to examine traditional markers of autophagy like Beclin-1 or LC3 spots.

Further validation of the roles that SMase hydrolysis and ceramide signaling play in the membrane may prove to be more problematic. One can easily study how the absence of SM hydrolysis affects integrin rearrangement, through use of inhibitors against acid or neutral SMases and histological staining for specific integrins, but it is harder to prove its involvement in response to strain without real-time visualization of the cell during strain on a microscope-mounted strain system. Ideally, ceramide accumulation at the site of integrins during rearrangement would be able to be visualized with fluorescent antibodies against ceramide and SMases.

This body of work also does not make an effort to specifically describe which of the numerous mechanisms proposed for mechanotransduction is the "correct" method, nor is it our intention to do so. It does seem likely that ceramide plays a critical role in lipid rafting associated with integrins and focal adhesions, as well as to perhaps perform second messenger signaling. As such, it would help to clarify the function of ceramide in the mechanotransduction response by examining how inhibition of SMases and *de novo* synthesis during strain alters

traditional signaling pathways, particularly MAPKs which are also modulated by ceramide. In particular, nSMase is associated with signaling through ERK1/2 to promote a pro-inflammatory phenotype, whereas aSMase is assicated with signaling through JNK to promote a pro-apoptotic phenotype [112]. Both of these pathways have been implicated in endothelial activation [25] and in mechanotransduction [44]. Thus, different sources of ceramide generated in response to cyclic strain may contribute to different aspects of the mechanotransduction response to cyclic strain and to the resultant phenotypic response, as shown in Figure 5.2.

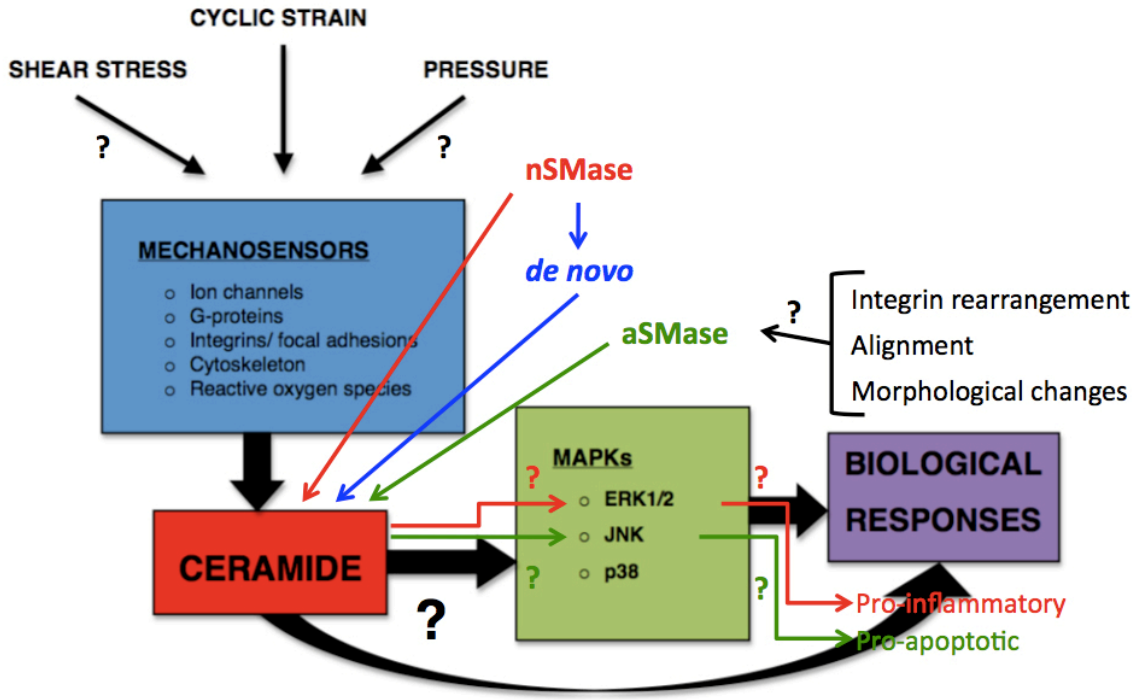

Figure 5.2. Different sources of ceramide generated in response to cyclic strain may contribute to different aspects of the mechanotransduction response and the resultant phenotypic response.

In assessing the importance of ceramide signaling in the mechanotransduction response, it would be necessary as well to examine the direct impact of the various ceramide events observed (nSMase activation, aSMase activation, and late *de novo* synthesis) on cellular alignment in ECs. Although not reported in the results, during experiments, cells pretreated with manumycin A appear, by visual inspection, to fail to align with 10% strain initially, although they do eventually align by 24 hours, which is potentially a very interesting finding. This observation suggests that ceramide signaling as a result of nSMase activity is necessary for alignment to occur. However, it should be noted that manumycin A is also a known inhibitor of the Ras pathway by way of inhibiting Ras farnesyl transferase. It has been proposed that some of the Ras inhibitory activities of manumycin may be attributable to nSMase inhibition. It is unclear whether nSMase inhibition occurs in parallel to Ras inhibition or upstream to it [111]. Initial pilot studies to quantify cellular alignment during strain in the presence of manumycin were disappointing, owing to the toxicity of manumycin to the cells at levels capable of full nSMase inhibition, especially when cells were grown at the subconfluent levels needed for clear alignment assessment by computer-assisted analysis of morphology. It would be helpful to repeat these experiments using another inhibitor of nSMase (i.e. scyphostatin), and to evaluate alignment in the context of a confluent monolayer, since this represents the most physiologically relevant culture condition for ECs.

Finally, it would be necessary to evaluate the overall role of ceramide as a contributing factor to the development of atherosclerotic lesions in an *in vivo* model. Apolipoprotein E (apoE)-deficient mice are a common animal model of atherosclerosis. Interestingly, two studies performed by others appear to validate the role of ceramide in atherosclerosis progression.

M. Sugita *et al*, in a study examining whether one of the antiatherogenic properties of statins is the ability of that drug class to inhibit protein farnesylation, treated apoE-deficient mice with manumycin A, which is a known inhibitor of Ras farnesyltransferase as well as nSMase. Their results showed that fatty streak lesions at the aortic sinus in mice treated with manumycin were only 42% of the size of those in untreated apoE-deficient mice and that the α-smooth muscle actin-positive area in the lesion was reduced to 29% of that in the untreated group [113]. While their results may be due specifically to inhibition of Ras farnesyltransferase, the possible function of nSMase inhibition, particularly in the strain setting of the aorta, may also play a role. Furthermore, nSMase has been show to stimulate Weibel-Palade body exocytosis in hAECs [26], strengthening the idea that nSMase activity contributes to EC activation and eventual dysfunction prior to the onset of atherosclerosis. Our own study showed that nSMase-associated ceramide signaling seems to be required for later *de novo* ceramide synthesis as well, which may help to propagate prolonged mechanotransduction responses.

Similar findings have been reported following inhibition of *de novo* ceramide synthesis *in vivo*. M. Hojjati *et al*. treated apoE-deficient mice with myriocin, an inhibitor of serine palmitoyl-CoA transferase, and therefore *de novo* ceramide synthesis, showing a reduction in atherosclerotic lesion size of 42% and 39% at the aortic root compared to control in mice fed a normal and high fat diet, and reduction in aortic lesion sizes *en face* of 36% and 37% in the same groups [114]. Considered together with the manumycin study in apoE-deficient mice, this argues strongly that prolonged ceramide production due to *de novo* synthesis in ECs may contribute to ultimate progression of atherosclerotic lesions.

In studying the vascular microenvironment, it is also important to consider that smooth muscle cells as well as ECs encounter the same cyclic strain forces and contribute to the

formation of atherosclerotic lesions. Although they do not encounter the same soluble sources of sphingolipids as ECs because of their separation from circulating blood, they do encounter the same intralesional sources of ceramide and ceramide metabolites. Thus, to properly assess the role of ceramide and its metabolites in atherogenesis and in response to cyclic strain, it would be very helpful to compare the response of SMCs to ECs by repeating the same studies in this cell type.

Likewise, experiences in vein to artery grafting and vessel stenosis argue that in addition to examining the ceramide response due to cyclic strain in arterial ECs, we should pursue studies of how ceramide changes in venous ECs where the ceramide response may prove to be even more pronounced.

5.5 CLOSING REMARKS

These studies have elucidated the time scale of the ceramide response and the ceramide biosynthetic and metabolic pathways that occur during the early response to cyclic strain. Ceramide signaling occurs as a result of distinct signaling events associated with nSMase, aSMase, and *de novo* ceramide synthesis. The nSMase signaling event appears to be necessary for the later *de novo* event to occur. The EC response to cyclic strain appears to be sensitive to strain magnitude, resulting in ceramide elevation at levels both above and below physiological strain magnitudes, suggestive of a wide variety of arterial pathological states.

These findings help to elucidate the early events in the mechanotransduction response to cyclic strain and represent a step towards bridging our understanding of the relationship between mechanotransduction and inflammation as it relates to endothelial cell activation and dysfunction

and vascular disease. Establishment of the involvement of the ceramide biosynthetic pathway in endothelial cells and the vascular environment provides us with new biomarkers and therapeutic targets to potentially protect against vascular activation, dysfunction, and atherogenesis.

APPENDIX A

ESI-MS/MS ANALYSIS OF PHOSPHOLIPIDS IN AORTIC ENDOTHELIAL CELLS

The ESI-MS/MS analysis of the total phospholipid profile in hAECs described in Section 2.2.4.3 yielded a wealth of information about the predominant species of PC, PE, plasmenyl PE, PG, PI, and PS present in hAECs. These spectra are presented in this appendix. Daughter ion spectra are labeled to show which fragments correspond to fatty acid side-chains, allowing for determination of the acyl/acyl composition of each species shown in Tables 2.1, 2.2, 2,3. 2.4, 2.5, and 2.6. Daughter ion spectra are also labeled with the phospholipid species identified from that scan.

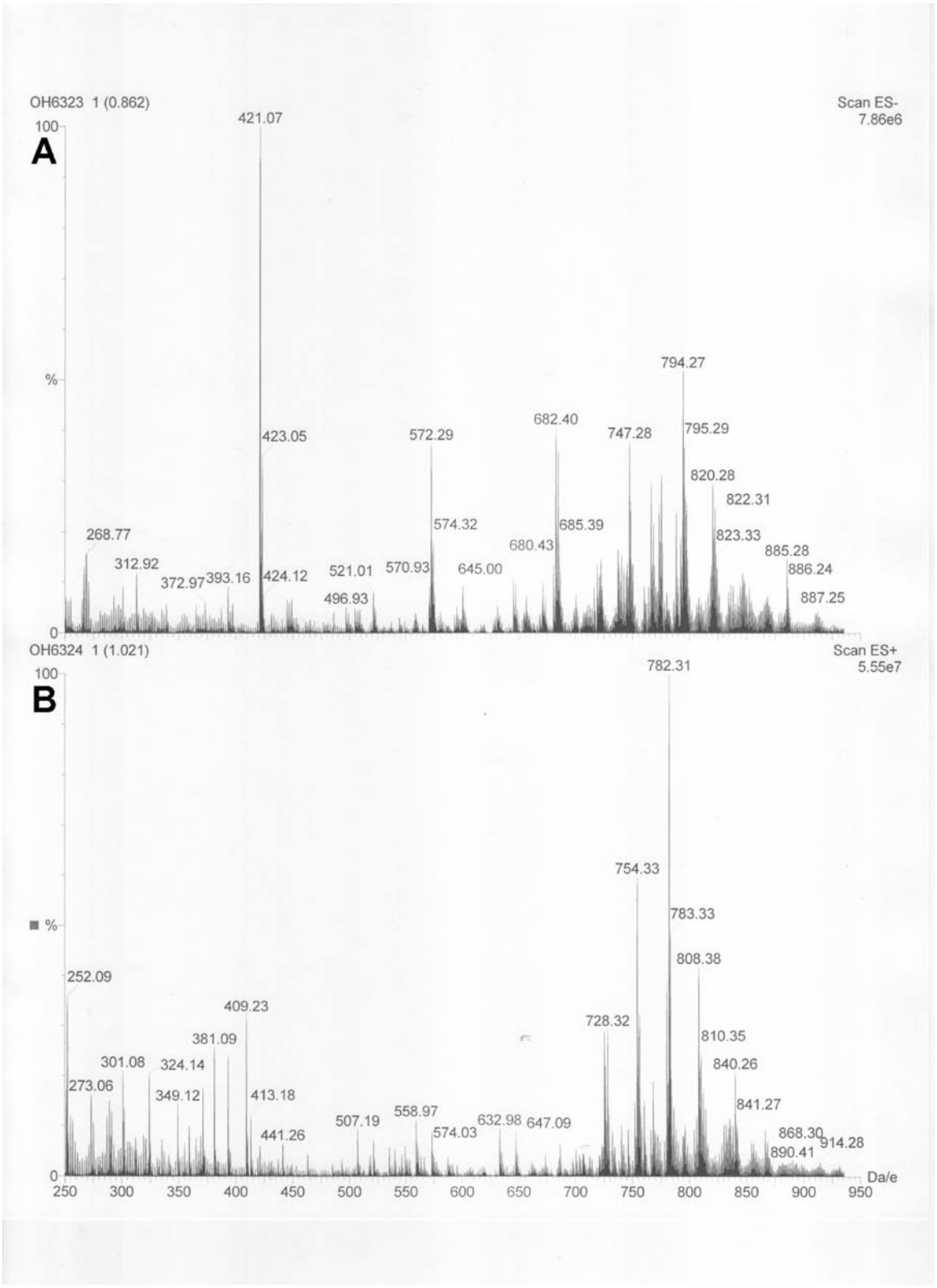

Figures A.A and A.B: (A) shows the full negative ion mode scan for hAECs. (B) shows the full positive ion modes scan for hAECs.

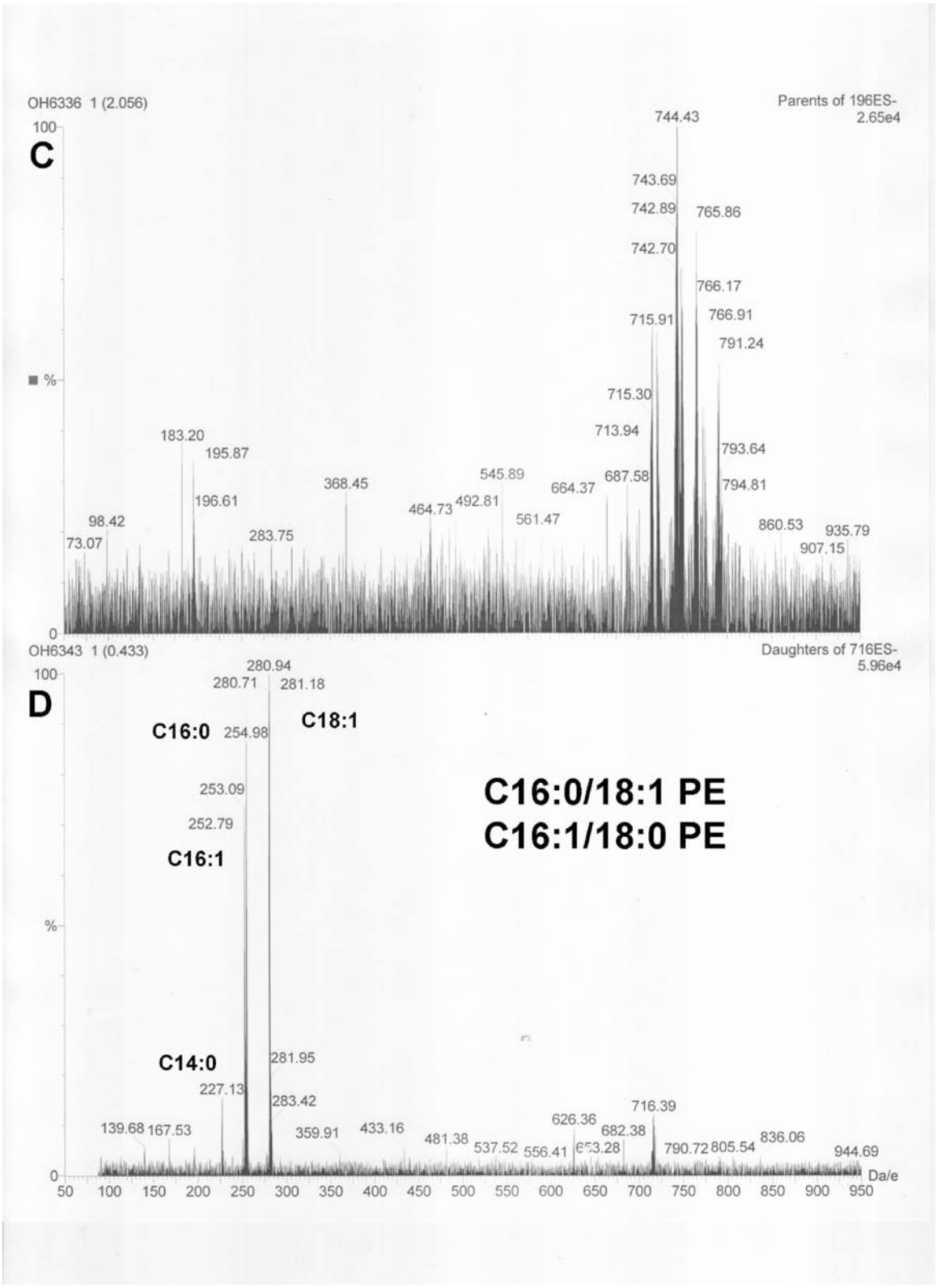

Figures A.C and A.D: (C) shows the parent ion scan of all ions producing a fragment with m/z of 196 indicating PE species. (D) shows the daughter ion scan of the parent at a m/z of 716, identified in (C).

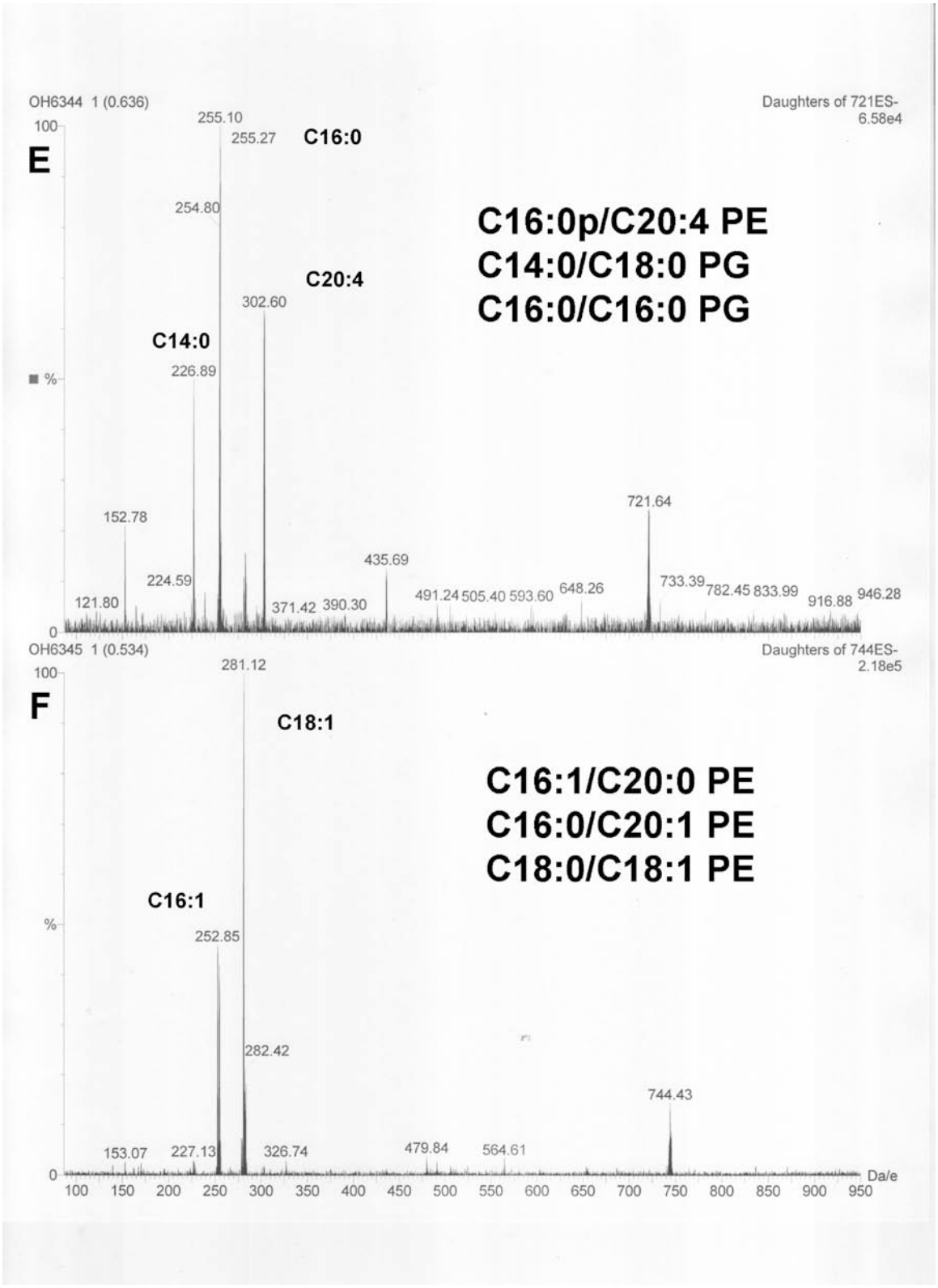

Figures A.E and A.F. (E) shows the daughter ion scan of the parent at a m/z of 721, identified in (C). (F) shows the daughter ion scan of the parent at a m/z of 744, identified in (C).

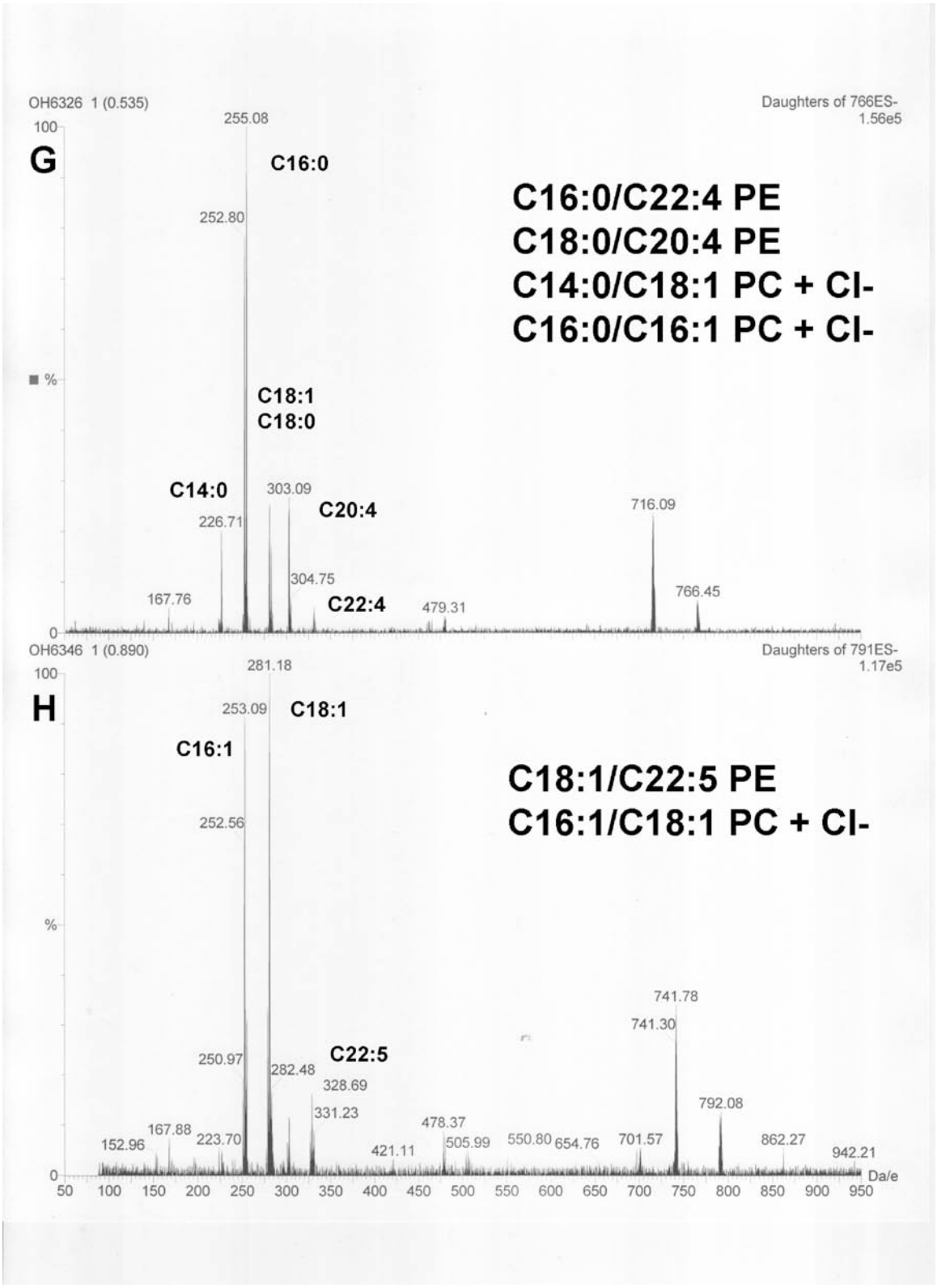

Figures A.G and A.H. (G) shows the daughter ion scan of the parent at a m/z of 766, identified in (C). (H) shows the daughter ion scan of the parent at a m/z of 791, identified in (C).

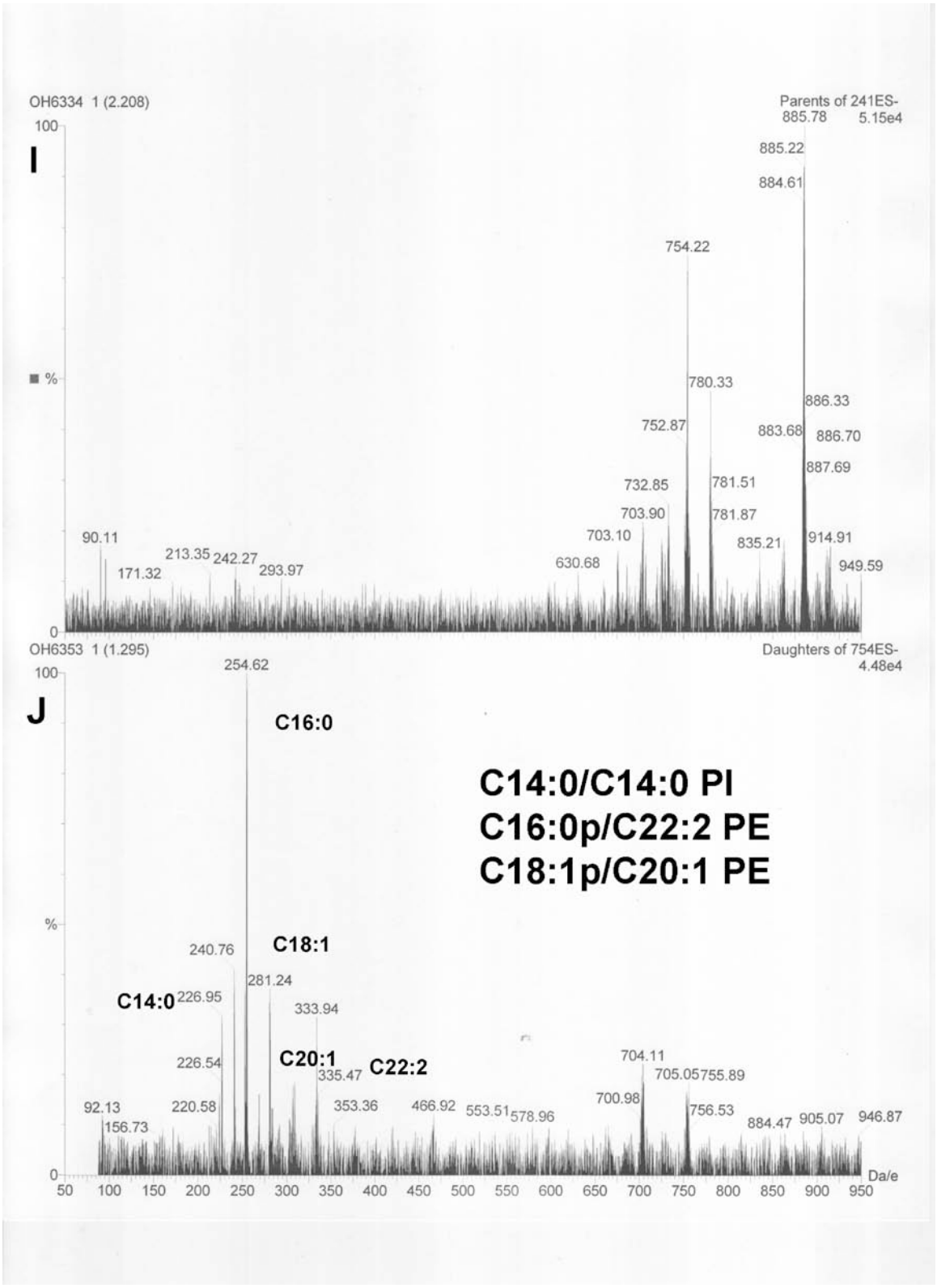

Figures A.I and A.J. (I) shows the parent ion scan of all ions producing a fragment with m/z of 241 indicating PI species. (J) shows the daughter ion scan of the parent at a m/z of 754, identified in (I).

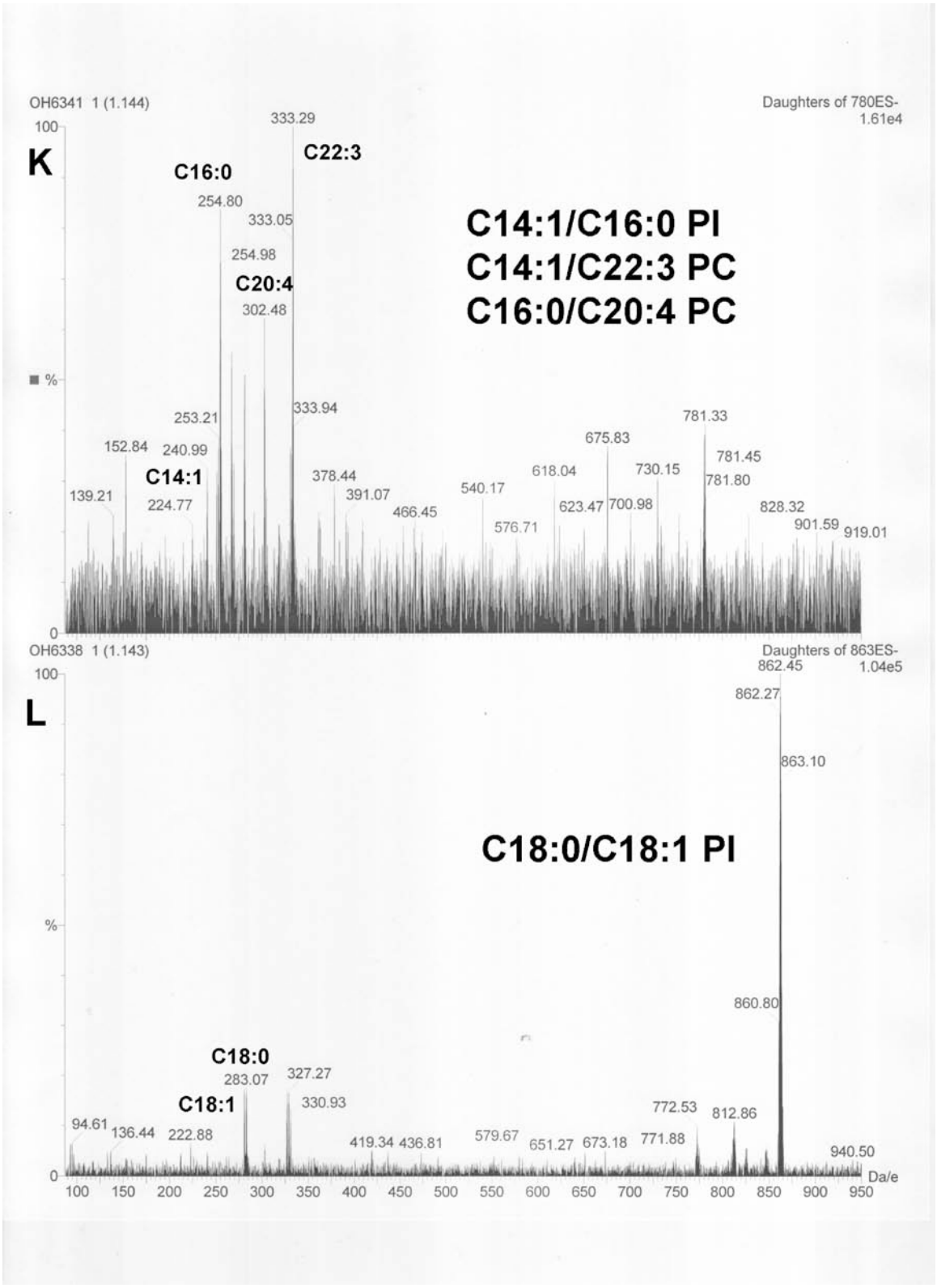

Figures A.K and A.L. (K) shows the daughter ion scan of the parent at a m/z of 780, identified in (I). (L) shows the daughter ion scan of the parent at a m/z of 863, identified in (I).

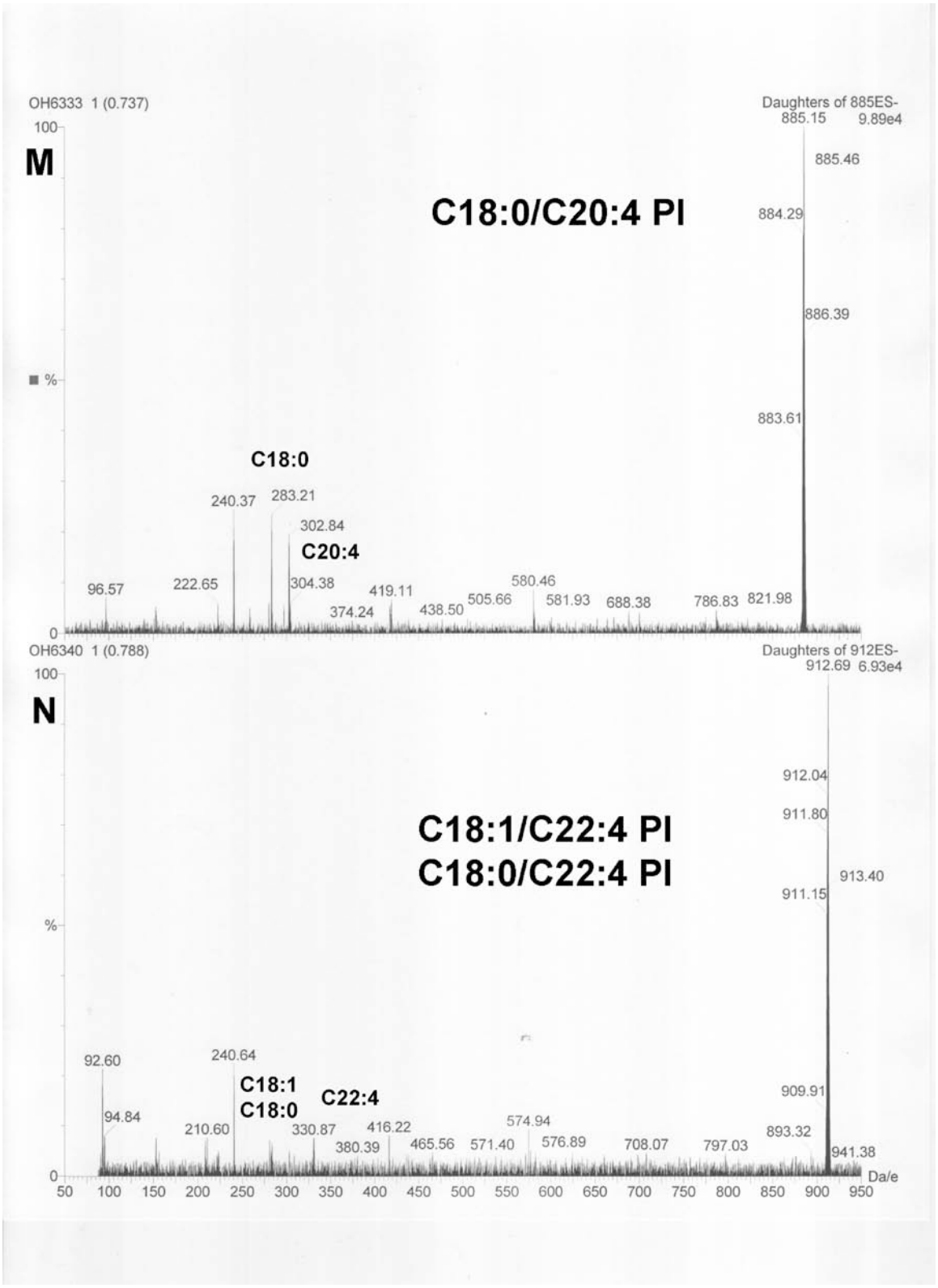

Figures A.M and A.N. (M) shows the daughter ion scan of the parent at a m/z of 885, identified in (I). (N) shows the daughter ion scan of the parent at a m/z of 912, identified in (I).

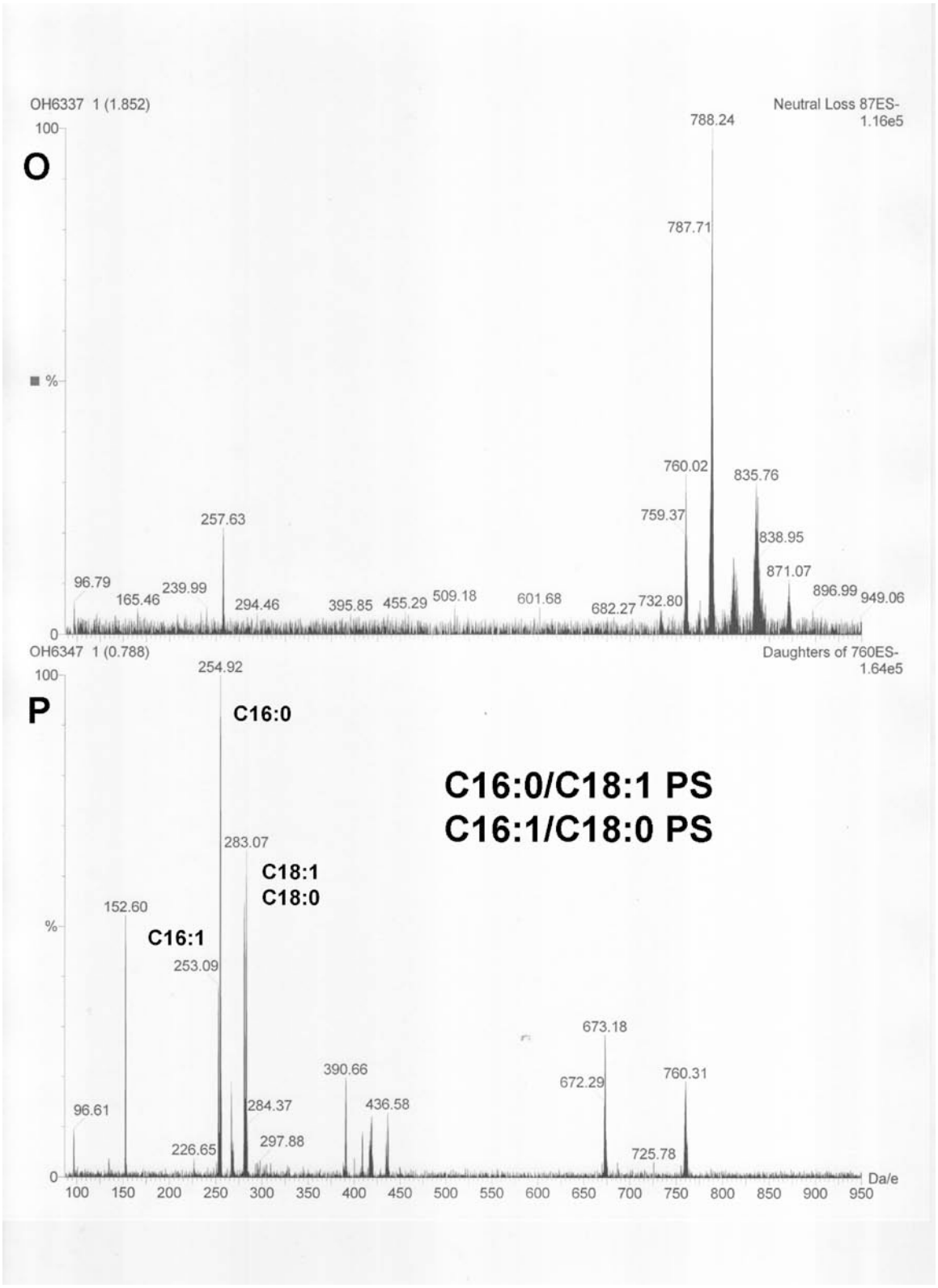

Figures A.O and A.P. (O) shows the neutral loss scan of all ions producing a fragment at m/z of 87 less than the parent, indicating PS species. (P) shows the daughter ion scan of the parent at a m/z of 760, identified in (O).

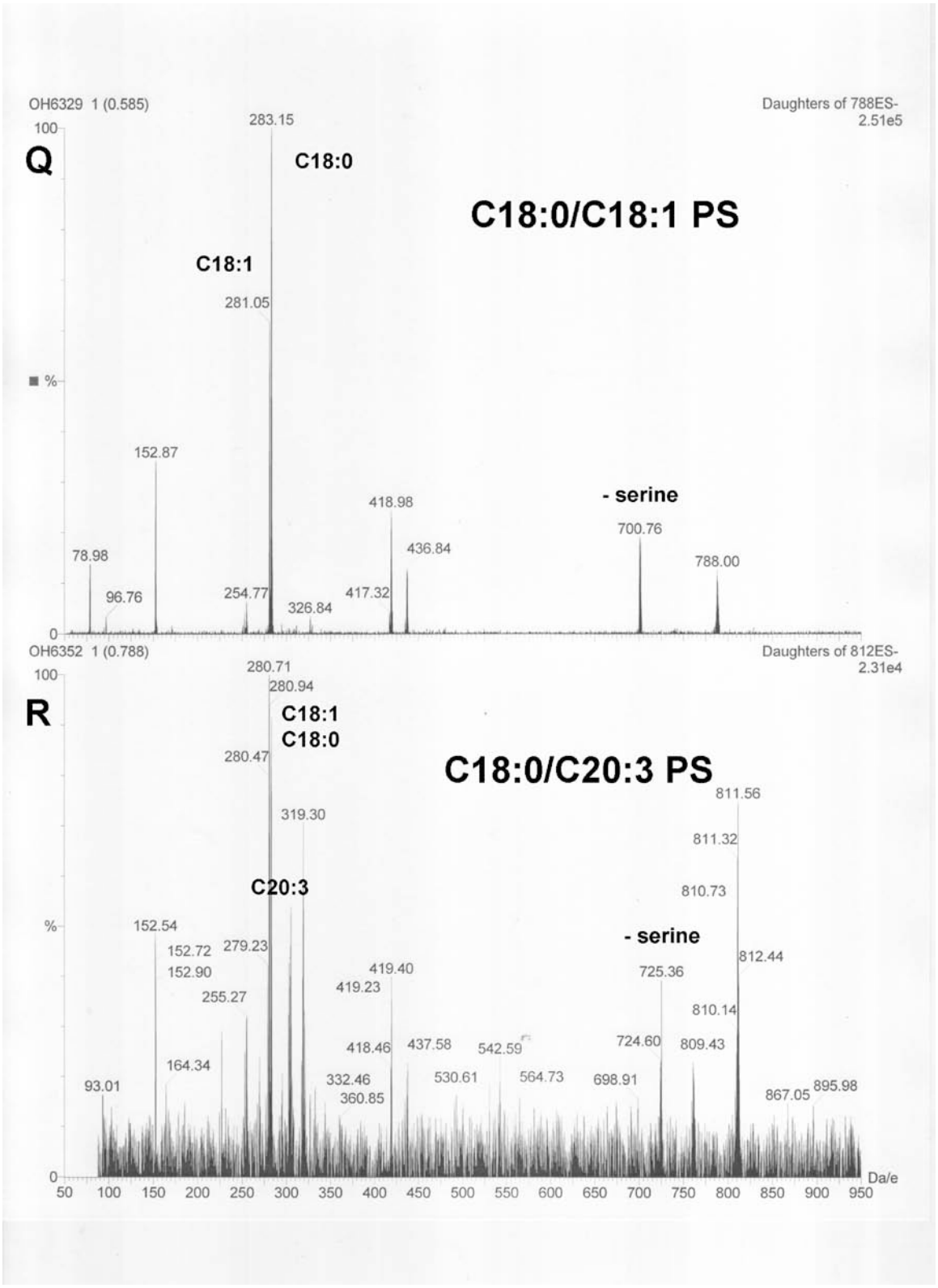

Figures A.Q and A.R. (Q) shows the daughter ion scan of the parent at a m/z of 788, identified in (O). (R) shows the daughter ion scan of the parent at a m/z of 812, identified in (O).

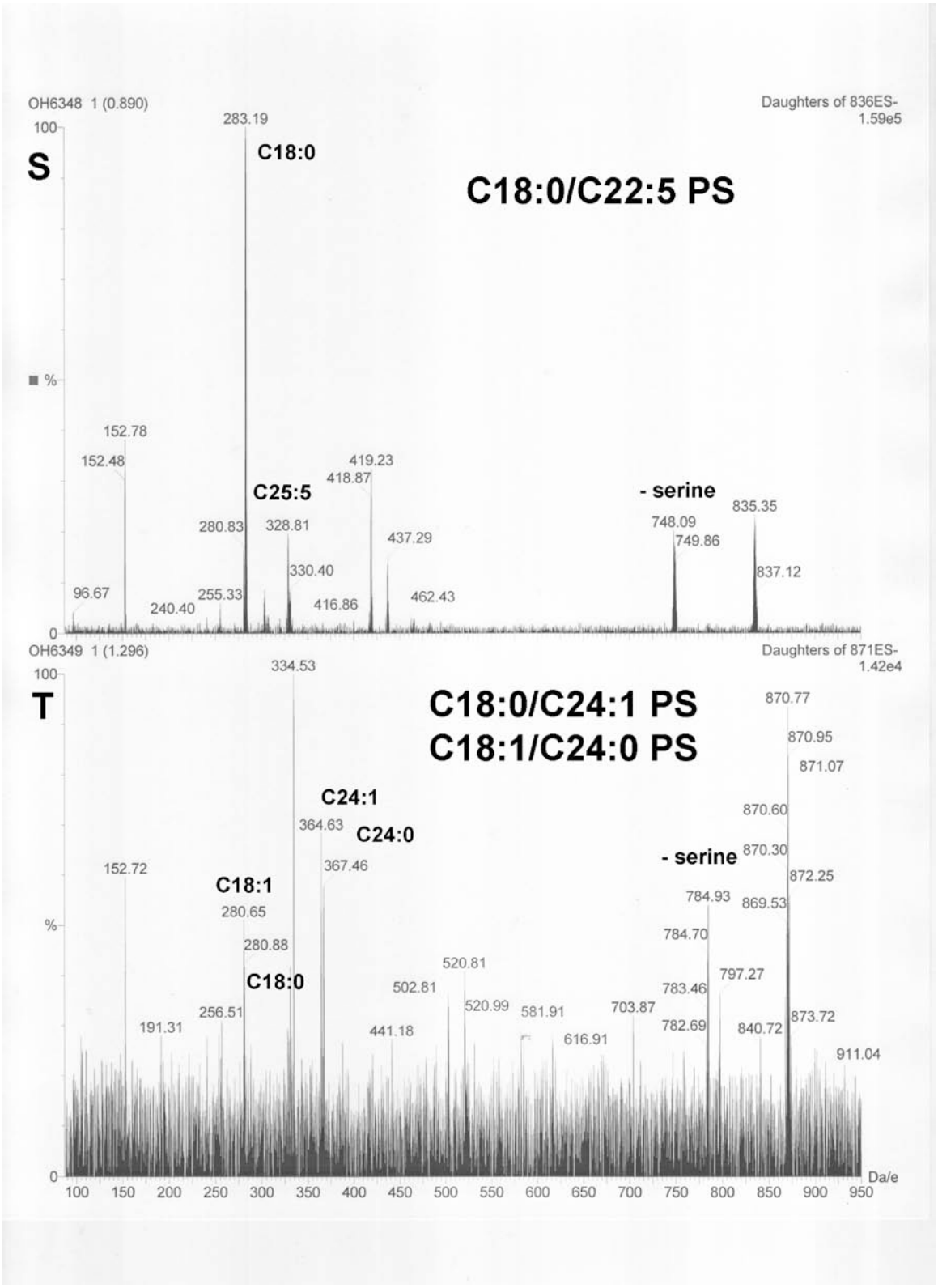

Figures A.S and A.T. (S) shows the daughter ion scan of the parent at a m/z of 836, identified in (O). (T) shows the daughter ion scan of the parent at a m/z of 871, identified in (O).

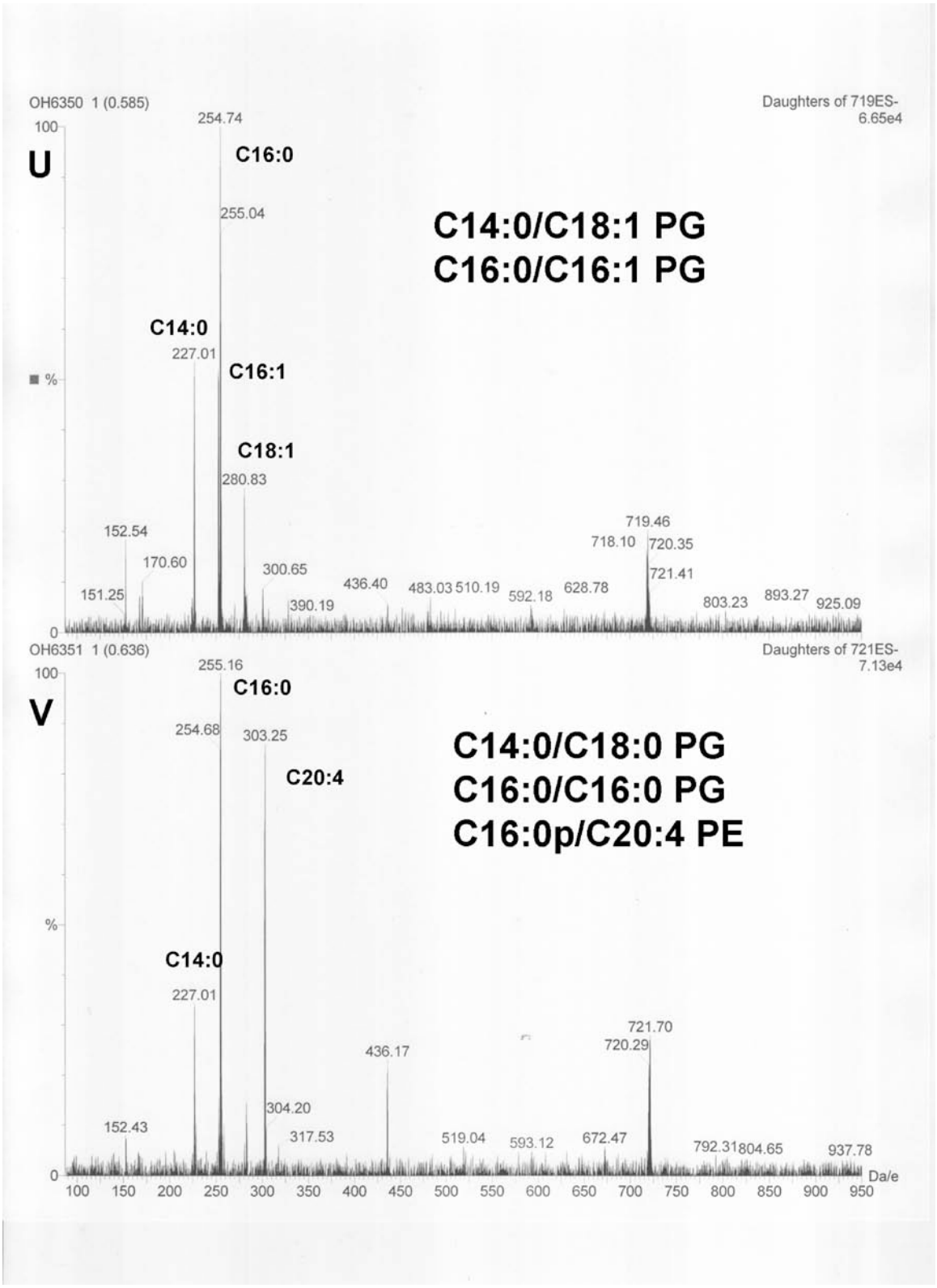

Figures A.U and A.V. (U) shows the daughter ion scan of the parent at a m/z of 719, identified in (A). (V) shows the daughter ion scan of the parent at a m/z of 721, identified in (A).

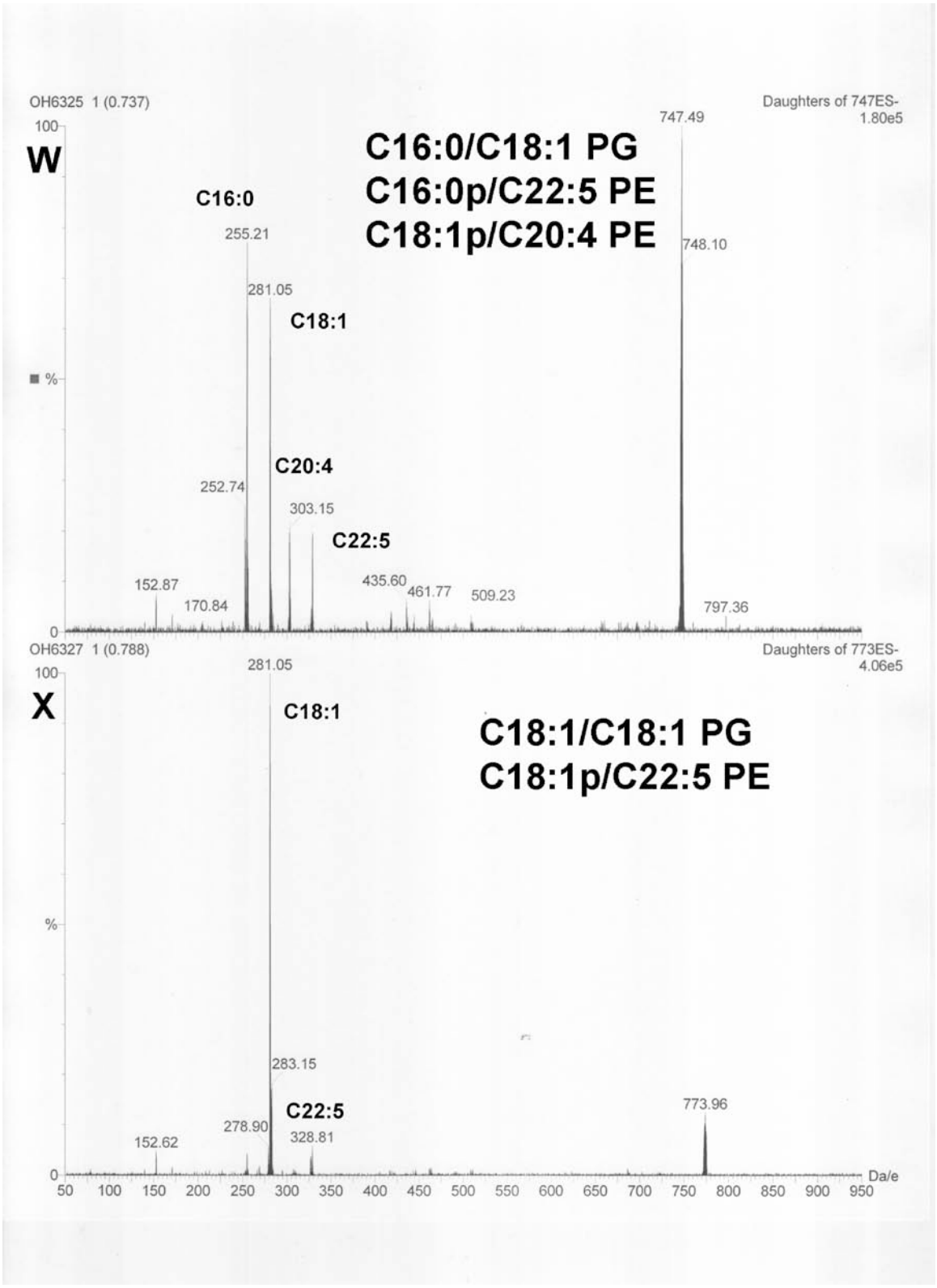

Figures A.W and A.X. (W) shows the daughter ion scan of the parent at a m/z of 747, identified in (A). (X) shows the daughter ion scan of the parent at a m/z of 773, identified in (A).

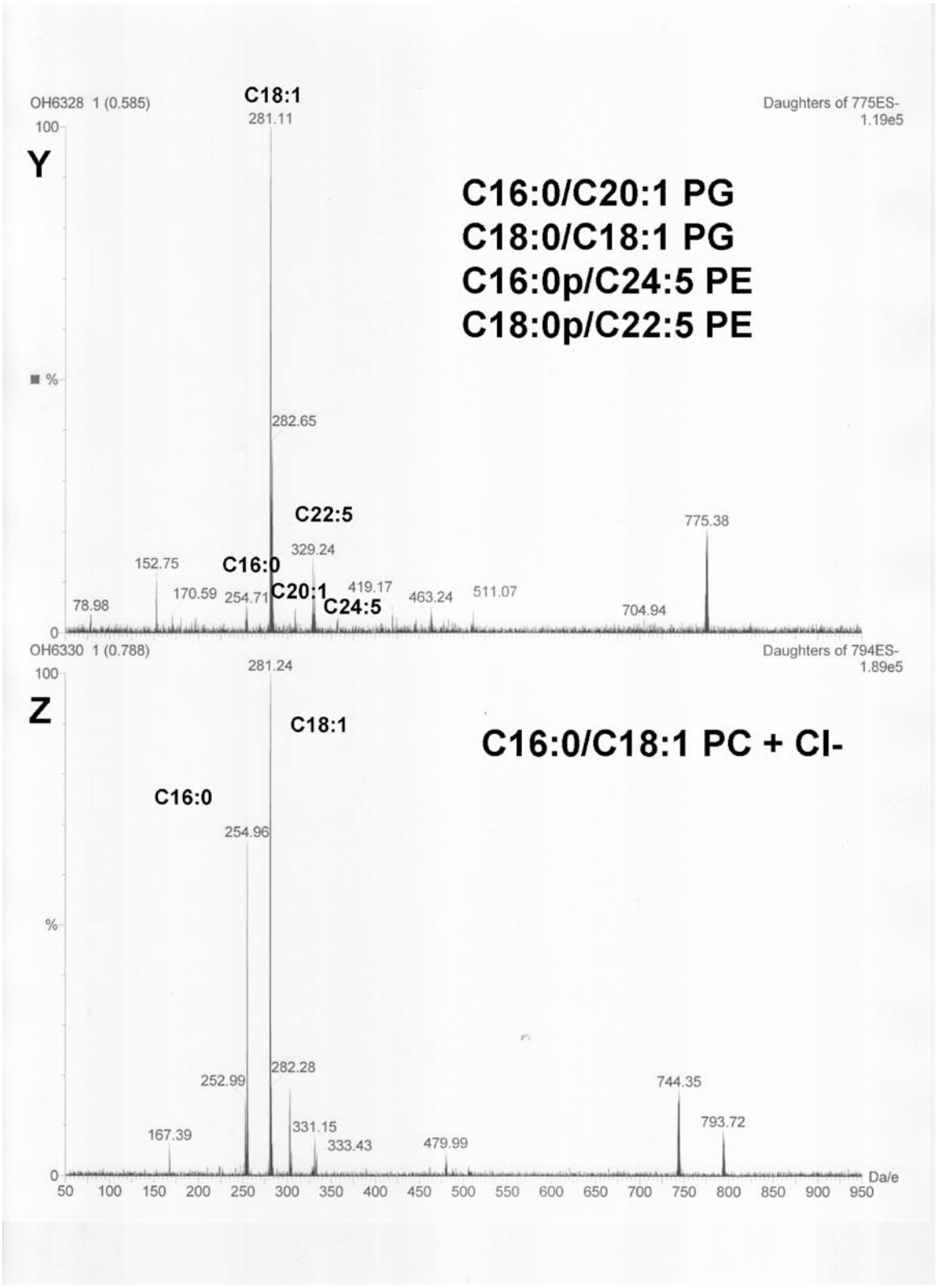

Figures A.Y and A.Z. (Y) shows the daughter ion scan of the parent at a m/z of 775, identified in (A). (Z) shows the daughter ion scan of the parent at a m/z of 794, identified in (A).

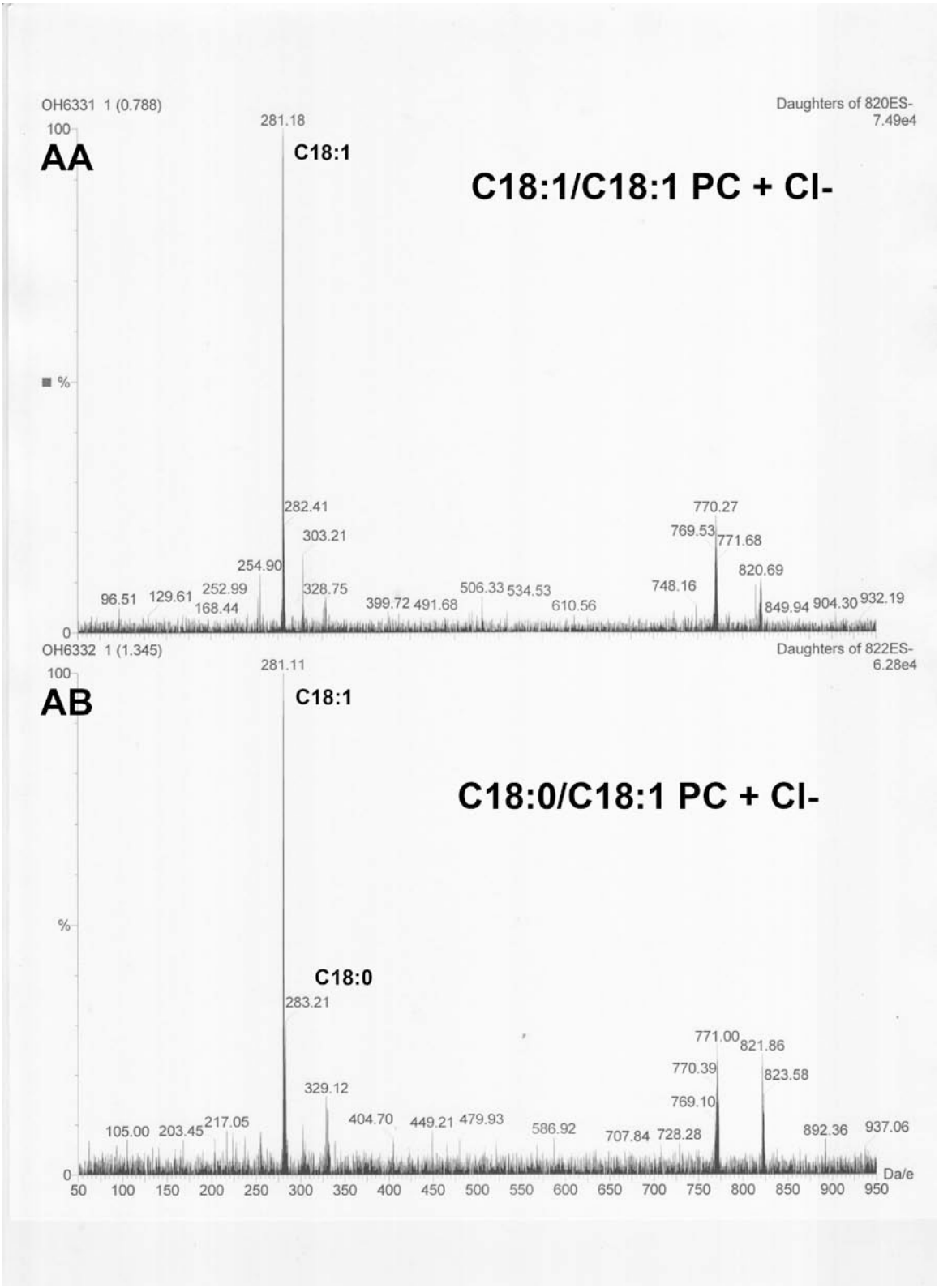

Figures A.AA and A.AB. (AA) shows the daughter ion scan of the parent at a m/z of 820, identified in (A). (AB) shows the daughter ion scan of the parent at a m/z of 822, identified in (A).

APPENDIX B

ESI-MS VERIFICATION OF SIMILARITY OF LIPID PROFILE BETWEEN HUMAN AND BOVINE AORTIC ENDOTHELIAL CELLS

To confirm that the same species of phospholipids and sphingolipids identified in hAECs are also present in bAECs, the full positive and negative ion mode spectra were compared following ESI-MS analysis of identically performed lipid extractions from both cell types. These spectra are presented in this appendix. For ease of comparison, the spectra have been expanded so that each figure shows a m/z range of 50 units unless otherwise specified. The negative ion mode scan covers the m/z range of 250-950 to include sphingosine (m/z of 299) and S-1-P (m/z of 379) in addition to the usual phospholipids and sphingolipids detected in the m/z range of 400-950. The positive ion scan covers the m/z range of 400-950. For each figure, the top spectra corresponds to hAECs and the bottom panel corresponds to bAECs.

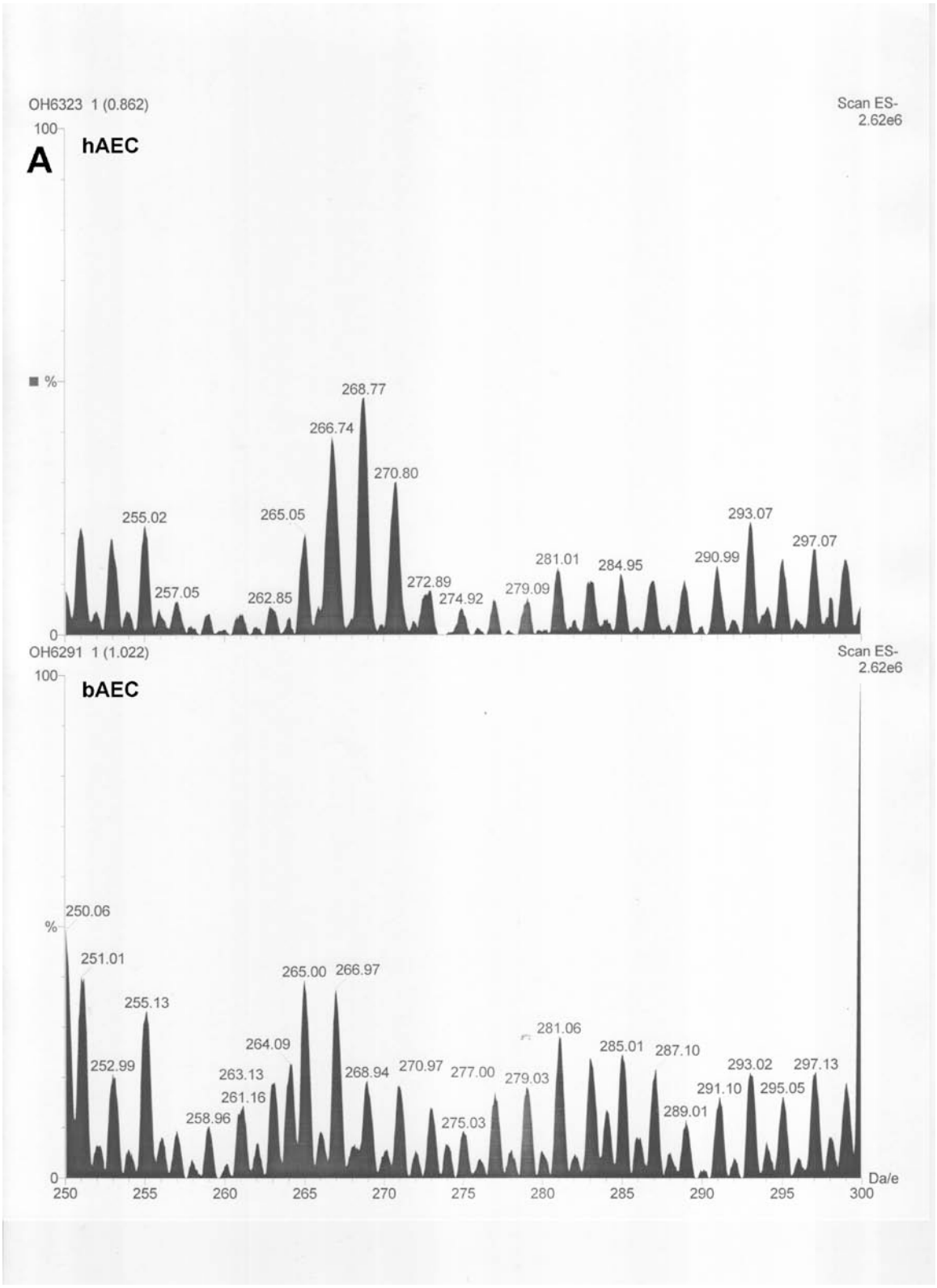

Figure B.A. ESI-MS comparison of hAECs and bAECs in the negative ion mode across the m/z range of 250-300.

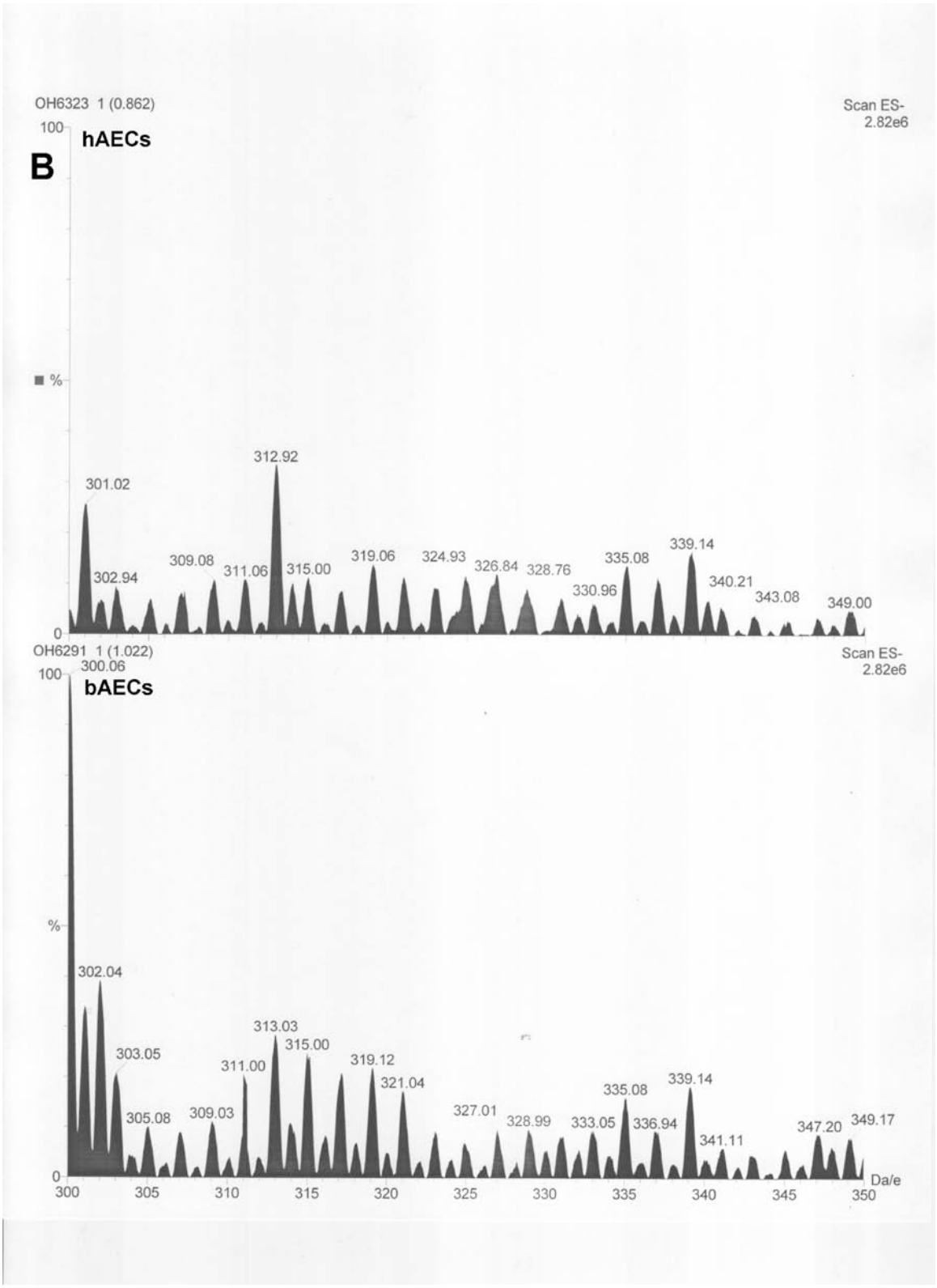

Figure B.B. ESI-MS comparison of hAECs and bAECs in the negative ion mode across the m/z range of 300-350.

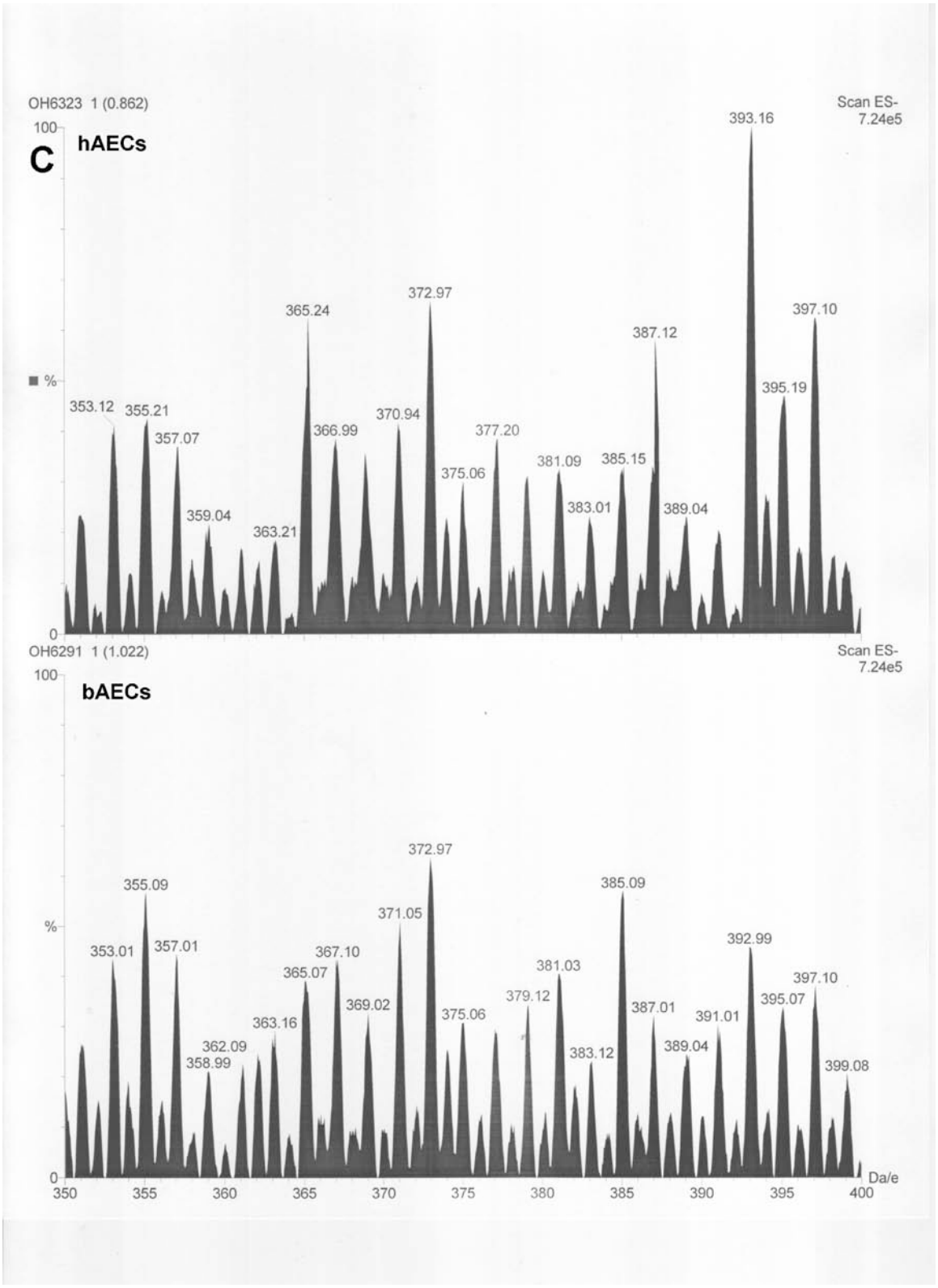

Figure B.C. ESI-MS comparison of hAECs and bAECs in the negative ion mode across the m/z range of 350-400.

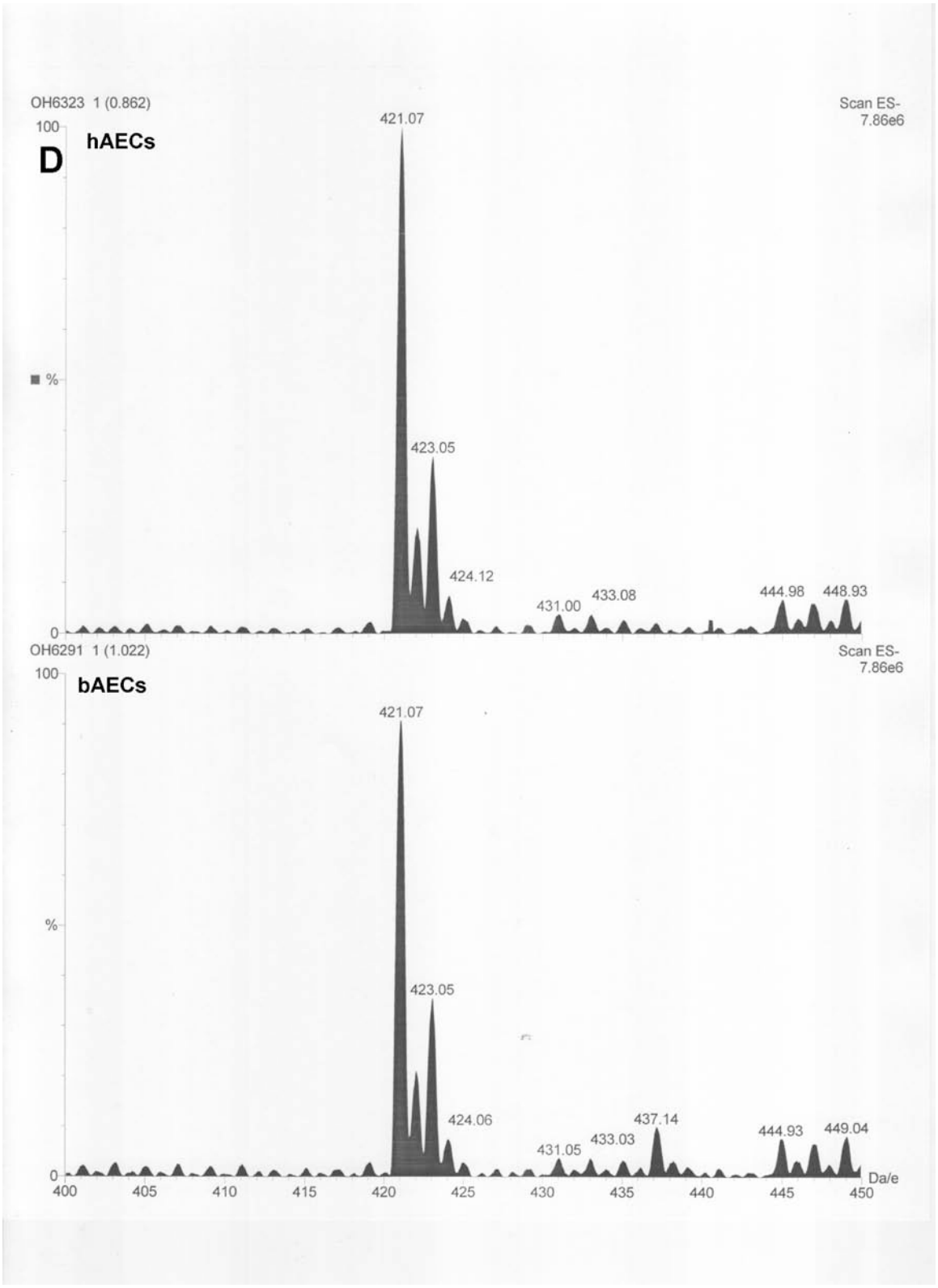

Figure B.D. ESI-MS comparison of hAECs and bAECs in the negative ion mode across the m/z range of 400-450.

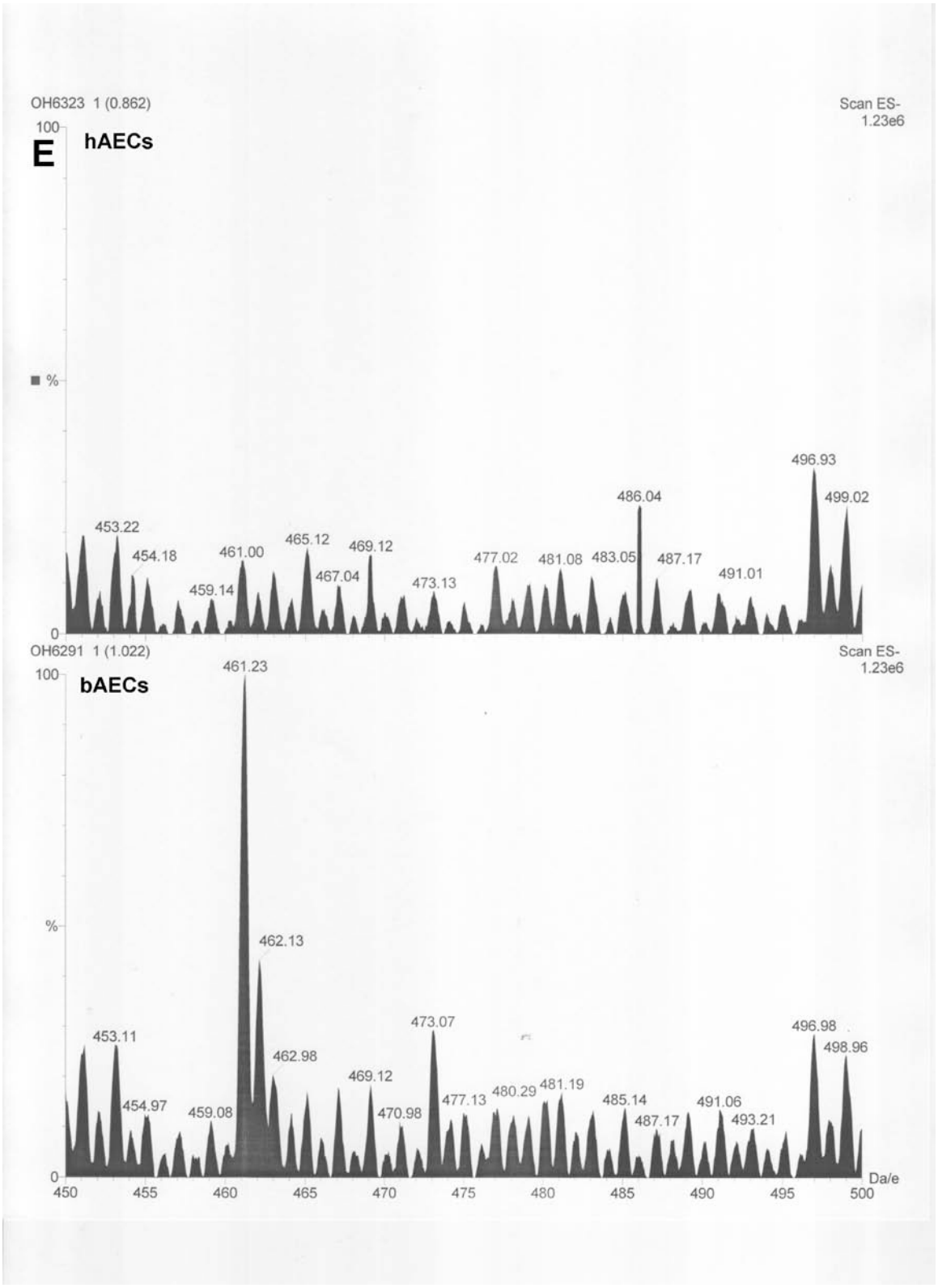

Figure B.E. ESI-MS comparison of hAECs and bAECs in the negative ion mode across the m/z range of 450-500.

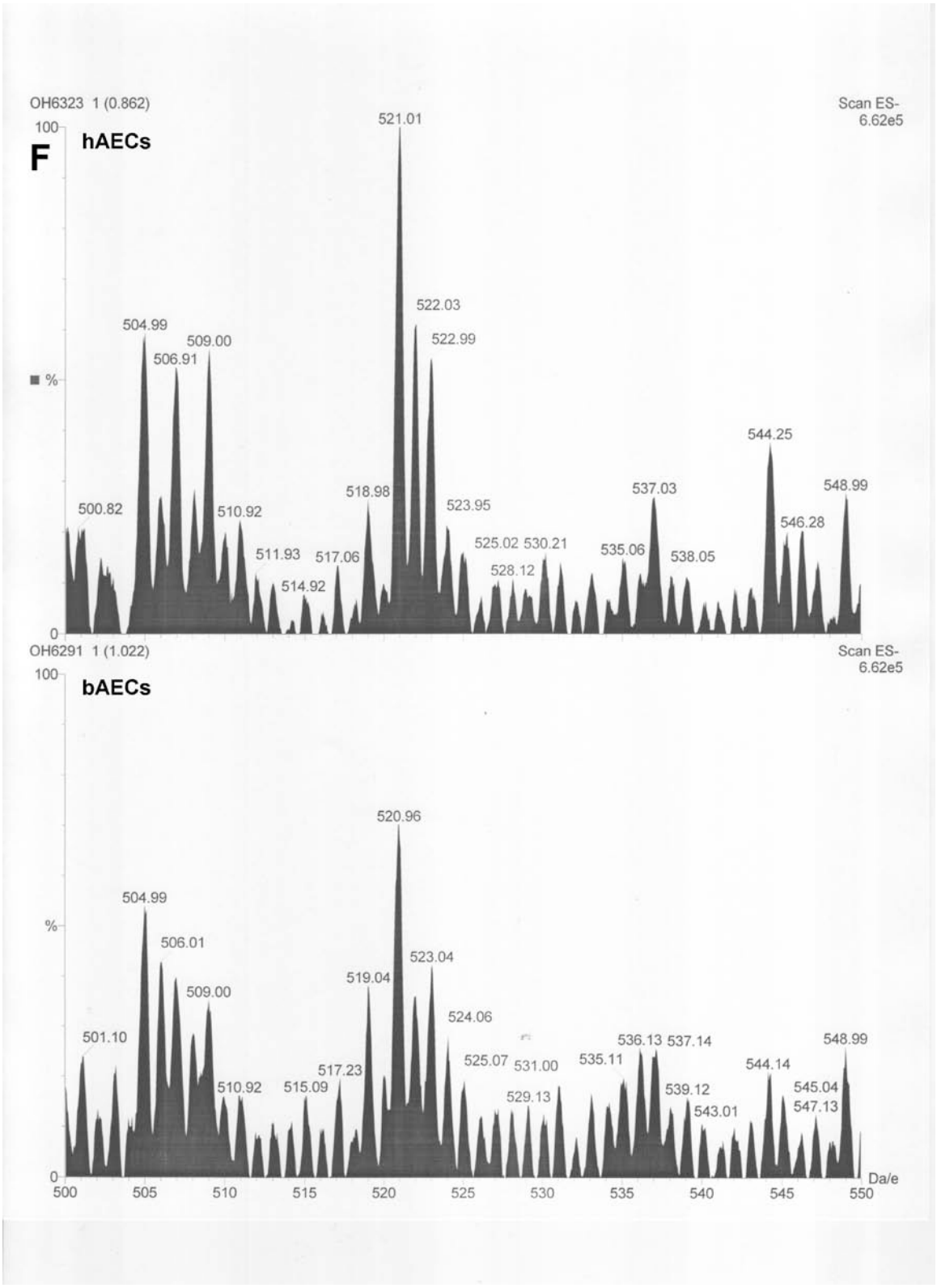

Figure B.F. ESI-MS comparison of hAECs and bAECs in the negative ion mode across the m/z range of 500-550.

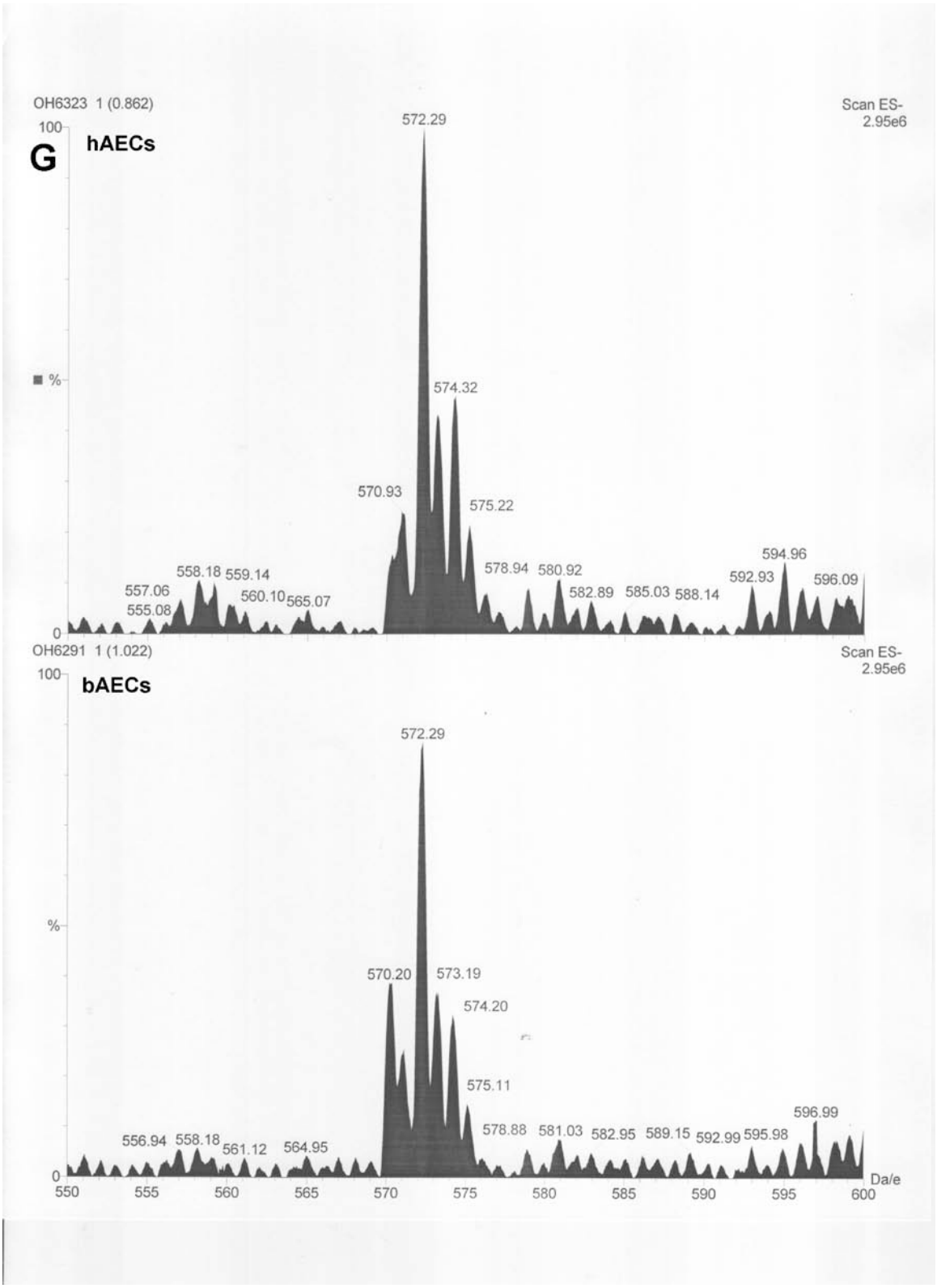

Figure B.G. ESI-MS comparison of hAECs and bAECs in the negative ion mode across the m/z range of 550-600.

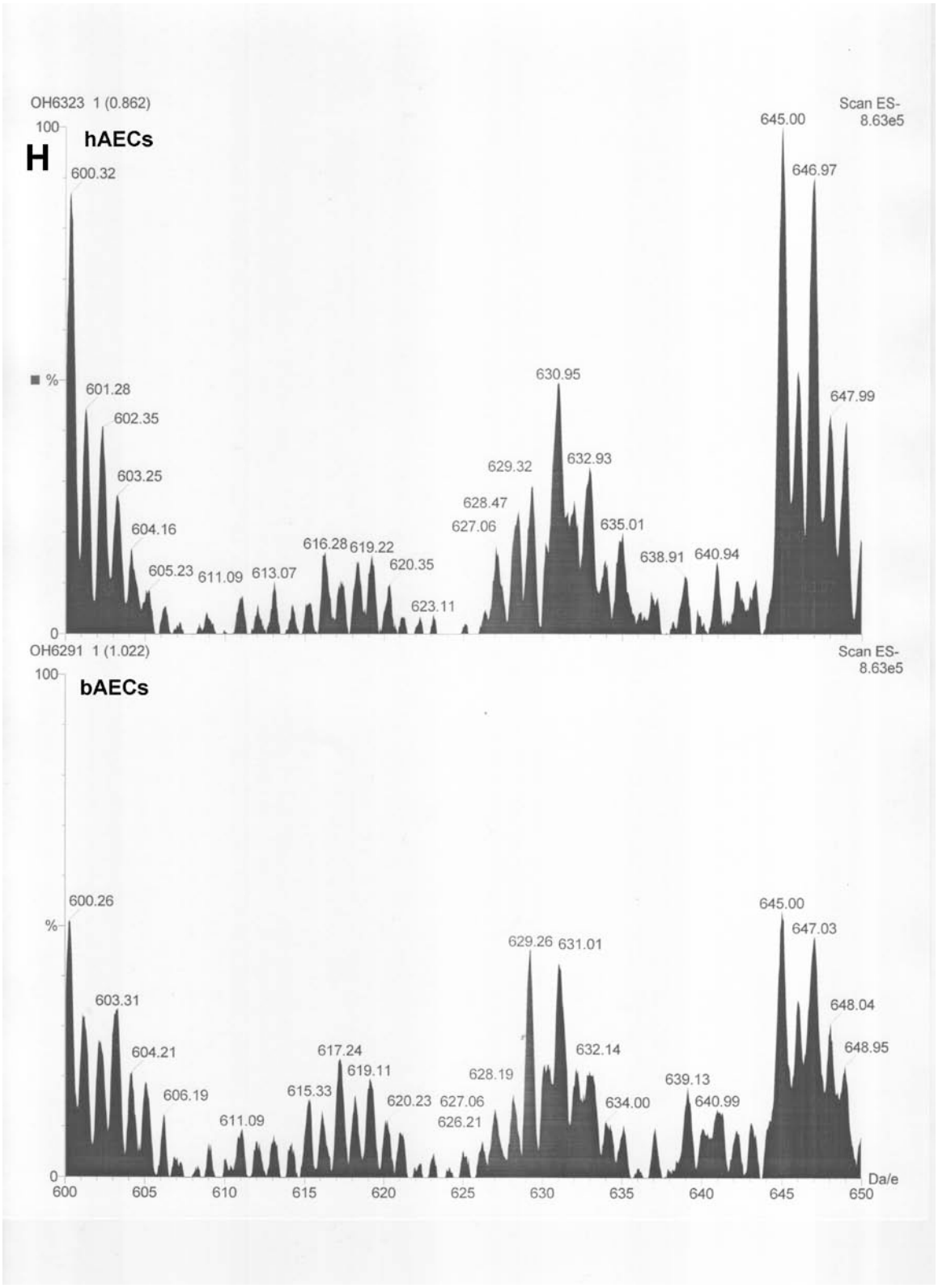

Figure B.H. ESI-MS comparison of hAECs and bAECs in the negative ion mode across the m/z range of 600-650.

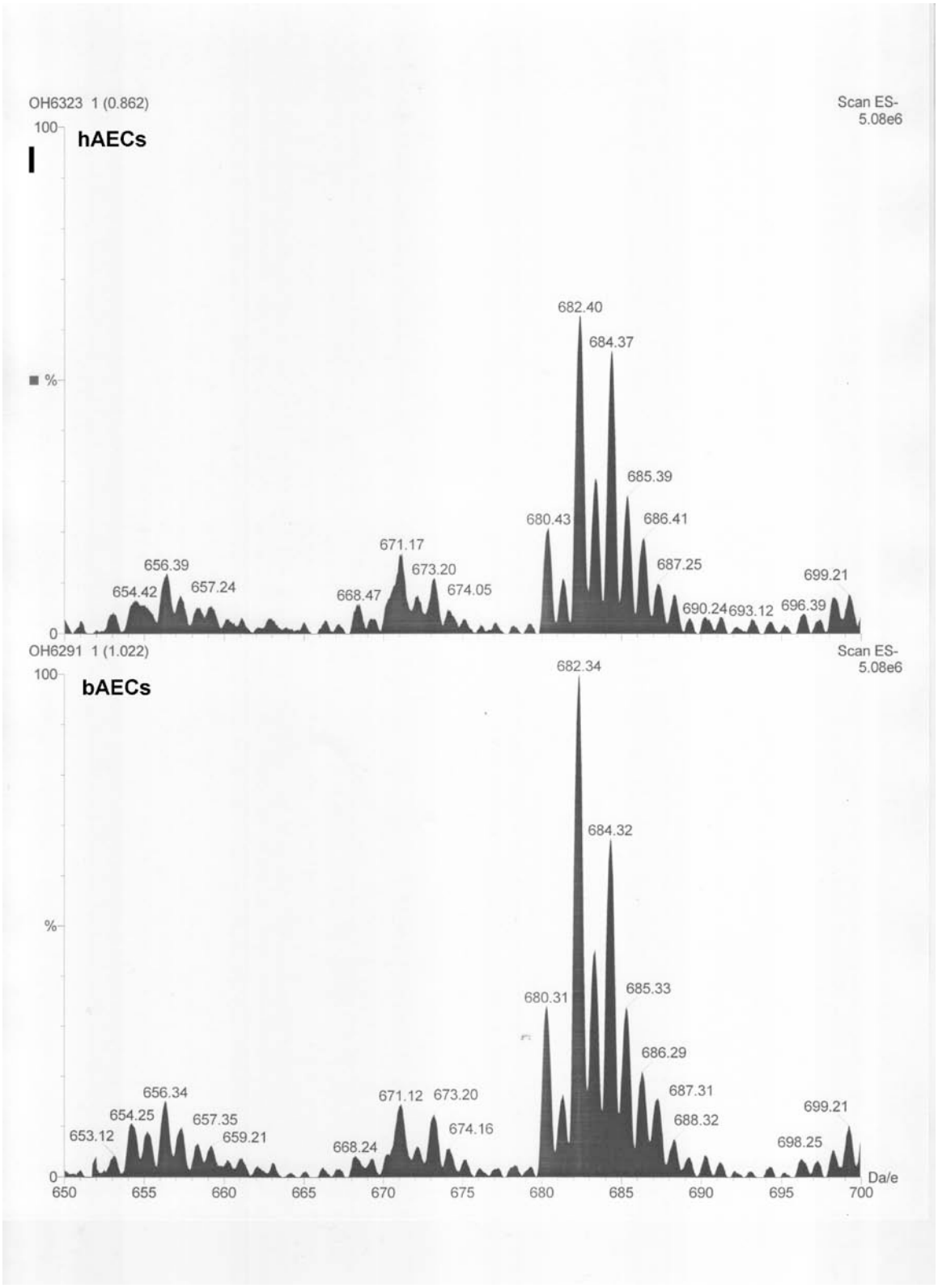

Figure B.I. ESI-MS comparison of hAECs and bAECs in the negative ion mode across the m/z range of 650-700.

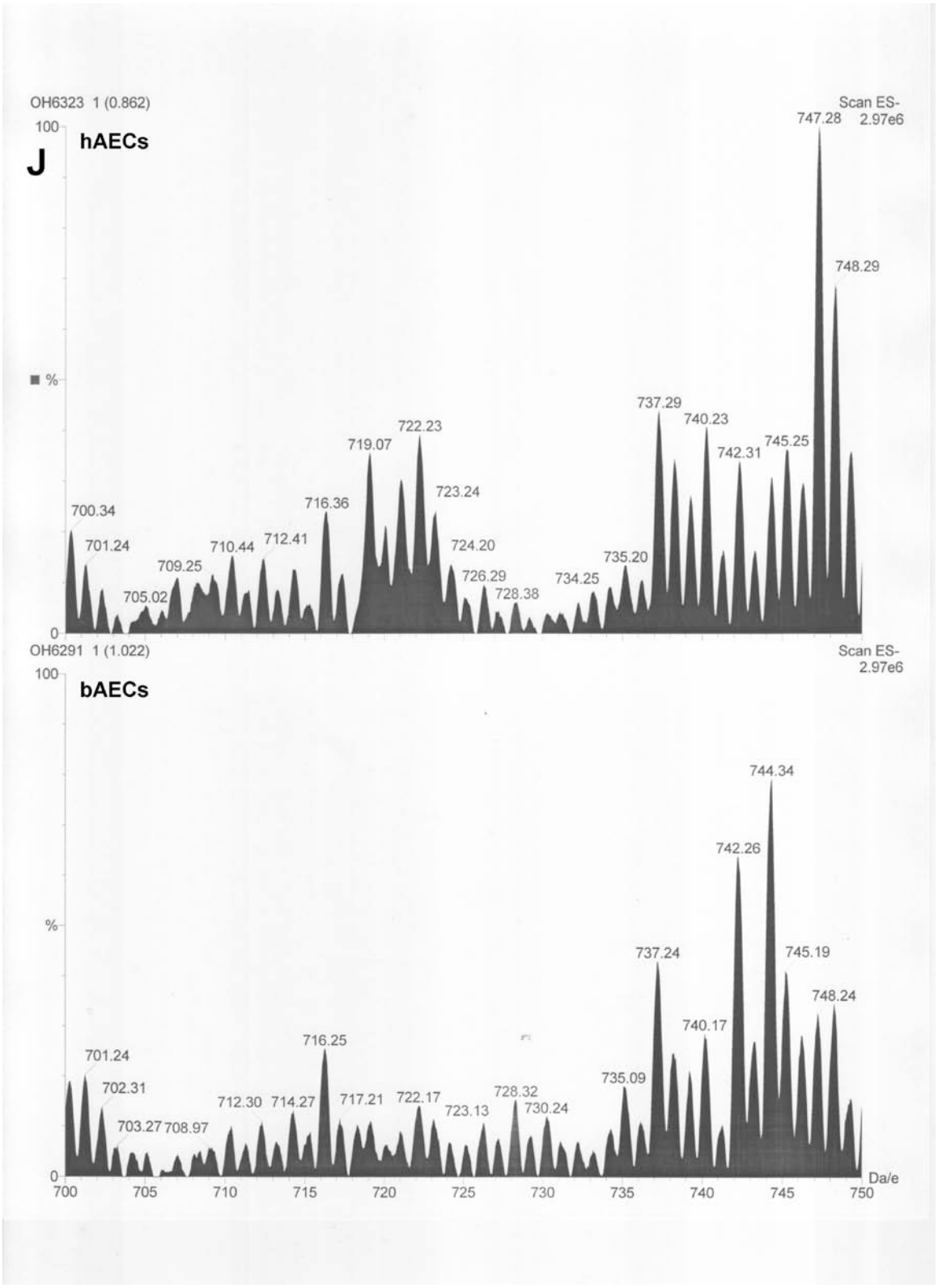

Figure B.J. ESI-MS comparison of hAECs and bAECs in the negative ion mode across the m/z range of 700-750.

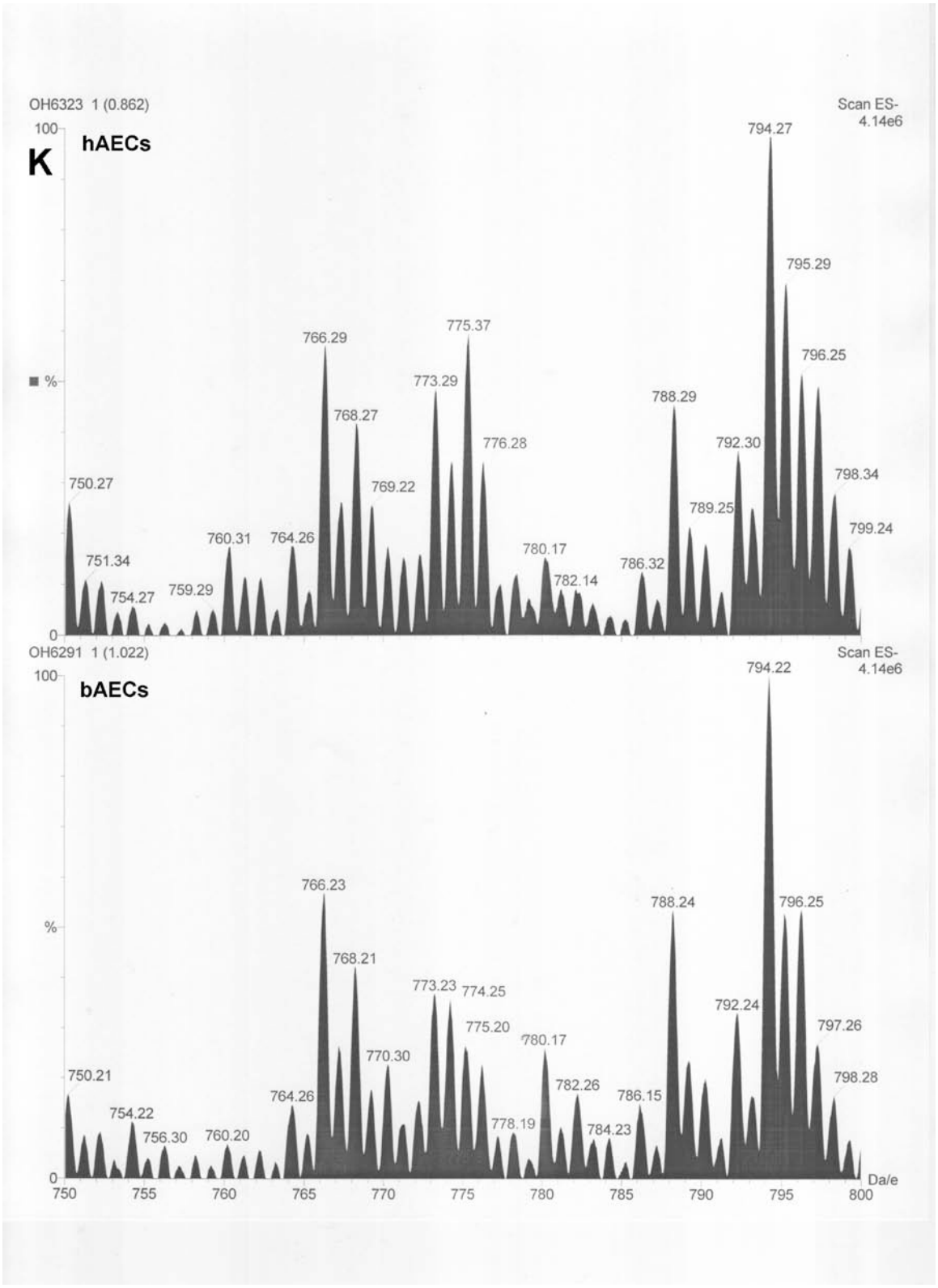

Figure B.K. ESI-MS comparison of hAECs and bAECs in the negative ion mode across the m/z range of 750-800.

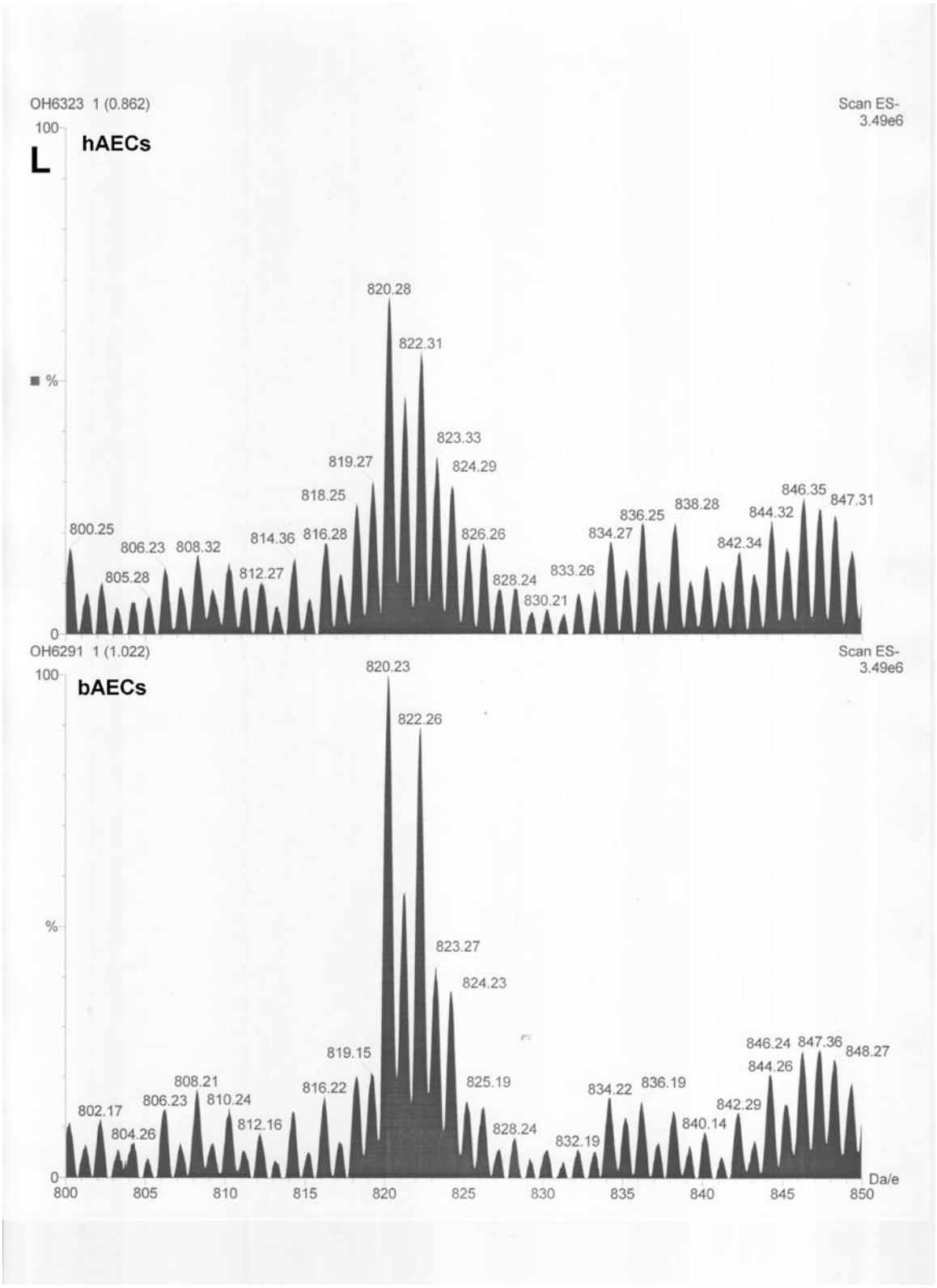

Figure B.L. ESI-MS comparison of hAECs and bAECs in the negative ion mode across the m/z range of 800-850.

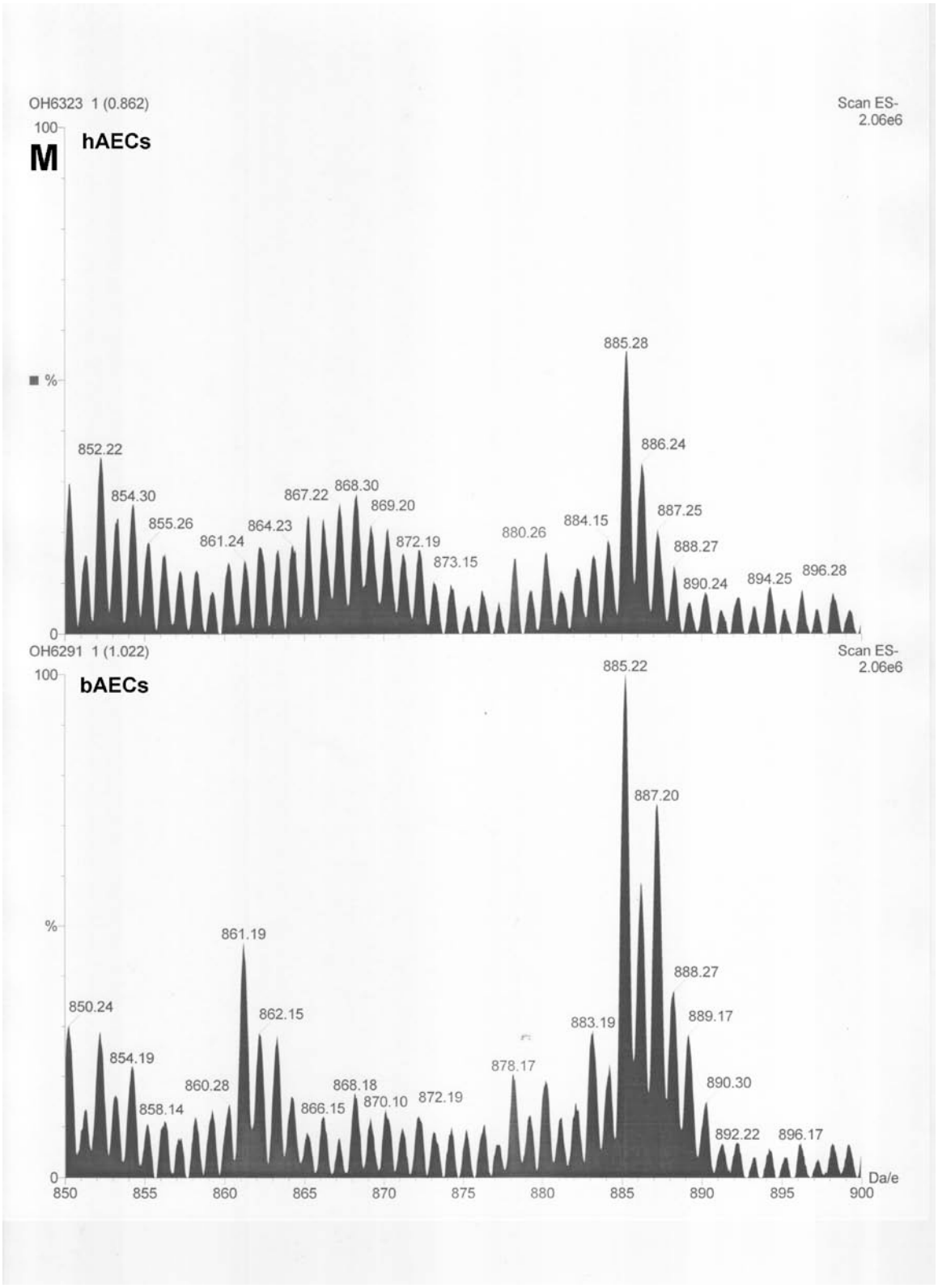

Figure B.M. ESI-MS comparison of hAECs and bAECs in the negative ion mode across the m/z range of 850-900.

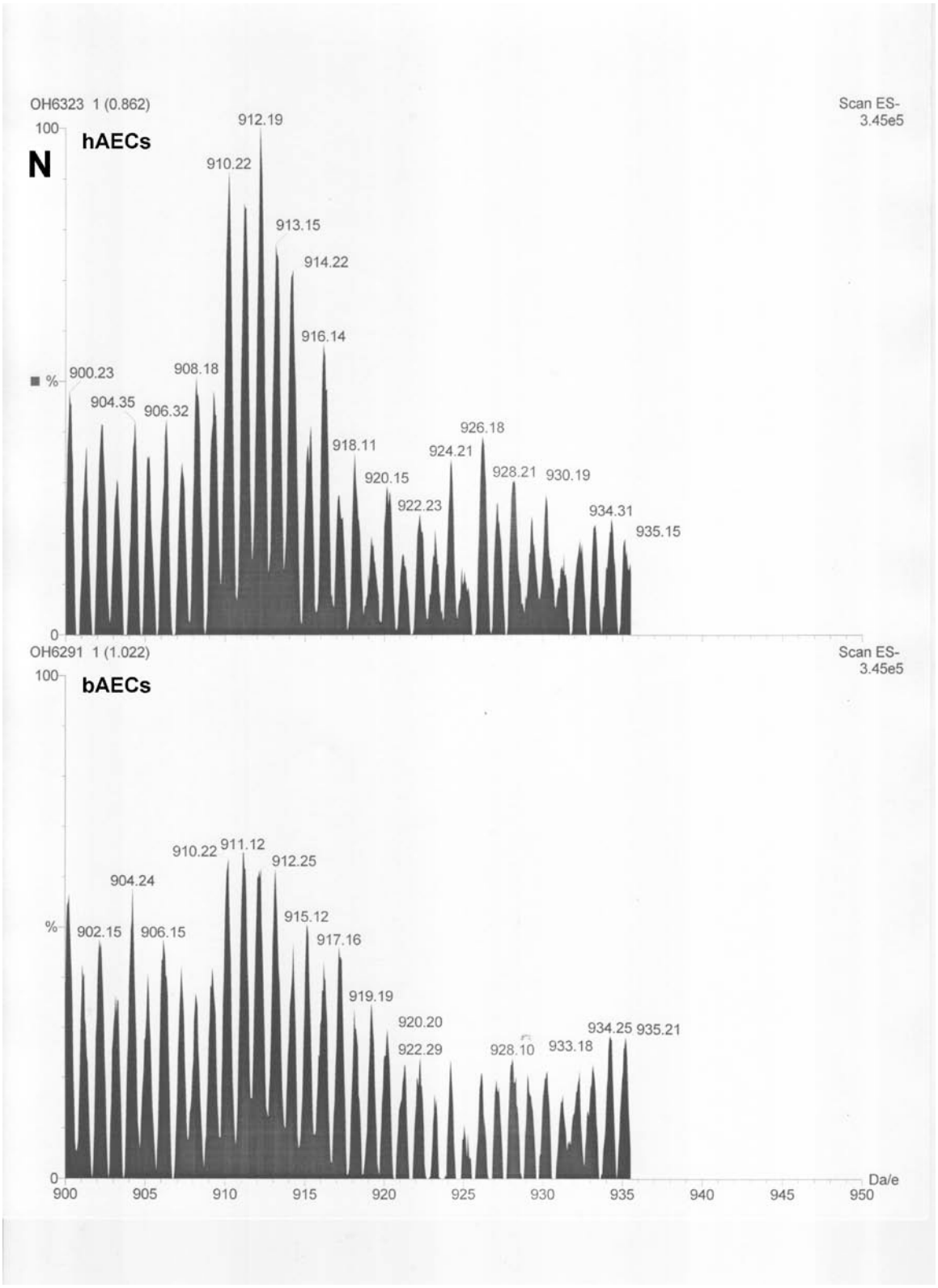

Figure B.N. ESI-MS comparison of hAECs and bAECs in the negative ion mode across the m/z range of 900-950.

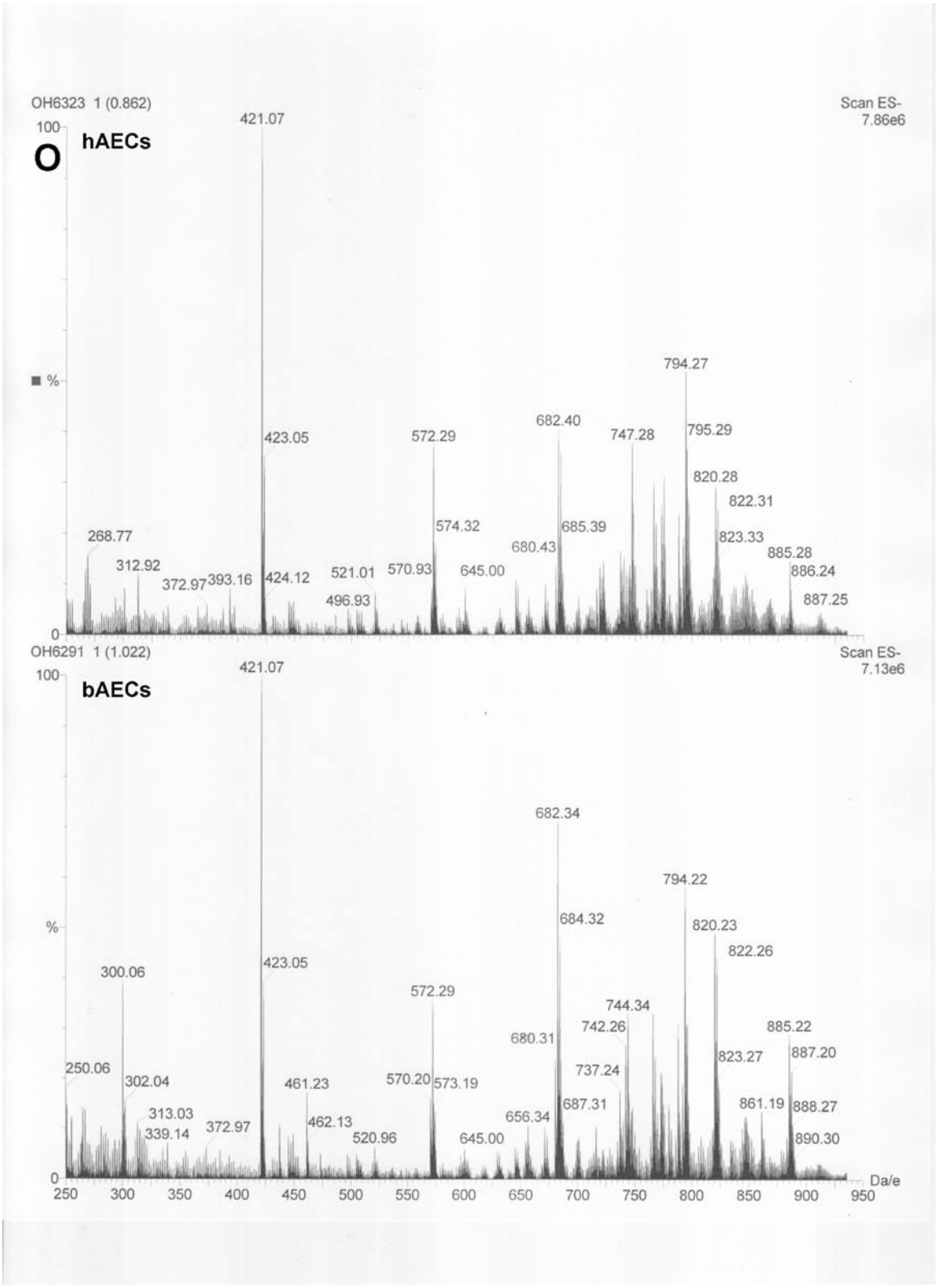

Figure B.O. ESI-MS comparison of hAECs and bAECs in the negative ion mode across the m/z range of 250-950.

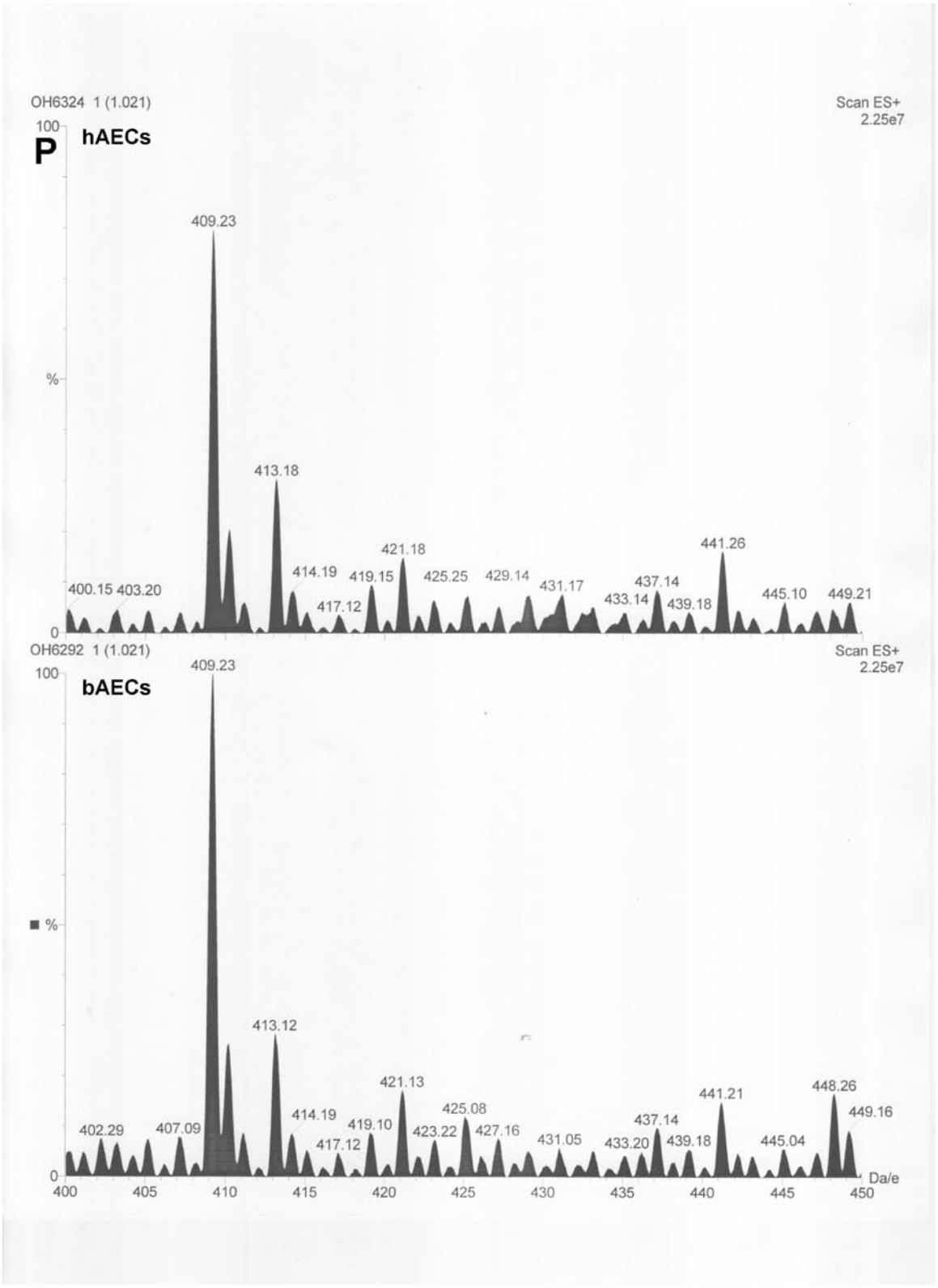

Figure B.P. ESI-MS comparison of hAECs and bAECs in the positive ion mode across the m/z range of 400-450.

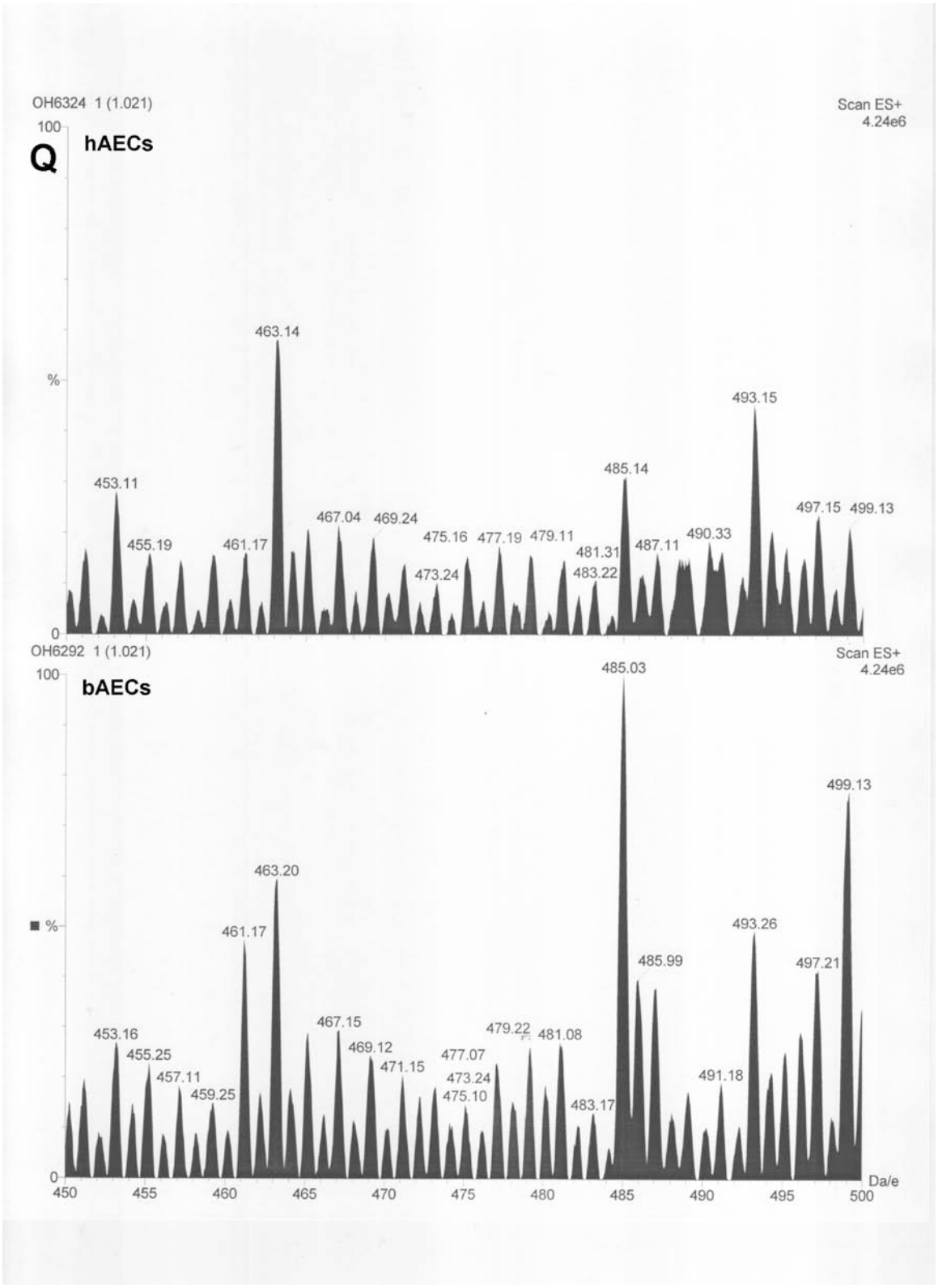

Figure B.Q. ESI-MS comparison of hAECs and bAECs in the positive ion mode across the m/z range of 450-500.

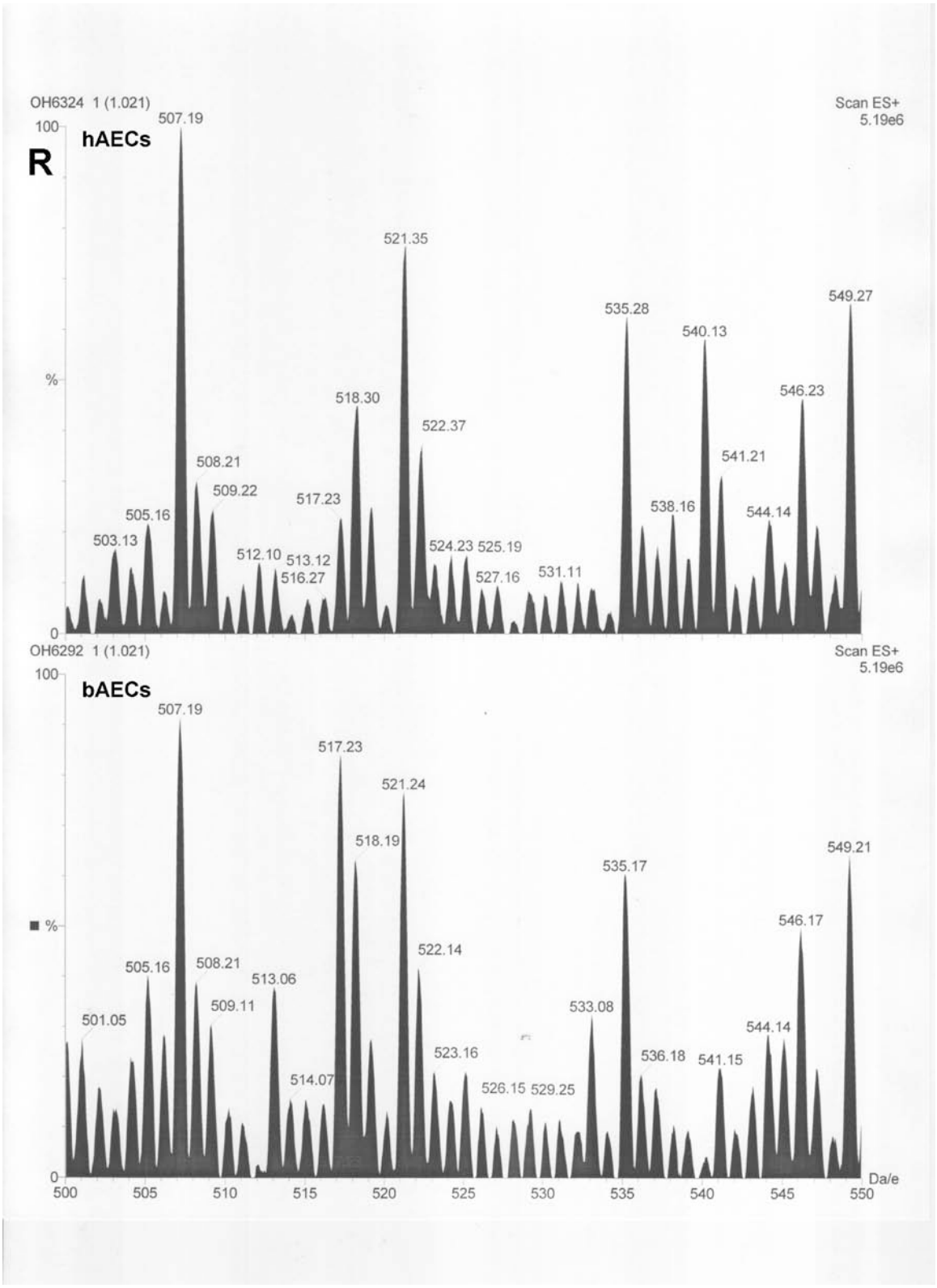

Figure B.R. ESI-MS comparison of hAECs and bAECs in the positive ion mode across the m/z range of 500-550.

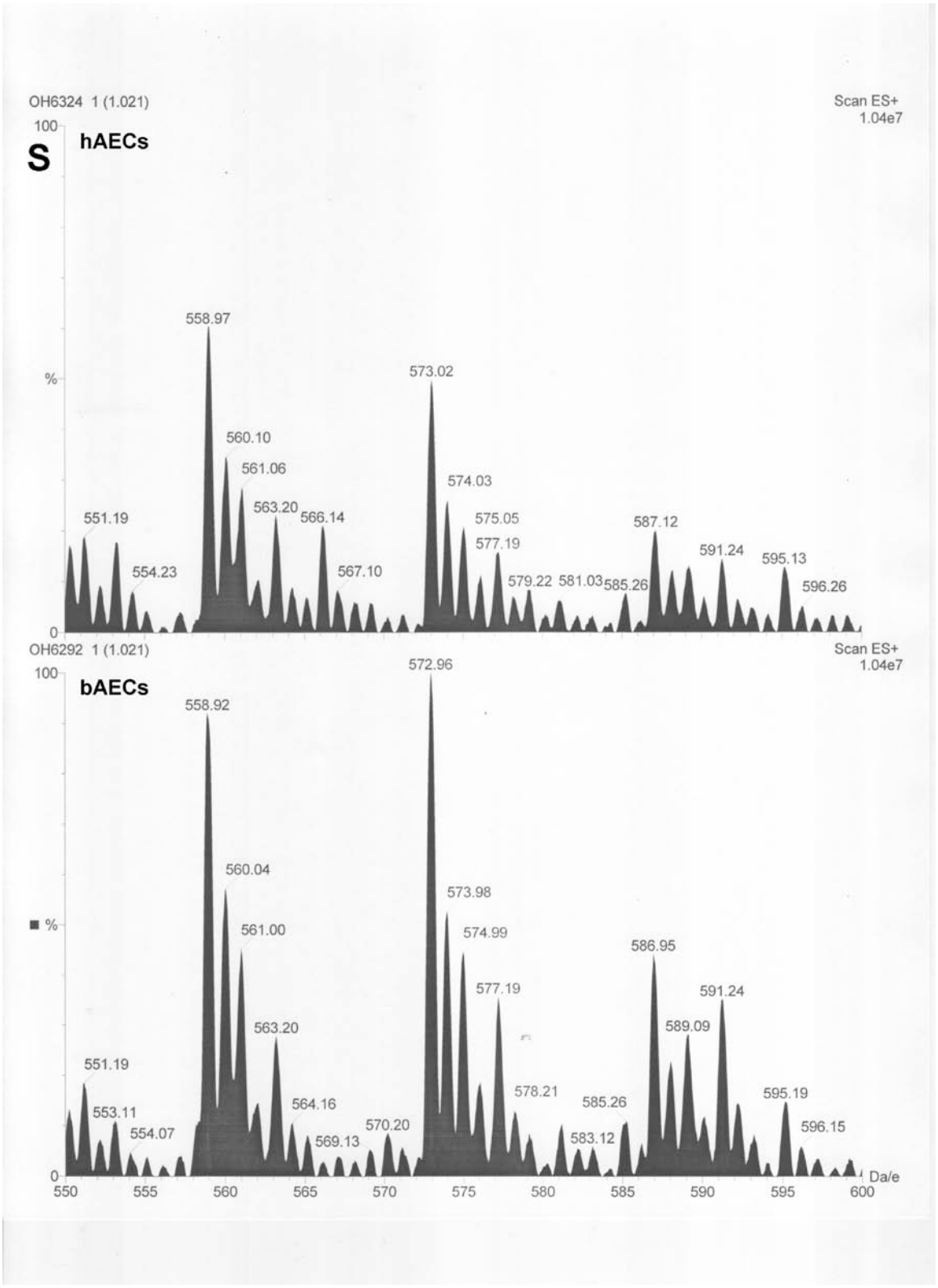

Figure B.S. ESI-MS comparison of hAECs and bAECs in the positive ion mode across the m/z range of 550-600.

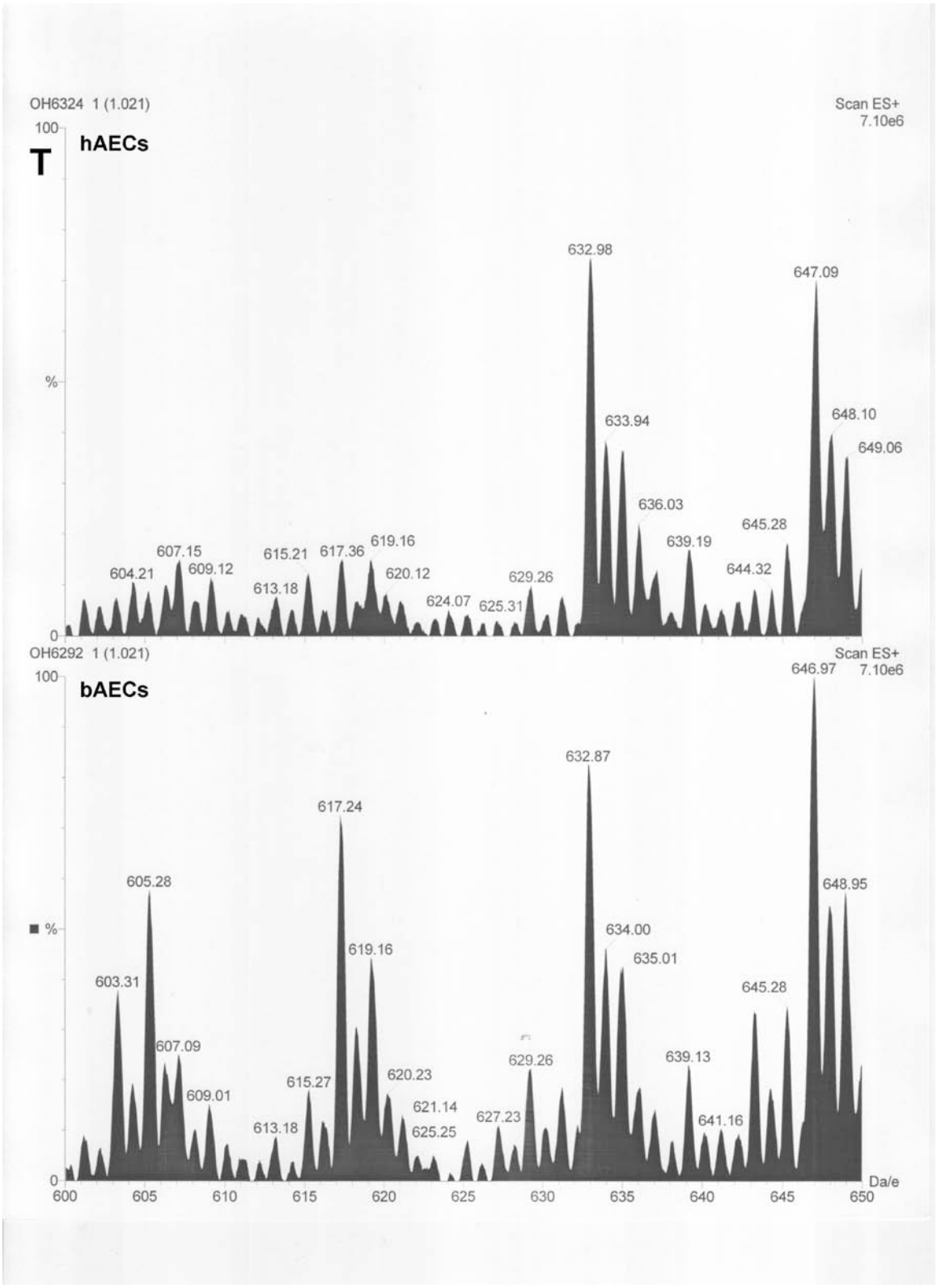

Figure B.T. ESI-MS comparison of hAECs and bAECs in the positive ion mode across the m/z range of 600-650.

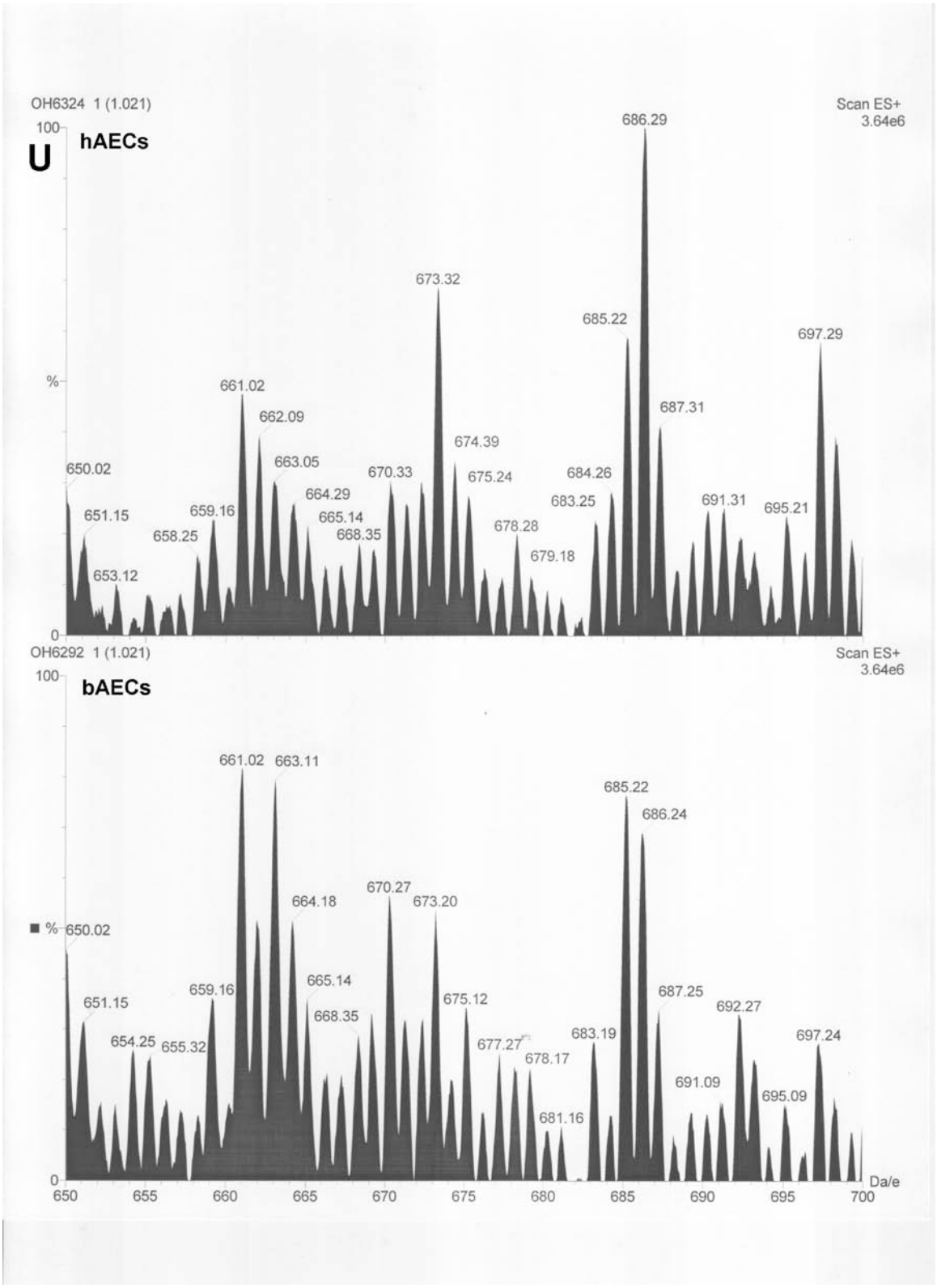

Figure B.U. ESI-MS comparison of hAECs and bAECs in the positive ion mode across the m/z range of 650-700.

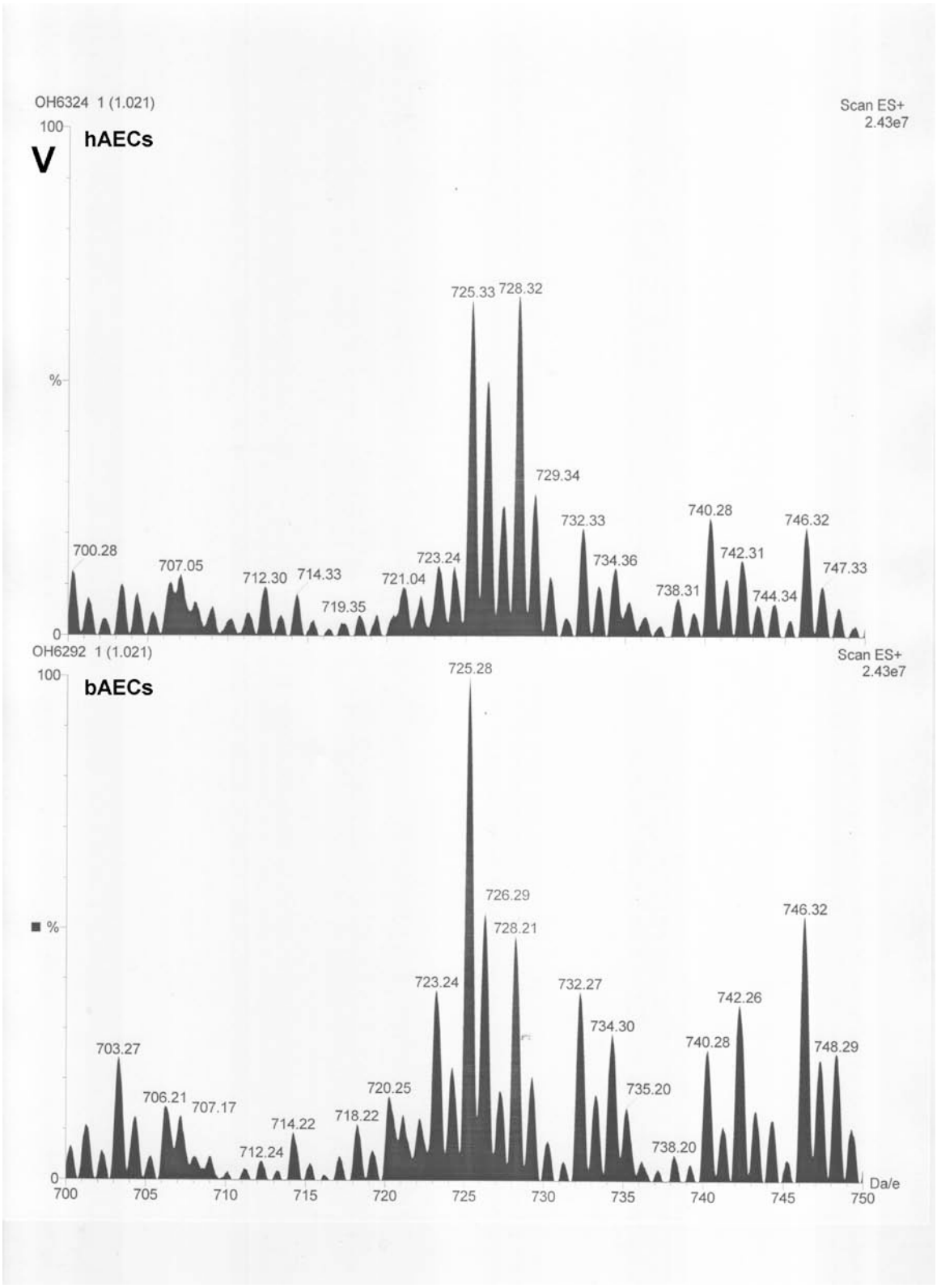

Figure B.V. ESI-MS comparison of hAECs and bAECs in the positive ion mode across the m/z range of 700-750.

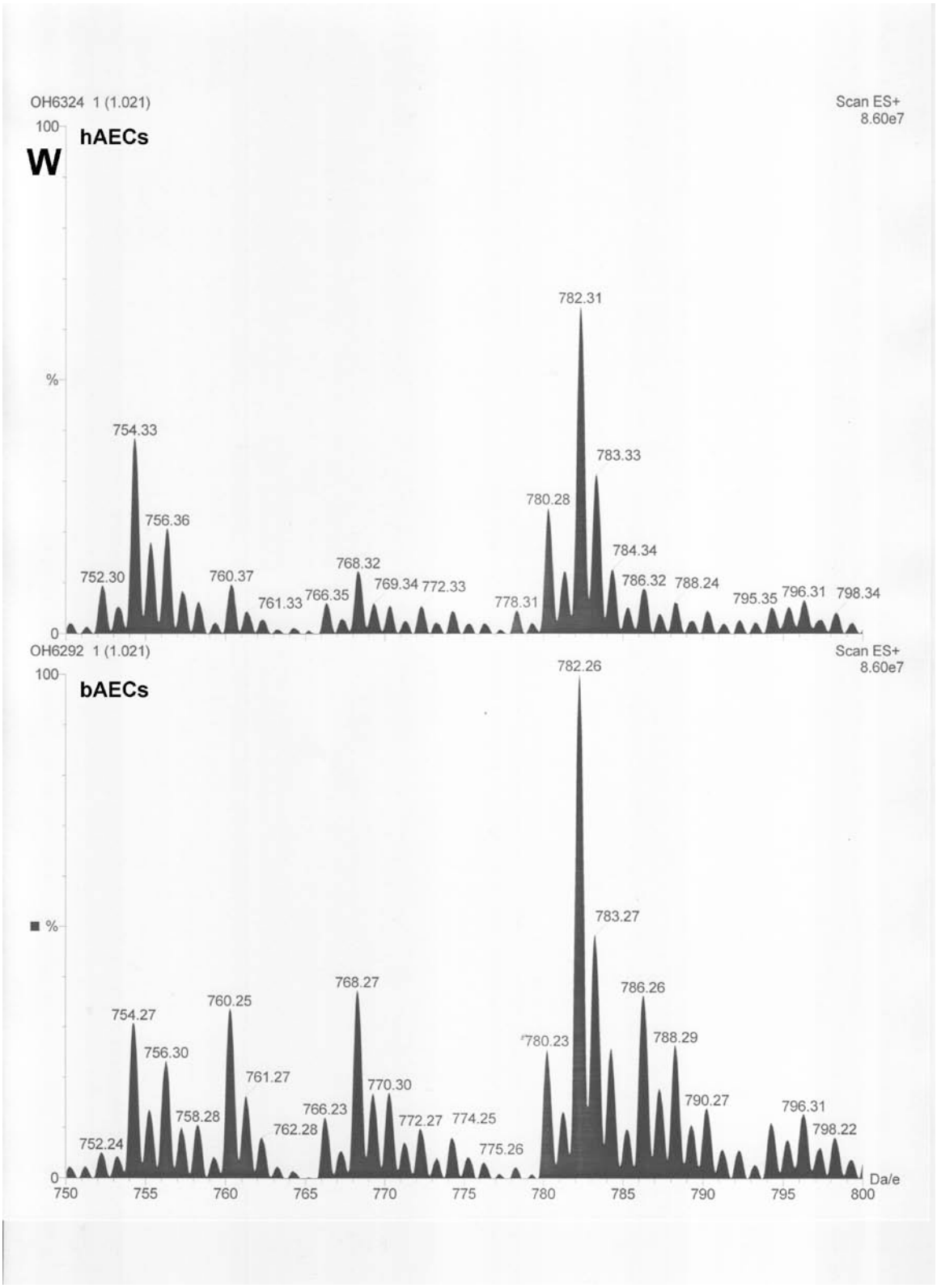

Figure B.W. ESI-MS comparison of hAECs and bAECs in the positive ion mode across the m/z range of 750-800.

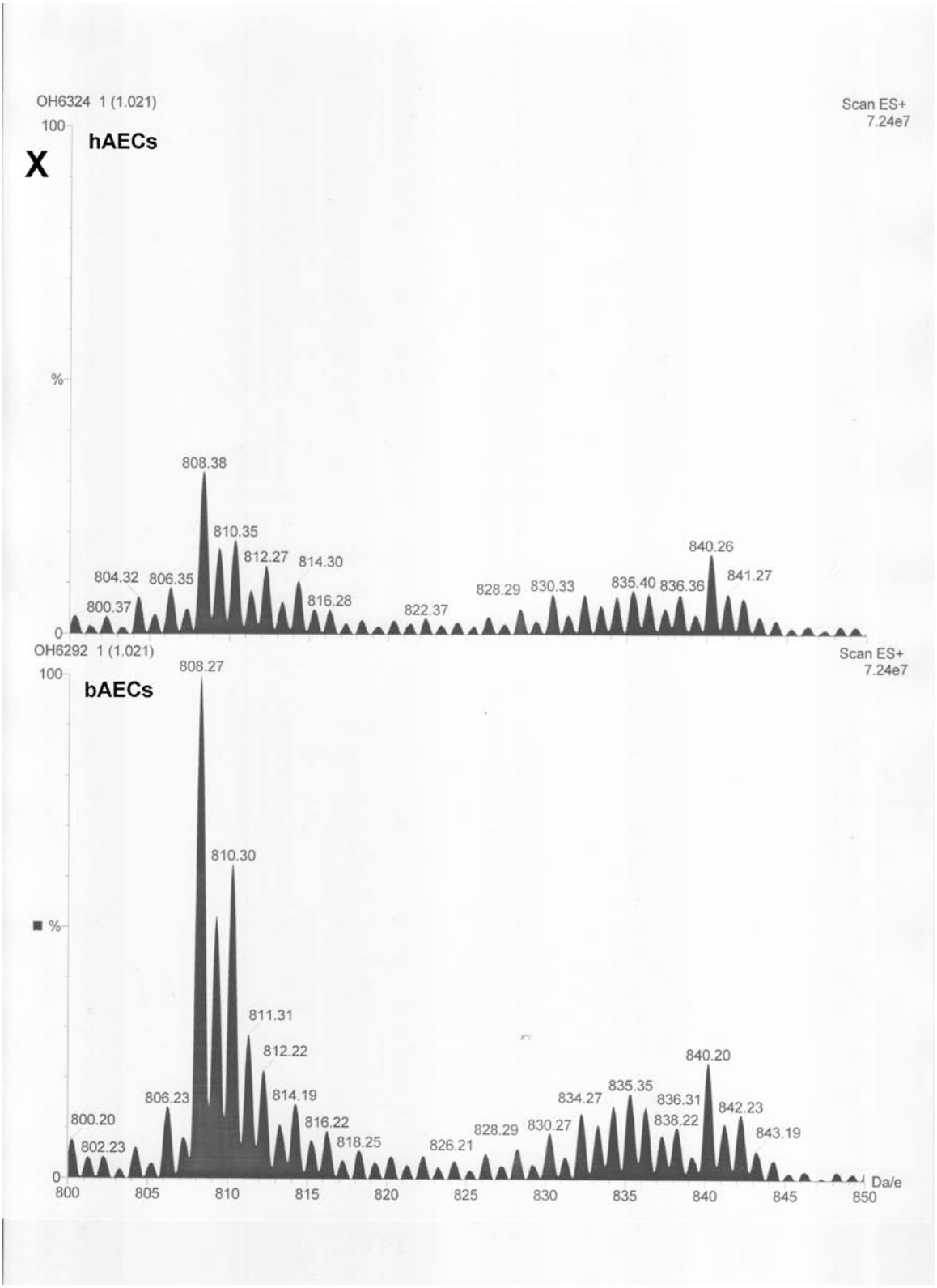

Figure B.X. ESI-MS comparison of hAECs and bAECs in the positive ion mode across the m/z range of 800-850.

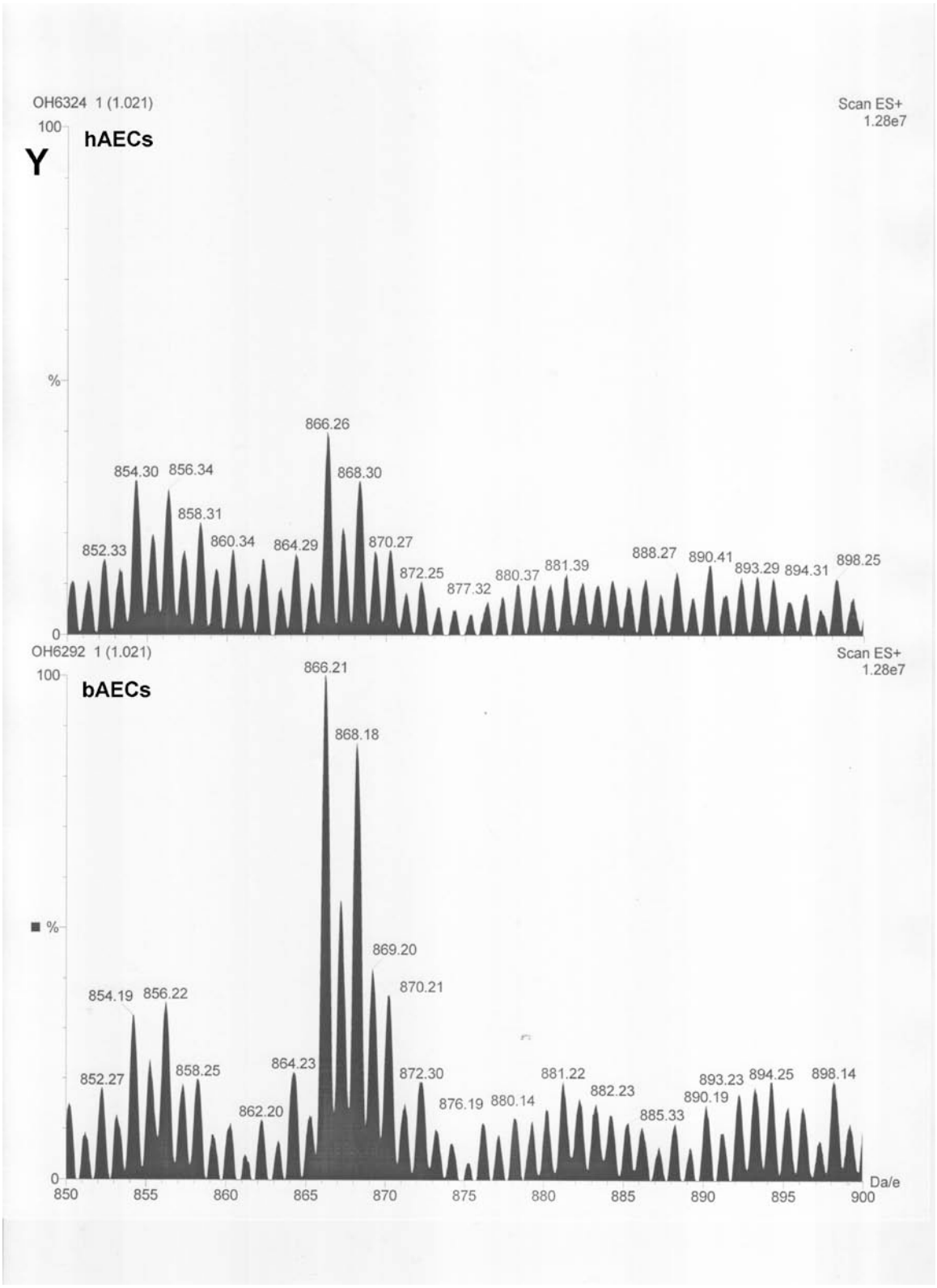

Figure B.Y. ESI-MS comparison of hAECs and bAECs in the positive ion mode across the m/z range of 850-900.

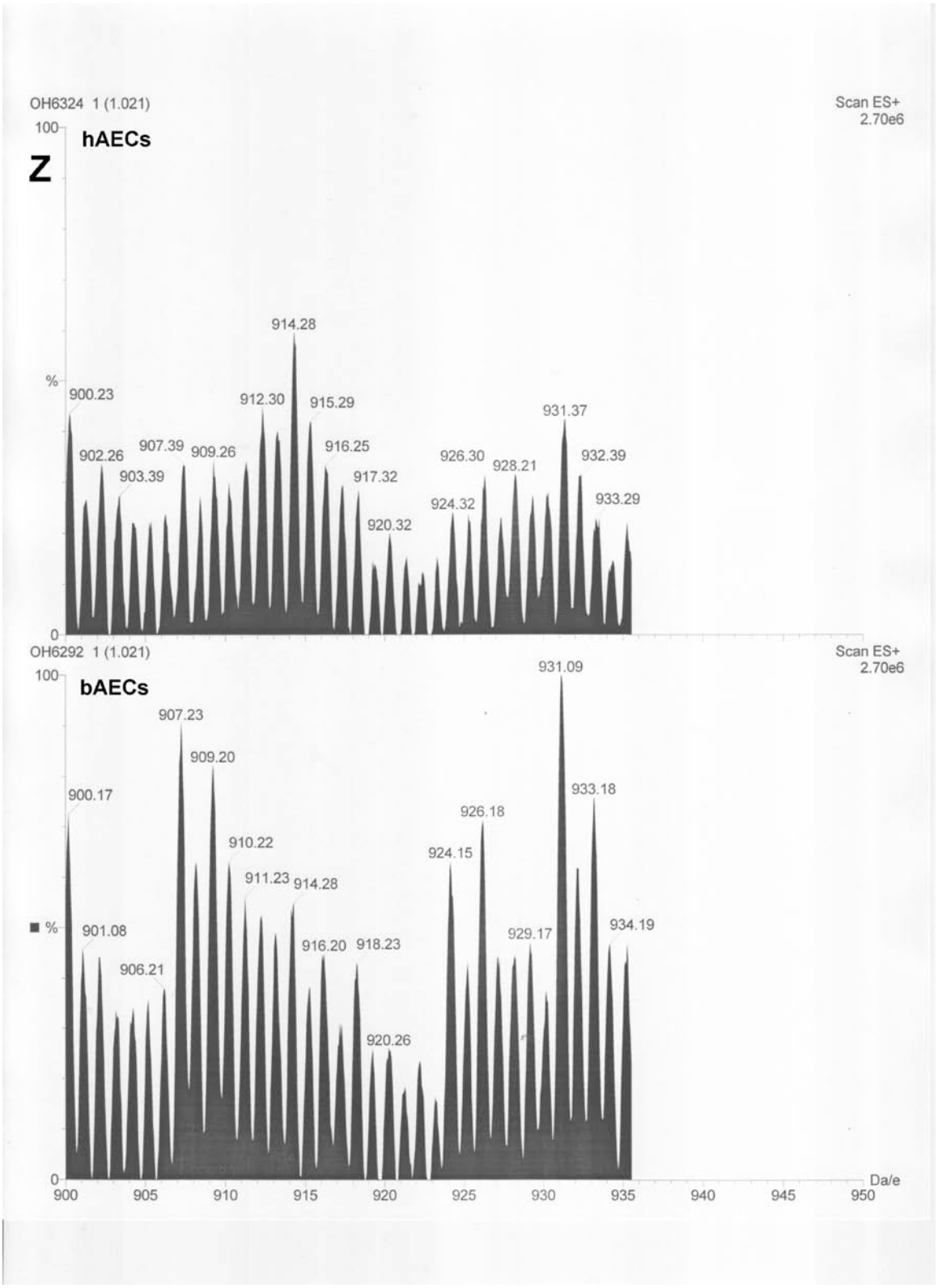

Figure B.Z. ESI-MS comparison of hAECs and bAECs in the positive ion mode across the m/z range of 900-950.

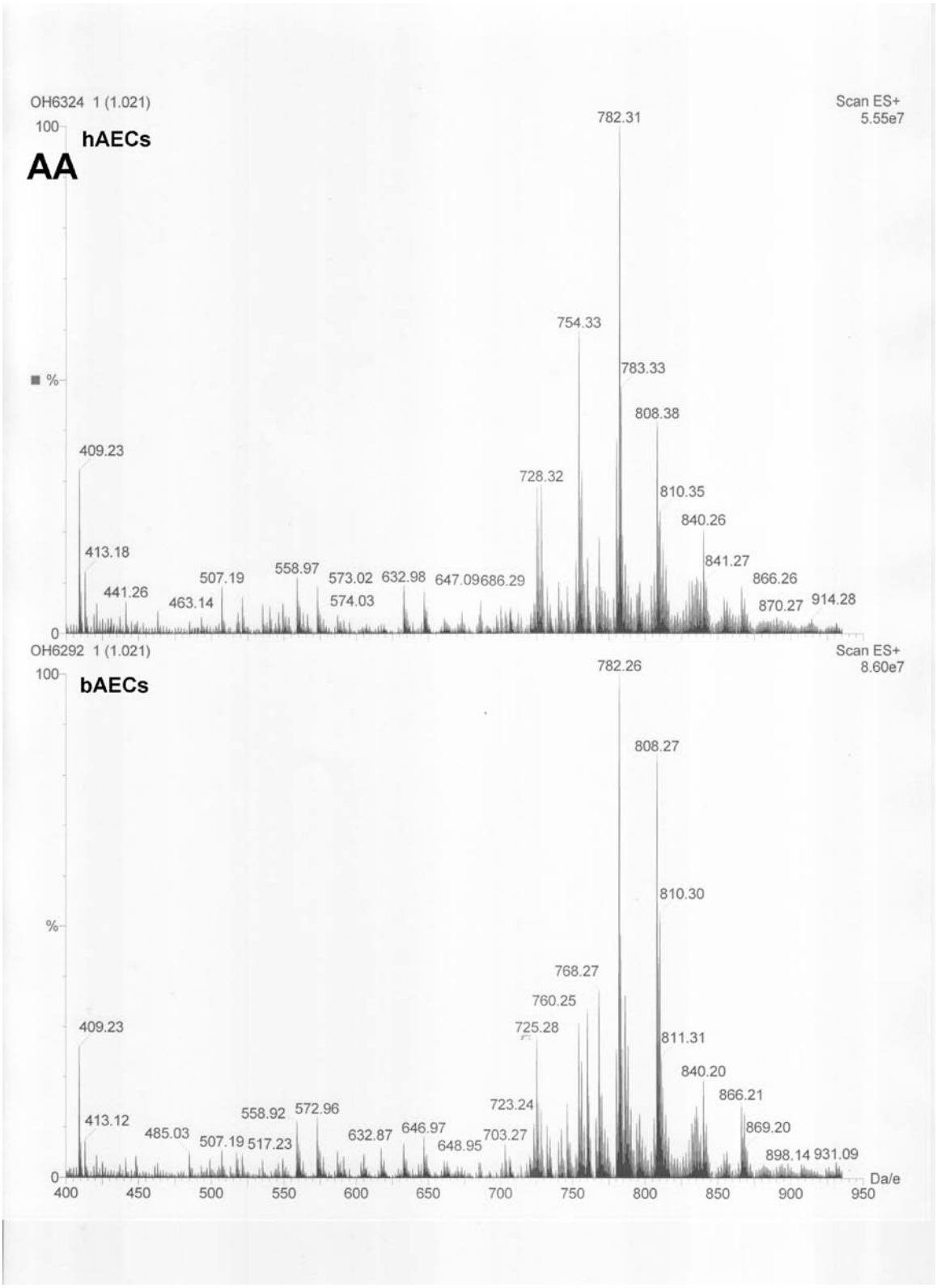

Figure B.AA. ESI-MS comparison of hAECs and bAECs in the positive ion mode across the m/z range of 400-950.

BIBLIOGRAPHY

1. Choy, J.C., et al., *Endothelial cell apoptosis: biochemical characteristics and potential implications for atherosclerosis.* Journal of Molecular & Cellular Cardiology, 2001. **33**(9): p. 1673-90.

2. Prokazova, N.V., et al., *Lipid second messengers and cell signaling in vascular wall.* Biochemistry-Russia, 2007. **72**(8): p. 797-808.

3. Sigal, L.H., *Basic science for the clinician 44: atherosclerosis: an immunologically mediated (autoimmune?) disease.* JCR: Journal of Clinical Rheumatology, 2007. **13**(3): p. 160-8.

4. Verma, S., M.R. Buchanan, and T.J. Anderson, *Endothelial function testing as a biomarker of vascular disease.[see comment].* Circulation, 2003. **108**(17): p. 2054-9.

5. Bonetti, P.O., L.O. Lerman, and A. Lerman, *Endothelial dysfunction: a marker of atherosclerotic risk.* Arteriosclerosis, Thrombosis & Vascular Biology, 2003. **23**(2): p. 168-75.

6. Hansson, G.K. and P. Libby, *The immune response in atherosclerosis: a double-edged sword.* Nature Reviews. Immunology, 2006. **6**(7): p. 508-19.

7. Libby, P., *Inflammation in atherosclerosis.* Nature, 2002. **420**(6917): p. 868-74.

8. Lloyd-Jones, D., et al., *Heart disease and stroke statistics--2009 update: a report from the American Heart Association Statistics Committee and Stroke Statistics Subcommittee.* Circulation, 2009. **119**(3): p. e21-181.

9. Verma, S. and T.J. Anderson, *Fundamentals of endothelial function for the clinical cardiologist.* Circulation, 2002. **105**(5): p. 546-9.

10. Lockhart, C.J., G.E. McVeigh, and J.N. Cohn, *Measuring endothelial function.* Current Diabetes Reports, 2006. **6**(4): p. 267-73.

11. Brunner, H., et al., *Endothelial function and dysfunction. Part II: Association with cardiovascular risk factors and diseases. A statement by the Working Group on*

Endothelins and Endothelial Factors of the European Society of Hypertension. Journal of Hypertension, 2005. **23**(2): p. 233-46.

12. Willerson, J.T. and D.J. Kereiakes, *Endothelial dysfunction.[comment].* Circulation, 2003. **108**(17): p. 2060-1.

13. Ross, R., *The Vessel Wall*, in *The Heart and cardiovascular system : scientific foundations*, H.A. Fozzard, et al., Editors. 1991, Raven Press: New York. p. 163-185.

14. Martini, F.H., *Fundamentals of Anatomy and Physiology*. 7th ed. 2006, San Francisco, CA: Pearson Education, Inc.

15. Mitchell, R.N. and P. Libby, *Vascular remodeling in transplant vasculopathy.* Circulation Research, 2007. **100**(7): p. 967-78.

16. dela Paz, N.G. and P.A. D'Amore, *Arterial versus venous endothelial cells.* Cell & Tissue Research, 2009. **335**(1): p. 5-16.

17. Moreno, P.R., et al., *Neovascularization in human atherosclerosis.* Current Molecular Medicine, 2006. **6**(5): p. 457-77.

18. Langheinrich, A.C., et al., *Vasa vasorum and atherosclerosis - Quid novi?* Thrombosis & Haemostasis, 2007. **97**(6): p. 873-9.

19. Wang, Y.X., *Do measures of vascular compliance correlate with endothelial function?* Current Diabetes Reports, 2007. **7**(4): p. 265-8.

20. Sima, A.V., C.S. Stancu, and M. Simionescu, *Vascular endothelium in atherosclerosis.* Cell & Tissue Research, 2009. **335**(1): p. 191-203.

21. Triggle, C.R., et al., *The endothelium in health and disease--a target for therapeutic intervention.* Journal of Smooth Muscle Research, 2003. **39**(6): p. 249-67.

22. Wagner, D.D. and P.S. Frenette, *The vessel wall and its interactions.* Blood, 2008. **111**(11): p. 5271-81.

23. Aird, W.C., *Spatial and temporal dynamics of the endothelium.* Journal of Thrombosis & Haemostasis, 2005. **3**(7): p. 1392-406.

24. Herrmann, J. and A. Lerman, *The endothelium - the cardiovascular health barometer.* Herz, 2008. **33**(5): p. 343-53.

25. Kuldo, J.M., et al., *Molecular pathways of endothelial cell activation for (targeted) pharmacological intervention of chronic inflammatory diseases.* Current Vascular Pharmacology, 2005. **3**(1): p. 11-39.

26. Bhatia, R., et al., *Ceramide triggers Weibel-Palade body exocytosis.* Circulation Research, 2004. **95**(3): p. 319-24.

27. van Gils, J.M., J.J. Zwaginga, and P.L. Hordijk, *Molecular and functional interactions among monocytes, platelets, and endothelial cells and their relevance for cardiovascular diseases.* Journal of Leukocyte Biology, 2009. **85**(2): p. 195-204.

28. Michaux, G. and D.F. Cutler, *How to roll an endothelial cigar: the biogenesis of Weibel-Palade bodies.* Traffic, 2004. **5**(2): p. 69-78.

29. Utgaard, J.O., et al., *Rapid secretion of prestored interleukin 8 from Weibel-Palade bodies of microvascular endothelial cells.* Journal of Experimental Medicine, 1998. **188**(9): p. 1751-6.

30. Wolff, B., et al., *Endothelial cell "memory" of inflammatory stimulation: human venular endothelial cells store interleukin 8 in Weibel-Palade bodies.* Journal of Experimental Medicine, 1998. **188**(9): p. 1757-62.

31. Zhang, H., et al., *Role of TNF-alpha in vascular dysfunction.* Clinical Science, 2009. **116**(3): p. 219-30.

32. Hansson, G.K., et al., *Innate and adaptive immunity in the pathogenesis of atherosclerosis.* Circulation Research, 2002. **91**(4): p. 281-91.

33. Csiszar, A., et al., *Inflammation and endothelial dysfunction during aging: role of NF-kappaB.* Journal of Applied Physiology, 2008. **105**(4): p. 1333-41.

34. Chironi, G.N., et al., *Endothelial microparticles in diseases.* Cell & Tissue Research, 2009. **335**(1): p. 143-51.

35. Mannarino, E. and M. Pirro, *Endothelial injury and repair: a novel theory for atherosclerosis.* Angiology, 2008. **59**(2 Suppl): p. 69S-72S.

36. Erusalimsky, J.D., *Vascular endothelial senescence: from mechanisms to pathophysiology.* Journal of Applied Physiology, 2009. **106**(1): p. 326-32.

37. Lockhart, C.J., et al., *End-organ dysfunction and cardiovascular outcomes: the role of the microcirculation.* Clinical Science, 2009. **116**(3): p. 175-90.

38. Liu, S.Q., et al., *A possible role of initial cell death due to mechanical stretch in the regulation of subsequent cell proliferation in experimental vein grafts.* Biomechanics & Modeling in Mechanobiology, 2002. **1**(1): p. 17-27.

39. Goldman, S., et al., *Long-term patency of saphenous vein and left internal mammary artery grafts after coronary artery bypass surgery: results from a Department of*

Veterans Affairs Cooperative Study. Journal of the American College of Cardiology, 2004. **44**(11): p. 2149-56.

40. Manninen, H.I., et al., *Angiographic predictors of graft patency and disease progression after coronary artery bypass grafting with arterial and venous grafts.* Annals of Thoracic Surgery, 1998. **66**(4): p. 1289-94.

41. Sasaki, Y., et al., *Role of endothelial cell denudation and smooth muscle cell dedifferentiation in neointimal formation of human vein grafts after coronary artery bypass grafting: therapeutic implications.* Heart, 2000. **83**(1): p. 69-75.

42. Liu, S.Q., M.M. Moore, and C. Yap, *Prevention of mechanical stretch-induced endothelial and smooth muscle cell injury in experimental vein grafts.* Journal of Biomechanical Engineering, 2000. **122**(1): p. 31-8.

43. Bundey, R.A., *Endothelial cell mechanosensitivity. Focus on "Cyclic strain and motion control produce opposite oxidative responses in two human endothelial cell types".[comment].* American Journal of Physiology - Cell Physiology, 2007. **293**(1): p. C33-4.

44. Kakisis, J.D., C.D. Liapis, and B.E. Sumpio, *Effects of cyclic strain on vascular cells.* Endothelium: Journal of Endothelial Cell Research, 2004. **11**(1): p. 17-28.

45. Lehoux, S., Y. Castier, and A. Tedgui, *Molecular mechanisms of the vascular responses to haemodynamic forces.* Journal of Internal Medicine, 2006. **259**(4): p. 381-92.

46. Tarbell, J.M., S. Weinbaum, and R.D. Kamm, *Cellular fluid mechanics and mechanotransduction.* Annals of Biomedical Engineering, 2005. **33**(12): p. 1719-23.

47. Ali, M.H. and P.T. Schumacker, *Endothelial responses to mechanical stress: where is the mechanosensor?* Critical Care Medicine, 2002. **30**(5 Suppl): p. S198-206.

48. Orr, A.W., et al., *Mechanisms of mechanotransduction.[erratum appears in Dev Cell. 2006 Mar;10(3):407].* Developmental Cell, 2006. **10**(1): p. 11-20.

49. Tarbell, J.M. and E.E. Ebong, *The endothelial glycocalyx: a mechano-sensor and -transducer.* Sci Signal, 2008. **1**(40): p. pt8.

50. Chien, S., *Molecular basis of rheological modulation of endothelial functions: importance of stress direction.* Biorheology, 2006. **43**(2): p. 95-116.

51. Mayr, M., et al., *Mechanical stress-induced DNA damage and rac-p38MAPK signal pathways mediate p53-dependent apoptosis in vascular smooth muscle cells.* FASEB Journal, 2002. **16**(11): p. 1423-5.

52. Liu, X.M., et al., *Physiologic cyclic stretch inhibits apoptosis in vascular endothelium.* FEBS Letters, 2003. **541**(1-3): p. 52-6.

53. Sotoudeh, M., et al., *Induction of apoptosis in vascular smooth muscle cells by mechanical stretch.* American Journal of Physiology - Heart & Circulatory Physiology, 2002. **282**(5): p. H1709-16.

54. Sung, H.J., et al., *Cyclic strain and motion control produce opposite oxidative responses in two human endothelial cell types.[see comment].* American Journal of Physiology - Cell Physiology, 2007. **293**(1): p. C87-94.

55. Lum, H. and K.A. Roebuck, *Oxidant stress and endothelial cell dysfunction.* American Journal of Physiology - Cell Physiology, 2001. **280**(4): p. C719-41.

56. Davies, P.F., *Hemodynamic shear stress and the endothelium in cardiovascular pathophysiology.* Nature Clinical Practice Cardiovascular Medicine, 2009. **6**(1): p. 16-26.

57. Garin, G. and B.C. Berk, *Flow-mediated signaling modulates endothelial cell phenotype.* Endothelium: Journal of Endothelial Cell Research, 2006. **13**(6): p. 375-84.

58. Davies, P.F., J.A. Spaan, and R. Krams, *Shear stress biology of the endothelium.* Annals of Biomedical Engineering, 2005. **33**(12): p. 1714-8.

59. White, C.R. and J.A. Frangos, *The shear stress of it all: the cell membrane and mechanochemical transduction.* Philosophical Transactions of the Royal Society of London - Series B: Biological Sciences, 2007. **362**(1484): p. 1459-67.

60. Harrison, D.G., et al., *Endothelial mechanotransduction, nitric oxide and vascular inflammation.* Journal of Internal Medicine, 2006. **259**(4): p. 351-63.

61. El Alwani, M., et al., *Bioactive sphingolipids in the modulation of the inflammatory response.* Pharmacology & Therapeutics, 2006. **112**(1): p. 171-83.

62. Gulbins, E. and P.L. Li, *Physiological and pathophysiological aspects of ceramide.* American Journal of Physiology - Regulatory Integrative & Comparative Physiology, 2006. **290**(1): p. R11-26.

63. Mathias, S., L.A. Pena, and R.N. Kolesnick, *Signal transduction of stress via ceramide.* Biochemical Journal, 1998. **335**(Pt 3): p. 465-80.

64. Futerman, A.H. and H. Riezman, *The ins and outs of sphingolipid synthesis.* Trends in Cell Biology, 2005. **15**(6): p. 312-8.

65. Pettus, B.J., C.E. Chalfant, and Y.A. Hannun, *Ceramide in apoptosis: an overview and current perspectives.* Biochimica et Biophysica Acta, 2002. **1585**(2-3): p. 114-25.

66. Taha, T.A., T.D. Mullen, and L.M. Obeid, *A house divided: ceramide, sphingosine, and sphingosine-1-phosphate in programmed cell death.* Biochimica et Biophysica Acta, 2006. **1758**(12): p. 2027-36.

67. Andrieu-Abadie, N., et al., *Ceramide in apoptosis signaling: relationship with oxidative stress.* Free Radical Biology & Medicine, 2001. **31**(6): p. 717-28.

68. Lee, Y.J. and A.A. Amoscato, *TRAIL and ceramide.* Vitamins & Hormones, 2004. **67**: p. 229-55.

69. Birbes, H., et al., *Mitochondria and ceramide: intertwined roles in regulation of apoptosis.* Advances in Enzyme Regulation, 2002. **42**: p. 113-29.

70. Seumois, G., et al., *De novo C16- and C24-ceramide generation contributes to spontaneous neutrophil apoptosis.* Journal of Leukocyte Biology, 2007. **81**(6): p. 1477-86.

71. Pavoine, C., et al., *Sphingomyelinases: their regulation and roles in cardiovascular pathophysiology.* Cardiovascular Research, 2009. **82**(2): p. 175-83.

72. Pilane, C.M. and E.F. LaBelle, *NO induced apoptosis of vascular smooth muscle cells accompanied by ceramide increase.* Journal of Cellular Physiology, 2004. **199**(2): p. 310-5.

73. Arena, S., et al., *Nitric oxide production stimulated by the basic fibroblast growth factor requires the synthesis of ceramide.* Annals of the New York Academy of Sciences, 2002. **973**: p. 94-104.

74. Clementi, E., N. Borgese, and J. Meldolesi, *Interactions between nitric oxide and sphingolipids and the potential consequences in physiology and pathology.* Trends in Pharmacological Sciences, 2003. **24**(10): p. 518-23.

75. Perry, D.K., *The role of de novo ceramide synthesis in chemotherapy-induced apoptosis.* Annals of the New York Academy of Sciences, 2000. **905**: p. 91-6.

76. Igarashi, Y. and Y. Yatomi, *Sphingosine 1-phosphate is a blood constituent released from activated platelets, possibly playing a variety of physiological and pathophysiological roles.* Acta Biochimica Polonica, 1998. **45**(2): p. 299-309.

77. Yatomi, Y., et al., *Sphingosine 1-phosphate, a bioactive sphingolipid abundantly stored in platelets, is a normal constituent of human plasma and serum.* Journal of Biochemistry, 1997. **121**(5): p. 969-73.

78. Lee, M.J., et al., *Vascular endothelial cell adherens junction assembly and morphogenesis induced by sphingosine-1-phosphate.* Cell, 1999. **99**(3): p. 301-12.

79. Bornfeldt, K.E., et al., *Sphingosine-1-phosphate inhibits PDGF-induced chemotaxis of human arterial smooth muscle cells: spatial and temporal modulation of PDGF chemotactic signal transduction.* Journal of Cell Biology, 1995. **130**(1): p. 193-206.

80. Spiegel, S. and S. Milstien, *Sphingosine-1-phosphate: an enigmatic signalling lipid.* Nature Reviews Molecular Cell Biology, 2003. **4**(5): p. 397-407.

81. Chatterjee, S., *Sphingolipids in atherosclerosis and vascular biology.* Arteriosclerosis, Thrombosis & Vascular Biology, 1998. **18**(10): p. 1523-33.

82. Czarny, M., et al., *Transient mechanoactivation of neutral sphingomyelinase in caveolae to generate ceramide.* Journal of Biological Chemistry, 2003. **278**(7): p. 4424-30.

83. Czarny, M. and J.E. Schnitzer, *Neutral sphingomyelinase inhibitor scyphostatin prevents and ceramide mimics mechanotransduction in vascular endothelium.* American Journal of Physiology - Heart & Circulatory Physiology, 2004. **287**(3): p. H1344-52.

84. Johns, D.G., H. Osborn, and R.C. Webb, *Ceramide: a novel cell signaling mechanism for vasodilation.* Biochemical & Biophysical Research Communications, 1997. **237**(1): p. 95-7.

85. Siskind, L.J., et al., *Enlargement and contracture of C2-ceramide channels.* Biophysical Journal, 2003. **85**(3): p. 1560-75.

86. Dumitru, C.A., et al., *Ceramide: a novel player in reactive oxygen species-induced signaling?* Antioxidants & Redox Signaling, 2007. **9**(9): p. 1535-40.

87. Shimizu, T. and T. Shimizu, *Lipid mediators in health and disease: enzymes and receptors as therapeutic targets for the regulation of immunity and inflammation.* Annual Review of Pharmacology & Toxicology, 2009. **49**: p. 123-50.

88. Kitatani, K., J. Idkowiak-Baldys, and Y.A. Hannun, *The sphingolipid salvage pathway in ceramide metabolism and signaling.* Cellular Signalling, 2008. **20**(6): p. 1010-8.

89. Pulfer, M. and R.C. Murphy, *Electrospray mass spectrometry of phospholipids.* Mass Spectrometry Reviews, 2003. **22**(5): p. 332-64.

90. Holthuis, J.C. and T.P. Levine, *Lipid traffic: floppy drives and a superhighway.* Nature Reviews Molecular Cell Biology, 2005. **6**(3): p. 209-20.

91. Vereb, G., et al., *Dynamic, yet structured: The cell membrane three decades after the Singer-Nicolson model.* Proceedings of the National Academy of Sciences of the United States of America, 2003. **100**(14): p. 8053-8.

92. Tillman, T.S. and M. Cascio, *Effects of membrane lipids on ion channel structure and function.* Cell Biochemistry & Biophysics, 2003. **38**(2): p. 161-90.

93. Leidl, K., et al., *Mass spectrometric analysis of lipid species of human circulating blood cells.* Biochimica et Biophysica Acta, 2008. **1781**(10): p. 655-64.

94. Patschan, S., et al., *Lipid mediators of autophagy in stress-induced premature senescence of endothelial cells.* American Journal of Physiology - Heart & Circulatory Physiology, 2008. **294**(3): p. H1119-29.

95. Bayir, H., et al., *Selective early cardiolipin peroxidation after traumatic brain injury: an oxidative lipidomics analysis.* Annals of Neurology, 2007. **62**(2): p. 154-69.

96. Thomas, R.L., Jr., et al., *Mass spectrometric identification of increased C16 ceramide levels during apoptosis.* Journal of Biological Chemistry, 1999. **274**(43): p. 30580-8.

97. The Waters Corpration. *Quattro II User's Guide*. [PDF users guid] [cited 2009; Available from: https://www.waters.com/webassets/cms/support/docs/quattro_2_guide_issue2.pdf.

98. Brites, P., H.R. Waterham, and R.J. Wanders, *Functions and biosynthesis of plasmalogens in health and disease.* Biochimica et Biophysica Acta, 2004. **1636**(2-3): p. 219-31.

99. Leray, C., J.P. Cazenave, and C. Gachet, *Platelet phospholipids are differentially protected against oxidative degradation by plasmalogens.* Lipids, 2002. **37**(3): p. 285-90.

100. Beckett, C.S., et al., *Phospholipase A2-catalyzed hydrolysis of plasmalogen phospholipids in thrombin-stimulated human platelets.* Thrombosis Research, 2007. **120**(2): p. 259-68.

101. Meyer, M.C. and J.M cHowat, *Calcium-independent phospholipase A2-catalyzed plasmalogen hydrolysis in hypoxic human coronary artery endothelial cells.* American Journal of Physiology - Cell Physiology, 2007. **292**(1): p. C251-8.

102. Pewzner-Jung, Y., S. Ben-Dor, and A.H. Futerman, *When do Lasses (longevity assurance genes) become CerS (ceramide synthases)?: Insights into the regulation of ceramide synthesis.* Journal of Biological Chemistry, 2006. **281**(35): p. 25001-5.

103. Scarlatti, F., et al., *Ceramide-mediated macroautophagy involves inhibition of protein kinase B and up-regulation of beclin 1.* Journal of Biological Chemistry, 2004. **279**(18): p. 18384-91.

104. Lavieu, G., et al., *Is autophagy the key mechanism by which the sphingolipid rheostat controls the cell fate decision?[comment].* Autophagy, 2007. **3**(1): p. 45-7.

105. Humphrey, J.D., *Vascular adaptation and mechanical homeostasis at tissue, cellular, and sub-cellular levels.* Cell Biochemistry & Biophysics, 2008. **50**(2): p. 53-78.

106. DeLoach, S.S. and R.R. Townsend, *Vascular stiffness: its measurement and significance for epidemiologic and outcome studies.* Clinical Journal of The American Society of Nephrology: CJASN, 2008. **3**(1): p. 184-92.

107. Hoshino, Y., K. Nishimura, and B.E. Sumpio, *Phosphatase PTEN is inactivated in bovine aortic endothelial cells exposed to cyclic strain.* Journal of Cellular Biochemistry, 2007. **100**(2): p. 515-26.

108. Morrow, D., et al., *Cyclic strain regulates the Notch/CBF-1 signaling pathway in endothelial cells: role in angiogenic activity.* Arteriosclerosis, Thrombosis & Vascular Biology, 2007. **27**(6): p. 1289-96.

109. Hirayama, Y. and B.E. Sumpio, *Role of ligand-specific integrins in endothelial cell alignment and elongation induced by cyclic strain.* Endothelium: Journal of Endothelial Cell Research, 2007. **14**(6): p. 275-83.

110. Davis, G.E. and D.R. Senger, *Endothelial extracellular matrix: biosynthesis, remodeling, and functions during vascular morphogenesis and neovessel stabilization.* Circulation Research, 2005. **97**(11): p. 1093-107.

111. Arenz, C., et al., *Manumycin A and its analogues are irreversible inhibitors of neutral sphingomyelinase.* Chembiochem, 2001. **2**(2): p. 141-3.

112. Pena, L.A., Z. Fuks, and R. Kolesnick, *Stress-induced apoptosis and the sphingomyelin pathway.* Biochemical Pharmacology, 1997. **53**(5): p. 615-21.

113. Sugita, M., H. Sugita, and M. Kaneki, *Farnesyltransferase inhibitor, manumycin a, prevents atherosclerosis development and reduces oxidative stress in apolipoprotein E-deficient mice.* Arteriosclerosis, Thrombosis & Vascular Biology, 2007. **27**(6): p. 1390-5.

114. Hojjati, M.R., et al., *Effect of myriocin on plasma sphingolipid metabolism and atherosclerosis in apoE-deficient mice.* Journal of Biological Chemistry, 2005. **280**(11): p. 10284-9.